DEPARTMENT OF ELECTRICAL ENGINEERING

UNIVERSITY OF CAPE TOWN

Penetration Level of Un-Conventional Rural Electrification Technologies on Power Networks

MICHAEL JUMA SAULO

Supervisor: Prof. C.T. GAUNT

Thesis submitted to the University of Cape Town

IN FULFILMENT OF THE REQUIREMENT OF THE AWARD OF THE DEGREE OF

DOCTOR OF PHILOSOPHY

IN THE

DEPARTMENT OF ELECTRICAL ENGINEERING

MAY 2014

DECLARATION

I hereby:

(a) Grant the university free license to reproduce the above thesis in whole or in part for the purpose of research;

(b) Declare that:

(i) The thesis is my own work, both in conception and execution, and that a part from the normal guidance from my supervisor, I have received no assistance apart from that stated below;

(ii) Except as stated below, neither the substance nor any part of the thesis has been submitted in the past, or is being, or is to be submitted for a degree in the University or in any other University.

(iii) I am now presenting the thesis for examination for the Degree of PhD.

Michael Juma Saulo **Date**

ACKNOWLEDGEMENTS

First and foremost, my thanks go to the Almighty God for giving me the faith, strength and the courage towards pursuing my doctoral studies, and for keeping me safe and clear of any major difficulties that could have hindered me from finishing the PhD degree. I thank you heavenly father in the name of Jesus Christ our Saviour for keeping me alive for the years that I have been able to breathe.

Secondly, I would like to offer my special appreciation to my supervisor/mentor Prof C.T Gaunt. You have been an inspiration, a person that I have always relied on for help when things were not going well. Thank you for keeping the trust in me by allowing me to do my research under your supervision.

Thirdly, I would like to thank my beloved wife Winnie and children, Amelia, Brenda, Collins, Dorcas and Emmanuela for allowing me to travel that long distance and be able to finish my degree. I know it has been hard with me sometimes away from home for many months. Thank you for your patience and support.

I don't want to forget all my friends at the University of Cape Town specifically Milton, Samuel and Oliver and at home, Dr. Mbogho and the electrical staff members at UCT and TUM; you have been supportive, and helpful in many ways.

Finally, I have to thank my sponsors The Technical University of Mombasa (TUM) and National Commission for Science and Technology (NACOSTI), for giving me this opportunity to be able to realize my dream of finishing my PhD. in Electrical Engineering. Thank you very much for your financial support.

ABSTRACT

The overall electricity access rate is still very low in most sub-Saharan African (SSA) countries. The rate is even lower in rural areas where most of the population in these countries lives. One of the main obstacles to rural electrification (RE) is the high cost of laying the distribution infrastructure owing to the dispersed nature of loads and low demand. Thus, electrifying the rural areas needs to be considered holistically and not just on the financial viability. To reduce cost, it is important that un-conventional rural electrification (URE) technologies, which are cheaper than the conventional ones be explored. Un-conventional rural electrification (URE) technologies have been tried successfully in some parts of the world. However, the literature review showed that no work had so far been done with regard to maximum penetration level of these technologies on power transmission networks, especially the Capacitor Coupled Sub-station (CCS) and Auxiliary Service Voltage Transformers (ASVTs). These two technologies have the ability to tap power directly from high voltage transmission lines and convert it to distribution level single or three phase supply for the purpose of rural electrification.

This thesis investigated the adoptability and maximum penetration level of sub-station based URE technologies in power transmission networks with regard to voltage quality, stability, and capacity constraints without steady and transient state voltage violation. Quantitative data collected from practical power transmission lines were used for empirical and analytical approaches developed in this research.

The research developed a method of determining maximum allowable penetration level of CCS without steady state voltage violation derived from a modified distributed generation analogy. The method was based on determination of voltage sensitivities from linearized power system model. Consequently, this method was used to validate repetitive power flow simulations carried out in the case studies

Conversely, the percentage penetration level of ASVT units in a power transmission network was explored based on voltage quality and stability constraints. This was done by comparing simulation results of ASVT(s) loadability curve, with the constructed Surge Impedance Loading (SIL) curves. The later curves were derived from the ABCD parameters of the transmission line under investigation.

Analysis of results and performance of URE systems were presented and based on findings; the hypothesis was validated. It was established from analysis and simulations, that there was no apparent optimum point of penetration for CCS or ASVT on power networks. The sub-stations could be installed at any point along the transmission line. However, it was established that there was a maximum number of CCS/ASVT units that could be installed in particular power networks. The maximum penetration level of CCS/ASVT was dependent on the transmission line ABCD parameters, size of the divider capacitors or the impedance of ASVT unit(s) integrated in the power network, real and reactive power of the load on the CCS/ASVT and loading condition of the line.

Furthermore, it was established that both innovative URE sub-station technologies are applicable to any HV transmission line as long as the line voltage is maintained within the ± 6% tolerance, while the load power factor is varied between 0.2 and unity power factor. Moreover, the loadability tests for the ASVT showed that the system could operate almost at all power factors at 1MW loading. On the other hand, the CCS could operate from 0.5 up to a maximum of 0.9 power factor for similar loading conditions. Apparently, this indicated that the ASVT system was more flexible than the CCS and could be used for a wider variation of power factors or loading. Consequently, merging the two loadability graphs for CCS and ASVT produces an optimum power factor or operating range that these two systems could operate within when integrated in power transmission lines.

Finally, it was demonstrated that these technologies may be applied in any transmission line in SSA, provided appropriate maximum penetration level analysis are performed with respect to voltage sensitivities for CCS and surge impedance loading (SIL) for ASVT systems. The analysis would be based on the maximum penetration level of URE acceptable at steady and transient state without violating the allowable voltage limitation.

LIST OF ACRONYMS

ASVTs	Auxiliary Services Voltage Transformers
CB	Circuit Breaker
CCS	Capacitor Coupled Sub-Station
CCS-IM	Capacitor Coupled Substation - Induction Motor
CCVT	Capacitor Coupled Voltage Transformer
CSA	Canadian Standard Association
CVT	Capacitor Voltage Transformer
ESR	Equivalent Series Resistance
FSC	Ferro-resonance Suppression Circuit
HV	High Voltage
IM	Induction Motor
KWh	Kilo Watt hour
LV	Low Voltage
MV	Medium Voltage
MW	Megawatt
NPV	Net Present Value
OECD	Organization for Economic Co-operation and Development
O&M	Overhead and Maintenance
PSB	Power System Blockset
PV	Photo Voltaic
RE	Rural Electrification
ROI	Return on Investment
ROW	Right Of Way
SIL	Surge Impedance Loading
SSA	sub-Saharan Africa
SSR	Sub Synchronous Resonance
SWL	Shield Wire Line
SWS	Shield Wire Scheme
URE	Un-conventional Rural Electrification
VSD	Variable Speed Drives
WEO	World Energy Outlook
W/m^2	Watt per metre square
WTP	Willingness to pay

TABLE OF CONTENTS

Declaration i

Acknowledgements ii

Abstract iii

List of Acronyms v

Table of Contents vi

List of Figures x

List of Tables xiii

1 Introduction 1

1.1 Background 1

1.2 Objectives of the Thesis 4

1.3 The Concept of URE Technologies 6

1.4 Justification for the Research 8

1.5 Hypothesis and Research Questions 9

1.6 Novel Element of the Research 10

1.7 Structure of the Thesis 10

1.8 Onward 11

2 Un-conventional Rural Electrification Technologies 12

2.1 Introduction 12

2.2 URE Technologies 12

2.3 Capacitor Coupled Sub-Station (CCS) 14

2.4 Auxiliary Service Voltage Transformers (ASVTs) 24

2.5 Comparison between ASVT and conventional distribution transformers 25

2.6 Why URE Technologies 28

2.7 URE System Modeling and Analysis 29

2.8 URE Technology Planning 30

2.9 The Scope for URE Technologies 31
2.10 Local conditions Suitable for URE technologies 32
2.11 Research Question Answered 33
2.12 Onward 35
3 Theoretical Model Development 36
3.1 Introduction 36
3.2 Modeling Of the Transmission Line 36
3.3 Modeling of Capacitor Coupled Sub-station (CCS) 39
3.4 System Design 43
3.5 Modeling of ASVTs 57
3.6 Penetration Level of ASVTs On a Power Network 62
3.7 Proposed Methodology 73
3.8 Onward 74
4 Capacitor Coupled Sub-stations in Power Networks (Case Study) 75
4.1 Introduction 75
4.2 Simulation Software for case study 75
4.3 Simulation Scenarios 77
4.4 model with CCS and without FSC and load at steady and transient states 78
4.5 Model without CCS for unloaded and loaded conditions 90
4.6 Models with CCS and FSC for unloaded and loaded conditions 93
4.7 CCS with FSC at different distances with line unloaded and loaded 94
4.8 Effect of a reactor in the line 95
4.9 Three CCS with reactor on and off line 99
4.10 CCS with FSC model for Transient Stability Case 100
4.11 CCS loadability test 103
4.12 Shunt Compensation using CCS 104
4.13 Analysis of Results 105

4.14 Onward 107
5 Penetration Level of Capacitor Coupled Sub-stations on Power Networks 108
5.1 Introduction 108
5.2 Analogy between DG and CCS 108
5.3 Slack Bus Treatment in Load Flow Solutions 110
5.4 Voltage Sensitivities determination 113
5.5 Validation studies for different Scenarios 116
5.6 Maximum Penetration level without violating voltage limit 119
5.7 Validation test using voltage sensitivities analysis. 121
5.8 Onward 125
6 Auxiliary Service Voltage Transformers on Power Networks: (Case Study) 126
6.1 Introduction 126
6.2 ASVT Design Using the Reverse Design Method 126
6.3 ASVT design flow chart 128
6.4 Simulation Scenarios 128
6.5 model for ASVT in the line at steady state condition with load 129
6.6 Models for ASVT in the line without and with load and reactor on/off 137
6.7 Penetration level of Combined ASVT and CCS unit(s) at different distances 142
6.8 Transient conditions for ASVT/CCS at different switching 144
6.9 ASVT Loadability test 150
6.10 Comparative analysis of ASVT with CCS 152
6.11 Analysis of Results 154
6.12 Onward 156
7 Penetration Level of Auxiliary Service Voltage Transformers 158
7.1 Introduction 158
7.2 Determination of transmission line parameters 159
7.3 Determining the SIL Curve 164

7.4 Line loadability curves 167
7.5 Comparison of stability limits. 168
7.6 Penetration level of ASVT 169
7.7 Onward 170
8 Conclusion 171
8.1 Implication of URE technologies 176
8.2 Way Forward 177
References 178
Appendices 189

LIST OF FIGURES

FIGURE 1.1 CAPACITIVE COUPLED SUB-STATION LINE DIAGRAM [PASAND AND AGHAZADEH 2003]....2
FIGURE 1.2 ASVT SINGLE LINE DIAGRAM [GOMEZ ET AL. 2010]. 2
FIGURE 1.3 PICTORIAL VIEWS OF THE TWO URE SCHEMES [ABB MANUAL 2000 AND GAUNT 2005] 3
FIGURE 1.4 OBJECTIVE OF THE THESIS 5
FIGURE 2.1 THREE-PHASE SWS DISTRIBUTION SYSTEM [ILICETO ET AL. 2005]. 13
FIGURE 2.2 CCS EQUIVALENT CIRCUIT [BOLDUC ET AL. 1997] 15
FIGURE 2.3 CONVENTIONAL POWER TRANSFORMER [ABB 2000] 27
FIGURE 2.4 AUXILIARY SERVICE VOLTAGE TRANSFORMER (ASVT) [GOMEZ ET AL 2010] 27
FIGURE 3.1 EQUIVALENT CIRCUIT OF A TRANSMISSION LINE 38
FIGURE 3.2 SECTIONS OF THE PI MODEL....38
FIGURE 3.3 CAPACITOR COUPLED SUB-STATION SCHEMATIC DIAGRAM [PASAND AND AGHAZADEH 2003] 40
FIGURE 3.4 ELECTRICAL CIRCUIT CAUSING FERRO-RESONANCE 42
FIGURE 3.5 ANALYTICAL VIEW OF FERRO-RESONANCE PROBLEM....42
FIGURE 3.6 CAPACITIVE VOLTAGE DIVIDER CONNECTED PHASE- TO- GROUND....43
FIGURE 3.7 GENERIC CVT STRUCTURE....46
FIGURE 3.8 ACTIVE AND PASSIVE FERRO-RESONANCE-SUPPRESSION CIRCUIT 47
FIGURE 3.9 SCHEMATIC REPRESENTATIONS 48
FIGURE 3.10 SYSTEMS EQUIVALENT CIRCUIT [RAPHALALANI ET AL. 2000] 49
FIGURE 3.11 PEAK POWER OVER THE DAILY PROFILE (KW) 52
FIGURE 3.12 AVERAGE POWER DEMAND CURVE FOR A TYPICAL RURAL VILLAGE 52
FIGURE 3.13 LOAD DURATION CURVE....53
FIGURE 3.14 ONE LINE DIAGRAM OF DISTRIBUTION FEEDER [BARAN AND WU 1989]....54
FIGURE 3.15 COMPONENT DIMENSION AND MATERIAL PROPERTIES OF A TRANSFORMER 58
FIGURE 3.16 STEINMETZ 'EXACT' TRANSFORMER EQUIVALENT CIRCUIT 59
FIGURE 3.17 TRANSMISSION LINE LOADABILITY CURVE (ST CLAIRS CURVE) [DUNLOP ET AL. 1979]....67
FIGURE 3.18 CONCEPTUAL CURVE FOR LINE LOADING [NAYAK ET AL. 2006]....68
FIGURE 3.19 SYSTEM DIAGRAM [HAO AND XU 2008] 69
FIGURE 3.20 POWER TRANSFER CAPABILITY CURVE [HAO AND XU 2008]....70
FIGURE 3.21 TRANSMISSION LINE MODEL AND ITS EQUIVALENT CIRCUIT [HAO AND XU 2008] 71
FIGURE 4.1 INTERFACING ELECTRICAL CIRCUITS WITH SIMULINK 76
FIGURE 4.2 TRANSIENT SIMULATION CIRCUITS....77
FIGURE 4.3 MODEL FOR THE LINE WITH ONE CCS AND WITHOUT FSC....78
FIGURE 4.4 MODEL FOR THE LINE WITH ONE CCS AND DISTURBANCE 81
FIGURE 4.5 WAVEFORMS FOR SIGNAL 1 INJECTION 84
FIGURE 4.6 WAVEFORMS FOR SIGNAL 2 INJECTION 86
FIGURE 4.7 WAVEFORMS FOR SIGNAL 3 INJECTION 88
FIGURE 4.8 WAVEFORMS FOR SIGNAL 3 INJECTION 90
FIGURE 4.9 MODEL FOR THE LINE WITHOUT LOAD AND CCS 91
FIGURE 4.10 SENDING AND RECEIVING VOLTAGE WAVEFORM FOR LINE WITHOUT LOAD AND CCS 91
FIGURE 4.11 MODEL OF THE LINE WITH LOAD AND WITHOUT CCS....92
FIGURE 4.12 SENDING AND RECEIVING VOLTAGE WAVEFORMS FOR LINE WITH LOAD AND WITHOUT CCS 92
FIGURE 4.13 MODELS WITH CCS MIDWAY BETWEEN THE LINE AND WITHOUT LOAD....93
FIGURE 4.14 SIMULATION FOR HV VOLTAGE WAVE WITH CCS MIDWAY THE UNLOADED LINE 93
FIGURE 4.15 MODELS WITH CCS MIDWAY BETWEEN THE LINE AND WITH LOAD....94
FIGURE 4.16 RECEIVING END VOLTAGE WAVE WITH CCS MIDWAY AND LINE LOADED 94

FIGURE 4.17 MODEL WITH CCS AND 10 MVAR REACTORS AT THE RECEIVING END 96
FIGURE 4.18 EFFECTS OF 125MW AND 10MVAR REACTOR ON THE TRANSMISSION LINE 96
FIGURE 4.19 MODEL FOR TWO CCS CONNECTED ON THE TRANSMISSION LINE 97
FIGURE 4.20 TWO CCS CONNECTED TO LOADED TRANSMISSION LINE AT DIFFERENT DISTANCES 98
FIGURE 4.21 VOLTAGE WAVEFORMS OF TWO CCS WITH A 10MVAR CONNECTED AT DIFFERENT DISTANCES 99
FIGURE 4.22 MODELS FOR THREE CCS AT DIFFERENT DISTANCES 100
FIGURE 4.23 SIMULATION RESULTS FOR THREE CCS AT DIFFERENT DISTANCES 100
FIGURE 4.24 MODELS FOR TRANSIENT STABILITY SIMULATION 101
FIGURE 4.25 MV AND LV VOLTAGE WITH BREAKER CLOSING AFTER 1 SECOND 101
FIGURE 4.26 MV AND LV VOLTAGE WITH BREAKER CLOSING AFTER 2 SECOND 102
FIGURE 4.27 MV AND LV VOLTAGE WITH BREAKER CLOSING AFTER 3 SECOND 102
FIGURE 4.28 CCS LOADABILITY TEST MODEL 103
FIGURE 4.29 VOLTAGE PROFILE FOR LOADABILITY TEST 104
FIGURE 4.30 CCS VOLTAGE PROFILE FOR COMPENSATED AND UNCOMPENSATED LINE 105
FIGURE 5.1 CCS MODIFIED VERSION OF THE POWER NETWORK SYSTEM 110
FIGURE 5.2 CCS EQUIVALENT CIRCUIT OF THE MODIFICATION 110
FIGURE 5.3 SINGLE LINE DIAGRAM OF KENYA TRANSMISSION NETWORK 118
FIGURE 5.4 SINGLE LINE DIAGRAM OF THE IEEE 30-BUS TEST SYSTEM 119
FIGURE 5.5 VOLTAGE PROFILES WITH CCS UNITS AT BUSES 8, 22, AND 28. 122
FIGURE 5.6 MAXIMUM ALLOWABLE POWER OF BUS 28. 123
FIGURE 5.7 VOLTAGE PROFILE FOR DIFFERENT POWER FACTORS FOR CCS UNIT 124
FIGURE 5.8 ASSESSMENT OF VOLTAGE SENSITIVITY 125
FIGURE 6.1 FLOW CHART FOR ASVT DESIGN 127
FIGURE 6.2 MODEL CIRCUIT WITH ONE ASVT (PI-SECTION = 440KM TRANSMISSION LINE) LINE LOADED 129
FIGURE 6.3 MODEL CIRCUIT WITH ONE ASVT WITHOUT LOAD 130
FIGURE 6.4 MODEL CIRCUIT WITH ONE ASVT (PI-SECTION =440KM TRANSMISSION LINE) 131
FIGURE 6.5WAVEFORMS FOR SIGNAL 1 INJECTION 133
FIGURE 6.6 WAVEFORMS FOR SIGNAL 2 INJECTION 134
FIGURE 6.7 WAVEFORMS FOR SIGNAL 3 INJECTION 136
FIGURE 6.8 WAVEFORMS FOR SIGNAL 4 INJECTION 137
FIGURE 6.9 MODEL FOR THE LINE WITHOUT LOAD AND ASVT 138
FIGURE 6.10 MODEL FOR THE LINE WITH LOAD AND ONE ASVT 138
FIGURE 6.11 RECEIVING END LV AND HV VOLTAGE 139
FIGURE 6.12 MODEL FOR THE LINE WITH LOAD AND TWO ASVTS 140
FIGURE 6.13 LV VOLTAGE AT 50 AND 100KM FROM RABAI 140
FIGURE 6.14 MODEL FOR THE LINE WITH LOAD AND THREE ASVTS 141
FIGURE 6.15 MODEL FOR THE LINE WITHOUT LOAD AND CCS 142
FIGURE 6.16 MODEL FOR COMBINATION OF ASVT AND CCS 142
FIGURE 6.17 MODEL FOR TRANSIENT SIGNAL OF ASVT/CCS COMBINATION 145
FIGURE 6.18 WAVEFORMS FOR SIGNAL 1 INJECTION 149
FIGURE 6.19 ASVT LOADABILITY MODEL 151
FIGURE 6.20 LOADABILITY TEST OF ASVT 151
FIGURE 6.21 ASVT/CCS COMPARISON. 153
FIGURE 7.1 SIMULATION CIRCUIT USED FOR LINE PARAMETER DETERMINATION 159
FIGURE 7.2SIMULATION RESULTS PARAMETERS FOR A 50KM SHORT LINE 160
FIGURE 7.3 SIMULATION RESULTS PARAMETERS FOR A 150KM MEDIUM LINE 161
FIGURE 7.4 SIMULATION RESULTS PARAMETERS FOR A 440KM LONG LINE 162
FIGURE 7.5 SIMULATION CIRCUIT USED FOR DRAWING THE SIL CURVE 164

FIGURE 7.6 SIL CURVE WITH POWER FACTOR OF 0.5 166
FIGURE 7.7 SIL CURVE WITH POWER FACTOR OF 0.9 166
FIGURE 7.8 SIL CURVE WITH MIXED POWER FACTORS 167
FIGURE 7.9 COMPARISON OF REALISTIC STABILITY LIMITS (UNCOMPENSATED) 168
FIGURE 7.10 COMPARISON OF REALISTIC STABILITY LIMITS (COMPENSATED) 169

LIST OF TABLES

TABLE 1.1 SAMPLE URE TECHNOLOGY OPTIONS 7
TABLE 1.2 ELECTRICITY ACCESS IN 2009-REGIONAL AGGREGATES (SOURCE: WEO -2011) 9
TABLE 4.1 SUMMARY OF VOLTAGES MEASURED AT DIFFERENT POINT IN THE MODEL 79
TABLE 6.1 MEASUREMENTS FOR DIFFERENT PENETRATION LEVELS OF ASVT AT STEADY STATE 129
TABLE 6.2 MEASUREMENTS FOR DIFFERENT PENETRATION LEVELS OF ASVT/CCS AT STEADY STATE 143
TABLE 6.3 COMPARATIVE ANALYSES OF ASVT AND CCS 153
TABLE 7.1 LOAD SIZES 160
TABLE 7.2 ERRORS INTRODUCED IN THE CALCULATED PARAMETERS (SHORT LINE) 161
TABLE 7.3 ERRORS INTRODUCED IN THE CALCULATED PARAMETERS (MEDIUM LINE) 162
TABLE 7.4 ERRORS INTRODUCED IN THE CALCULATED PARAMETERS (LONG LINE) 163
TABLE 7.5 PARAMETER FOR TRANSMISSION LINES SHOWN IN FIGURE 7.1 163
TABLE 7.6 SIZE OF IMPEDANCE LOAD IN CONJUCTION WITH TIME 165

1 INTRODUCTION

1.1 BACKGROUND

The overall electricity access rate is still very low in most sub-Saharan African (SSA) countries. The rate is even lower in rural areas where most of the population in these countries lives. One of the main obstacles to rural electrification (RE) is the high cost of laying the distribution infrastructure owing to the dispersed nature of loads and low demand. Thus, electrifying the rural areas needs to be considered holistically and not just on the financial viability. To reduce cost, it is important that un-conventional rural electrification (URE) technologies, which are cheaper than the conventional ones be explored.

In most SSA rural areas, the concentration of electricity users is low and cost of deploying a conventional sub-station is prohibitive. As a result, in many cases power utilities will not be able to generate an adequate return on the large investment necessary to bring a conventional distribution sub-station on line. Conversely, there are large numbers of rural communities in these areas living around or in close proximity to high voltage transmissions lines but are un-electrified. The main obstacle is that these lines are carrying high voltages that cannot be directly and cheaply used for electrification. Therefore, in order to address the drawbacks associated with prohibitive costs of conventional sub-stations, URE sub-station are explored in this thesis [Anderson and Yanev 2010, Pasand and Aghazadeh 2003].

The focus of this study is based on two types of URE sub-station technologies namely; Capacitor Coupled Sub-station (CCS) that taps directly into the transmission overhead lines and Auxiliary Service Voltage Transformers (ASVTs) which allows direct connection to high voltage lines or bar, and directly transforms energy from voltage up to 230kV down to 600V or smaller in one step [Gomez et al. 2010].

Figure 1.1, shows a single line diagram of the CCS sub-station technology. Where; C_1 and C_2 are the divider capacitors, L is the inductor added in series to cancel the Thévenin reactance that is;

$C_{th} = C_1 + C_2$ at 50Hz, FSC is the Ferro-resonance suppression circuit and Tx is the fixed turns ratio isolating transformer connected to the load. Figure 1.2 is an ASVT single line diagram. Whereas, Figure 1.3 is the pictorial diagrams for the two systems respectively.

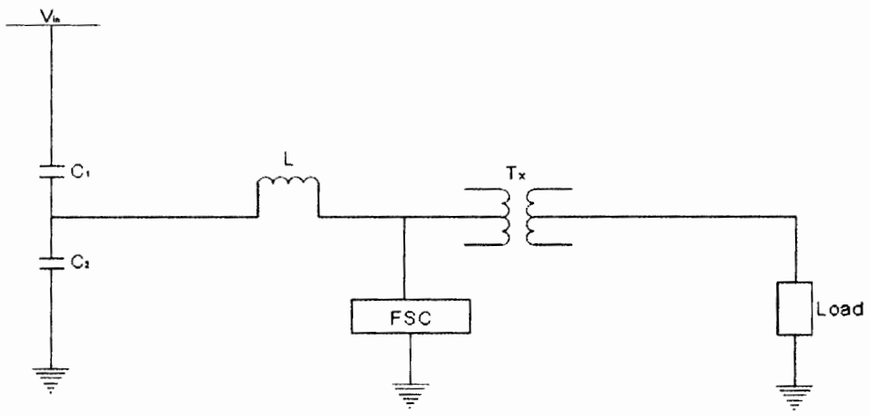

Figure 1.1 Capacitive Coupled Sub-station line diagram [Pasand and Aghazadeh 2003].

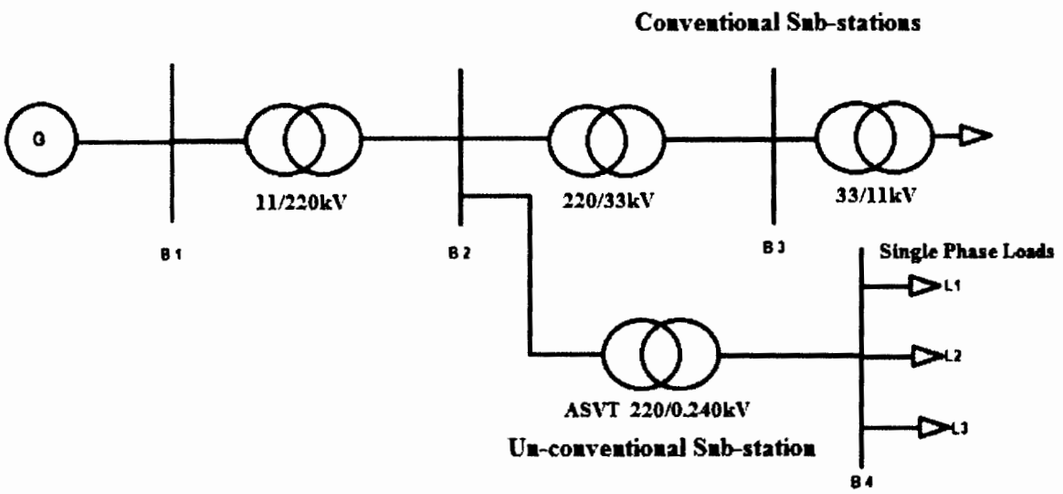

Figure 1.2 ASVT single line diagram [Gomez et al. 2010].

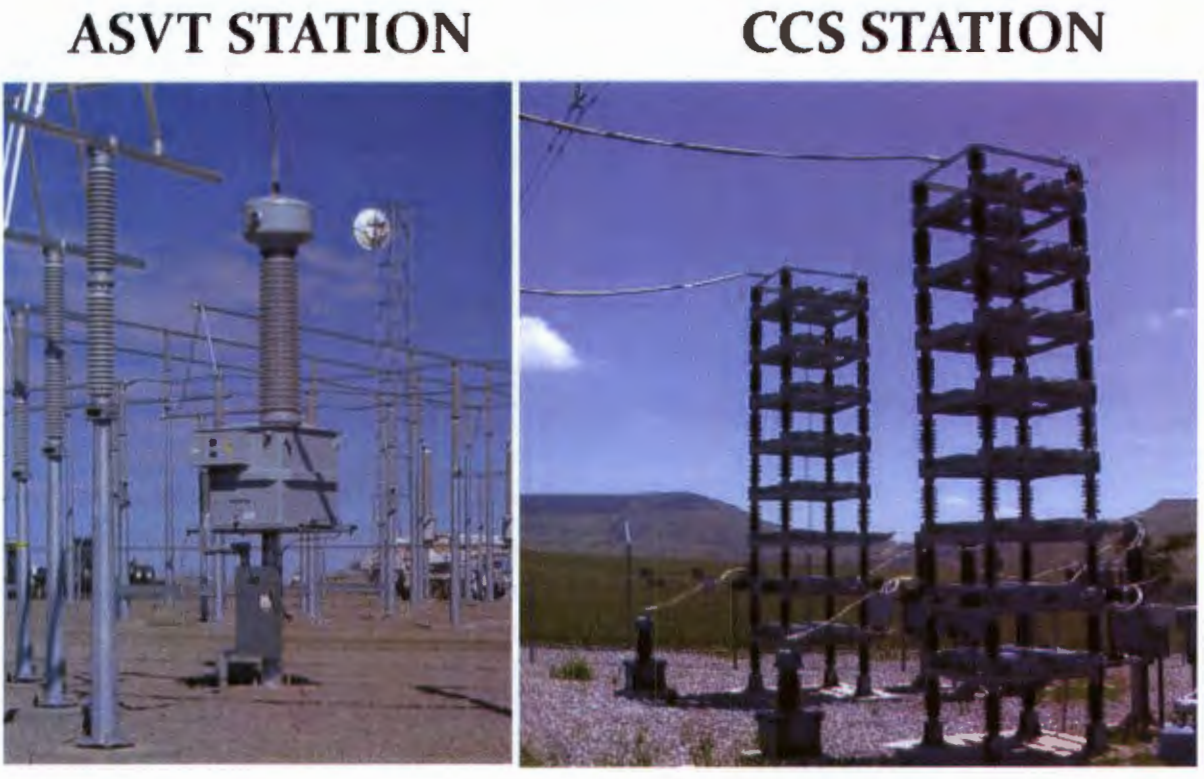

Figure 1.3 Pictorial views of the two URE schemes [ABB Manual 2000 and Gaunt 2005]

These two URE sub-station technologies offer major opportunities for reduction of construction, operating and maintenance costs of grid-based rural electrification in SSA. In many cases, careful attention to system design enables construction cost to be reduced by up to 30%, contributing significantly to the pace, scope and affordability of the rural electrification services [Barnes and Foley 2004, Barnes 2005].

Grid-based electricity offers a cheaper option for lighting and small appliances usage in rural settlements in SSA. Therefore, there is no need to apply the design standards used for more heavily loaded urban systems when designing rural electrification networks. The rural distribution system can be designed for actual loads, often not more than a few kilowatt-hours per month, imposed to it by rural households [Barnes 2005, Zomers 2003]. Although consumptions grow, this is usually at a slow pace and provided necessary design provisions are made, systems can be upgraded relatively cheaply later.

Each developing country has had their own un-conventional way of cost-saving opportunities for rural electrification planners. For example, in Thailand, materials were standardized and manufactured locally, reducing procurement, material handling, and purchase expenses [Barnes and Foley 2004].

In Costa Rica, the Philippines and Bangladesh, adoption of the well proven single-phase distribution systems, used in the US rural electrification program of the 1930s, brought major savings over the three-phase conventional system still widely used in Africa and elsewhere [Ledwich et al. 2007]. In Australia and Brazil, Single Wire Earth Return (SWER) distribution lines achieved even greater cost reduction in their rural electrification programs [Barnes 2007, and Anil 2005].

Therefore, careful and empirical analysis of URE system design and implementation practices has great potential for significant cost savings, which can improve affordable access of electricity to rural consumers, contributing to sustainability of electricity services in rural areas [Saulo et al. 2011].

1.2 OBJECTIVES OF THE THESIS

Electricity alone is not enough to develop a nation or a country, but it generates substantial benefits, including the promotion of commercial and industrial production, better health and education [Kooijman 2009]. However, some factors such as low population density, difficult terrain and low consumption, amongst others, make rural electrification substantially more costly to develop than urban schemes. Historically, this has been one of the main reasons for low electrification rates in rural areas of most developing countries in SSA [Barnes 2007].

Rural electrification has two primary objectives. First, to improve the economic status of the rural population by increasing the productivity of human and labor and secondly, to promote rural welfare by providing an environment equal in comfort and convenience to that enjoyed in urban areas [Cecelski 2002, Kooijman 2009]. This research project has three objectives illustrated in Figure 1.4;

Objective 1: Is the overall objective of the thesis. The objective is to evaluate the adoptability and maximum allowable percentage penetration level of the sub-station based URE technologies in power networks with regard to voltage quality, stability and capacity constraints without steady state voltage violation.

Objective 2: Determine the maximum allowable percentage penetration level of CCS in power networks with regard to voltage quality, stability, and capacity constraints without steady state voltage violation.

Objective 3: Determine the maximum allowable percentage penetration level of ASVTs in power networks with regard to voltage quality, stability, and capacity constraints without steady state voltage violation.

In this research project the analysis is focused on developing countries with emphasis in sub-Saharan Africa. However, case studies are done on Kenyan power transmission networks.

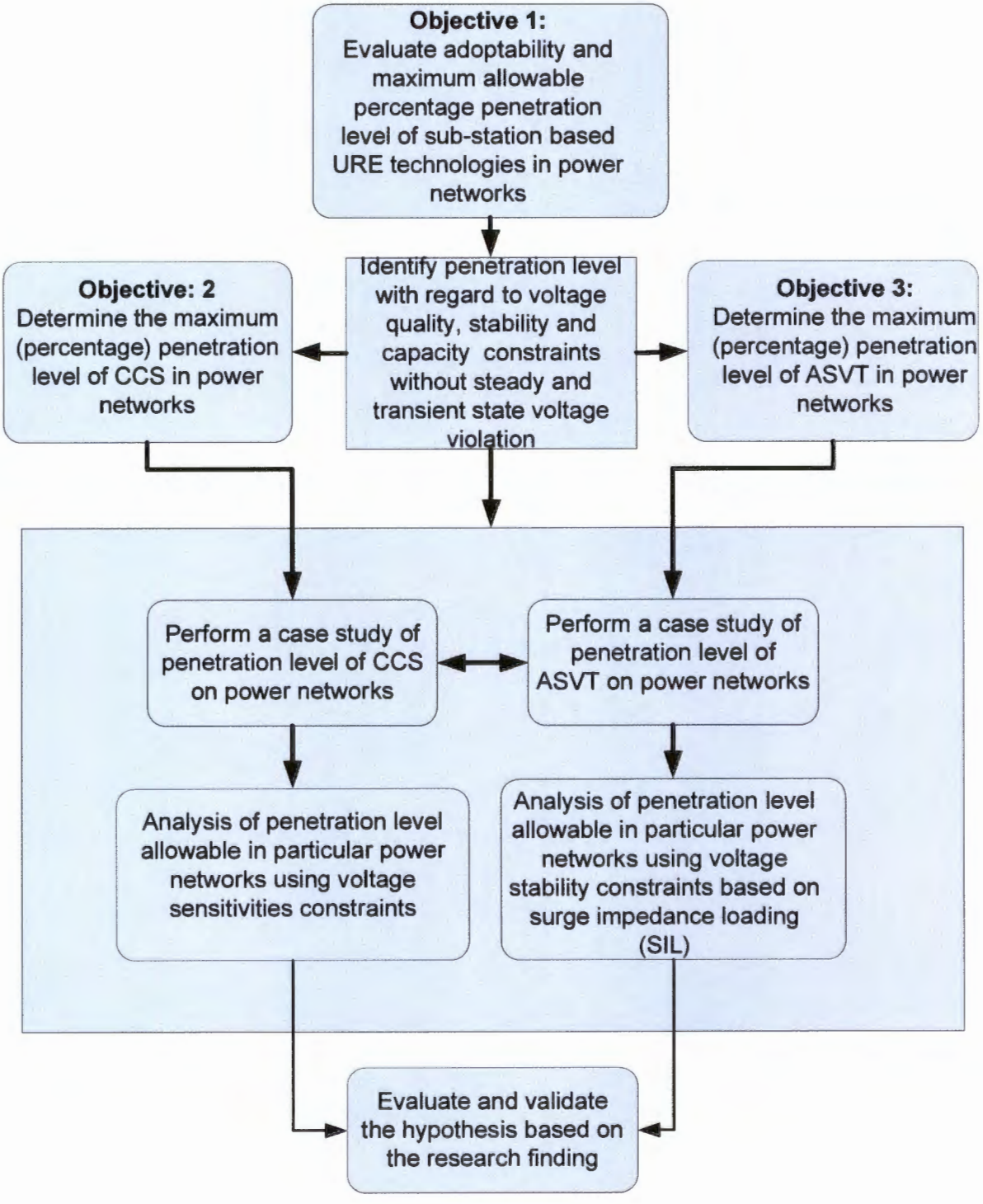

Figure 1.4 Objective of the thesis

1.3 THE CONCEPT OF URE TECHNOLOGIES

This section considers three aspects of URE in developing countries;

- Factors leading to URE technologies
- The URE technology options
- Penetration levels of URE technologies

1.3.1 FACTORS LEADING TO URE TECHNOLOGIES

A World Bank report [2000] recommended, "There is a need to break out from the traditional conventional mould, to review specific needs of rural community, to go back to basic principles, and to develop designs that most cost-effectively address their needs." Surprisingly, these calls have remained largely ignored, especially in SSA. These are evidenced by the common centralized generation with high voltage transmission to regional sub-stations. Consumers are then supplied using lower voltage lines reducing the voltage closer to the customers [Ledwich et al. 2007].

Quite often rural networks are over-designed, since there is a perception that under design carries more risk for organizations than the over-design because the former provide criticism in the future. Therefore, designers of URE based technologies need to take advantage of already existing built-in extra infrastructure capacity, especially where there is an extensive system in place when designing the URE projects.

Most transmission networks in SSA were built more than 50 years ago during the colonial era. These lines on their path from power source to major urban centers typically transverse many un-electrified rural areas. In recent times these areas have developed and their need for electrical energy has actually doubled if not tripled. Consequently, there is dire need to approach rural electrification planning and design from un-conventional perspective. In other words planning following existing developments [Saulo et al. 2010].

In this research project, URE technologies concept are taken to mean "the rural electrification technologies which do not follow traditional methods" for example, three phase distribution system with three or four wires, conventional vertical transmission and distribution approach and conventional bulky transformer sub-stations among others.

1.3.2 THE URE TECHNOLOGY OPTIONS

Table 1.1 shows URE technology options that have been successfully tested and tried in various parts of the world. It is important to note that SWER and SWS are URE line technologies while CCS and ASVT are sub-station based URE technologies.

Table 1.1 Sample URE technology options

URE Technologies	Countries where URE are used
Single Wire Earth Return (SWER) at a variety of voltages.	South Africa, Botswana, South American countries, Australia, New Zealand, Asia, North Africa.
Shield wire scheme (SWS)	Brazil,Ethiopia,Ghana
Auxiliary Service Voltage transformers (ASVTs)	Mexico, Brazil.
Capacitor Coupled Sub-station (CCS)	Brazil, Australia, Botswana, South Africa

Rural networks mostly supply low-density loads typically a significant distance from the conventional distribution substations. There are a range of supply needs ranging from village lighting to intensive support of computerized agriculture and comfort lifestyle. This leads to variety in load density and reliability expectations. For some cases the best solutions are isolated supply systems to individual customers; in other cases local generation for a limited set of customers is used. The common tradition is to use centralized generation with high voltage transmission to a regional sub-station and then supply the load using lower voltage lines reducing the voltage closer to the customer as shown in Figure 1.2 (conventional sub-station).

In this research project, two possible URE sub-station based technologies are considered focusing on their delivery capability. The first preliminary task is to determine the viability of each individual URE technology with regard to cost, reliability capacity constraints and local conditions. Secondly, the maximum penetration level of each URE technology on the power network without steady state voltage violation is determined with regard to voltage quality, stability, and capacity constraints.

There is a variety of tools ranging from linear programming, evolutionary algorithms to multi-criteria decisions analysis (MCDA) techniques that may be used for this work. The choice of tools depends on the data collected from literature and the field data from the prevailing local conditions [Celli et al. 2005].

1.3.3 PENETRATION LEVELS OF URE TECHNOLOGIES

There is a growing need to understand the quantifiable relationship setting up how much URE technology would be 'right' for particular power network. The URE technologies being proposed here have great impact on the transmission and distribution network structure; hence the knowledge of a quantifiable level of penetration is necessary. Most of the URE technologies shown in Table 1.1 are still immature technologies in developing countries especially in SSA.

Maximum penetration level of the URE technologies in power networks is a totally new concept in this research project. This argument is based on the literature survey carried out and the fact that these technologies are still immature in most parts of the world.

Therefore, it is plausible to research the maximum penetration level of URE technology on an existing power network using modified analogies from other similar and proven penetration level optimization techniques. The definition of penetration level of URE technologies according to this research project is "the maximum capacity of URE technologies connected into power networks ensuring the system can operate safely, economically and reliably without steady state voltage violation" [Jinfu et al. 2007].

Penetration level relates to many factors, such as the short circuit currents, stability and reliability. It is a complicated problem to calculate penetration level if all the factors are considered, and the result may not be universal. For example, the existing method of calculating penetration level for distributed generation (DG) mainly considers capacity constraints from one of several aspects. According to Chao Wang et al. (2007), the computation of maximum penetration level is analysed considering tap hunting constraints. The approach to calculate the penetration level based on voltage amplitude limitation is also presented by Morren et al. [2006].

These approaches with some modification are considered in this research bearing in mind, that connecting CCS or ASVT unit(s) to a transmission line changes the voltage profile of the line. The exact penetration limits will depend critically on the in-depth analysis of these two URE sub-station technologies when connected to power networks.

1.4 JUSTIFICATION FOR THE RESEARCH

Rural electrification, a key ingredient in the delivery of modern life's basics like health, education, communication and light, remains largely elusive for most African rural communities. There is no other region in the world with a lower per capita level of electrification than SSA [Ilskog 2008, Haayinka 2008].

Table 1.2 shows the regional electrification aggregates as at 2009. The overall electrification rates in SSA stand at 14.2% with the urban and rural area figures standing at 59.9% and 30.5% respectively. One way of tackling this problem is the use of URE technologies. It is evidence from the table that SSA has the lowest percentage rural and urban electrification access [WEO 2011].

Table 1.2 Electricity access in 2009-regional aggregates (source: weo -2011)

Continents/ sub-continents	Population without electricity in million	% age Electrification rate	% age Urban electrification rate	% age Rural electrification rate
Africa	587	41.8	68.8	25.0
North Africa	2	99.0	99.6	98.4
sub-Saharan Africa	585	30.5	59.9	14.2
Developing Asia	675	81.0	94.0	73.2
China & East Asia	182	90.8	96.4	86.4
South Asia	493	68.5	89.5	59.9
Latin America	31	93.2	98.8	73.6
Middle East	21	89.0	98.5	71.8
Developing countries	1314	74.7	90.6	63.2
World*	1317	80.5	93.7	68.0

* World total includes OECD and Eastern Europe / Eurasia

In 1973, the government of Kenya started the rural electrification program (REP) with the aim of electrifying the whole countryside especially those remote areas that would not automatically attract power utility companies [LCPDP 2009].

The aim was mainly to encourage agro based and small-scale rural enterprises. Unfortunately, the overall performance of this parastatal enterprise was dismal, after 17 years of its existence, REP had electrified only 62,000 households or 2% but with a staggering expenditure of 600million US dollars which translates to just under US $10,000 per household [KPLC 2007b]. Such a huge cost of rural electrification thus justifies research into improving the performance of electrification programs and their operation in SSA.

Consequently, there is a need to re-evaluate URE technologies especially the cost reduction apparently offered by these technologies. Maximum percentage penetration level of each of these available technologies with regard to voltage quality, stability, and capacity constraints needs to be identified to help policy makers and network utility companies in their planning and operation.

1.5 Hypothesis and Research Questions

The hypothesis that this research project tests is whether:

There is a maximum allowable percentage penetration level of sub-station based URE technologies on power networks with regard to steady state voltage quality, stability, and capacity constraints without steady and transient state voltage violation.

The guiding research questions to be explored in testing the validity of the hypothesis include:

- Is there a consistent method of determining the percentage penetration level of URE technologies with regard to steady state voltage quality, stability, and capacity constraints?

- What is the scope of URE technologies to be considered?
- What factors restrict each of the URE technologies highlighted?
- What criteria may be used to compare the two URE sub-station technologies?
- What methods should be used to explore the implication and adaptability of implementing various URE technologies in SSA?
- Is there a consistent and reliable way to analyze the cost, reliability and performance implications of URE with conventional rural electrification technologies?
- What methods/tools/models would be appropriate for this research project?
- Do any environmental factors affect the choice of URE sub-station technologies?

1.6 Novel Element of the Research

The nature of this research project is such that it incorporates several interesting novel aspects, requiring particular careful attention as the analysis develops. The research;

- Provides insight on quantifiable relationship of how much percentage of sub-station based URE technology would be 'right' for particular power networks.
- It provides appropriate mechanisms for improving access to reliable and affordable electricity to the rural consumers in developing countries of SSA.
- The research project investigates a planning model that may be used in optimizing a mix of both URE and conventional RE technologies in power networks.
- The research enhances an understanding of the cost, reliability and performance implications of RE technologies by comparing conventional with URE technologies.
- It provides understanding of the implication, adoptability and maximum penetration level of the URE technologies in the Kenyan power network and by extension for power networks in SSA.

1.7 Structure of the Thesis

The structure of this thesis is determined by the objectives of the research, the relevance to rural electrification programs, and the processes needed to test the hypothesis. The various chapters are described briefly below. To put the work in context, each section of the research is developed coherently.

Chapter 2: Identifies useful contribution from literature on URE sub-station technologies in the context of the research questions. This also considers conditions under which URE projects were implemented, their technical and economic implications.

Chapter 3: Covers the theoretical model development for URE technologies and lay a foundation for the subsequent case studies.

Chapter 4: Presents a case study on penetration level of CCS technologies on power networks.

Chapter 5: Provides analysis of the penetration level of CCS technologies allowable in particular power networks using voltage sensitivities constraints.

Chapter 6: Presents a case study on penetration level of ASVT technologies on power networks.

Chapter 7: Provides analysis of penetration level of ASVTs allowable in particular networks using voltage quality and stability constraints based on Surge Impedance Loading of that particular line.

Chapter 8: Summarizes the findings of the research, evaluates the hypothesis and comments on the implication of the finding.

1.8 ONWARD

Providing an affordable and reliable electricity supply to rural communities is seen by countries round the world as one of the major keys to development. A good quality and stable electricity supply can provide a wide variety of benefits including lighting (allowing evening activities), clean cooking and heating, access to television/radio, telephone (including mobile), improved health (due to example refrigeration), and many small industrial uses.

Often this can be provided by extending the main electricity network to the community. However, for remote rural areas the costs involved can be very high. Therefore, URE technologies are thus very relevant, particularly for countries in SSA, as they have potential to make connection to the electricity network affordable. While such systems are already in use, there penetration level is very low. Hence, if the penetration level of such system in power network increases, what is the effect on power and voltage quality, stability and capacity constraints of the overall system? What are the limiting factors, and how can this limit be determined for any particular rural electrification project. This are some of the major questions that this thesis intend to address progressively. The next chapter reviews the literature on URE technologies in the context of the research questions. The intention is to have insight into the broader application of the "lessons".

2 UN-CONVENTIONAL RURAL ELECTRIFICATION TECHNOLOGIES

2.1 INTRODUCTION

The URE technologies are still un-developed technologies in the African contest and especially in SSA. Even in places like South Africa and Botswana where URE line and sub-station technologies have been tried, the penetration level of these technologies are almost insignificant. Researchers and engineers have argued that these technologies lead to important cost reduction when compared with conventional alternatives [Zomers 2003, Barnes 2007, Anderson and Yanev 2010].

Consequently, there was a dire need to develop appropriate models to investigate these technologies and understand the reason for their paucity especially in rural electrification of SSA despite their claimed benefits. It was reported that many people in rural areas of SSA do not have access to electricity and even electrification of the metropolitan areas and suburbs was incomplete or unreliable [Nasser et al. 2009]. Literature indicated that more than 1.6 billion people, mostly in developing countries, do not have access to electricity and that most of them live in rural areas [Cecelski 2002, Kooijman 2009].

In this chapter the literature survey was directed to:

- Investigating from published literature, technological trends and adoptability of URE technologies identified in chapter 1. This was done with a view of establishing their technical and economic capability in an appropriate context.
- Identify existing methods or possibilities for new approaches to determine the penetration level of these technologies in particular power networks with regard to steady state voltage quality, stability, and capacity constraints.

2.2 URE TECHNOLOGIES

The identified URE technologies, captured in Table 1.1 were listed as follows:

- Single Wire Earth Return (SWER)
- Shielded Wire Schemes (SWSs)
- Capacitor Coupling Sub-stations (CCSs).
- Auxiliary Service Voltage transformers (ASVTs)

As mentioned earlier it is important to note that SWER and SWS are URE line technologies while CCS and ASVT are sub-station based URE technologies.

SWER technology was proposed by Lloyd Mandeno (1888-1973) in New Zealand in 1925 and widely became popular within the country. It later spread to Australia, where they currently have approximately 200,000km of SWER lines, i.e. 20% of the entire network [Nasser and Rattray 2008]. The technology has also found use in many developing countries of the world, such as South Africa, Brazil, Mozambique and Laos among others [Chapman 2001, Nasser and Rattray 2008].

Therefore, against this backdrop SWER technology may now be considered as conventional with regard to this research project. In addition, the Shielded Wire Schemes (SWSs) shown in Figure 2.1 is a modified single phase earth or metallic return system [Iliceto et al. 2005]. This system is mostly strung on the same support as the high voltage lines. SWSs schemes have widely been used in the world and as a result of that, it is also considered as conventional [Iliceto et al. 2004]. In terms of the hypothesis in this study, the penetration of SWS in rural areas is limited to the extent of the HV lines.

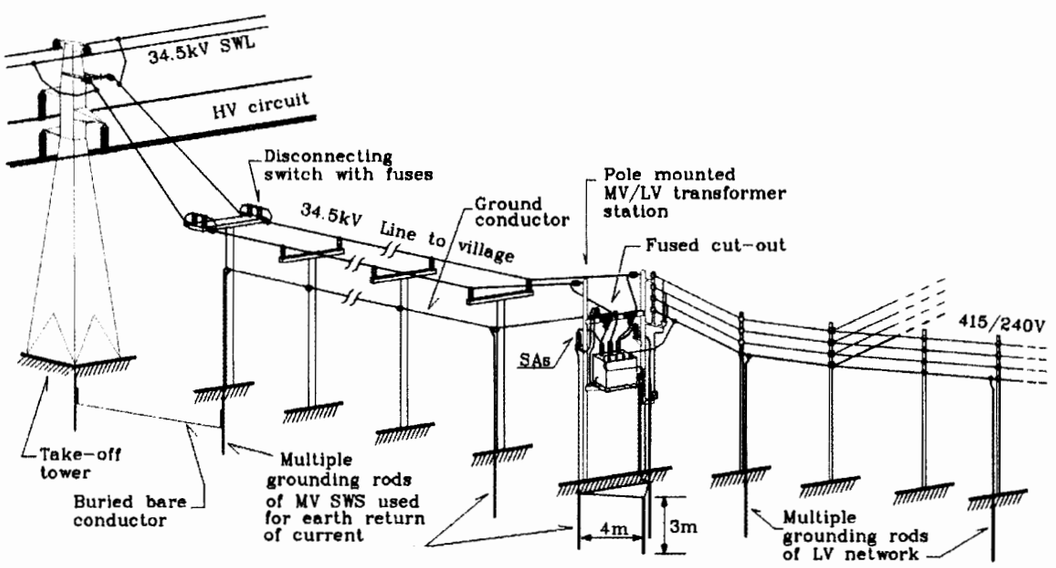

Figure 2.1 Three-phase SWS distribution system [Iliceto et al. 2005].

The literature review therefore focuses on only two URE sub-station technologies namely, capacitor coupled sub-station (CCS) and auxiliary service voltage transformer (ASVT). They both have capability to tap power from high voltage transmission lines.

The scope for rural electrification in this research project was limited to rural areas that are in close proximity (10 km radius) to high voltage transmission lines. The next sections describe fundamentals of each of these two URE sub-station technologies with reference to the research questions posed in Section 1.4 of Chapter 1.

2.3 CAPACITOR COUPLED SUB-STATION (CCS)

The concept of a capacitor voltage transformer (CVT) from which CCS derives its main principle of operation is not new. Most transmission sub-stations use CVTs for metering and protection purposes. The CVT application is usually of limited burden (a few VA) and prone to complex resonant oscillations or Ferro-resonance [Daqing and Roberts 2000].

Figure 2.2 shows the equivalent circuit for CCS. The transformation ratio depends on the required output voltage. This can be obtained using values of the divider parameters (C_1 and C_2), $C_1/ (C_1+ C_2)$. Where C_1 and C_2 are high voltage and low voltage capacitors respectively. V_T is tap-off voltage between the capacitor divider.

This divider has inherent poor voltage regulation due to high capacitive impedance introduced by equivalent capacitance of C_1 and C_2. However this can be corrected by inserting a compensating reactor L in series with the load. The inductance is chosen so that the system operates at resonance for a reasonable variation of the load. The latter can be achieved by using tapped reactor. Tapping mechanism can be manual or automatic.

The selection of the tuning reactor takes into account a number of variables, viz. feeder, transformer, load reactance's and resistance of the reactor. It therefore means that each value has its own range of reasonable operation.

Phenomenon such as Ferro-resonance made it difficult to design CCS in the past. However, development of a passive damper filter by "Hydro-Quebec Company Limited" of Canada has made it possible to design a CCS with a capacity of up to 1.5 – 2 MW [Bolduc et al. 1997].

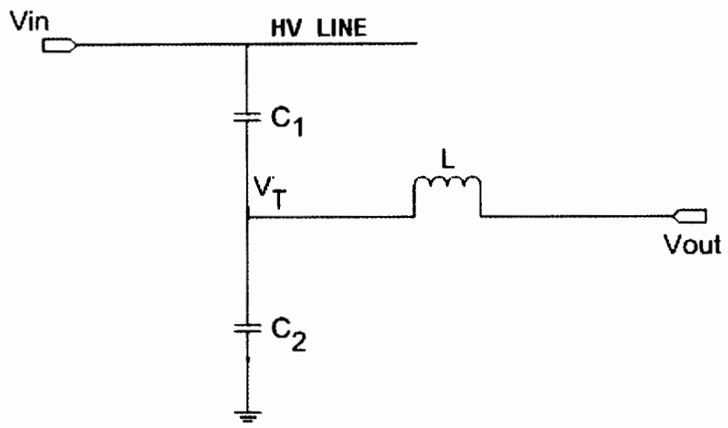

Figure 2.2 CCS equivalent circuit [Bolduc et al. 1997]

The capacitive divider technique (or CCS technology) has been known for quite a while but using this technology to transform high voltage to medium voltage for delivering electric power to remote areas is more recent. With this technique, energy is drawn from electric field of high voltage transmission line by use of discrete capacitors.

This technique leads to important cost reduction when compared with the more conventional electromagnetic coupling systems like the high voltage power transformer. In comparison with the conventional magnetic coupling transformer sub-stations, the CCS has the following benefits:

- It is cheaper, at almost one quarter of the cost of a conventional magnetic coupled transformer sub-station of same size. This is due to low usage of iron, copper as well as insulation since voltage reduction is done by the capacitors [Sarmiento 1990].
- It readily adapts to lines operated at voltages of 100 to 275kV. The modest cost compared to a conventional sub-station makes it an ideal choice for application in rural areas traversed by high voltage lines [Schilder et al. 2005].
- Can be made easily transportable and therefore can access remote areas without major road infrastructure [Anderson and Yanev 2010].
- No need of constructing recuperation pits since the oil content is very small thus not much spillage in case of damage.
- If constructed midway in a transmission network, the capacitive reactance of the sub-station helps in cancelling out some of the inductive reactance thus improving power transfer capability of the existing transmission line [Pasand and Aghazadeh 2003].

- The development of various aspects of damper-filter has made it possible to achieve a stable CCS for rural electrification based on a simple capacitor divider principle. [Bolduc et al. 1997, Ferracci 1998].

However, there are limitations with this kind of technology. Following on-site field tests and laboratory tests on a CCS carried out by Schilder et al. [2005] and Reeves et al. [2011] on different applications of the system, some of the major issues they experienced were;

- The CCS can be energized as well as operated successfully preferably with a resistive load.
- When a CCS was used for supplying a large induction motor (IM), self-excitation occurred, resulting in significant sub-synchronous voltage, current and speed oscillations.
- When a CCS was used to supply Variable Speed Drive (VSD) pump motor and auxiliaries, it was found that at 68% of CCS rating caused severe Sub-Synchronous Resonance (SSR) in the output voltage of the CCS.
- The SSR was observed as flicker at the sub-station during start-up and when the motor was running at approximately 60% of rated speed.
- When used to supply large motors accurate equivalent circuit parameters are required to predict the instabilities experienced in a practical installation.

One of the common issues experienced in the CCS is Ferro-resonance and switching resonance. Therefore, a brief literature of Ferro-resonance in high voltage power system is presented below to put the literature in the right perspective.

2.3.1 FERRO-RESONANCE IN HIGH VOLTAGE POWER SYSTEMS

According to Jacobson and Menzies [2001], the term "Ferro-resonance", which appeared in literature for the first time in 1920, refers to all oscillating phenomena occurring in an electric circuit which must contain at least:

- Non-linear inductance (ferromagnetic and saturables),
- Capacitor,
- Voltage source (generally sinusoidal),
- Low losses.

Ferro-resonance is a special case of disturbance that involves high levels of voltage and current waveform distortion. This phenomenon can severely affect voltage transformers and its consequences can be catastrophic.

Ferro-resonance effect has been a subject of many studies for a long time. It is generally a complex resonance oscillation in a series R-L-C circuit with non-linear inductance. At times much higher voltages at higher frequencies than the system power frequency. These voltages are produced during:

- System switching with or without connected load.
- Short circuit conditions.
- Load rejection conditions.
- Transformer magnetic saturation during switching
- Lightening

Power networks are made up of a large number of saturable inductance power transformers, voltage measurement inductive transformers (VT), shunt reactors, capacitor voltage transformers and series or shunt capacitor banks. Therefore, they present scenarios under which Ferro-resonance can occur.

The main feature of this phenomenon is that more than one stable steady state response is possible for the same set of the network parameters. Transients, lightning over-voltages, energizing or de-energizing transformers or loads, occurrence or removal of faults, may initiate Ferro-resonance. The response can suddenly jump from one normal steady state response (sinusoidal at the same frequency as the source) to another Ferro-resonant steady state response characterized by high over-voltages and harmonic levels which can lead to serious damage to the equipment [Jacobson et al.1999].

A practical example of such behavior is the de-energization of a voltage transformer by the opening of a circuit-breaker. As the transformer is still fed through grading capacitors across the circuit-breaker, this may lead either to zero voltage at the transformer terminals or to permanent highly distorted voltage of amplitude well over normal voltage.

To prevent the consequences of Ferro-resonance which may result to untimely tripping of protection devices, destruction of equipment such as power transformers or voltage transformers and production of losses. It is necessary to understand the phenomenon and know how to predict, identify and a void or eliminate it [Jacobson 2000, Ferracci 1998].

Currently, the term Ferro-resonance is firmly established in the power system engineer's vocabulary and is used not only to describe the jump to a higher current fundamental frequency state but also divergences to sub-harmonic, quasi-periodic and even chaotic oscillations in any circuit containing a nonlinear inductor [Jacobson and Menzies 2001].

However, it appears there is a slight difference between Ferro-resonance and switching resonance. The former being sustained in the circuit for a longer period of time while the latter takes place for a short duration of time during disturbances before the circuit settles down to steady state condition. For designing the desired FSC, the following points should be considered: [Pasand and Aghazadeh 2003].

- When the amplitude of over-voltages is more than a threshold, the firing pulses must be issued to switch-on the damping resistor. For implementation of this point, the voltage amplitude is obtained using a resistive divider circuit. This signal should be compared to the maximum threshold voltage.
- The damping resistor should be switched-off when the load is reconnected to system.
- Power electronic switches go to off mode in negative half cycle of voltage but the damping resistor should be connected continuously to secondary side of the transformer during the whole period of over-voltages

The results of different simulations indicate that the occurrence of Ferro-resonance in this situation depends on conditions such as:

- The residual fluxes circulating in the core of the transformer before its energization,
- The closing instants of the circuit breaker which initiates the energization of system or the initial angle of the input voltage,
- The type of transformer winding connection,
- The switching sequence of system energization such as single phase switching or three phase simultaneous switching.

All notwithstanding, application of CCS technology still displays a better cost effective way of supplying electricity where HV transmission lines traverse rural villages or in close proximity to the rural communities. The main question that arises is "why are these systems not widely spread in developing countries and especially SSA"? [Saulo and Mbogho 2011]. The subsequent sections provide probable solutions to this question with regard to cost, capacity constraints, and reliability.

2.3.2 COST IMPLICATION OF CCS TECHNOLOGY

Electrification of rural areas has progressed at low rates mainly due to high costs associated with extending electricity grids and developing decentralized systems [Barnes 2005]. Rural areas particularly in developing countries are usually characterized by low population densities with scattered clusters of premises usually inhabited by poor communities. Consequently, rural electricity supply systems are characterized by dispersed consumers, low consumption and low load factors. These areas are usually served by long overhead lines that are susceptible to adverse weather conditions resulting in poor quality of supply.

Because of the long distances involved in connecting new customers, the installation costs per customer are usually higher than in urban areas. Due to these backdrops there is lack of interest among electricity supply companies to service such areas since they are not economical viable [Kooijman 2009, Mutale et al. 2007, Ledwich et al. 2007].

One of the major criteria used to supply electricity to a customer is the willingness and ability to pay (WTP). Although most rural customers are willing to pay they are limited by ability [Eberhard 1986]. Numerous alternatives to rural electrification exists e.g. Micro/Pico hydro, Solar, Wind, Diesel generators etc., but all these alternatives have a cost setback [Bekker et al. 2008, Haayinka 2008].

The present grid conventional technology in most of SSA uses centralized generation integrated with high voltage transmission lines to convey power to regional sub-stations. Customers are supplied through lower voltage lines. As the supply is extended to more remote rural regions, cost per connection with conventional three phase technology increase to levels that are unaffordable [Chapman 2001, Bekker et al. 2008]. Achieving savings requires that the capacity of a delivery network be matched to the load in the network planning stages. Therefore, optimum design of URE sub-station technologies consistent with planning approach, safety, reliability and maintenance is necessary, leading to low total or lifetime cost [Gaunt 2003].

2.3.3 CAPACITY CONSTRAINTS OF CCS TECHNOLOGY

As mentioned earlier the CCS borrows from the CVT principle of operation. Consequently, it has the ability to decrease voltage but cannot increase current as opposed to wound electromagnetic transformers [Daqing and Roberts 2000]. Therefore, this poses a serious capacity constraint on the system. Secondly, the system can only reduce voltages and not increase as compared to a conventional transformer. The later limitation can be mitigated by the inclusion of an isolating transformer at the output terminal of CCS. While this is a viable solution it also has challenges of Ferro-resonance when the transformer saturates.

CCS studies done by Hydro-Quebec showed that for a 2MVA load, an equivalent of 8.7 MVAR had to be injected in the transmission line from the CCS sub-station [Bolduc et al. 1997]. This was done to maintain the system at resonance for a reasonable variation of load. The addition of some MVAR is also an extra benefit since it improves the line voltage profile. It reduces system losses by cancellation of some of the reactive current [Jacobson 2000]. Nevertheless, this adds a new dimension to the power system. Greater attention is necessary in considering the economic and technical effects of this capacitive reactance that are constantly in the system

In addition, the location of the CCS in a power network is important, since in certain system operations, the sub-station may find itself at the end of the line. In this case, voltage profile may rise to a higher value more than the maximum designed capacity. This rise of system voltage may cause stress to equipment insulation and accelerate failure [Sarmiento et al. 1990, Bolduc et al. 1997].

Methods of voltage control in energy transmission network are well known. Thus, in order to keep the voltage within the statutory requirements, active and reactive power is dispatched into the system in a controlled manner. Hence, reactive power balance is a concern when using CCS technologies to ensure voltage and power capacity constraints limits are not violated.

The research done by Hydro-Quebec which resulted in the construction and commissioning of Riviera Ste-Anne sub-station was an example of an application of CCS [Bolduc et al. 1997].

The study showed that the technology was adaptable to voltages ranging from 100 kV to 275 kV. This was within the range of many SSA countries transmission line voltages. Therefore, there was a motivation to study the technology with the intention of determining penetration level of this technology in power networks.

In this research project, locations of village(s) were considered carefully for the application of an effective CCS technology. Villages in close proximity to the 220kV overhead transmission lines with capacity of up to 100 household and an estimated power demand of about 100kW (see the average load demand in section 3.4.3 of chapter 3) were taken into consideration. Other important factors considered were;

- The conductor parameters
- Length of longest feeder from the sub-station
- Load distribution
- Amount and direction of reactive power flow.

Thus, capacity constraints of this sub-station technology can be effectively mitigated by ensuring that the system is well designed with provision for reactive power balance.

2.3.4 RELIABILITY OF CCS TECHNOLOGY

This type of URE technology has been met with a number of problems in the past. Ferro-resonance remains a serious threat to proper operation of CCS. This is the oscillation of energy storage between the two energy storage elements present in the circuit, capacitor and reactor.
These oscillations can reach extremely high voltages if not properly addressed. [Gonen. 2008, Raphalalani et al. 2000].

The development of a damper-filter has made it possible to achieve a stable CCS based on the simple principle of a capacitive divider [Bolduc et al. 1997, Pasand and Aghazadeh 2003].

This system does not require a costly power-transformer or circuit breakers. It readily adapts to line operated at voltages of 100 to 275kV as earlier mentioned. Its modest cost compared to a conventional sub-station makes it an ideal choice for application in rural areas traversed by high voltage transmission lines [Schilder et al. 2005].

Tests carried out on the South African; Meru field sub-station and in the laboratory on a CCS system connected to a rural feeder for supply of a pumping station showed that the system worked better with resistive loads as opposed to induction motor loads especially above 40kW [Reeves et al. 2011]. This is because of the electrical interaction between the region of resonant operation of the CCS and the torque characteristic of the motor during starting. This is particularly important given that the rural load power factors can be very low at times for the purposes of starting an induction motor.

Hence, the system reliability is dependent on the type of loads connected. In other words for the system to work effectively then control of the type and size of load on the rural feeders must be evaluated.

2.3.5 VOLTAGE STABILITY OF CCS TECHNOLOGY

Voltage stability refers to the ability of a power system to maintain steady voltages at all buses in the system after being subjected to a disturbance from a given initial operating condition. Voltage stability is a very important aspect of overall power system stability. The voltage stability is analogous to stability of any other physical system [Wadhwa 2010]

Voltage stability aspects cover a very wide range of phenomenon from a slow phenomenon involving the mechanical tap changing to a fast phenomenon involving the induction motors, air conditioning loads or HVDC links [Kundur and Paserba 2004].

Voltage stability or voltage collapse has been seen as a steady state problem involving static power flow studies for analysis. The ability to transfer reactive power from sources to sinks during steady operating conditions is a major aspect of voltage stability. It is, however to be noted, that the network maximum power transfer limit is not necessarily voltage stability limit only but many other factors like the distance of the transmission line must also be considered [Kundur and Paserba 2004].

A CCS system is said to be voltage instable, if for at least one bus in the system, the voltage magnitude decreases as the reactive power injection is increased. Voltage instability results in progressive fall or rise of voltages of some buses. This mostly depends on the amount of reactive power a CCS penetrates in a power network [Pasand and Aghazadeh 2003].

Large scale effect of voltage instability leads to voltage collapse. This is a process by which the sequence of events accompanying voltage instability leads to a blackout or abnormal low voltages in a significant part of the power system. Voltage instability problems are also experienced at terminals of HVDC links connected to weak ac systems [Kothari and Nagrath 2006].

The maximum power transfer problem becomes much more complicated by the presence of synchronous machines in power system. The power transfer for long lines is limited by the magnitude of voltages at the two ends, reactance between the two ends and the sine of the angle between the two voltages [Wadhwa 2010]

The voltage stability, sometimes called load stability, however, is now a major concern in planning and operating electric power system as the power to be transferred is increased, the interconnection of networks is also increased because of obvious advantages and there is need for more intense use of available transmission facilities. More and more electric utilities are facing voltage stability imposed limitations. Voltage instability and collapse have in the past resulted in several major system failures or blackouts. [EPRI TR 1993].

Studies concerning loadability curve including voltage stability constraints by [Hao and Xu 2008] concluded that;

- The voltage quality limit has dominating influence on the loadability of short lines, while the voltage stability limit is the main constraint for long lines.
- Both analytical and numerical results showed that, for the uncompensated line, it was not possible to transfer power without causing voltage stability problem when the line length was over 588km.

- The resistance has remarkable effect on line loadability, especially for low voltage levels. This effect will be decreased as voltage class increases.

- With shunt compensation it becomes possible to transfer power over long distance without violating the voltage stability or voltage quality limits.

2.3.6 VOLTAGE QUALITY OF CCS TECHNOLOGY

Conventionally, power is known to flow from the transmission network to the distribution network. There are different problems that may arise while power flows from utility side network to load side network. However, major issues related with flow of power in the distribution network that determines voltage quality can be categorized as [Wadhwa 2010];

- Voltage drop.
- Power loss.
- Power quality.

Voltage drop in the distribution circuits during peak loads and voltage rise during low loads is the main determinant of voltage quality for both a CCS technology and a conventional transformer. The total voltage drop in the secondary circuit of distribution system is highest at the remote end [Liu and Bebic 2008].

To minimize the secondary circuit length, distribution engineers locate distribution transformers close to the load centers and try to have the secondary service drops to the individual customers as close as possible. The reasons behind high voltage drop include [Kothari and Nagrath 2006];

- Lower distribution system voltage levels – Larger conductors have lower voltage drop and lower power losses, but they cost more, so there is a trade-off between savings due to lowered losses and increased costs of the conductors. Utilities commonly have design guidelines that are based on underlying economic considerations. Practicality of carrying varying sizes of conductors in stock and other considerations such as feeder pick up from an adjacent sub-station for increased reliability is necessary
- Poor power factor causes power system losses which may lead to voltage drops. Excessive voltage drops can cause overheating and premature failures on motors and other inductive equipment.
- Single-phase circuits due to insufficiently sized wiring or of other faults within the wiring system, such as high resistance connections.

- Unbalanced circuits - A three-phase power system is called balanced or symmetrical if the three-phase voltages and currents have the same amplitude and are phase shifted by 120^{o} with respect to each other. If either or both of these conditions are not met, the system is called unbalanced or asymmetrical.

The transformers with bulk power delivery may have load tap changers (LTC) or there may be a voltage regulator in series with the transformer on the Secondary (LTC) side. For voltage stability the impedance of transformer is important. Leakage impedance of power delivery transformer varies between 8 and 11% on its base. Impedances of distribution transformers normally range between 2 to 4%. The bulk power delivery transformers represent a major portion of the distribution system impedance [Kothari and Nagrath 2006].

2.4 AUXILIARY SERVICE VOLTAGE TRANSFORMERS (ASVTS)

The ASVT or sometimes known as a station service voltage transformer (SSVT) is insulated in SF6 gas and combines the characteristics of an instrument voltage transformer with power distribution capability [Gomez et al. 2010].

The transformer has power capability of up to about 50kVA to 1MVA for both single and three phase supply. Note that, 1MVA is approximately equivalent to 3x330kVA for single phase units. In this transformer the high voltage side is connected directly to the overhead transmission lines. While, typical secondary voltage ratings are 115V, 230V, 240V, 277V, 480V, and 600 volts.

Other voltage level supplies can be designed on order. The system was originally designed to suit supply for auxiliary services within the sub-station such as lighting loads, motor loads and instrumentation purposes [Arteche manuals 2010, Saulo et al. 2012a].

In developing countries where transmission line infrastructure is already in place but a wide-spread distribution infrastructure is lacking, the un-conventional ASVT sub-station technologies can be used as a compact transformer to greatly reduce the electrification costs for small villages or compounds. The ASVT can either be used with its low voltage output to directly supply needed power for in-close loads near the transmission right of way, or simply step up the ASVT low voltage output through distribution transformers for a local distribution network. Small sub-stations can be sited specific to the load requirements without a large distribution network. Tapping the high voltage transmission line and connecting an ASVT with a small footprint sub-station will provide affordable, readily-available electricity to many rural dwellers in close proximity to high voltage lines and presently without power [Gomez et al. 2010, Barnes 2007].

A pilot project was successfully carried out in the rural town of Tubares in Mexico, where ASVTs were used to supply the villagers. The ASVT tapped power from a line of 123kV and transformed it to 230V for distribution purposes. It was reported that a good return on investment was achieved, though not the major objective of the project.

The project brought great developments in the area and has encouraged other rural electrification projects in the region to use the same technology. According to Gomez et al. [2010], the system involves very simple station engineering and presents a successful and economically viable alternative, for electrification of rural communities with load requirements up to 330kVA single phase to 1MVA at three phase arrangement, supplying enough power for applications like refrigeration, water pumping, lighting and other low voltage applications. The use of ASVTs for RE provides the following benefits [Gomez et al. 2010];

- Very high reliable power potential (the number of interruptions in a transmission line are minimum compared with the interruptions usually experienced in a conventional distribution line).
- Solution cost is three times lower than a traditional sub-station. This makes it economically viable for the electrification of rural areas that otherwise would not have opportunity to have the electric service.
- The ASVT is used in a dual function, as a source of power and as an instrument transformer in a single unit, being also used for metering and relaying application.

The main limitation of the system is capacity constraint. Additionally, since the main voltage transforming device of the ASVT is used as a dual function, the failure of one function may lead to the failure of the rest of the system, resulting in power failure to the consumers. Standardization is another barrier with this type of technology. This system has very minimum literature available and this creates curiosity or motivation for investigation.

2.5 COMPARISON BETWEEN ASVT AND CONVENTIONAL DISTRIBUTION TRANSFORMERS

ASVT are designed to transform voltage from the high values in the transmission and distribution system to the low value in one step that can be utilized by low voltage devices. Its applications include: metering for energy billing and transaction purposes; protection control for system protection and protective relaying purposes; load survey for economic management of industrial load. On the other hand, distribution transformers are used to transform a relatively lower voltage to a low voltage suitable for distribution to low power users [ABB 2000]

Industry recommendations are that the insulation class of ASVT should be at least equal to the maximum line to line voltage existing on the system at the point of connection. This is because under fault conditions these units could be subjected to line to line voltage. The system has the ability to handle extra high voltage in one step down to low voltage.

This is not the case with conventional distribution transformers which utilizes a series of step down transformers before finally supplying the low load consumers [ABB 2006]. The dielectric material used must have an excellent insulation; due to the high pressures and temperatures in voltage transformers. Cycloaliphatic Epoxies was used in the 1970's due to its very good resistance to humidity ultra violet radiation; outdoor pollution and chemicals. It has an outstanding mechanical strength and dielectric properties [IEG 1993]

Incorporated inductive voltage transformer insulation and magnetic performance readily accommodates high momentarily and maximum continuous operation voltage to distribution transformers. Fully rated impulse levels provide improved ability to withstand high transients' currents. Reliable transmission voltage access for sub-station power; provides very reliable control power access available directly from the transmission lines. It eliminates the need to bring in the outside distribution voltage and it is not typically subject to line outages [ABB 2000]

In sub-station where the power transformers do not have the tertiary windings, controlled power must be supplied by an alternative means. ASVT can be mounted on the bus as well as a bus potential transformer with measuring winding and a controlled power source which makes it carryout a dual function [ABB 2000].

Low profile, compact overall size and weight relative to distribution transformer; makes the ASVT not to require expensive pad; simply a support stand and small foundation. Hence, it has minimal sub-station foot print. In other words, it is a pad mounted type transformer which allows the connection directly either to a high voltage line or bar, and directly transforms energy from voltages up to 230kV down to 600V or less in one step. The high thermal rating of this device makes it able to accommodate from 50kVA up to 330kVA per phase despite its physical size compared to the conventional power transformer of the same rating. Usually, the power transformer thermal rating is governed by [Susa 2005];

- Design limits (e.g. 110 °C hot spot) not necessarily operational limit.
- Transformer winding and oil temperature
- Conservative hot spot temperature.
- Continuous load at rated current

Figure 2.3 and 2.4 shows pictorial views of the sub-station power transformer and ASVT respectively.

Figure 2.3 Conventional power transformer [ABB 2000]

Figure 2.4 Auxiliary Service Voltage Transformer (ASVT) [Gomez et al 2010]

2.6 WHY URE TECHNOLOGIES

For many decades, distribution transformers have been used for distributing low voltage power to both domestic and commercial users. To get this low voltage power, several stepdown transformer have to be incoporated in the process.

In Kenyan rural electrification planning model, the power obtained from this distribution transformer is limited to serve custmers who are within radius of 600m from the transformer [KPLC 2007a , LCPDP 2009]. The installation cost is usually sub-divided among this customers. The installation cost of a single phase supply for those customers within the 600m radius of the low distribution transformer is between US$ 450 and US$ 600 for three phase, while those outside this radius the cost is almost 300 times that of those within the radius [KPLC 2007a].

This cost has discouraged rural communities from enjoying the benefits of electricity. Thus the conventional distribution system have not been favourable in rural areas where the communities are sparsely populated [LCPDP 2009]. Technological evolution has introduced other types of rural electrification technologies that require consideration. The un-conventional CCS and ASVT, which have ability to step down high voltage from 220 kV to 240 V in one step have been analysed in this research project [Saulo et al. 2012a].

Many rural areas in SSA and especially in Kenya are marginalized. Though most African governments have put in place RE programs, the impact is still minimal [DFID 2007, REA 2007]. Most government budgets are limited; hence their priorities are channeled to other sectors of poverty alleviation, health, agriculture and water. Therefore, RE becomes a secondary priority to most governments with very small budget allocation [Invernizzi et al. 2007, Iskog 2008].

Additionally, most power utility evaluates the return on investment (ROI) before they embark on any RE projects. Therefore, for any such project to attract the utility it must be cost effective or must yield good returns. Unfortunately, most RE projects are non-attractive because of many factors mentioned earlier in chapter one [Kooijman 2009]. Hydro-power generating stations which form a large percentage of most countries power sources in SSA, are located in rural areas along the river sources. The transmission lines integrated to these stations transverse a large un-electrified part of rural areas on their way to the load centers mostly located in urban areas. These rural populations are left without electricity since the transmission lines carry very high voltage which must be stepped down in steps by use of conventional distribution transformer sub-station [Anderson and Yanev 2010, Saulo et al. 2012b].

Consequently, careful and empirical analysis of URE system design and implementation practices could have great potential for significant cost savings, which can improve affordable access of

electricity to the rural consumers, contributing to sustainability of the electricity services in these rural areas [Kooijman 2009]. It is also worth noting that URE technologies for the electrification of rural and slum areas are not yet mature but still evolving. It also comprises more than technology [Kaijuka 2007, Kooijman 2009].

Important observations from literature include that electrification of these areas needs a multi-disciplinary approach, and that decision makers need appropriate information, structures and tools as a basis for consistent and appropriate decision-making [Kersting 2002, Bekker 2008]. The URE methods of tapping power from high voltage transmission lines for direct low voltage distribution is a concept that has been analyzed in-depth in this research project due to the claimed advantages.

2.7 URE System Modeling and Analysis

In recent years computer programmes have become available so that the transmission and distribution engineers and planners can develop a feel for how the transmission and distribution system is operating. With tools, power flow studies can be run to present loading conditions and to help with the long range planning of new facilities [Saulo and Mbogho 2012].

The tools also provide an opportunity for the engineer to do such things as optimize capacitor placement in order to minimize losses. Different switching scenarios for normal and emergency conditions can also be simulated. Short-circuit studies can be carried out to generate necessary data for the development of a reliable coordinated protection plan for fuses, reclosers, and relay circuit breakers [Kersting 2001, Neimane 2001].

In short, the distribution engineer now has the required tools. The main problem now is that the data required for distribution modeling are more extensive. In fact, some of the data may not be readily available. This leads to the use of approximate methods of modeling and analysis. In these methods it is normally assumed that all loads are balanced three phase, and all segments will be three-phase and perfectly transposed. With these assumptions, a single line-to-neutral equivalent circuit for the feeder may be used [Kersting 2001, Loveday and Turner 2004].

It is evident that both sub-station based un-conventional technologies discussed in the foregoing sections have their own modeling techniques using different tools. The normal approach to most distribution system designs is by:

- Mathematical modeling
- Iterative design methods
- Simulations.

There is a growing need for understanding the quantifiable relationship of how much URE technology would be 'right' for a particular power network. Penetration level techniques of URE are ill researched and no tangible work so far has been carried out in these areas.

Therefore, the feasible measure is to research on the maximum penetration level of URE technologies on an existing power network, using modified well developed techniques for penetration level analysis [Saulo et al. 2012b].

This may be possible since the problem of optimal siting, sizing and penetration level of systems with DG have been well investigated by a number of works [Celli et al 2005, Gozel et al. 2009, Aryes et al. 2010].

In some works the problem has been approached by using metaheurastic-based methods or other non-classical methods which demand the solutions of several power flows. In other works, AC optimal power flow; or other classical techniques; have also been successfully applied to analyze the problem.

The penetration level of CCS and ASVT technologies may also be analogized from different relevant perspectives, with common constraints imposed on them. This kind of treatment requires rigorous testing as will be seen in the successive chapters.

2.8 URE TECHNOLOGY PLANNING.

In SSA most urban centres have electricity access, but rural coverage is uneven and inadequate. In such cases, there are several alternative frameworks to guide planning. These include [Munasinghe 1988, Zomers 2001];

- ***Integrated rural development*** - Electricity is treated as a component of infrastructure development, area coverage (quickly reach as many customers in a particular area as possible).
- ***Grid extension*** - Prioritize households close to the grid.
- ***Isolated generation***- Evaluate local generation sources in remote regions
- ***Intensification*** - focus on adding connections in electrified areas

Regardless of which approach is chosen, the first step is to understand where people live and how best to reach them given existing infrastructure; this suggests distribution planning as the natural starting point for a national analysis [Saulo and Gaunt 2010].

Geographic Information Systems (GIS), a powerful tool for analyzing information on where and how people live, can be used to improve people's access to services and markets. For this reason, GIS systems are being employed in development planning in SSA in a range of sectors, including electricity-planning efforts.

A certain Ugandan study, for example, mapped energy demand centers and developed a ranking system to prioritize locations based on the number of households and institutions [Kaijuka 2007].

This research may need to use both maps to visualize the distribution of households, institutions and prim algorithm to develop network topology, into the planning model. Therefore, it distinguishes the approach from planning efforts that use GIS solely as an organizational or visualization tool [Munasinghe 1988]. Efforts to further develop grid electricity infrastructure in SSA face a range of financial, technical and institutional challenges including lack of access to capital, poor coordination across sectors and institutions, and high levels of poverty resulting in low ability to pay for services [Cecelski 2002, Haanyika, 2008]. Moreover, electrification by itself has not always lived up to the touted development benefits [World Bank 2000, Mainali and Silveria 2010].

Addressing these issues is mostly beyond the scope of this research project. Instead, we investigate the most cost-effective way to reach the target population regardless of projected impacts on development. As mentioned earlier a multi-displinary approach may be used to address target groups of electricity consumers in rural areas. Some accommodation for ability to pay is made by adjusting electricity demand levels based on poverty data and utility company estimates, but this is done exogenously and does not factor into the definition of cost-effective. One sure thing that motivates this work is that the un-conventional approach to RE technology has a high capability of cost reduction when integrated in RE planning [Saulo et al. 2011].

2.9 THE SCOPE FOR URE TECHNOLOGIES

There are envisaged development plans in SSA countries and especially in Kenya for RE programmes [REA 2007]. The scope of this research is based on two options of URE sub-station based technologies discussed in the foregoing sections that are the CCS and ASVTs. These two URE technologies offer an opportunity to carry out some good fundamental research in these areas.

A new outlook is required on these two URE sub-station based technologies with regard to their adaptability and penetration level in power networks especially in SSA. In other words, rural distribution network planning requires a new approach [World Bank 2000].

Consequently, system study applying extensive modeling and simulation is necessary for better understanding of the sub-station based URE technologies and their suitability in different situations and circumstances. This should be done in order to maximize the predicted benefit of these technologies to the rural consumers and overall power system reliability [Saulo et al. 2011]

2.10 LOCAL CONDITIONS SUITABLE FOR URE TECHNOLOGIES

Each RE technology in SSA was developed concurrently with the prevailing local conditions. Demand for electricity in rural areas in SSA has traditionally been met by extending the electricity distribution network out from the cities and towns (load centers) that were the first areas to be electrified. As the years have passed and with the lower consumer density in the new rural areas being served, the cost of bringing power to each new consumer has increased. At the same time, these new consumers have less disposable income and purchase less electricity [Mainali and Silveria 2010].

In light of increasing construction costs per consumer, low revenues, logistical difficulties and associated costs encountered in managing rural systems, most electricity utility companies in SSA have found it increasingly difficult to meet demand for electricity in rural areas.

According to Kirubi [2006] and Bekker et al [2008], if the cost of photovoltaic (PV) modules drops as envisaged by the world economic forum of 2005, then interest will be focused on harnessing PV technology for rural electrification (RE). This can be done using centralized PV battery charging stations or PV hybrid systems managed by an entrepreneur, the local community, or the government [Bekker et al. 2008].

Individually-owned PV solar home systems (SHS) have proved more popular in some SSA rural homes. A niche market exists for this technology, but drawbacks still remain, including the following:

- Both capital and recurring costs are and will remain high for some time to come;
- Any subsidies to reduce cost tend to benefit the wealthier segment of the population that can more easily afford these systems; and
- The small quantity of electricity generated is limited to basic lighting and entertainment.

Therefore, such a large per-household investment, contributes very little to the economic development of rural areas or to amenities and services for the general population. Other alternatives exist, each with advantages and disadvantages.

Small hydropower plants can produce power at low cost but need a high capacity factor to be able to capitalize on their low cost. This is often difficult to achieve in rural areas where most of the load is residential and where no grid exists to absorb excess generating capacity. Furthermore, during the dry season, stream flows may be inadequate to generate sufficiently to meet demand.

Diesel plants are generally a low-cost option; however, in remote areas access to fuel year-around may be difficult and costs high, coupled with the fact that most rural roads in SSA are in very poor state. Sufficient mechanical skills must also be available to maintain the equipment in proper operating condition. Therefore, no single "best" option stands out for supplying affordable electricity to rural areas. Consequently, for each local condition, the appropriateness of each RE option should be assessed with regards to the prevailing environmental factors, proportionate technology and available geographical features.

2.11 RESEARCH QUESTION ANSWERED

This chapter has provided preliminary answers to some of the research questions posed in first chapter as follows:

- **Is there a consistent method of determining the percentage penetration level of URE technologies with regard to steady state voltage quality, stability, and capacity constraints?**

There is a growing need for understanding the quantifiable relationship between setting up and how much URE technology would be 'right' for a particular power network. The definition of penetration level of URE technologies according to this research: is the maximum capacity of URE technologies connected into the network ensuring the system can operate safely, economically and reliably [Jinfu et al. 2006]. Penetration level relates to many factors, such as the short circuit currents, stability and reliability. It will be a complicated problem to calculate penetration level if all the factors are considered, and the result may not be universal. The existing methods of calculating penetration level for DG mainly consider the capacity constraints from one or several aspects.

The approach to calculate the penetration level based on voltage amplitude limitation is presented in by Chao et al [2007] and Ayres et al [2010]. These approaches, with some relevant modification may be considered in this research bearing in mind, that connecting capacitors in the form of CCS to a transmission line affects the system voltage profile. The exact penetration limits will depend critically on the steady state voltage quality, stability and capacity constraints.

Additionally, the inclusion of ASVT on a transmission line affects the voltage quality and stability. Therefore, penetration level of CCS and ASVT technologies may be analogized from different relevant perspective, with common constraints imposed on them. This kind of treatment requires rigorous testing as will be seen in the succeeding chapters.

- **What factors restricts the use of each URE technologies highlighted?**

The URE technologies discussed in this chapter have their own limitations as described in section 2.2.The CCS and ASVT with appropriate modification seem to be able circumvent most of their limitations. The un-conventional system issues like standardization and staff training are not beyond reach and proper mitigation strategies can be put in place during the planning stages.

- **Is there a consistent and reliable way to analyze the cost, reliability and capacity constraints implications of un-conventional and conventional rural electrification technology(s)?**

The technology for the electrification of rural and slum areas are not yet mature but still evolving. It also comprises more than technology. Important observations from literature are that electrification of these areas needs a multi-disciplinary approach, and that decision makers need appropriate information, structures and tools as a basis for consistent and appropriate decision-making. The most suitable method of electricity provision (technological or institutional model) will usually depend on the combination of the geographic context, the consumer need, and the possibilities that are available and affordable to provide the energy requirements. Therefore, the most appropriate solutions in one place might be quite unsuitable in another.

- **What methods/tools would be appropriate for this task?**

It is evident that both the URE technologies have their own modeling techniques using different tools. The normal approach to most distribution system designs is by:

- Mathematical modeling
- Iterative design methods
- Simulations.

This question may be concluded by stating that there is no fixed methodology or set of tools for any given research activity. The choices of methodology or tools are determined by the depth of hypothesis and research questions one wishes to answer to validate it. However, it should be noted that the methodology choice made will most likely constrain the questions one can ask and conversely certain research questions can best be addressed using certain methodologies.

2.12 ONWARD

The literature has reviewed URE technologies with regard to technological trends and adoptability of the two sub-station based URE technologies. Largely, application of URE technologies still displays a better cost effective way of supplying electricity where HV transmission lines traverse rural villages or in close proximity to the rural communities. The main question that arises is "why are these systems not widely spread in developing countries and especially SSA"? Consequently, there is a dire need to develop appropriate models to investigate these technologies and understand the reason for their paucity especially in rural electrification of SSA despite their claimed benefits. Existing methods or possibilities for new approaches to determine the penetration level of these technologies in particular power networks with regard to steady state voltage quality, stability, capacity constraints and local conditions need to be investigated.

It is evident that URE technologies require a new outlook with regard to their adaptability and penetration level in power transmission networks. RE planning requires new approaches that are able to integrate the innovative URE technologies in transmission and distribution power networks so as to reap maximum benefit from these technologies. The next chapter describes "theoretical model development" that forms the foundation for case studies that finally leads to analysis of practical issues.

3 THEORETICAL MODEL DEVELOPMENT

3.1 INTRODUCTION

Theoretical model development for URE technologies is a very important foundation for subsequent case studies. It guides in studying the behavior of power transmission networks at steady and transient state conditions when integrated to CCS / ASVT. The model developed should describe the component of the system as accurately as possible if the results are to produce the correct practical situation. The developed models are then analyzed in a computer software environment as will be shown in the succeeding chapters. The following data are therefore necessary for modeling of the systems;

- The distances at which the CCS or ASVT can be installed relative to the sending and receiving end voltage.
- Line capacity.
- Conductor type and size.
- Transmission line parameters (Inductance, charging capacitance, and resistance of conductor).
- Line transformers and generators data
- Active and reactive power flow on the power transmission line
- Surge impedance loading (SIL) of the line.

The complete data of a 220kV, 440 km (Kiambere-Rabai) transmission line in Kenya were used for case studies and are provided in appendix A and B. This chapter describes the theoretical model development for both the CCS and ASVT systems. This forms the foundation for case studies in chapter 4 and 6, which finally leads to measurement and analysis of maximum penetration levels of the two systems in power transmission network in chapter 5 and 7.

3.2 MODELING OF THE TRANSMISSION LINE

Traditionally, transmission lines may be modeled under two possible scenarios i.e. steady and transient state. For transient analysis, a power line may be represented as a matrix of differential equations, while for steady-state; a set of hyperbolic equations or regular models may be used [Glover and Sarma 1987, Mrimal 1992].

In order to achieve a model that is representative of the CCS / ASVT with their associated switch gear, analyses of mathematical equations are applied. The approach taken here is first to model different system parameters separately then integrate them to the respective power transmission line. This is done based on the available data (See appendix A and B). In a transmission line, voltage and current are time and position dependent. [Mrimal 1992, Arthur and Vijay 2000, Kersting 2001]. Therefore, for a long line continuous parameters;

We can say;

$$V_S = V_R \cosh yl + I_R Z_C \sinh yl \quad (3.1)$$

$$I_S = I_R \cosh yl + V_R / Z_C \sinh yl \quad (3.2)$$

Where V_S and I_S are source or sending voltage and current respectively and V_R and I_R are received voltage and current respectively. These equations can be re-arranged to solve for received voltage and current given source voltage and current as shown in equation (3.3) and (3.4):

$$V_R = V_S \cosh yl - I_S Z_C \sinh yl \quad (3.3)$$

$$I_R = I_S \cosh yl + V_S / Z_C \sinh yl \quad (3.4)$$

These are equations used for solving problems for continuous long transmission lines. Since the project entails tapping line to neutral voltage, the line voltage shall be divided by a factor of $\sqrt{3}$ to obtain the phase voltage value.

It is well known that the line constants (resistance, inductance, capacitance and conductance) of a transmission line are uniformly distributed over the entire length of the line. So far it has been assumed that the line has lumped constants and the line calculations made with such assumptions gave results with reasonable accuracy for medium lines. If such an assumption of lumped line constants is applied to long transmission lines (>200km), serious errors are introduced in the line performance calculation.

Therefore, the performance calculations of long transmission lines are made with line constants uniformly distributed over the entire length of the line so that the results with fair degree of accuracy are obtained. Rigorous mathematical treatment is required for the solution of such transmission lines.

However, in this thesis the analysis of the long transmission lines are carried out in a computer software environment. Hence, the lumped parameter equivalent circuit of pi (π) or tee (T) models are used. For this project the pi model is used, because of its easier adoption to the system formation of an actual long line [Mrimal 1991]. Figure 3.1 illustrated the line parameters.

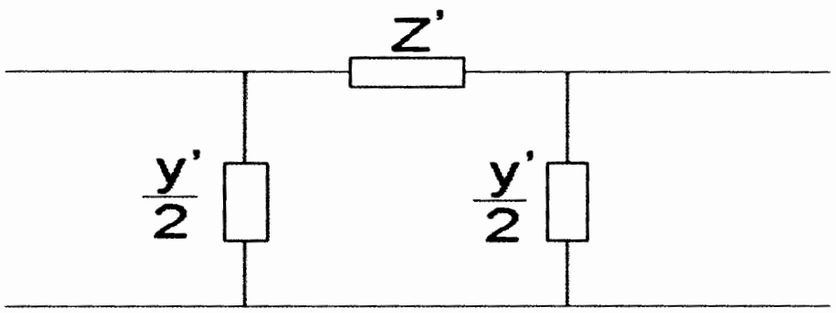

Figure 3.1 Equivalent Circuit of a Transmission Line

To derive the model shown in Figure 3.1, the line is considered on a differential per section basis.

By solving the system Z' can be defined; $Z' = Z\frac{Sinh(\gamma l)}{\gamma l}$, where $\gamma l = \sqrt{yz}l$ and $\frac{y'}{2} = \frac{y}{2}\frac{\tan \gamma l/2}{\gamma l/2}$

Due to the complexity of the model, manual calculation can prove tedious and time wasting. A graphical icon based program under MATLAB Sim Power Systems is used instead; this icon based simulation has been proved to be accurate [Mrimal 1991, Kothari and Nagrath 2006]. The pi section line block model implements per phase transmission line with parameters lumped in pi sections. For a transmission line, the resistance, inductance, and capacitance are uniformly distributed along the line. An approximate model of the distributed parameter line is obtained by cascading several identical pi sections to limit the loss of accurancy in the pi model, as shown in Figure 3.2.

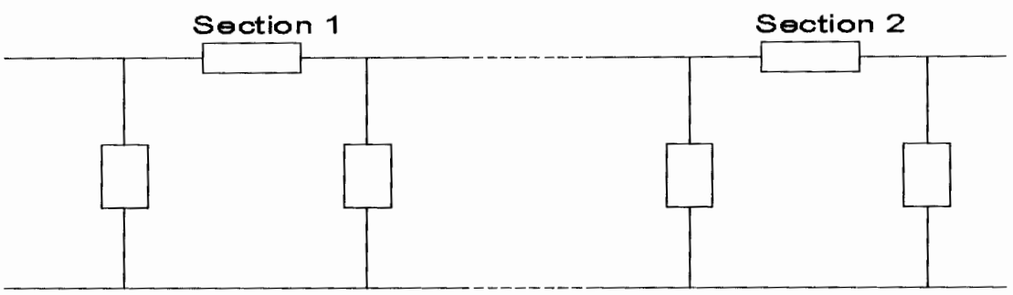

Figure 3.2 Sections of the pi model

The pi section linear model has a finite number of states that permit linear state-space model computation. The number of sections used depends on the frequency range to be represented. A good approximation of the maximum frequency range represented by the pi line model is given by the following equation [Sim Power Systems 1997];

$$f_{max} = \frac{Nv}{8l} \tag{3.5}$$

Where: N - Number of sections

v: Propagation speed in km/s $= \frac{1}{\sqrt{LC}}$, L in H/km, C in F/km

l: Line length in km.

For this research project the 440 km long Kiambere – Rabai line in Kenya is being used for case studies (see appendix A and B). Therefore, a section has a length of 110km which translates to a frequency limitation of 340Hz. However the total line is represented by approximately 4 pi sections, which converts to 1.36 kHz frequency limit. It is important to note that each configuration of pi section has a different line length in kilometers. Therefore, different frequency limitations are expected for different configuration. Consequently, the case studies in chapter 4 and 6 are limited to these frequencies.

3.3 Modeling of Capacitor Coupled Sub-station (CCS)

The un-conventional CCS has been known for quite a while, but using this technology to transform high voltage (HV) to medium voltage (MV) for delivering power is still a new concept in developing countries, especially in SSA [Bolduc et al. 1997, Schilder et al. 2005].

Figure 3-3 represents a CCS line diagram. If the CCS technique is used as a sub-station for feeding remote loads or for rural electrification, it normally includes an isolating transformer (Tx) as a passive circuit installed on the outgoing feeders. It is conceivable that these transformer cores get saturated in some transient cases and interaction of their saturated core with the capacitive divider may result in Ferro-resonance [Pasand and Aghazadeh 2003]. From the figure, an inductor L is added to the capacitive voltage divider C_1 and C_2 to cancel the Thévenin impedance $C_{th} = C_1 + C_2$ at 50Hz (see the equivalent circuit in figure 3.4). The regulation is done by adjusting C_1, C2 and L so that they satisfy $LC\omega^2 = 1$, where $\omega = 2\pi 50$.

The FSC block in the figure represents the Ferro-resonance suppression circuit. This circuit is important since Ferro-resonance and over voltage transients problems can occur in these sub-stations during different conditions. The FSC comprises a capacitor C_3, an inductor L_1 connected in parallel and a damping resistor R connected in series as shown in Figure 3.3. Values of capacitor C_3 and inductance L_1 are calculated as $[2\pi f]^2 L C = 1$, where f is frequency of power signal. The value of R is calculated so that; $3\sqrt{L/C} < R < \left(\frac{2}{3}\right)\sqrt{\frac{L}{C}}$ whereby dampening of resonance is obtained.

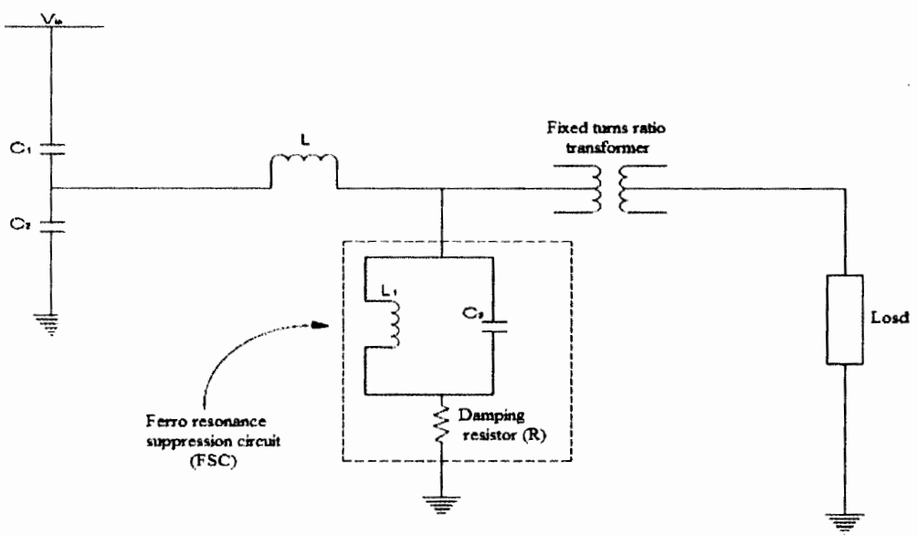

Figure 3.3 Capacitor Coupled Sub-station schematic diagram [Pasand and Aghazadeh 2003]

If a voltage is applied to the primary winding of a conventional distribution transformer, the secondary voltage increases proportionately to the primary voltage. As the primary voltage increases the secondary voltage continues to increase up to a point of discontinuity, or secondary resonance, where an abrupt increase, in secondary voltage occurs. The resonance effect immediately increases the secondary flux density and causes saturation of that portion of the core [Bolduc et al. 1997, Pasand and Aghazadeh 2003].

The saturation effects are characterized by high sustained over-voltages and over-currents with maintained levels of current and voltage waveform distortion, producing extremely dangerous consequences. Depending on the application, high speed suppression of the transient Ferro-resonant oscillations may be needed, which requires a more sophisticated Ferro-resonance suppression circuit (FSC) as explained in section 2.3 of chapter two.

Active and passive Ferro-resonance suppression circuits (FSCs) are normally proposed to damp Ferro-resonance oscillations as already explained. The impact of Ferro-resonance may vary from relay or control mis-operation to catastrophic equipment failure. The awareness of the various situations in which Ferro-resonance oscillations may occur, allows appropriate mitigation strategies to be designed before equipment's are put into service and problems develop [Bolduc et al.1997, Jacobson 2000]. Different methods exist for analysing of Ferro-resonance oscillations [Araujo et al. 1993, Chakravarthy 1995].

One useful way of evaluating the risk is to calculate the natural frequency with saturated and non-saturated transformer cores. The range of frequencies between which Ferro-resonance phenomenon may occur is given by the expression in equation (3.6) [Bolduc et al. 1997].

$$\frac{1}{2\pi\sqrt{C_{th}(L+M)}} \leq f \geq \frac{1}{2\pi\sqrt{C_{th}(L+M_{sat})}} \tag{3.6}$$

Where;

C_{th} is the Thévenin equivalent of the capacitor voltage divider.

L is the inductance of the inductor coil

M is the mutual inductance of the isolating transformer

M_{sat} is the mutual inductance of the isolating transformer at saturation

Taking an analytical view of the problem at fundamental frequency, Figure 3.5 shows the element impedances of Figure 3.4. It can be seen that there are three possible solutions of which **A** and **C** are stable. Solution **A** is the normal linear solution of the capacitive sub-station system.

In case of some transients such as an output short circuit or upon system energisations, solution **B** or **C** may be reached instead, and therefore Ferro-resonance is experienced [Bolduc et al. 1997]

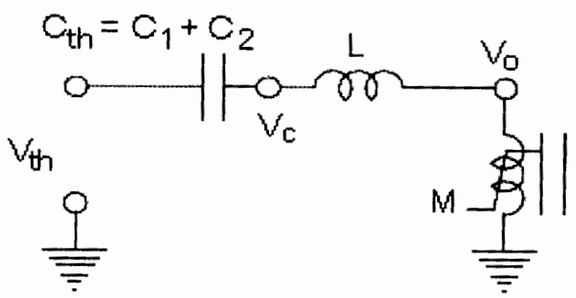

Figure 3.4 Electrical circuit causing Ferro-resonance

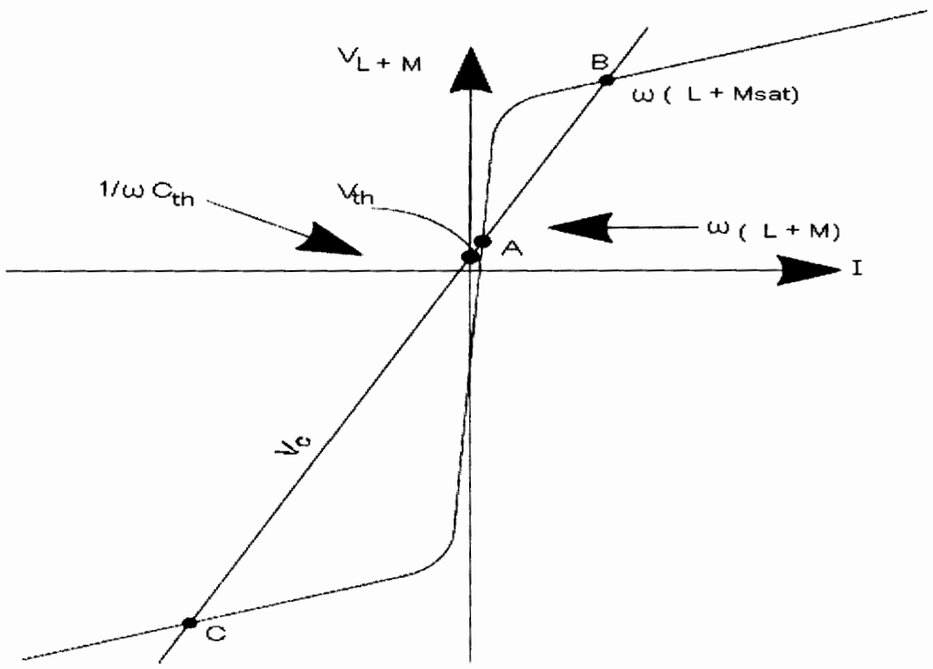

Figure 3.5 Analytical view of Ferro-resonance problem

3.4 SYSTEM DESIGN

The design of a voltage divider which forms the CCS system includes several steps in steady state considerations and transient state analysis. The subsequent section discusses these designs from two perspectives i.e. (i) modeling CCS without transmission line (ii) modeling CCS on a transmission line. The later sections also consider the CCS placement on a transmission line before finally coming up with the practical design of the CCS parameters.

3.4.1 MODELING CCS WITHOUT TRANSMISSION LINE

Steady State Consideration

The purpose of a CCS is to reduce the high voltage of a transmission line to a distribution voltage level. For this reason, the system is usually referred as a capacitive transformer. Figure 3.6 illustrates the operating principle of the capacitor divider considering a phase to ground connection [Sarmiento et al. 1990, Raphalalani et al. 2000, and Schilder et al. 2005].

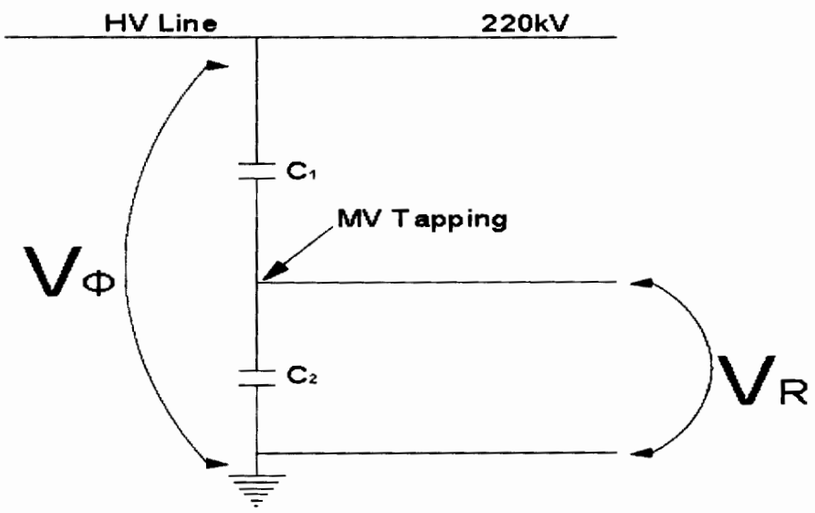

Figure 3.6 Capacitive voltage divider connected phase- to- ground

Let $V_{Ø}$ and V_R be the transmission line and the reduced voltage respectively then the voltage ratio as a function of the divider impedances (Z_1 and Z_2) or capacitance C_1 and C_2 is:

$$V_R = \frac{Z_2}{Z_1 + Z_2} V_\phi = \frac{C_1}{C_1 + C_2} V_\phi \qquad (3.7)$$

The coefficient $Z_1/ (Z_1+Z_2)$ is the transformation ratio of the system. The impedance of the Thévenin circuit from Figure 3.6 is very high and causes poor voltage regulation with big loads. The choice of capacitor C_1 and C_2 must satisfy two conditions.

The first one is the voltage across bank C_2 for a no load condition corresponds to the selected distribution voltage V_R. This condition can be defined by equation 3.8 in the form of,

$$\frac{Z_1}{Z_2} = \frac{V_\phi}{V_R} - 1 \qquad (3.8)$$

The second condition to be satisfied is that the maximum steady state voltage V_{max} across each capacitor unit must be less than or equal to its normal voltage V_n . This condition can be stated for bank C_1 for the most critical situation which is a full resistive load and it is expressed by the following inequality [Sarmiento et al. 1990].

$$V_{C1(max)} \leq V_{nC2} \qquad (3.9)$$

Where; $V_{C1(max)} = \sqrt{(I_L Z_L)^2 + (V_\phi - V_R)^2}$

$$V_{nC2} = \sqrt{P_{nC2} Z_2}$$

I_L = Maximum current through the load

P_{nc1} = Nominal power of bank C_1

Z_L = Impedance of an inductor connected in series with load.

On the other hand, the worst case for bank C_2 is a full inductive load. Assuming that the lowest power factor that can be encountered is 0.8, and then the following inequalities can be expressed as follows [Sarmiento et al. 1990]:

$$V_{C1\max} = \sqrt{(0.8 I_L Z_L)^2 + (V_R + 0.6 I_L Z_L)^2}$$

$$\leq V_{nC1} = \sqrt{P_{nC2} Z_2} \qquad (3.10)$$

Given that: $Z_L = \frac{Z_1 Z_2}{Z_1 + Z_2}$ (3.11)

Where: P_{nC2} = nominal power of bank C_2

By substituting Z_L in both inequalities 3.9 and 3.10, two quadratic inequalities are obtained, having Z_1 and Z_2 as variables as expressed below:

$$Z_1^2\left(\frac{I_L}{1+\frac{Z_1}{Z_2}}\right)^2 - Z_1 P_{nC2} + (V_\Phi - V_R)^2 \le 0 \qquad \textbf{(3.12)}$$

$$Z_2^2\left(\frac{I_L}{1+\frac{Z_1}{Z_2}}\right)^2 - Z_2\left(P_{nC2} - 1.2\frac{I_L V_R}{1+\frac{Z_2}{Z_1}}\right) + V_R^2 \le 0 \qquad \textbf{(3.13)}$$

By choosing the nominal power P_n of each bank the inequalities 3.12 and 3.13 yield intervals of feasible values for C_1 and C_2 .The interval for C_2 can be converted into the interval for C_1 when multiplied by the constant ratio Z_1/Z_2. The intersection of this interval with the one obtained from P_{nC1} yields a range of feasible values of C_1, and the corresponding range of C_2 for the previously selected powers P_{nC1} and P_{nC2}.

This technique can be directly applied when all the units of the banks are identical. This involves an iterative process in which the nominal powers are increased until the feasible intervals allow a selection of single phase units that best approximate the impedance ratio in equation 3.8.

If the capacitors units are of different voltage class or power rating, the nominal voltage V_n of the bank may be obtained as follows: First define the nominal current of each unit "j".

$$I_{nj} = \frac{P_{nj}}{V_{nj}} \qquad \textbf{(3.14)}$$

Then determine the minimum current $I_{n\ min}$ found and multiply it by the summation of their impedances:

$$V_n = I_{n(\min)}\left(\sum_j \frac{V_{nj}^2}{P_{nj}}\right) \qquad \textbf{(3.15)}$$

By following this procedure the capacitor units of the prototype systems may be chosen.

Transient state considerations

Capacitor voltage transformers (CVTs) are common in high voltage transmission lines and have similar characteristics to the CCS. These same applications require a fast, yet secure protection.

However, as the requirement for faster protective relays grows, so does the concern over the poor transient response of some CVTs for certain conditions. Figure 3.7 shows a generic CVT structure.

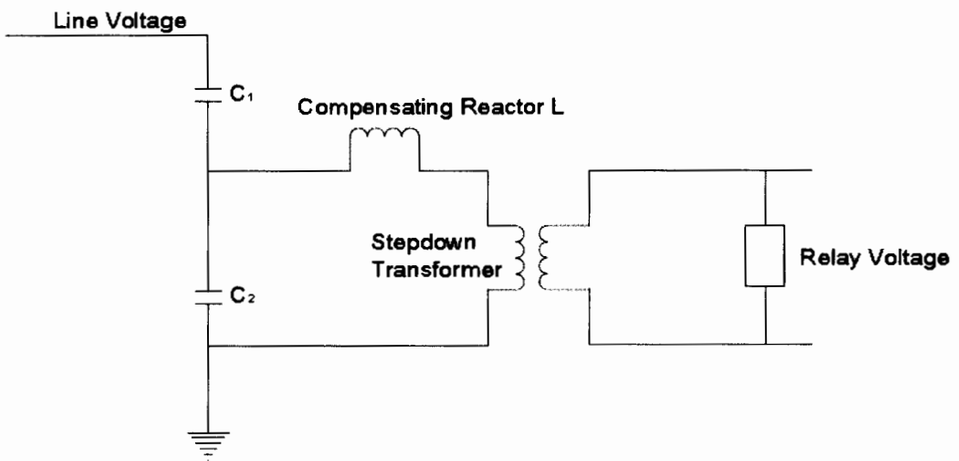

Figure 3.7 Generic CVT structure

As mentioned earlier the CCS operation principles is based on the CVT design. Consequently, the transient response characteristics are similar and depend on two factors [Daqing and Roberts 2000],

- The coupling capacitor value
- Ferro resonance – suppression circuit design

The coupling capacitor value

A CVT/CCS is made of a number of capacitor units connected in series. The number of capacitor units depends on the applied primary voltage level. The CVT capacitance is represented by two values: one for the equivalent capacitance above the intermediate voltage point (C_1) and the other for the intermediate capacitance below the intermediate voltage point (C_2).

The Thévenin equivalent capacitance value (C_1 and C_2) is different from the total capacitance $C_1.C_2 / (C_1+C_2)$ normally given by CVT manufacturers [Kirchesch 2000].

Some manufacturers differentiate CVTs as normal high or extra high capacitance CVTs. The high capacitance value in a CVT decreases the transient magnitude. Increasing the CVT capacitance value can increase the CVT cost but decreases the CVT transient response. Thus, the protection engineer must strike a balance between CVT performance and cost [Daqing and Roberts 2000].

Ferro-resonance – Suppression circuit design

The transient response characteristics are governed by two types of Ferro-resonance – suppression circuit design i.e. Active Ferro-resonance – suppression circuit (AFSC) or the passive Ferro-resonance – suppression circuit (PFSC) design. Figure 3-8 shows both designs [ANSI C93.1-1990, Ferracci 1998, Jacobson and Menzies 2001].

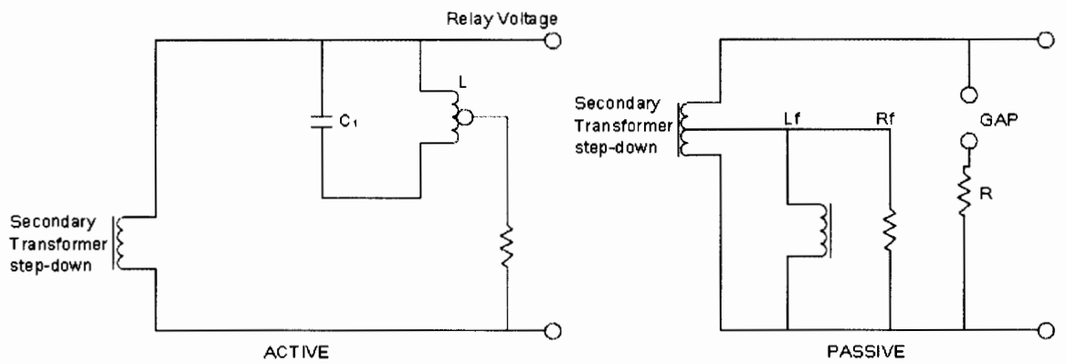

Figure 3.8 Active and passive Ferro-resonance-suppression circuit

(I) Active Ferro-resonance – Suppression Circuit (AFSC)

AFSC consists of an LC parallel tuning circuit with a loading resistor. The LC tuning circuit resonates at the system frequency and presents a high impedance voltage to the fundamental voltage.

The loading resistor is connected to a middle tap of the inductor to increase the resonant impedance of the circuit. For frequencies above or below the fundamental frequency (off nominal frequency), the LC parallel resonant impedance gradually reduces to the resistance of the loading resistor and attenuates the energy off-nominal-frequency voltage. This research project has adopted this type of FSC for its application.

(II) Passive Ferro-resonance – Suppression Circuit (PFSC)

PFSC consists of a permanently connected loading resistor R_f, a saturatable inductor L_f, and an air-gap loading resistor R. Under normal operating conditions, the secondary voltage is not high enough to flash over the air gap, and the loading resistor R has no effect on the CVT performance.

Once a Ferro-resonance oscillation exists, the induced voltage flashes over the gap and shunts in the loading resistance, to attenuate the oscillation energy. L_f is designed to saturate at about 150% of nominal voltage to further prevent a sustained Ferro-resonance condition.

3.4.2 MODELING CCS ON A TRANSMISSION LINE

Figure 3.9 shows the schematic representation of CCS connected to the transmission line. An equivalent circuit is shown in Figure 3.10 where *k* is a factor between zero and one [Raphalalani et al. 2000].

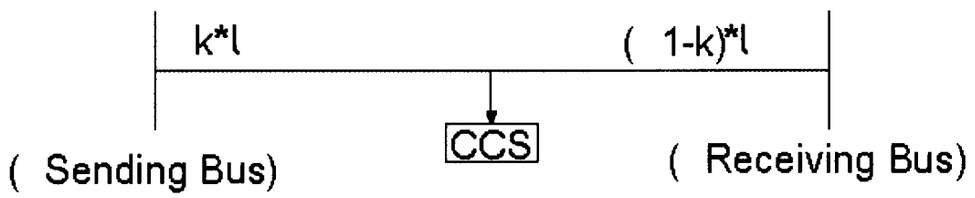

Figure 3.9 Schematic representations

This factor defines the location of CCS along the length of the transmission line and *l* is the length of the transmission line. The transmission line parameters are obtained using factor k. Variable with subscript 'a' refers to the first portion of the line whose length equals k**l* while subscript 'b' refers to the last portion of the line. Length of this portion is equal to (1-k)**l*.

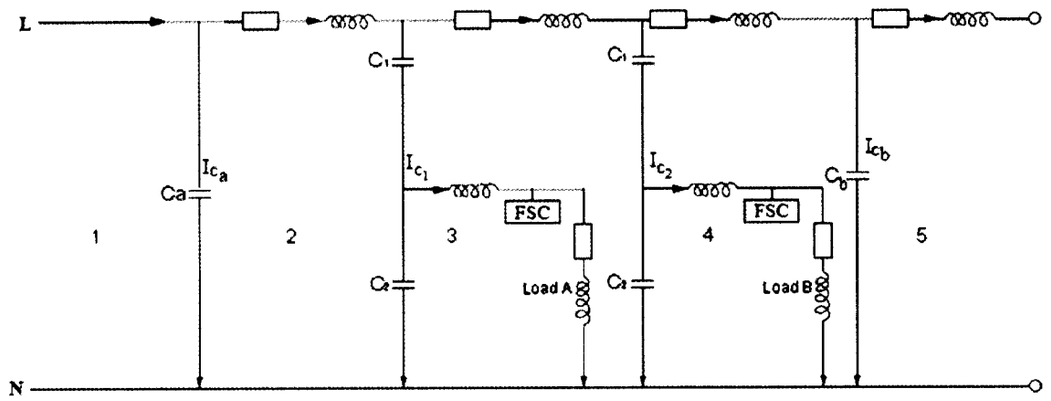

Figure 3.10 Systems equivalent circuit [Raphalalani et al. 2000]

Steady state Modeling

Steady state equations have been derived [Raphalalani et al. 2000] from the models shown in Figure 3.10 the equations relate to the receiving and sending end voltage and current of the transmission line including the load terminal of the CCS unit.

$$V_R = \left[\frac{2}{(1+j\omega C_b Z_b)}\right]\left[\frac{V_d}{C_{12}} + \frac{I_d Z_a}{C_{12}} - \frac{V_s}{2}(1+j\omega C_a Z_a) + \frac{I_s Z_a}{2}(2+j\omega C_a Z_a) - \frac{I_R Z_b}{2}(2+j\omega C_b Z_b)\right] \quad (3.16)$$

$$I_R = \left[\frac{1}{(1+j\omega C_b Z_b)}\right]\left[I_s(1+j\omega C_a Z_a) - j\omega C_b V_R + j\omega C_2 V_d - j\omega C_a V_s - I_d(1-j\omega C_2\right] \quad (3.17)$$

Transient Modeling

The equivalent circuit used for modeling is the one in Figure 3.10. The circuit has been divided into five loops (loop numbers have been indicated in Figure 3.10). Equations derived are shown below;

$$R_a\frac{di_1}{dt} + L_a\frac{d^2 i_1}{dt^2} + \frac{1}{C_a}(i_1 - i_2) = \frac{dV_s(t)}{dt} \quad (3.18)$$

$$\frac{1}{C_a}(i_2 - i_1) + R_a\frac{di_2}{dt} + L_a\frac{d^2 i_2}{dt^2} + \frac{1}{C_1}(i_2 - i_4) + \frac{1}{C_2}(i_2 - i_3) = 0 \quad (3.19)$$

$$\frac{1}{C_1}(i_3 - i_2) + R\frac{di_3}{dt}(i_3 - i_4) + L\frac{d^2 i_3}{dt^2} + (i_3 - i_4) + \frac{dV_d(t)}{dt} = 0 \quad (3.20)$$

$$\frac{1}{C_1}(i_4 - i_2) + R_b\frac{di_4}{dt} + L_b\frac{d^2 i_4}{dt^2} + \frac{1}{C_b}(i_4 - i_5) - \frac{dV_d(t)}{dt} + L\frac{d^2 i_4}{dt^2}(i_4 - i_3) + R\frac{di_4}{dt}(i_4 - i_3) = 0 \quad (3.21)$$

$$R_b\frac{di_5}{dt} + L_b\frac{d^2 i_5}{dt^2} + \frac{dV_R}{dt} + \frac{1}{C_b}(i_s - i_4) = 0 \quad (3.22)$$

These equations may be used to show the variation of load voltage with load power. The idea is to find an optimum operating load that can be supported before the voltage begins to collapse. The load tests are done at variable load power factor. The load model used is that of a series R-L.

The system is tested at different level of demand. Real power demand (P) may be fixed to a different value and reactive power demand (Q) varied to operate at different load power factor between 0.2 lagging and unity [Raphalalani et al 2000].

3.4.3 MODELING PRACTICAL CCS ELEMENTS

Section 3.3 showed the theoretical design of a CCS unit at steady state condition. It is important to note that the capacitors used for the design of CCS have inherent equivalent series resistance (ESR). Hence, they experience losses based on ESR designed value.

The practical approach to design is to ensure that the voltages V_{C1} and V_{C2} for capacitor C_1 and C_2 (see Figure 3.6) do not exceed nominal values under extreme steady state loading conditions. MATLAB Sim Power program is used to analyse transient behaviour for designs of low and high impedance obtained at steady state conditions. In order to determine the value of the capacitor we consider two boundary conditions namely:

- The heat dissipated should be such that the temperature rise should not exceed the maximum temperature rise of the capacitor based on its ESR designed value.

- The combination of the capacitors that make the capacitor divider circuit should result in the target output phase voltage which in this case is 33kV (Note: 33kV is the main distribution voltage used for rural electrification in Kenya).

According to Kothari and Nagrath [2006], It can be shown by use of the charge conservation law, that heat dissipated by the capacitor divider circuit composed of C_1 and C_2 is given by;

$$\Delta E = \frac{C_1 C_2}{C_1 + C_2} \frac{(\Delta V)^2}{2} \tag{3.23}$$

Where ΔE is the energy dissipated as heat and ΔV is the change in voltage.

In this case ΔV = (127-33) kV = 94kV, (Note: $220kV/\sqrt{3} = 127kV$)

Therefore;

$$\Delta E = \frac{C_1 C_2}{C_1 + C_2} \frac{(94 \times 1000)^2}{2} = \frac{C_1 C_2}{C_1 + C_2} \frac{94^2}{2} 10^6 \tag{3.24}$$

Equation 3.24 suggests that the capacitive equivalent has to be in the order of microfarads in order to keep losses as low as possible. The values of C_1 and C_2 are arrived at by use of iterative method. Capacitors are chosen in such a way that C_1 is smaller than C_2 by a factor that can give the desired voltage level at the output.

Therefore, considering the desired voltage of ± 6% of 33kV.and using equation 3.7, the capacitor voltages are chosen as follows; C_1= 0.5 μF and C_2 = 1.5μF.

This can be demonstrated by the calculation shown below, where; $V_\emptyset$ is the transmission line voltage per phase and V_R is the reduced or output voltage.

$$V_R = \frac{C_1 V_\phi}{C_1 + C_2} = \frac{0.5 \times 127 \times 10^{-6} \times 10^3}{(0.5 + 1.5) \times 10^{-6}} = 31.75kV$$

Thus, 31.75kV becomes our base voltage which is within ±6% of 33kV. From Figure 3.3, an inductor L is added to the capacitive voltage divider C_1 and C_2 to cancel the Thévenin impedance $C_{th} = C_1 + C_2 = C_f$ at 50Hz (see the equivalent circuit in figure 3.4). The regulation is done by adjusting C_1, C2 and L so that they satisfy $LC\omega^2 = 1$, where $\omega = 2\pi 50$. Therefore, the value of L is calculated as;

$$L = 1/C_f\omega^2 = \frac{1}{(0.5 + 1.5) \times 10^{-6} (314)^2} = 5.071H$$

For designing the desired Ferro-resonance suppression circuit (FSC) the following points are considered: The capacitor C_3 is connected in parallel to the inductor L_1 and both are connected in series with a damping resistor R. Thus, $C_f = C_{th} = C_1 + C_2 = 0.5+1.5 = 2.0\mu F$.

And $L_f \leq \frac{1}{(2\pi f)^2 C_f}$, Therefore; $L_1 = L_f \leq 5.071H$.

The damping resistor R should be in the range of the system load. Figure 3.11 and 3.12 shows the peak power over the daily load profile load and average power demand curve respectively for a typical rural village in Kenya [KPLC 2007a]

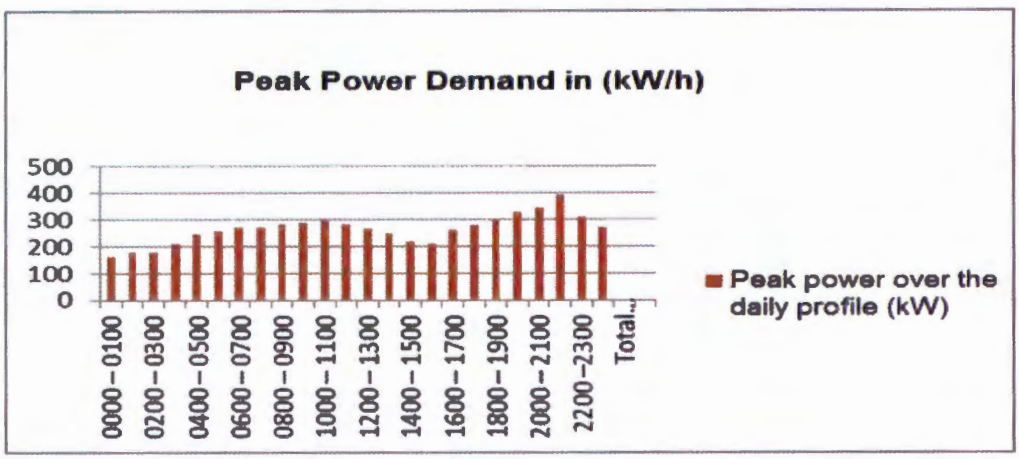

Figure 3.11 Peak power over the daily profile (kW)

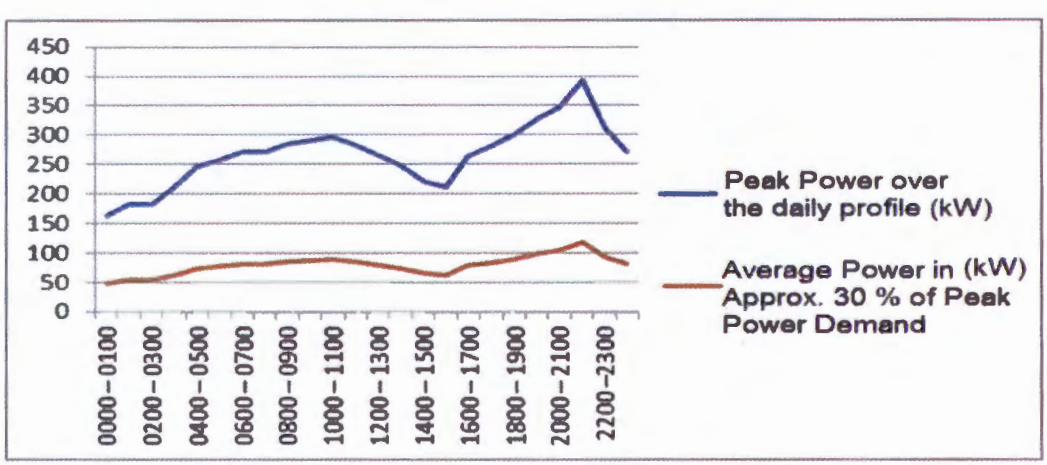

Figure 3.12 Average power demand curve for a typical rural village

Figure 3.11 shows the peak power demand over the daily load profile. The peak load is considered at 391.40.kW. The average load requirement for these rural communities is taken as 30% (based on the diversity factor of the rural loads) of the peak power demand over the daily profile as shown in Figure 3.12. The average power demand was modeled with regards to the communities continuous rating load requirement. Based on these findings an average load of 100kVA at unity power factor was considered for the optimum design of the CCS and ASVT units. The design assumption was that, the tap-off voltage was at ±6% of 33kV then stepped down using the isolating transformer to 33kV /0.240kV for distribution purposes.

3.4.4 CAPACITOR PLACEMENT PROBLEM

The general capacitor placement problem consists of placing the capacitor (determining their number and the location) and determining the types and sizes. The objective is to attain optimum power and keep energy losses low while maintaining the cost of capacitors at a minimum [Baran and Wu 1989]. For this research project, the objective is to place the CCS units in the network so as to determine the maximum allowable penetration of the units without steady-state voltage violation. Therefore, a capacitor placement problem formulation becomes necessary.

Since we are interested in the energy loss with regard to penetration level of the capacitor units, it is necessary to take into account the load variations for a given period of time, T. We assume that the load variation can be approximated in discrete levels. Furthermore, the loads are assumed to vary in a conforming way (all the loads enjoy pattern of variation, this is typical of rural loads) [Ledwich 2007, Dagbjartsson et al. 2007]. Let S (τ) be the common Load Duration Curve as shown in Figure 3.13. [Baran and Wu 1989].

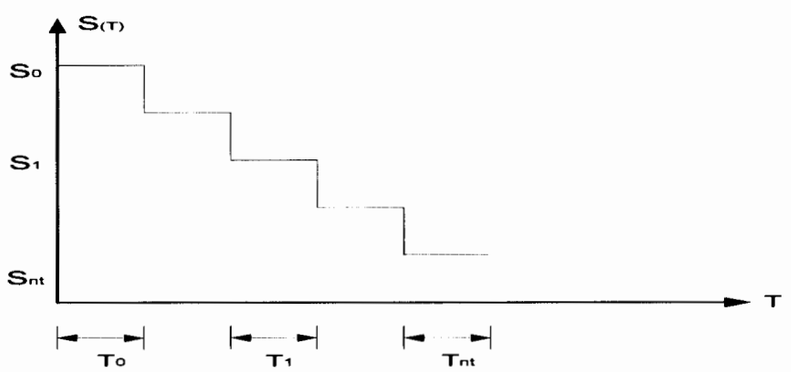

Figure 3.13 Load duration curve

Then a load say Q_L, Can be represented as;

$$Q_L(\tau) = Q_L^0 S(\tau) \quad (3.25)$$

Where Q_L^0 represents the peak value.

Under these assumptions, the time period, T can be divided into intervals during which the load profile of the system is assumed to be constant.

Let there be *nt* such load levels (load profile) where *n* represents the number of levels/branches or nodes. Then for each load level we have;

(i) Power flow equations

(ii) Voltage constraints as bounds on the magnitude of the system node voltages

(iii) Capacity and control constraints on the control variables (capacitors)

The constraints imposed by power flows on a radial distribution system by a new set of AC power flow equations called *DistFlow* equation is presented. They substitute for the conventional AC power flow equations [Baran and Wu 1989].

To summarize the idea, consider a three phase balanced radial distribution feeder with *n* branches/nodes, *l* laterals, and *nc* shunt capacitors placed at nodes of the system. Figure 3.14 shows the one line diagram of the system.

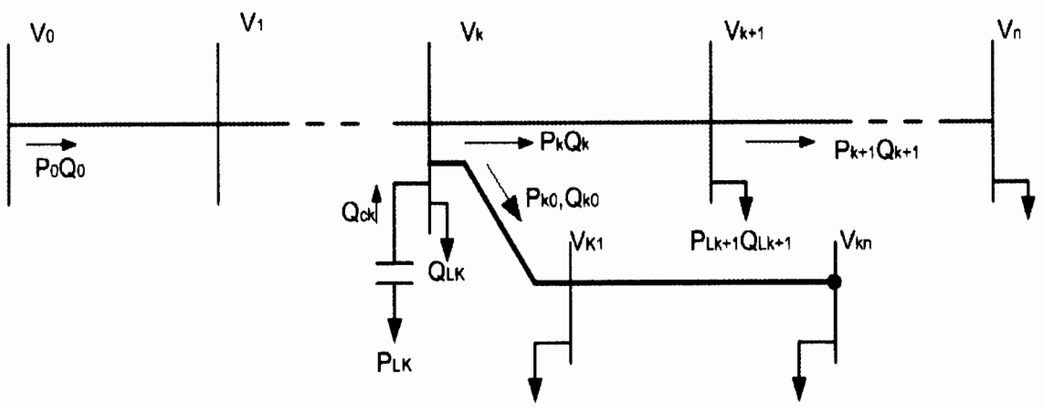

Figure 3.14 One line diagram of distribution feeder [Baran and Wu 1989].

It can be shown that power flow through each branch in the lateral can be described by the following recursive equations [Baran and Wu 1988].

$$P_{k+1} = P_k - r_{k+1}P_k^2 + Q_k^2 / V_k^2 - P_{Lk+1} \quad \textbf{(3.26)}$$

$$Q_{k+1} = Q_k - x_{k+1}P_k^2 + Q_k^2 / V_k^2 - Q_{Lk+1} \quad \textbf{(3.27)}$$

$$V^2{}_{k+1} = V_k^2 - 2(r_{k+1}P_k + x_{k+1}Q_k) + (r^2{}_{k+1} + x^2{}_{k+1})/P_k^2 + Q_k^2 / V_k^2 \quad \textbf{(3.28)}$$

Where:

P_kQ_k : Real and reactive power flows into the receiving end of branch k+1 connecting node k and node k+1,

V_k : bus voltage magnitude at node k,

Q_{ck} : reactive power injection from capacitor at node k.

Equation 3.26 to 3.28 called the branch flow equation has the following form

$$x_{k+1} = f_{k+1}(x_k, u_{k+i}) \quad \textbf{(3.29)}$$

Where, $x_k = [P_kQ_kV_k^2]^T$ and $u_{k+1} = Q_{ck+1}$

Note that if there is no capacitor in node k, then u_k does not appear in equation 3.29. By using notation, we may use $\boldsymbol{u}$ as an *nc* dimensional vector containing the *nc* capacitors i.e.

$u^T = [\, u_1 \ldots u_{nc}] = [Q_{cn_1} \ldots Q_{cn_m}]$

In addition to the branch flow equation of 3.29, there are terminal conditions to be satisfied for each lateral (counting the main feeder as the o^{th} lateral). For example for lateral k shown in Figure 3.14, we have the following terminal conditions:

(i) At the branching node k where the lateral is connected to the main feeder, a dummy variable is defined V_{ko} and let

$$x_{ko_3} = V_{ko}^2 = V_k^2 = x_{ok_3} \quad \textbf{(3.30)}$$

(ii) At the end of the lateral there is no power sent to the other branches, that is;

$$x_{kn_1} = P_{kn} = 0 \quad ; \quad x_{kn_2} = Q_{kn} = 0 \tag{3.31}$$

Therefore, for the general feeder considered, there are 3(n+l +1) Dist Flow equations corresponding to 3.26 to 3.28 and equation 3.30 to 3.31 are presented by the following equations.

$$G(x, u) = 0 \tag{3.32}$$

$$\text{Where, } x = [x_1^T \ldots x_l^T x_0^T]^T, x_k = [x_{ko}^T \ldots x_{kn}^T]^T \tag{3.33}$$

DistFlow equations can be used to determine the operating point, $\boldsymbol{x}$ of the system for a given load profile, P_{Li} , Q_{Li} i = 1 ....n and the capacitor settings $\boldsymbol{u}$. The *DistFlow* equation is preferred over the conventional AC power flow equations because the special structure of the *DistFlow* equation can be utilized to develop a computationally efficient and numerically robust solution algorithm. The detail of such algorithm is presented by Baran and Wu [1988].

For the capacitor placement problem, since there is *nt* different load profiles to be considered, the overall DistFlow equations are;

$$G(x^i, u^i) = 0 \quad ; \quad i = 0, 1 \ldots nt \tag{3.34}$$

Where $\boldsymbol{x^i}$, $\boldsymbol{u^i}$ represents the state and the control variables corresponding to the load profile $\boldsymbol{i}$ respectively.

The voltage constraints can be taken into account by specifying upper and lower bounds on the magnitude of the node voltages as follows,

$$V_{\min 2} \le V_j^{i2} = v_j^i(x^i) \le V_{\max 2} \quad j = 1... \quad i=0, 1 \ldots nt \tag{3.35}$$

These bounds constitute a set of functional inequality constraints of the form,

$$H^i(x^i) \le 0 \quad i=0, 1 \ldots nt \tag{3.36}$$

In this research project the CCS are modeled as capacitance dependent on voltage. Hence;

$$u^0 = u^1 = \ldots u^{nt} \tag{3.37}$$

3.5 MODELING OF ASVTs

The developments of transformer design tools and their electromagnetic field for finite elements as well as networks modeling programs allowed the transformers manufacturers to develop the ASVT which can transform high voltage energy from upto 420kV to (below 600V) in one step. ASVTs have high reliability and enough power to fulfill most of the low voltage load application, like control system, pump motors, instrumentation and illumination [Gomez et al. 2010].

To develop an ASVT model it is first important to understand the magnetic circuit theory and finite element analysis of a conventional transformers. Ideally, a transformer stores no energy - all energy is transfered instantaneously from input to output. In practice, all transformers do store some undesired energy,through the following ways [Bell and Bodges 2007];

- Leakage inductance, which reperesents energy stored in the non-magnetic regions between Windings, caused by imperfect flux coupling. In the equivalent electrical circuit, leakage inductance is in series with windings, and the stored energy is proportional to load current squared.

- Mutual inductance (magnetizing inductance), represents energy stored in the finite permeability of the magnetic core and in small gaps where the core halves come together. In the equivalent circuit, mutual inductance appears in parallel with the windings. The energy stored is a function of the volts-second per turn applied to the windings and is independent of load current.

Two models of analysing transformers are considered for the ASVTs design, the first model is based on the magnetic circuit theory and the second is based on magneto-static finite element analysis. In this research project the transformer reverse design method is incorperated for the two models.

3.5.1 REVERSE TRANSFORMER DESIGN

In the conventional method of transformer design, the terminal voltages, VA rating and frequency are specified. In the reverse design approach the physical characteristics and dimensions of the windings and core are the specifications. By manipulating the amount and type of material actually to be used in the transformer construction, its performance can be determined.

This is essentially the opposite of the conventional transformer design. It allows for customized design, as there is considerable flexibility in meeting the performance required for a particular application.This type of design is suitable for ASVT models since they are meant for customized application [Bell and Bodges 2007].

In the reverse design method, the transformer is built up from the core outwards. The core cross section dimensions (diameter for a circular core and side lengths for a rectangular core) are selected from cataloques of available materials. A core length is chosen. Laminations that are availabe can be specified in thickness. A core stacking factor can be estimated from the ratio of iron to total volume.

Figure 3-15 shows a transformer profile of known material characteristics and dimensions [Bell and Bodges 2007].

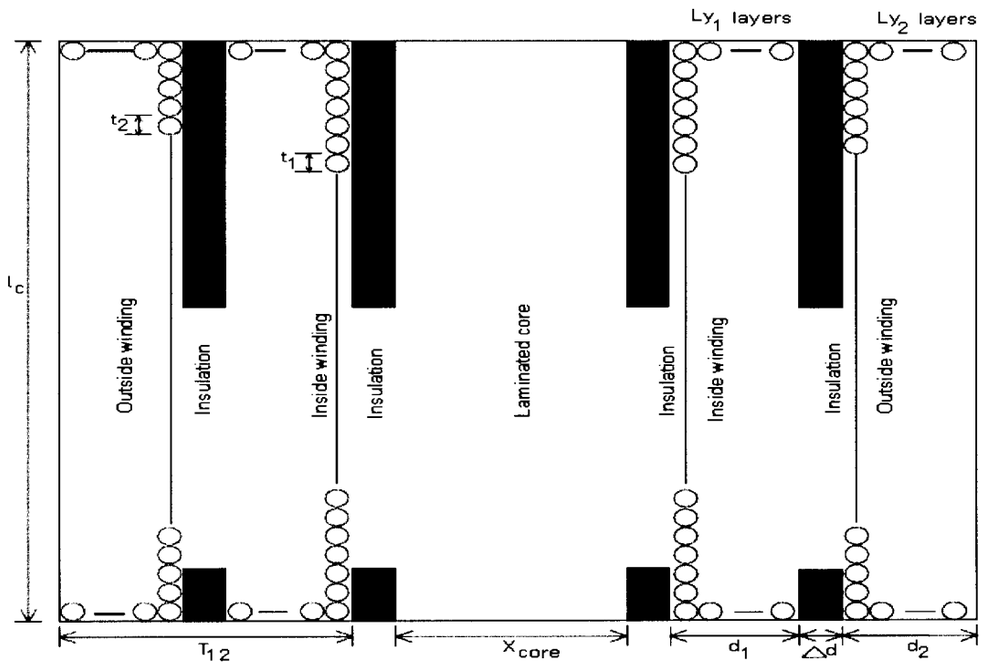

Figure 3.15 Component dimension and material properties of a transformer

Given the core length l_c and diameter,(or b_{core} and w_{core} for a rectangular core), the inside winding usually low voltage winding is wound on layer by layer. The wire size can be collected from catalogues. Insulation thickness is also specified. The designer can then specify how many layers of each winding are wound.

Insulation is placed between core and the inside winding (fomer) and between each layer for high voltage applications. The outer winding usually the HV windings is wound over the inside winding,with the insulation between layers according to the voltage between them.

Windings current densities and volt per turn become a consequence of the design, rather than a design specification. The only rating requirements are the primary voltage and frequency.

The secondary voltage and transformer VA rating are a consequence of the construction of a transformer. The number of turns are estimated to be ;

$$N_1 = \frac{l_c L_1}{t_1}, N_2 = \frac{l_c L_2}{t_2} \quad (3.38)$$

Where;

l_c is the length of core

L_1, L_2 Number of primary and secondary winding layers

$t_1 t_2$ axial thickness of primary and secondary wire

This calculation assumes that the winding length is equal to the core length. The actual winding lengths may be used if the primary and the secondary winding lengths are different and do not fully occupy the winding window height.

3.5.2 EQUIVALENT CIRCUIT MODELS

The Steinmetz 'exact' transformer equivalent circuit shown in Figure 3.16 is used to reperesent the transformer at supply frequency. Each component of the equivalent circuit can be calculated from the transformer material characteristics and dimensions [Paul et al. 1986, Margueron and Keradec 2007].

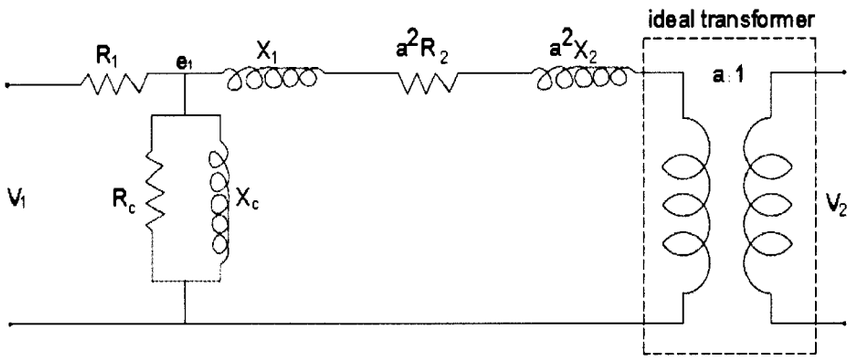

Figure 3.16 Steinmetz 'exact' transformer equivalent circuit

Based on the equivalent circuit model shown in Figure 3.16 different aspect of resistance models can be calculated or analysed.

Core loss resistance

The losses in the core consist of two major components, the hysteresis loss and the eddy current loss. The hysteresis loss can be calculated using [Paul et al. 1986].

$$P_k = k_h f B^x WT \tag{3.39}$$

Where : k_h = Constant depending on the material typically 0.11.

x = Steinmetz factor, typically 1.85

WT = Weight of the core.

B = Peak flux density, calculated from the transformer equation

$V_l = 4.44 f N_1 \phi$ (ϕ = B A_c)

The eddy current is expressed as

$$P_{ec} = \frac{c_l^2}{12 p_c} \frac{l_c}{N_l^2 A_c} e_1^2 k_v \tag{3.40}$$

Where:

c_l = lamination thickness

p_c = Operating resistivity of the core

A_c = cross-sectional area of the core

e_1^2 = induced primary winding voltage

k_v = total core volume/central limb volume

The variation of resistivity with temperature should be accounted for, since the transformer will be heated up under operation. The operating resitivity for a material at temperature ^{0}C is,

$$\rho = \rho_{20^0C}(1 + \Delta\rho(T - 20) \tag{3.41}$$

Where: $\Delta\rho$ = thermal resistivity coeficient

ρ_{20^0C} = material resistivity at 20^0C

The hysterisis and eddy current losses can be expressed in terms of induced voltage e_1,

$$p_h = \frac{e_1^2}{R_h}, p_{ec} = \frac{e_1^2}{R_{ec}} \quad (3.42)$$

Where, R_h = hysteresis loss equivalent resistance

R_{ec} = eddy current loss equivalent resistance

Thus, both R_h and R_{ec} can be included in the model as the core loss resistance R_c, calculated as,

$$R_c = \frac{R_h R_{ec}}{R_h + R_{ec}} \quad (3.43)$$

Inductive reactance models

Magnetizing reactance is given by [McLyman 2004],

$$X_m = \frac{\omega N_1 \mu_0 \mu_{rc} A_c}{I_{eff}} \quad (3.44)$$

Where; $\omega = 2\pi f$

μ_0 = Permeability of free space (4π x10 $^{-7}$ H/m)

μ_{rc} = Relative permeability of core.

I_{eff} = effective path length for mutual flux.

Leakage reactances

The primary and secondary leakage reactances are assumed to be the same, when referred to the primary, and are each half of the total transformer leakage reactance. One form of the expression is [Lindbolm 2004],

$$X_1 = a^2 X_2 = \frac{1}{2}\frac{\mu_0 N_1^2}{l_c}\left(\frac{l_p d_1 + l_s d_2}{3}\right) + l_{ps}\Delta d \quad (3.45)$$

Where; $l_p\, l_s$ = mean circumferential length of primary and secondary windings.

l_{ps} = mean circumferential length of interwinding space.

d_1, d_2 = Thickness of primary and secondary windings

Δd = Thickness of interwinding space.

Having obtained the component values, the equivalent circuit can be solved. Open circuit, short circuit and loaded circuit performances can be estimated by putting an impedance $Z_L = R_L + jX_L$ across the output and varying its value.

Consequently, performance measure of voltage regulation and power transfer efficiency for any load condition can be readily calculated. Current flows and densities in the windings can be calculated and compared to desired levels.

3.6 PENETRATION LEVEL OF ASVTS ON A POWER NETWORK

The ASVT is an inductive voltage transformer with a very high thermal rating in comparison to the conventional instrument transformers. In other words, it is a pad mounted type transformer which allows connection directly either to a high voltage line or bar, and directly transforms energy from voltages up to 230 kV down to 600V or smaller in one step, with a thermal rating capacity of 50 kVA to about 330kVA per phase.

This is equivalent to a thermal rating of 1MVA three phase power. It is neither an instrument transformer nor a power transformer. Therefore, it may be assumed as a transformer of high impedance closer to that of an instrument transformer, but 'permeable' enough to allow 50kVA to 1MVA load connected and still offer a good voltage regulation (see also section 2.5 for comparison) [Gomez 2010].

This transformer is a specially designed oil insulated high voltage transformer, similar to hipot designs but with large capacity. Integrating this type of transformer units into a high voltage (HV) transmission long line results to reactive power imbalance which may cause change in the voltage profile of the line. There are two possible methods of determining the optimum penetration level of ASVTs in a power transmission line without steady state voltage violation namely;

- Use of X/R ratio and comparing it with voltage level on the receiving end of the line.
- Using the surge impedance loading (SIL) level of the transmission line.

Maintaining adequate voltage profile in a power system has become a major problem because many utilities are squeezing maximum possible capacity from the transmission network to avoid the capital cost of building new lines and generation facilities. Low voltage can result in loss of stability and voltage collapse, and ultimately lead to power outages [Gonen 2008].

Voltage instabilility is mostly analysed by considering the characteristics of transmission systems and then examining how the phenomenon is influenced by characteristics of generators, load and reactive power compensation devices [Kundur 1994, Nayak et al. 2006].

The maximum power that can be delivered to loads and relationship between load power and network voltage are the two basic properties that require riqourous analysis.

According to Shukla and Sekar [2003], In their case study, where the line lengths were varied keeping X/R ratio and power factor constant. The following conclusions were drawn;

- High X/R ratio decreases the maximum power transfered and affects the voltage stability adversely.
- Low power factors have detrimental effect on voltage stability characteristics.
- Line capacitance tends to improve the voltage characteristics.

In a typical power transmission line, the SIL is of concern but is not a maximum power condition though it can be used as an indicator to gauge penetration level of ASVT unit(s).

On the other hand, typical R/X ratio for a power transmission line is small and the resistance has very little to do with the line impedance of the line. Therefore, it is plausible to use SIL as opposed to R/X ratio for penetration level measurement of ASVTs and especially for long transmission lines.

3.6.1 SURGE IMPEDANCE LOADING

Surge Impedance Loading (SIL) is defined as the amount of active power that is transfered to a load at unity power factor.This make the line appear purely resistive [Nayak et al. 2006]. It means that the line capacitance provides all the reactive power that is absorbed by the inductance of the line. This implies depending on the system load, the line can be either absorbing or providing reactive power.

In other words, balance of both consumption and production of reactive power by a line at a particular loading level may results to a flat voltage profile along the line and keep the angular and voltge stability within limit.

However, this can only be true if the line resistance is zero. Although, this is impractical since the resistance of the line cannot be zero. Therefore, a resonable balance has to be determined, so as to have a good voltage profile (not neccessarily flat). The SIL value can be determined by using the capacitance and inductance of the total line shown in equation 3.46

$$SIL = \frac{|V_L|^2}{\sqrt{L/C}} \tag{3.46}$$

The voltage V_L is the line to line voltage of the three phase transmission line. The SIL value in the equation is given in watts. When a line is loaded below SIL value the line is providing reactive power.

The inverse also applies that when the line is loaded above the surge impedance value it absorbs reactive power. When a transmission line absorbs reactive power, additional sources of reactive power has to be supplied for the line. This is done by means of capacitor banks that support power transfer over lines under heavy loading conditions[Nayak et al. 2006, Glover and Sarma 2002].

The SIL curve can be drawn using the parameters of equation 3.46 . Traditionally, this graph is drawn for a transmission line providing power to loads at specific power factors. That is, reactive power that is absorbed or provided by the line is plotted against the active power delivered to the load.

By changing the amount of power that is being supplied to the load , and recording the resultant change in reactive power, a SIL curve can be constructed. The SIL value for a transmission line can be read off the SIL curve. The SIL value will be the active power on the graph that results to zero net reactive power on the line.

SIL is defined by V, L and C as already indicated in equation 3.46, but L and C are defined by conductor size and arrangement. SIL is not affected by length directly, but the reactive power developed in the line is affected by length when the load is not SIL. A SIL curve is usefull as it it can be applied to determine the following;

- The size of reactance support needed to sustain a certain load on the line can be closely estimated.
- Stability limit of the transmission line can be determined.
- The current loading on the line can be used to determine whether it would be possible to increase the power transfer across the line.

3.6.2 DETERMINATION OF TRANSMISSION LINE PARAMETERS

Before surge impedance loading (SIL) curves can be constructed it is important to determine the transmission line parameters. The method used is based on syncronised phasor measurements This method uses the two-port ABCD parameters that is defined in [Grainger and Stevenson 1994].

The ABCD parameters give the relationship between the voltages and currents at two points. For a transmission line this means that the ABCD parameters represents the influence that the capacitance, inductance and resistance of the line has on the voltage and current values measured at the sending and receiving end sides. The relationship is given by the following equations [Wilson et al. 1999].

$$\begin{bmatrix} V_S \\ I_S \end{bmatrix} = \begin{bmatrix} AB \\ CD \end{bmatrix} \begin{bmatrix} V_r \\ I_r \end{bmatrix} \tag{3.47}$$

A and B are defined by the following equations.

$$A = \cosh \gamma l \tag{3.48}$$

$$B = Z_C \sinh \gamma l \tag{3.49}$$

$$\text{Where} \quad Z_C = \sqrt{\frac{z}{y}} \tag{3.50}$$

From the preceding equation it is seen that once A and B are known, z and y can be calculated. Therefore, z and y have been defined as the series impedance and shunt admittance per unit length. In order to solve for A and B two operating points that are linearly independent have to be considered. A matrix can be constructed for the measurements of the two cases.

$$\begin{bmatrix} V_S 1 \\ V_S 2 \end{bmatrix} = \begin{bmatrix} Vr1 I_r 1 \\ V_r 2 I_r 2 \end{bmatrix} \begin{bmatrix} A \\ B \end{bmatrix} \tag{3.51}$$

Using Cramer's Rule A and B can be calculated.

$$A = \frac{\det \begin{bmatrix} V_S 1 I_r 1 \\ V_S 2 I_r 2 \end{bmatrix}}{\det \begin{bmatrix} V_r 1 I_r 1 \\ V_r 2 I_r 2 \end{bmatrix}} \tag{3.52}$$

$$B = \frac{\det \begin{bmatrix} V_r 1 V_S 1 \\ V_r 2 V_S 2 \end{bmatrix}}{\det \begin{bmatrix} V_r 1 I_r 1 \\ V_r 2 I_r 2 \end{bmatrix}} \quad (3.53)$$

To calculate y and z the results from (3.52) and (3.53) are substituted into (3.48) and (3.49) while Z_C is substituted with equation (3.50) and $\gamma l = \sqrt{yz}l$

This will provide two equations with two unknown to solve. The method is very useful since the impedance is given as a value with an angle. This means that the resistance and inductance are given as separate values. This is also the only method that gives the shunt admittance (y) from where the capacitance can be calculated. This method is used in chapter seven to help in constructing the SIL curve.

3.6.3 SURGE IMPEDANCE LOADING CURVES

Transmission line loadability curve also known as St Clair curve has been a valuable tool for quickly estimating the power transfer capability of a transmission line. This is due to their universal characteristic that is applicable to all voltage levels. St Clair curve are generally accepted in the industry as a convenient reference for estimating the maximum loading limits of transmission lines [Hao and Xu 2008].

Figure 3.17 shows the St Clair curve for loadability of transmission line in terms of their SIL [Dunlop et al. 1979]. It is well known that the per-unit line data normalized using SIL and surge impedance is constant, that is dependent of line construction (arrangement) and voltage rating as explained earlier in section 3.6.1.

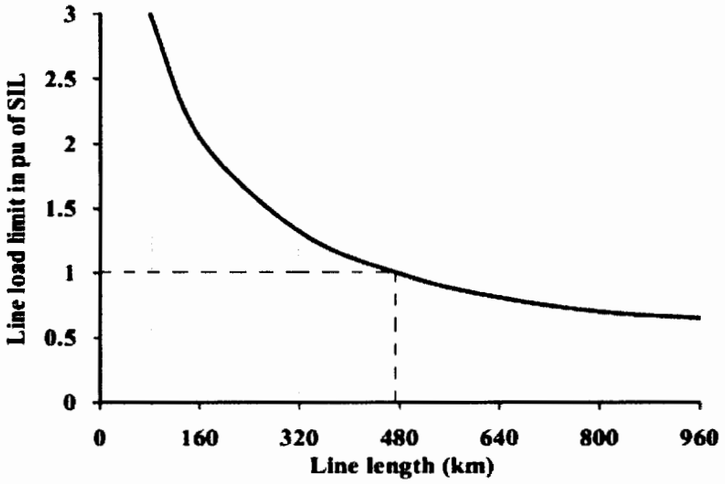

Figure 3.17 Transmission line loadability curve (St Clairs curve) [Dunlop et al. 1979].

In recent years, the power system voltage stability has attracted considerable interest in industry. St Clair curve concerns three limiting factors: thermal limit, voltage quality (or drop) limit and angular stability limit [Hao and Xu 2008]. In this research project, the focus is on long lines.

Therefore, voltage stability limit of the line loadability curve is used to estimate the penetration level of ASTV unit(s) on the transmission power line.

Figure 3.18 is a conceptual curve that captures these three attributes of transmission lines (note that the numbers are typical and limits for any particular line may vary). Additionally, the vertical axis is given as a percentage of SIL, simply because SIL provides a convenient characteristic of a transmission line that captures an attribute related to its power handling capability as a function of its physical construction. However, SIL does not capture the influence of length on power handling capability [Dunlop et al. 1979, Glover and Sarma 2002]

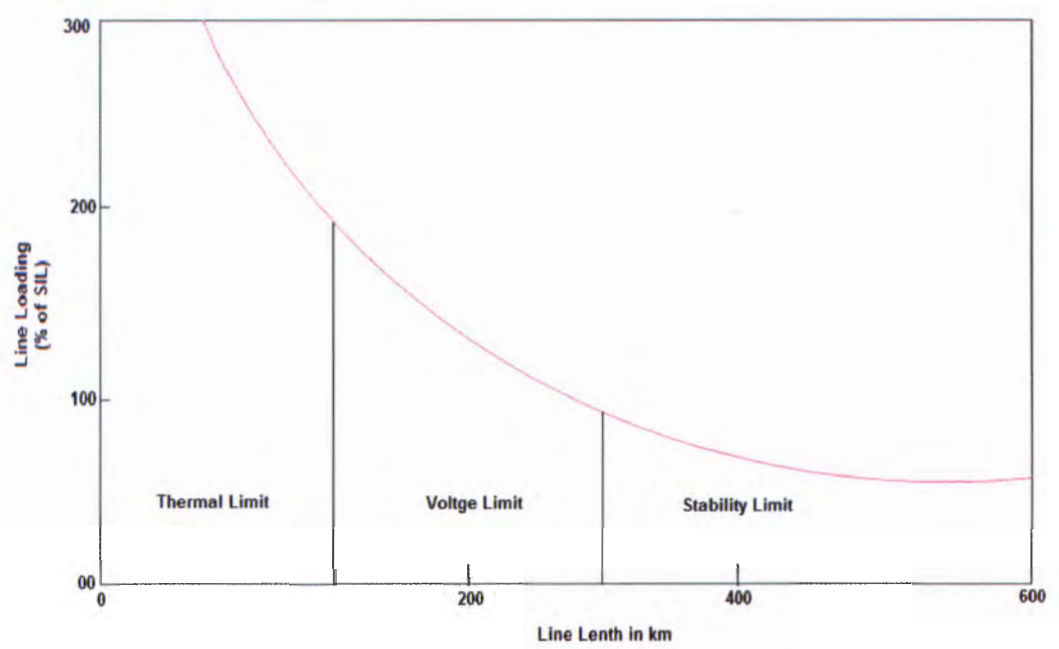

Figure 3.18 Conceptual curve for line loading [Nayak et al. 2006]

Considering Figure 3.18, it can be observed that:

- Power limit decreases with line length
- Short lines are limited mainly by thermal problems.
- Medium length lines tend to be limited by voltage-related problems.
- Long lines tend to be limited by stability problems.

The line under investigation is a 440km line, which falls under the long line category. Hence, voltage instability problems are most likely to affect it. In order to analyze the voltage stability problem it is important to first develop an ideal model as shown in the subsequent section.

3.6.4 VOLTAGE STABILITY LIMIT

A simple system is shown in Figure 3.19 To simplifies the calculation, the voltage phase angle at the receiving end is seen as a reference, and voltage magnitude of the sending end, V_s is constant [Dunlop et al. 1979, Mohamedi et al. 2007, Hao and Xu 2008].

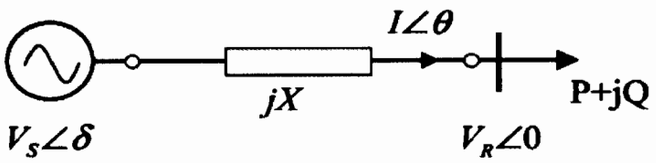

Figure 3.19 System diagram [Hao and Xu 2008]

At the receiving end,

$$V_R I^* = P + jQ \tag{3.54}$$

So, $$I = \frac{P - jQ}{V_R} \tag{3.55}$$

$$V_s = V_R + \left(\frac{p - jQ}{V_R}\right)jX = \left(V_R + \frac{QX}{V_R}\right) + j\left(\frac{PX}{V_R}\right) \tag{3.56}$$

The corresponding magnitude equation is

$$V_S^2 = \left(V_R + \frac{QX}{V_R}\right)^2 + \left(\frac{PX}{V_R}\right)^2 \tag{3.57}$$

The power delivered to the load as a function of receiving end voltage when Q = 0 can be solved as:

$$P = \frac{\sqrt{V_S^2 - V_R^2}}{X} V_R \tag{3.58}$$

Since V_S is constant and close to 1 per unit, and X and V_R are the only variables that can vary, then, when X is constant the power will vary with V_R as shown in Figure 3.20

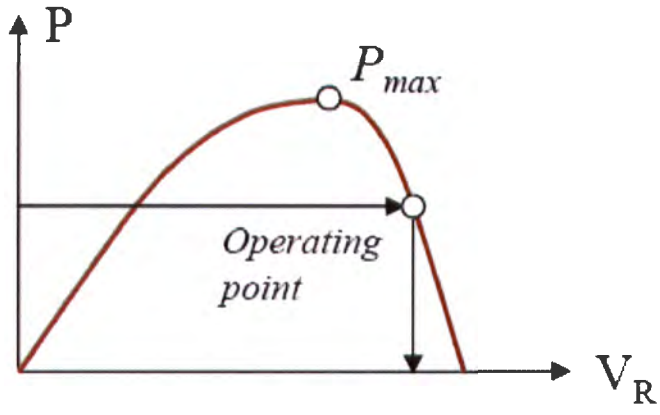

Figure 3.20 Power transfer capability curve [Hao and Xu 2008]

The maximum power that can be transmitted is reached when $dP/dV_R = 0$, which can be determined as;

$$P_{\max\_V_{Stab}} = \frac{V_S^2}{2X} \tag{3.59}$$

The voltage corresponding to equation 3.59 is given by;

$$V_{nose} = \frac{V_S}{\sqrt{2}} \tag{3.60}$$

Where,

V_{nose} is the nose point voltage

Equation 3.59 is the *voltage stability limit* of the power transmission. Considering nominal PI configuration, the transmission scheme and its equivalent circuit can be presented as shown in Figure 3.21.

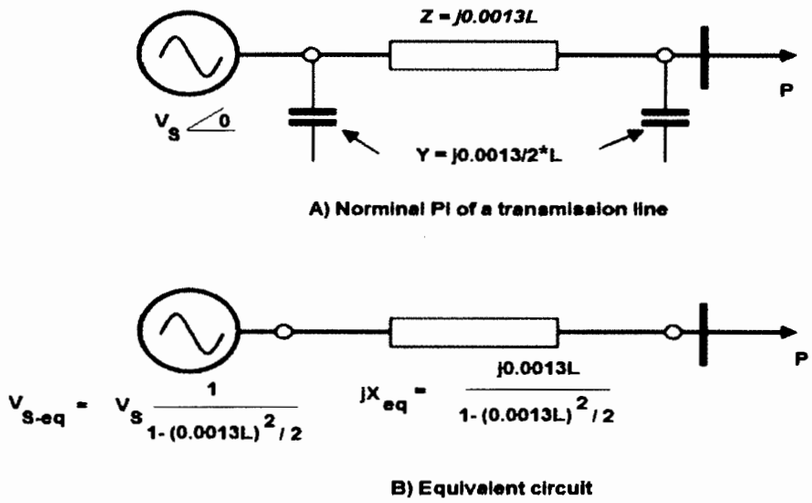

Figure 3.21 Transmission line model and its equivalent circuit [Hao and Xu 2008]

It can be seen from the equivalent circuit, when the line length increases, the open circuit voltage $V_{s\text{-}eq}$ increases accordingly because of the line charge. This is known as Ferranti effect. The effect leads to the increase of the nose point voltage.

We can further deduce from the Figure 3.21 that when the length increases to a specify value the nose point voltage will become higher than the sending end voltage. When this happen it becomes impossible to operate the system at any operating point with acceptable voltage level below the nose point voltage, which is unstable case. The line length at which the nose point will move above the sending end voltage can be determined using the following conditions [Dunlop et al. 1979, Mohamedi et al. 2007]:

$$V_{nose} = V_S \tag{3.61}$$

Assuming that the receiving end Q load is equal to 0 we can establish

$$V_{nose} = \frac{V_{S-eq}}{\sqrt{2}} = \frac{V_S}{\sqrt{2}} \frac{1}{1-(0.0013L)^2/2} = V_S \tag{3.62}$$

Solving the above equation yields

$$L = \sqrt{\frac{2-\sqrt{2}}{(0.0013)^2}} = 588.7km \quad (3.63)$$

This demonstrates that the power transfer capability is limited by voltage stability concern when the line length is greater than 588.7km. Note that this is for an ideal condition.

The transmission capacity of a partcular line is limited by its thermal capacity. However, in case of long high voltage AC lines efficiency of transmission capacity is below its thermal limit and restricted by angular and voltage stability limits which restricts line loadability upto to its Surge Impedance Loading (SIL) level. This is to ensure optimal utilization and efficient use of the transmission infrasructure [Nayak et al. 2006].

The quantum of power that a given high voltage transmission line can safely carry depends on various limits. These limits can be categorised into two types thermal and Stability/Surge Impedance Limit (SIL) limits. In case of long lines the capacity is limited by its SIL level only which is much below its thermal capacity due to large inductance. Decrease in line inductance and surge impedance shall increase the SIL and transmission capacity. Thermal capacity is the ultimate capacity of a line corresponding to its capability to withstand the heat generated due to line loss[Nayak et al. 2006, EPRI TR 1993]. It depends on the;

- type of conductor
- maximum permissable conductor temperature
- ambient coditions
- other enviromental factors

However, traditional line design limits power transfer distance and/or capacity. This is because of large inductive reactance of the transmission line which results into large angular separation and voltage drop between two adjacent nodes which may lead to instability in the system. Subsequently, restricts power transfer capacity of a long line (> 200km) to its SIL level. Hence, the use of SIL to measure penetration level of ASVT unit(s) is applied in this research project.

3.7 PROPOSED METHODOLOGY

This research project has three objectives as illustrated in Figure 1.4 of chapter one. The first objective which is the overall objective of this thesis is to evaluate the adoptability and maximum allowable percentage penetration level of the two sub-station based URE technologies in power networks individually and collectively with regard to voltage quality, stability and capacity constraints without steady and transient state voltage violation. Analysis of results and performance of URE systems will be presented and based on findings; the hypothesis will either be or not validated. It is important to note that the analyses are focused to developing countries with emphasis in sub-Saharan Africa. However, case studies will be done on Kenyan power networks.

The second objective is to determine the maximum allowable percentage penetration level of CCS in power networks with regard to voltage quality, stability, and capacity constraints without steady state voltage violation. This objective is to be achieved by first carrying out repetitive power flow simulations as will be shown in chapter 4. System energisation at no-load and load on/off will be carried out. Simulations are first done with the line not loaded, followed by a loaded line and finally the line under short circuit conditions. Voltage and power variable constraints will be taken into considerations. The CCS units are included at different distances. The line is cascaded with pi sections to increase the speed of convergence and reduce delays in the MATLAB SimPower software used. Ode 23t, an integration algorithm (Runge and Kutta 2^{nd} &3^{rd} Order) and a stiff solver will be used for simulation.

Subsequently, repetitive power flow simulations carried out in the case studies of chapter 4 will be validated using the voltage sensitivity analysis as described in chapter 5. This study uses a method of determining maximum allowable penetration level of CCS without steady state voltage violation derived from a modified distributed generation analogy. The method is based on determination of voltage sensitivities from linearized power system model.

The third objective is to determine the maximum allowable percentage penetration level of ASVTs in power networks with regard to voltage quality, stability, and capacity constraints without steady and transient state voltage violation. This objective will be achieved by first designing an ASVT using the reverse design approach developed in section 3.5. System energisation at no-load and load on/off are carried out similar to the CCS system. Simulations will first be done with the line not loaded, followed by a loaded line and finally the line under short circuit conditions. Voltage and power variable constraints will be taken into considerations. The ASVT units are included at different distances as shown in chapter 6.

The line is cascaded with pi sections to increase the speed of convergence and reduce delays in the MATLAB Sim Power software used. Loadability analysis is also done to show the variation of the voltage profile with load power (MW) at different power factors.

The line parameters of the line under study are first determined using the method described in section 3.6.2 based on the ABCD parameter determination. The SIL curve is then constructed centered on these parameters and compared to the loadability simulation results presented in chapter 6. This comparison will then be used in chapter 7 to estimate the maximum penetration level of the ASVT in the power network. This will be done with regard to the voltage quality and stability constraints limitations.

3.8 ONWARD

Most rural areas in SSA remain the main source of raw materials, agricultural products and cheap human labour. Therefore, availability of reliable electricity in these areas is a great concern to most governments. Although, most of these governments are willing to support electrification programmes, other competing needs like reliable water supply, health, and education becomes an impediment to electrification. The application of CCS and ASVT sub-station technologies is aimed at providing a cheaper and reliable alternative means of electricity supply to areas where the high voltage transmission lines passes through and are yet to be electrified. With envisaged development in SSA countries and especially in Kenya, the theory developed for the two options of URE sub-station technologies offers opportunities to carry out some good fundamental research in this area. The next chapter presents the case study for CCS technologies when integrated into transmission power networks.

4 CAPACITOR COUPLED SUB-STATIONS IN POWER NETWORKS (CASE STUDY)

4.1 INTRODUCTION

It is important to accurately model and analyze distribution systems. There are many different sub-station designs possible. Sub-stations serve one or more radial feeders. Each feeder must be modeled as accurately as possible in order for analysis to present valid results. Sometimes the most difficult task for the designer/engineer is to acquire all the necessary data.

In this chapter actual data collected (Appendix A and B) are used to model multiple configurations of a real power network in Kenya with varying topologies. The configurations are derived from the models developed in chapter 3. The 3phase, 220kV line is modeled per phase for the purpose of this study. The 440km (Kiambere – Rabai) line under study has generation at both ends, with load capacity of 210MVA.

4.2 SIMULATION SOFTWARE FOR CASE STUDY

The simulation circuits shown in this chapter are built using SimPowerSystem which work together with Simulink in MATLAB software environment to model transmission line networks. SimPowerSystem are design tool that provide a modern design tool that will allow scientists and engineers to rapidly and easily build models that simulate power systems. SimPowerSystem uses the Simulink environment, allowing a model to be built using simple click and drag procedures.

Not only can you draw a circuit topology rapidly but your analysis of the circuit can include its interactions with mechanical, thermal, control and other disciplines. This is possible because all the electrical parts of the simulation interact with the extensive Simulink modeling library. Since Simulink uses MATLAB as the computational engine, designers can also use MATLAB toolboxes and Simulink blocksets.

The power system block set allows you to build and simulate electrical circuits containing linear and non-linear elements. The circuits drawn in this chapter represent the 220kV, 440km, long Kiambere- Rabai transmission line in Kenya.

Figure 4.1 [mathwork.com 2008], shows an interface of electrical circuit with Simulink. The voltage measurement block acts as an interface between Power System Blockset (PSB) and the Simulink blocks.

The voltage measurement blocks convert the measured voltage into Simulink signals. Note that the current measurement block from the measurement library of *powerlib* can also be used to convert any measured current into a Simulink signal.

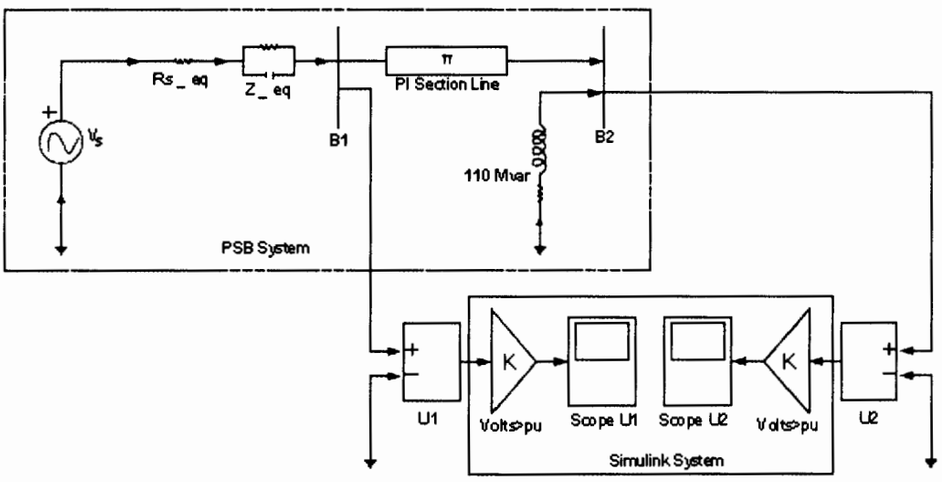

Figure 4.1 Interfacing electrical circuits with Simulink

4.2.1 SIMULATING TRANSIENTS

One of the main uses of Power System Blockset is to simulate transient in electrical circuits. This can be done either with mechanical switches (circuit breakers) or switches using power electronics devices. The circuit breaker is a non-linear element modeled by an ideal switch in series with resistance. Because of modeling constraints, this resistance cannot be set at 0. However, it can be set to a very small value, say 0.001Ω, that does not affect the performance of the circuit.

Figure 4.2 [mathwork.com 2008], shows a power system blockset for transient simulation. A circuit breaker is inserted in order to simulate the line.

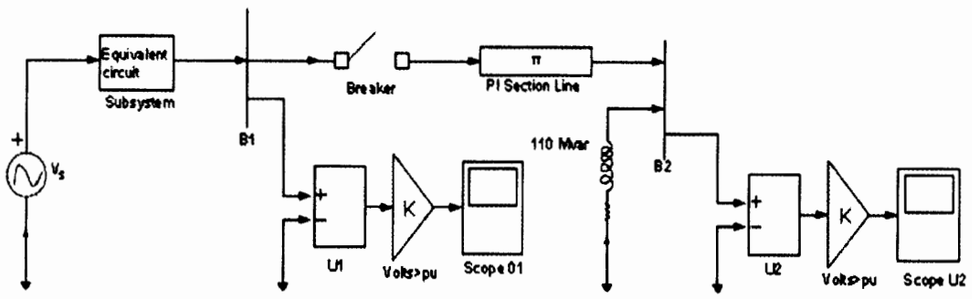

Figure 4.2 transient simulation circuits

The waveforms for sending and receiving end voltages are observed in scope U1 and U2 respectively. The line is cascaded with pi sections to increase the speed of convergence and reduce delays in the MATLAB SimPower software used. Ode 23tb, an integration algorithm (Runge and Kutta 2^{nd} &3^{rd} Order) and a stiff solver is used for simulation. Ode 23tb is fast and accurate with tolerance of 10^{-4}.

4.3 SIMULATION SCENARIOS

System energisation at no-load and load on/off were carried out. Simulations were first done with the line not loaded followed by a loaded line and finally the line under short circuit or transient conditions. Voltage and power variable constraints were taken into considerations. The CCS unit(s) was included at different distances. Simulations scenarios with different configurations of the system were carried out to investigate the transmission systems steady and transient state behavior. The CCS units were subjected to the same loading conditions and ratings as follows;

- Actual Load of transmission line - 125MW.
- Transformer rating - 70kVA.
- CCS heavy Load – 100kW.
- CCS Light Load – 1kW.
- C_1 – Varying between 0.12 to 0.5 μF.
- C_2 –Varying between 0.4 to 1.5 μF
- L Varying between 2.5 to 5.071H

- Occasionally switching on/off the 10MVAr reactor.

Different system configurations for simulations were classified as follows;

- Models with CCS and without FSC and load at steady and transient states
- Models without CCS for unloaded and loaded conditions
- Models with CCS and FSC for unloaded and loaded conditions
- CCS with FSC at different distances with line unloaded and loaded
- CCS with FSC models for transient stability cases.

Loadability analysis was also done to show the variation of the voltage profile with load power (MW) at different power factors. The steady state simulations focused and analyzed three main voltage points on the system, namely;

- Tap-off voltage (V_T), the point at which voltage is tapped on the transmission line.
- Voltage divider (V_D), the voltage between the capacitor bank C_1 and C_2 or voltage at the capacitive divider point.
- Load terminal voltage (V_L) is the voltage at the load point.

4.4 MODEL WITH CCS AND WITHOUT FSC AND LOAD AT STEADY AND TRANSIENT STATES

4.4.1 CCS MODEL WITHOUT THE FSC AND LOAD AT STEADY STATE

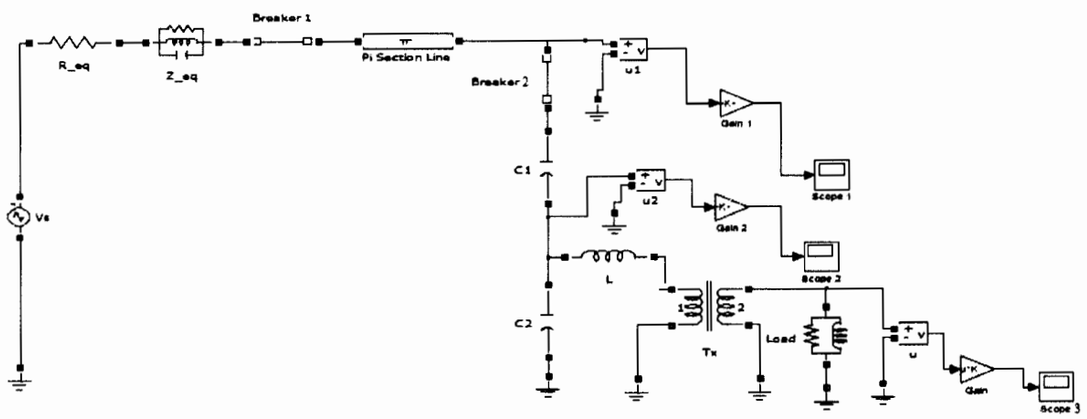

Figure 4.3 Model for the line with one CCS and without FSC

Figure 4.3 shows a sample model for the line with one CCS and without FSC used for steady state simulation scenario. Scope 1 measured the tap off voltage (V_T), while scope 2 measured voltage at the capacitive divider point (V_D) and scope 3 measured the load voltage (V_L). It is important to note that, the position of the CCS did not change the result for one CCS penetration. Appendix D1 and D2 shows the same model with two and three CCS penetration respectively. For the purpose of this research the CCS were assumed to be located with uniform distance. Table 4.1 presents the measured steady state voltages at different points on the system and at various CCS penetration distances.

Table 4.1 Summary of voltages measured at different point in the model

Length of Transmission line in Kilometers										
No of CCS	**Voltage in kV**	48.88	97.77	146.66	195.55	244.44	293.33	342.22	391.11	440.00
1	V_T									153.33
	V_D									38.332
	V_L									0.2388
2	V_T				148.12					177.51
	V_D				37.032					44.377
	V_L				0.232					0.246
3	V_T			141.84			150.08			153.42
	V_D			35.462			37.521			38.312
	V_L			0.221			0.2337			0.2389
4	V_T		138.9		146.64		151.84			154.81
	V_D		34.724		36.656		37.964			38.703
	V_L		0.216		0.223		0.237			0.241
5	V_T	130.4		131.73		132.69		133.27		133.46
	V_D	32.600		32.933		33.173		33.239		33.365
	V_L	0.203		0.205		0.2063		0.2072		0.2075

In appendix D1 each pi section represented 220km while in appendix D2 each pi section represented 147km. It was important to note that the value of C_1 C_2 and L used were derived from the values developed in chapter three. The values of C_1 C_2 and L could be varied to give different voltage measurements as long as the allowable voltage violation limit of 240V with ± 2.5% at the load terminal (V_L) was not surpassed for the low voltage side. However, for the high voltage side, that is the tap-off (V_T) and divider voltage (V_D), the allowable voltage violation was 6% of the nominal voltage. Therefore, with respect to Table 4.1, allowable tap-off voltage (V_T) and divider voltage (V_D) ranges between (119.38 to 134.62kV) and (31.02 to 34.98kV) respectively. While, the load terminal voltage (V_L) ranges between (0.234 to 0.246 kV).

Five configurations of the models were considered during simulation, ranging from a single CCS penetration at the end terminal of the transmission line to five CCS penetrating the system. Different arrangements at specific distances on the transmission line were considered and measurements taken as shown in table 4.1. The CCS simulation results showed that the tap-off voltage (V_T) on the transmission line reduced as the number of CCS penetration increased. The tap-off voltage drop of the five CCS units connected on the transmission line conformed to the allowable voltage drop. .Thus, no voltage compensation technique was required for the five CCS units penetration at steady state. This meant that the system was self-compensated for this scenario. Even though, at lower penetration of CCS units (i.e. 1 to 4 units), the voltage magnitude was slightly higher and above the acceptable range.

Therefore, in such instance compensation was necessary. Interestingly, the divider voltage (V_D) and the tap-off voltage (V_T) seemed to be within the allowable voltage drop for all the five configurations. Although, for the same scenario load voltage (V_L) was below the acceptable value. In summary it was observed that penetration of five CCS units can be adopted for this scenario as long as a tap changing transformer is installed at the output of the system to mitigate the low voltage on the load side. Therefore, five CCS units penetration gave the most probable acceptable voltage profile for the steady state scenario with FSC and unloaded condition.

4.4.2 CCS MODEL WITHOUT FSC AT TRANSIENT STATE

Transient state means any sudden change in a circuit, as a result of disturbance. This may occur during switching (closing or opening of a circuit), short circuit or even saturation. In this case the transient state condition was simulated by the use of switching on/off a circuit breaker and injecting a disturbance signal. Figure 4.4, below shows the layout of the CCS system model used for simulating transient conditions including monitoring instruments and disturbance (signal 1-4) injected.

The resulting transients after disturbance signal injection are presented in Figure 4.5 to 4.8 (a-e) for each signal injected. The waveform measurements were displayed out as follows;

Scope 1 measured the tap off voltage (V_T)

Scope 2 measured the divider voltage (V_D)

Scope 3 measured the system current

Scope 4 measured the load current

Scope 5 measured the load voltage (V_L)

It is important to note that, all the graphs in this section are labeled in the following manner. Graph (c) and (d) waveforms represent graphs of current against time in (seconds) and graphs (a), and (e) waveforms are graphs of per unit kilovolt (kV) against time (seconds). Graph (b) waveform is a graph of kilovolt (kV) against time (seconds)

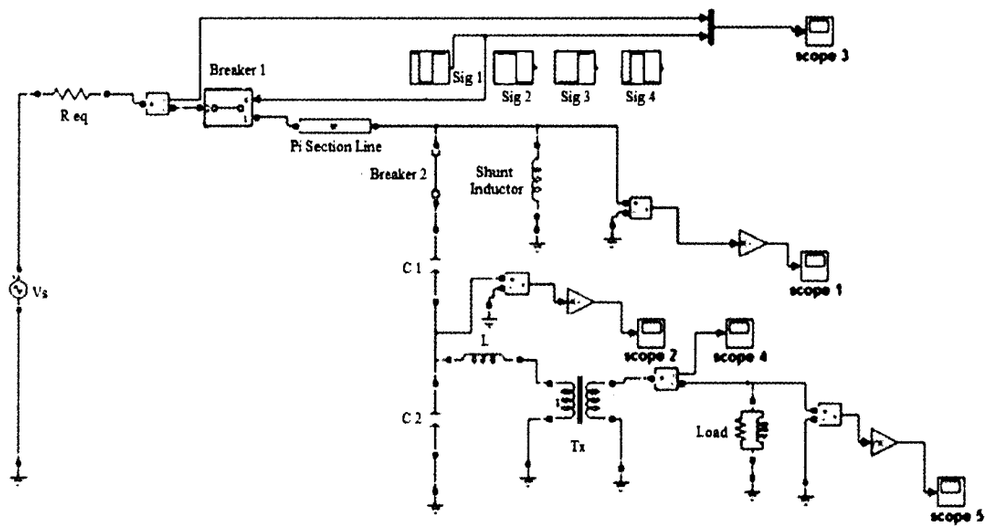

Figure 4.4 Model for the line with one CCS and disturbance

Signal 1

In this case the breaker device was initially closed, an opening command was given at t = 5 cycles and then ordered to close again at t = 15 cycles. When the system was switched off, a spike current of about 10 times normal system current and about 8 times normal system current when switched on was observed see Figure 4.5(c).

Additionally, a voltage overshot of about 1.3 time's normal tap-off voltage when the system was switched on or off was also observed. Further, the effect of switching resonance was clearly depicted on the system current and tap of voltage waveforms. Load current and load voltage waveform were observed to be in phase.

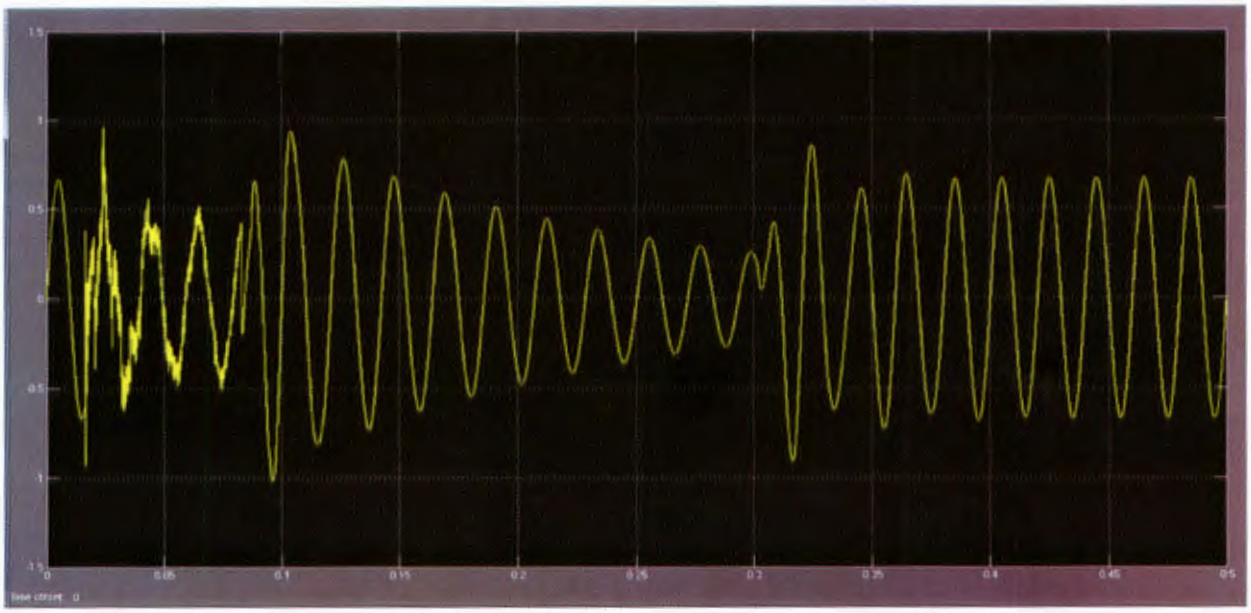

TAP-OFF VOLTAGE WAVEFORM (SCOPE 1)

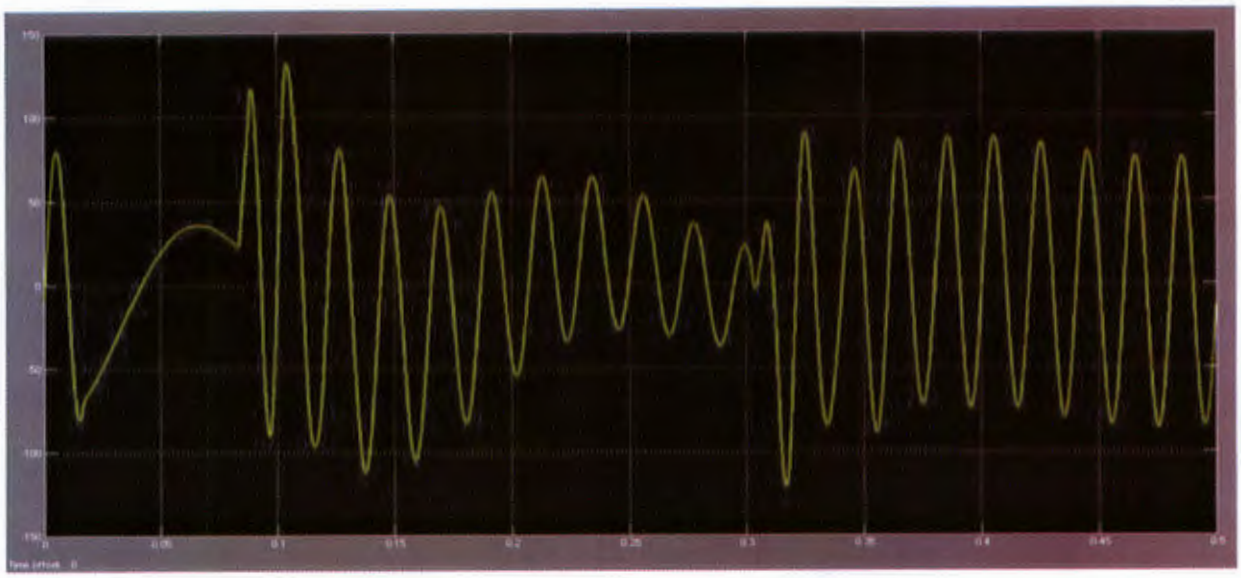

DIVIDER VOLTAGE WAVEFORM (SCOPE 2)

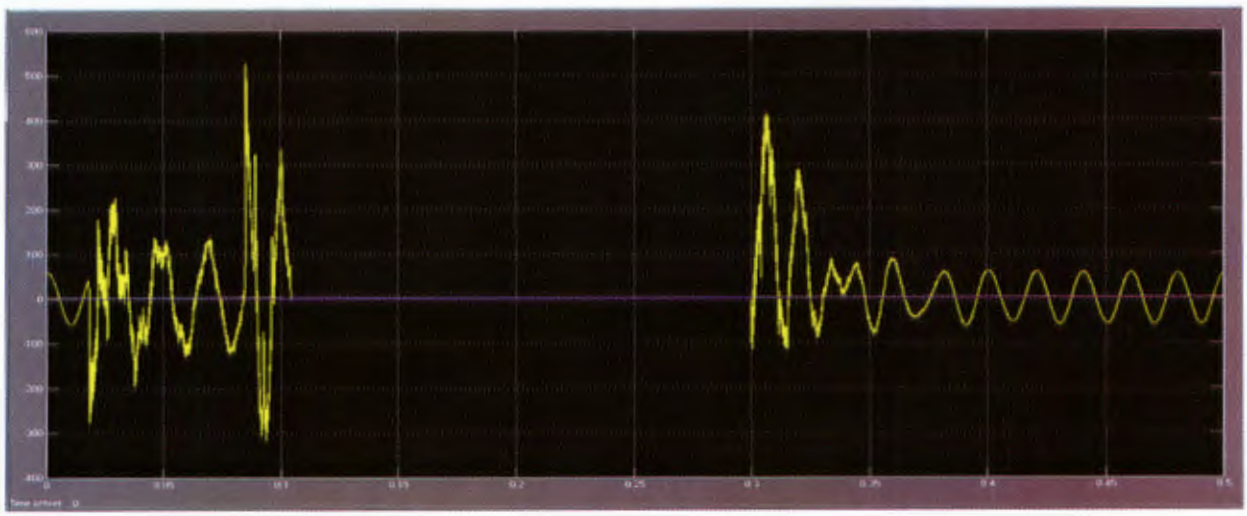

SYSTEM CURRENT WAVEFORM (SCOPE3)

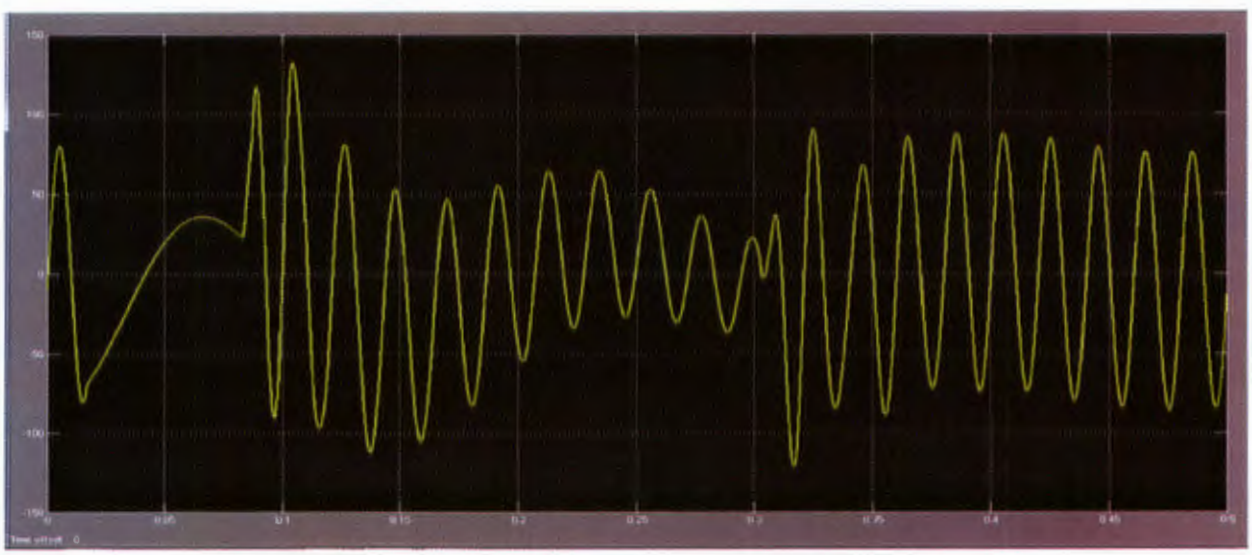

(D) LOAD CURRENT WAVEFORM (SCOPE 4)

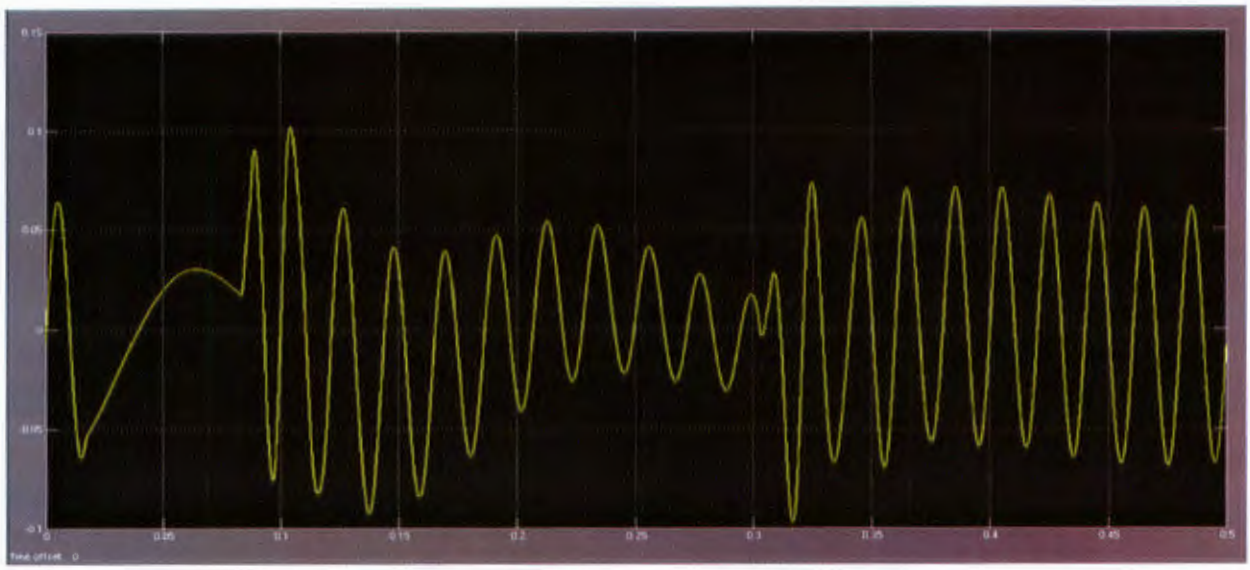

(E) LOAD VOLTAGE WAVEFORM (SCOPE 5)

Figure 4.5 Waveforms for Signal 1 Injection

Signal 2

The breaker device was initially closed and opening order was given at t = 15 cycles. Figure 4.6 (c) exhibits spike current at t = 5 cycles point of about 10 times the normal system current and an overshot voltage of about 1.5 times normal tap-off voltage. Ferro-resonance effect was observed on the divider voltage, load current and load voltage waveform but cleared out gradually after some cycles.

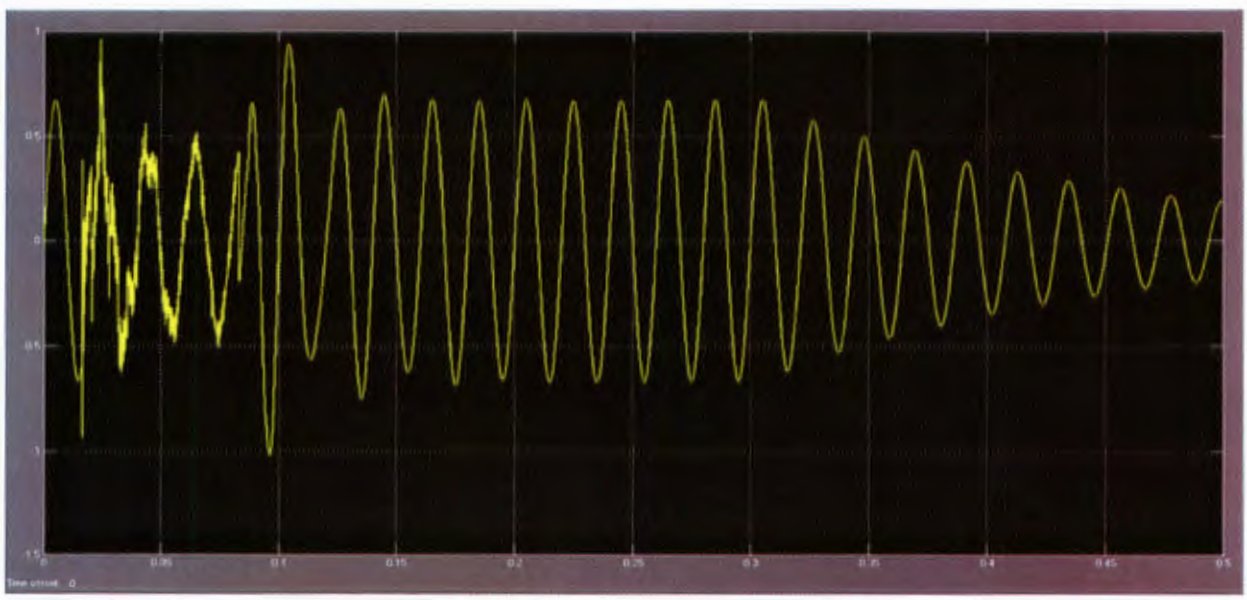

TAP- OFF VOLTAGE WAVEFORM (SCOPE 1)

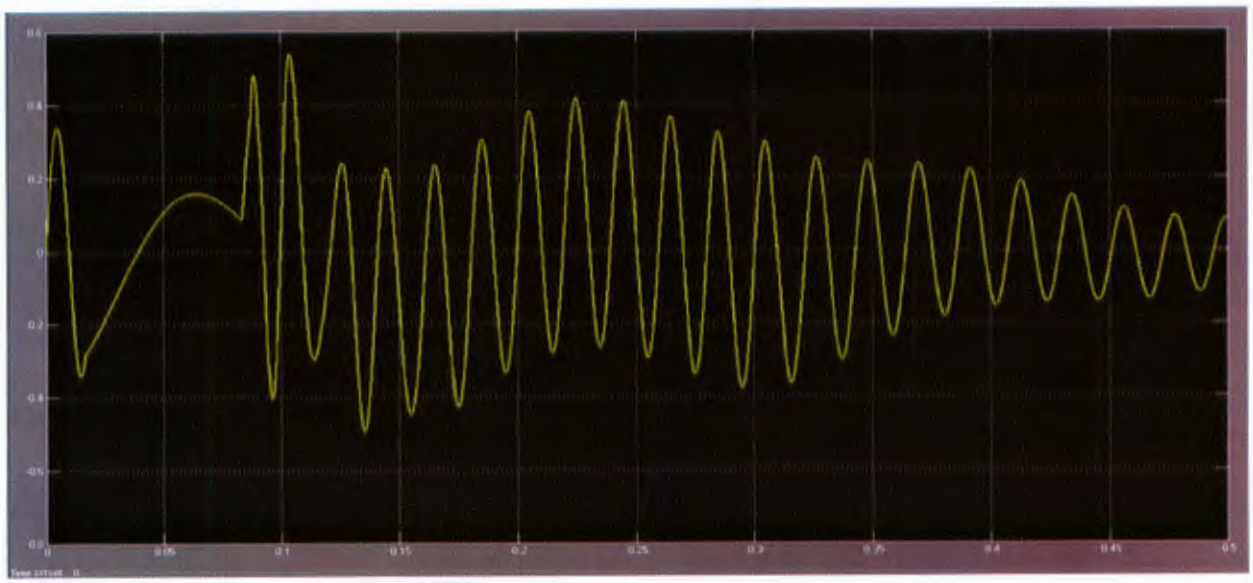

(B) DIVIDER VOLTAGE WAVEFORM (SCOPE 2)

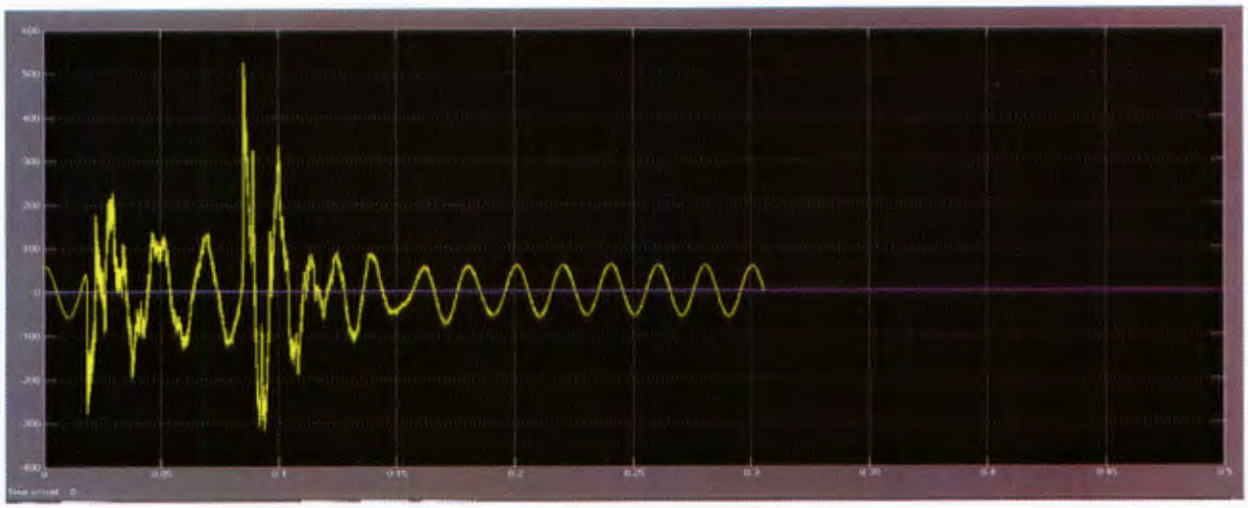

(C) SYSTEM CURRENT WAVEFORM (SCOPE 3)

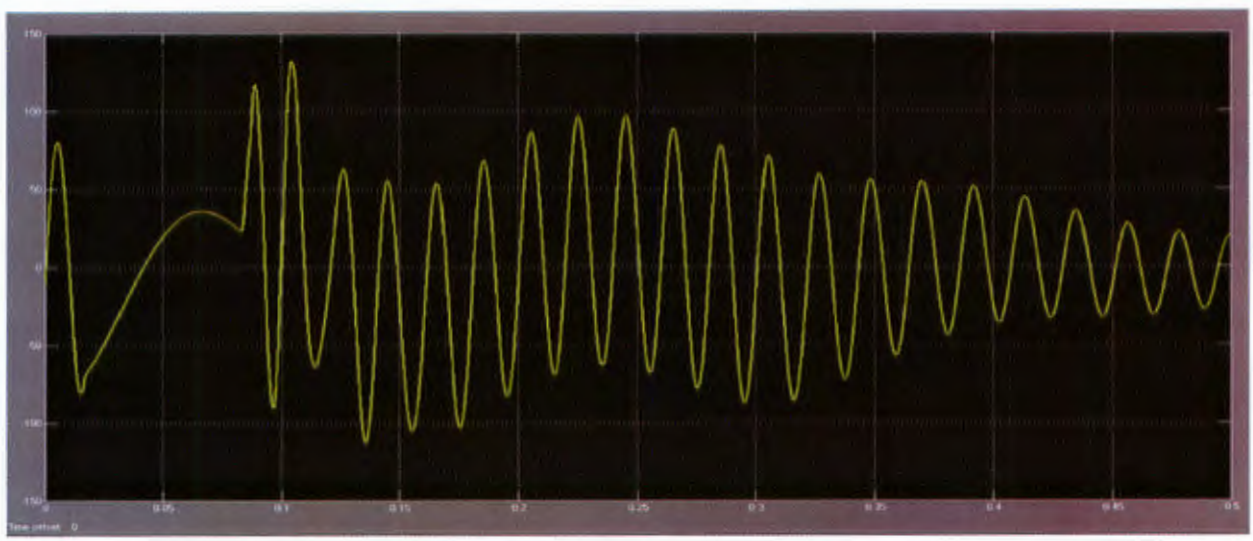

(D)LOAD CURRENT WAVEFORM (SCOPE 4)

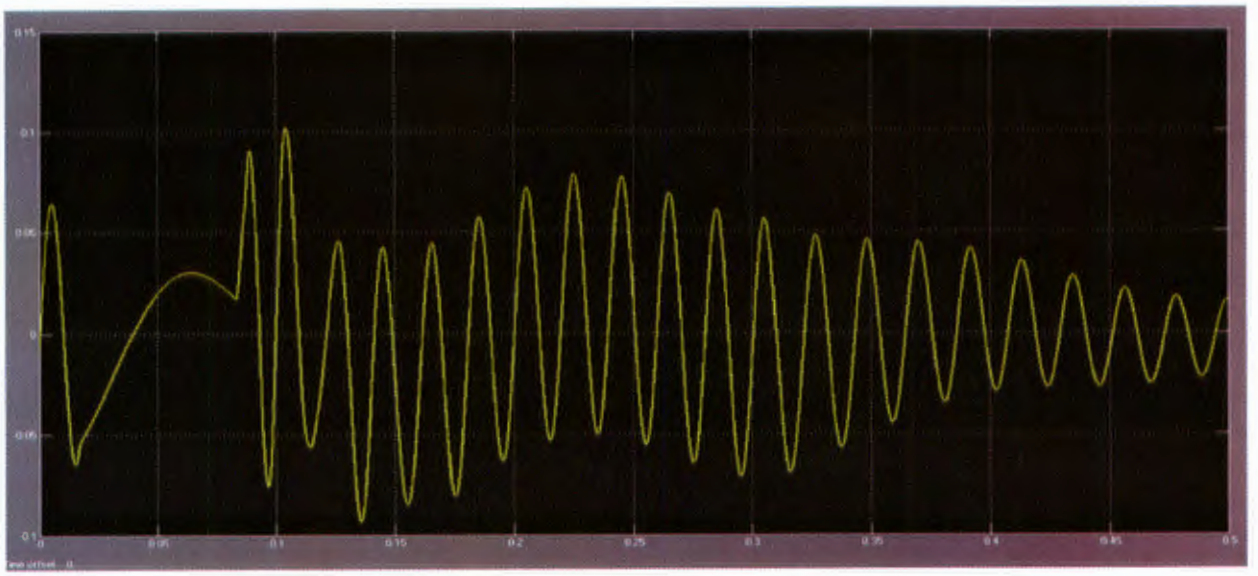

(E) LOAD VOLTAGE WAVEFORM (SCOPE 5)

Figure 4.6 waveforms for signal 2 injection

Signal 3

In this scenario, when the model was simulated the breaker device was initially off and closing order was given at t = 15 cycles. A spike current of about 7 times the normal system current and voltage overshot of about 1.5 times the normal tap-off voltage were observed. Ferro-resonance effect was experienced on the load voltage, load current and divider voltage waveforms as shown in Figure 4.7 (a-e)

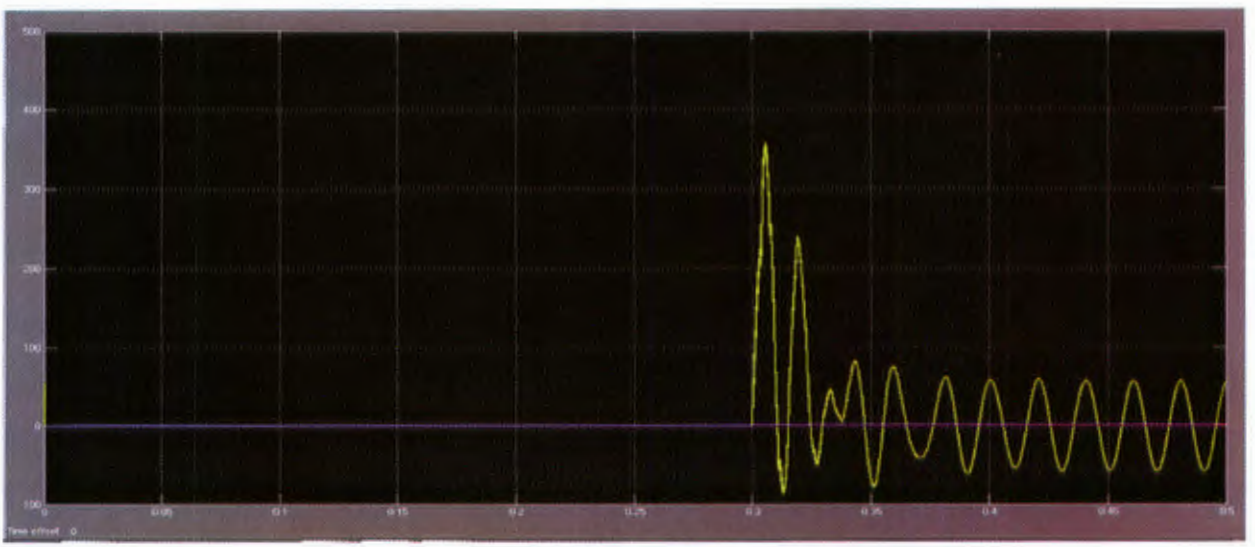

(A) TAP-OFF VOLTAGE WAVEFORM (SCOPE 1)

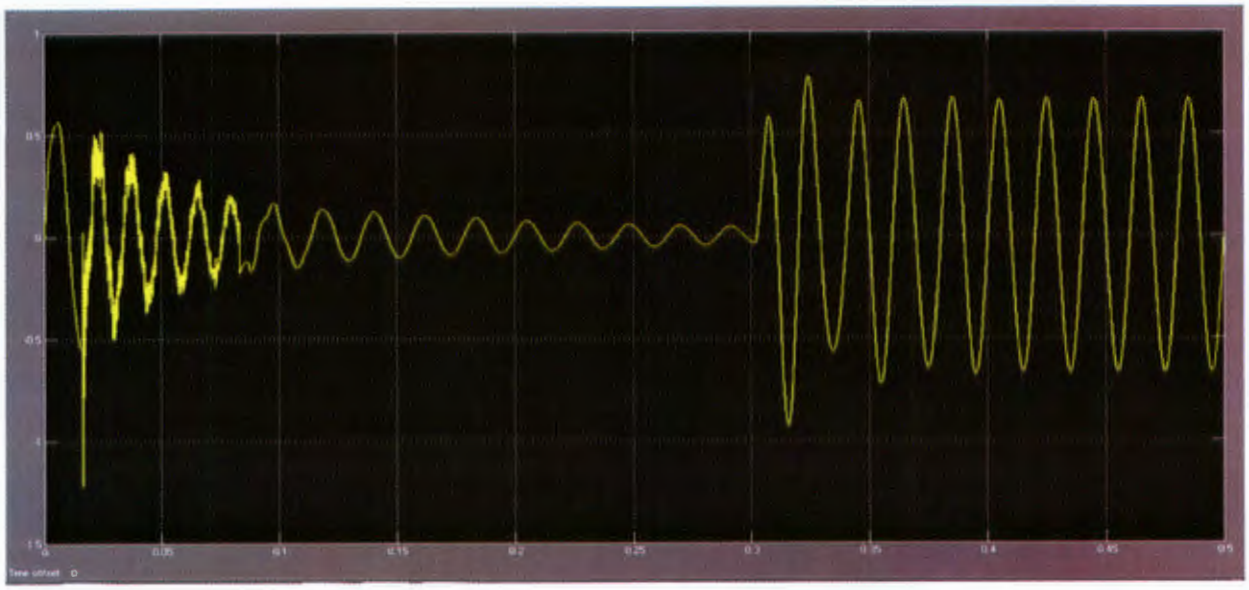

(B) DIVIDER VOLTAGE WAVEFORM (SCOPE 2)

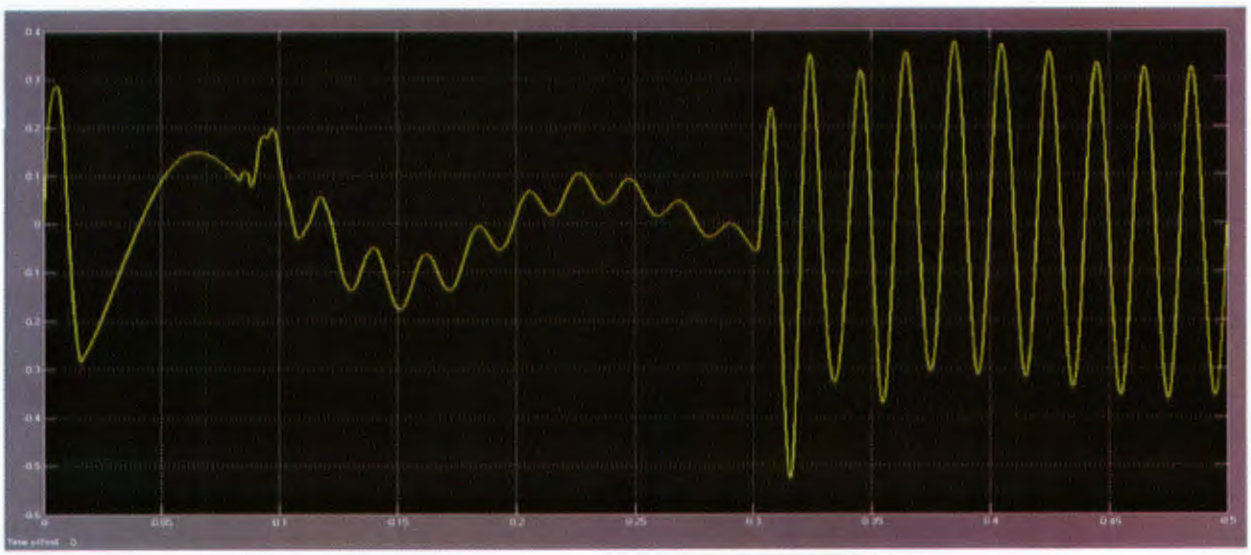

(C) SYSTEM CURRENT WAVEFORM (SCOPE 3)

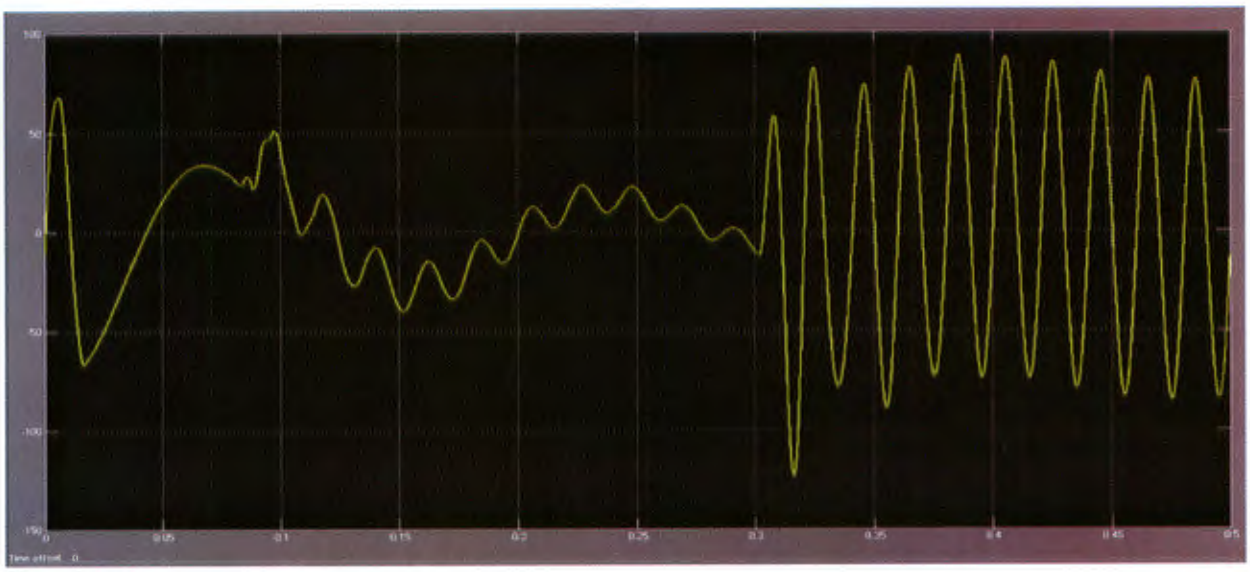

(D)LOAD CURRENT WAVEFORM (SCOPE 4)

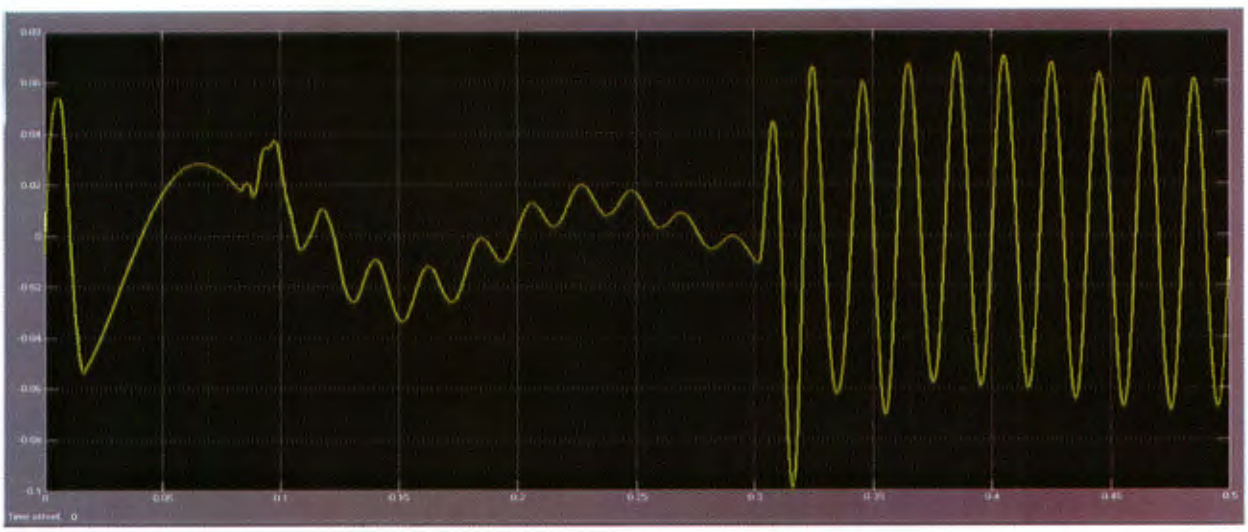

(E) LOAD VOLTAGE WAVEFORM (SCOPE 5)

Figure 4.7 Waveforms for signal 3 injection

Signal 4

The breaker device in this case was initially off and closing order was given at t = 5 cycles and then commanded to open at t = 15 cycles.

Figure 4.8, illustrates the spike current of about 8 time's normal system current and about1.5 time's normal tap-off voltage. Effect of Ferro-resonance was observed on the divider voltage, load current and load voltage waveforms but cleared out gradually after some cycles

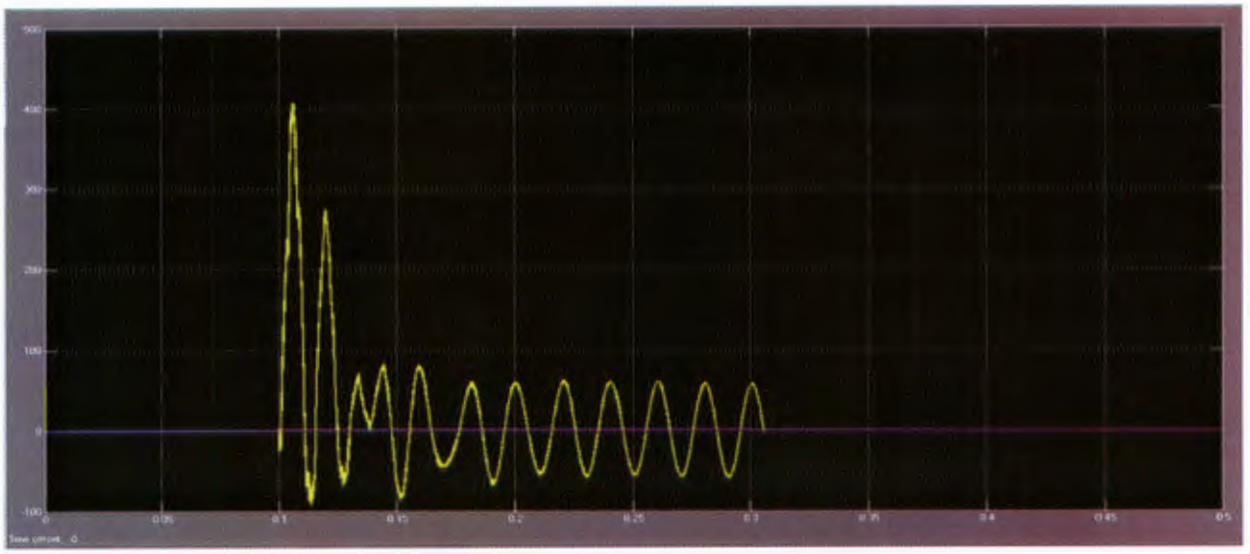

(B) TAP-OFF VOLTAGE WAVEFORM (SCOPE 1)

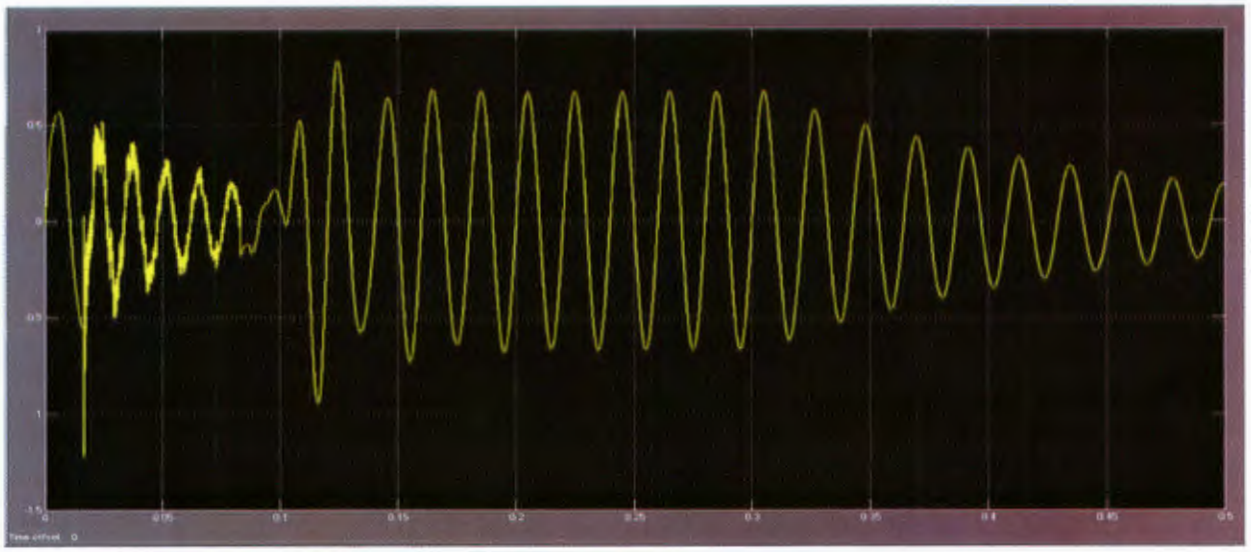

(B) DIVIDER VOLTAGE WAVEFORM (SCOPE 2)

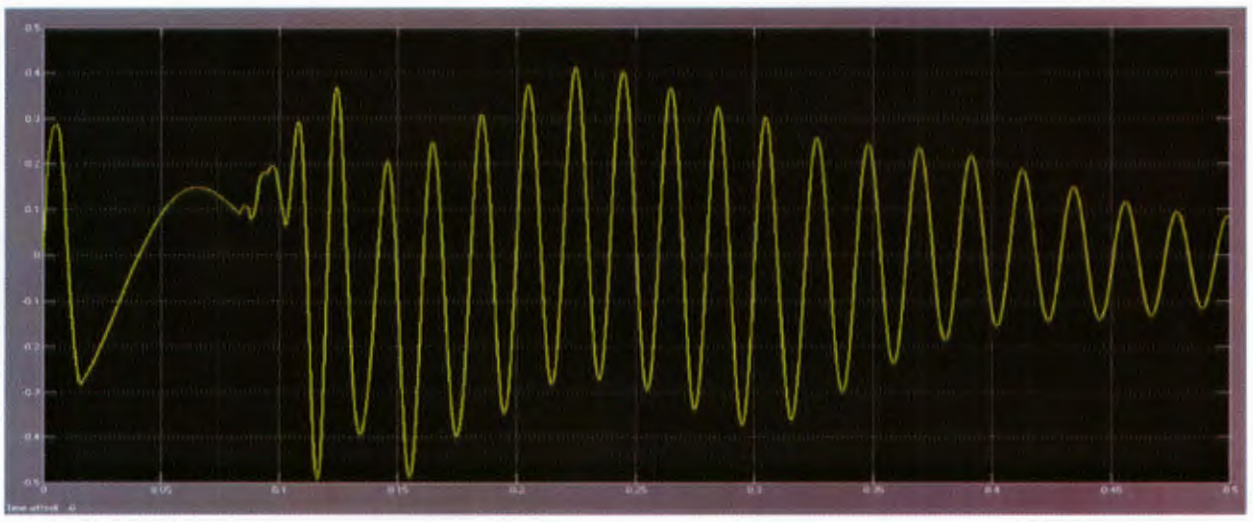

(C) SYSTEM CURRENT WAVEFORM (SCOPE 3)

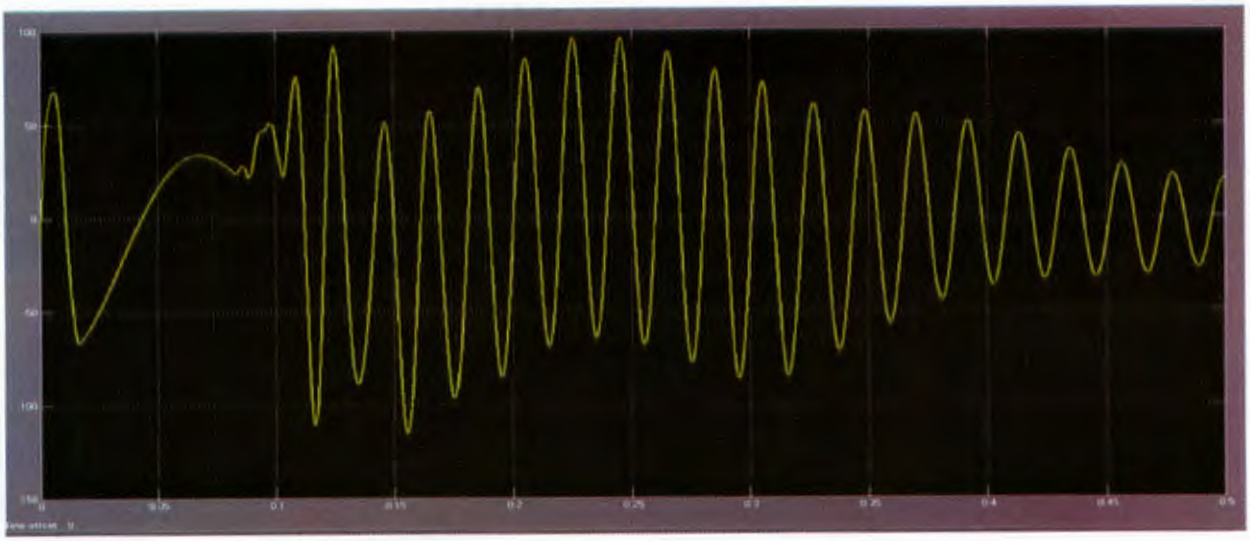

(D)LOAD CURRENT WAVEFORM (SCOPE 4)

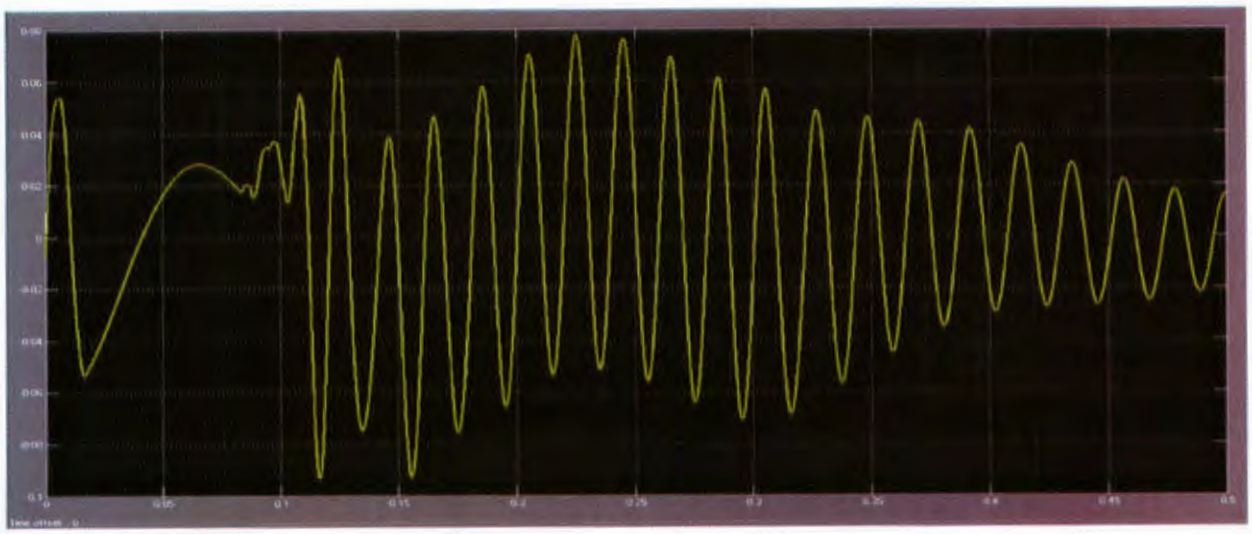

(E)LOAD VOLTAGE WAVEFORM (SCOPE 5)

Figure 4.8 waveforms for signal 3 injection

4.5 MODEL WITHOUT CCS FOR UNLOADED AND LOADED CONDITIONS

4.5.1 WITHOUT CCS AND UNLOADED

In this case, we consider steady state behavior of the line voltage without the CCS installed. The simulations were carried out with the line not loaded. The model is shown in Figure 4.9. It is important to note that the font looks smaller which was a direct output from the software and presents the system configuration.

Figure 4.10 (a) and (b) shows simulated voltage waveforms for the sending and receiving end voltage. The y-axis on the graph shows the voltage magnitude in kV while the x-axis shows the time in seconds on a scale of 0.02seconds representing one segment or cell.

It was observed that both the sending end and receiving end voltage experienced some switching resonance effect as seen in Figure 4.12 (a) and (b). It can be seen that the switching resonance is more intensive at the receiving end. The HV voltages are 148.92kV and 131.64kV respectively. Considering per phase value of ±6% of 127kV, an over shoot for one case was noted.

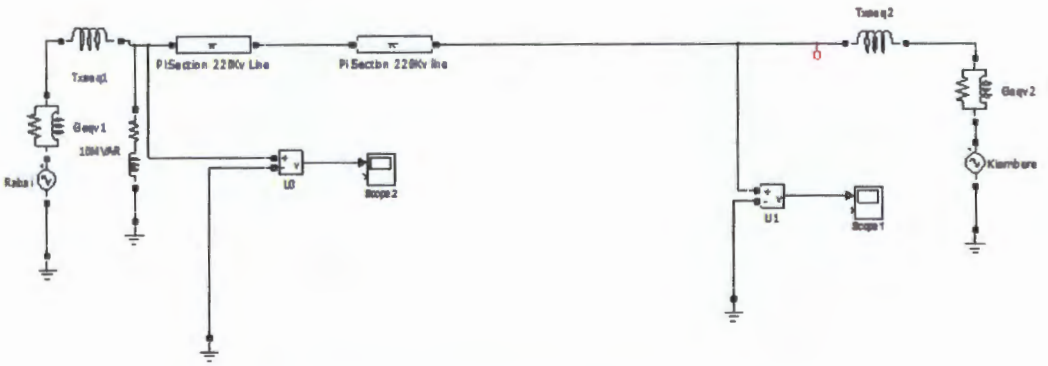

Figure 4.9 Model for the line without load and CCS

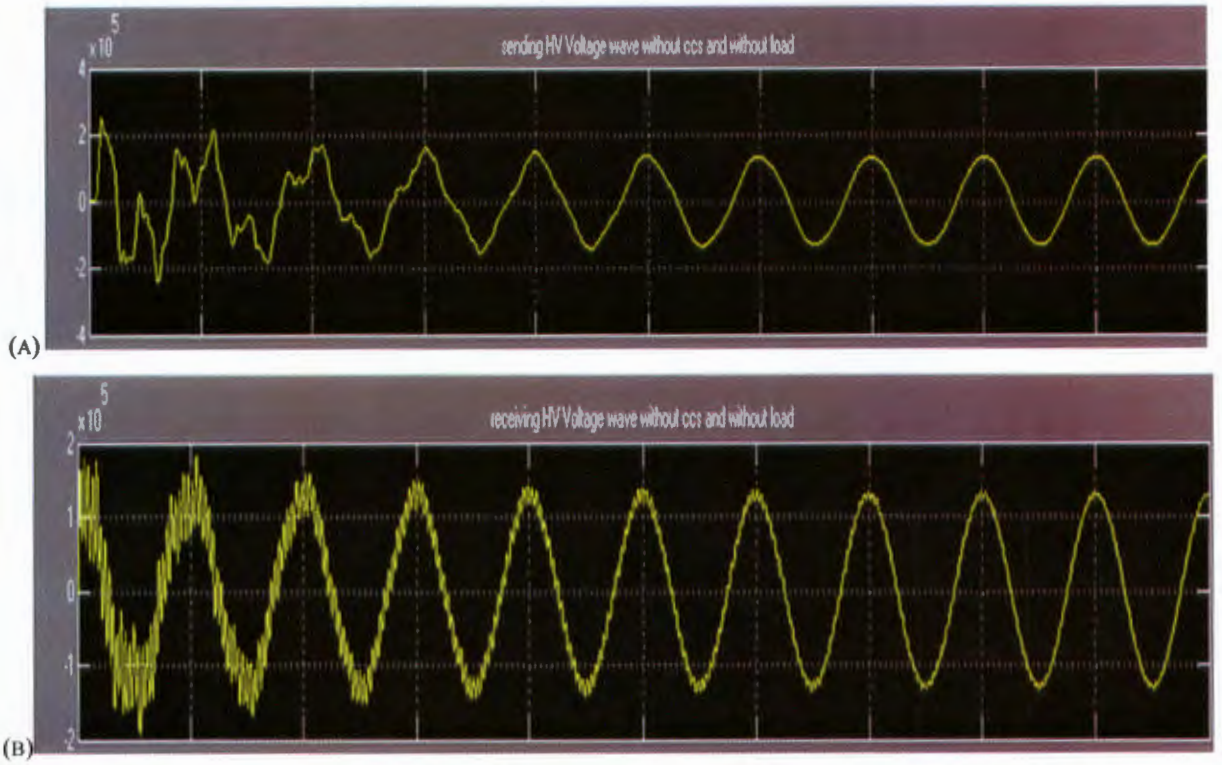

Figure 4.10 Sending and receiving voltage waveform for line without load and CCS

4.5.2 WITHOUT CCS BUT WITH LOAD

In this case, we still considered steady state behavior of the line voltage with a load of 125MVA at unity power factor that is 125MW but without the CCS. The model is shown in Figure 4.11. Figure 4.12 (a) and (b) shows simulated voltage waveforms for the sending and receiving end voltage. It was observed that the sending end voltage experiences some mild switching resonance effect as seen in Figure 4.12 (a). The receiving end voltage does not experience any switching resonance effect. The HV voltages are 145.96kV and 129.64kV respectively. The over shoot was still experienced in one case.

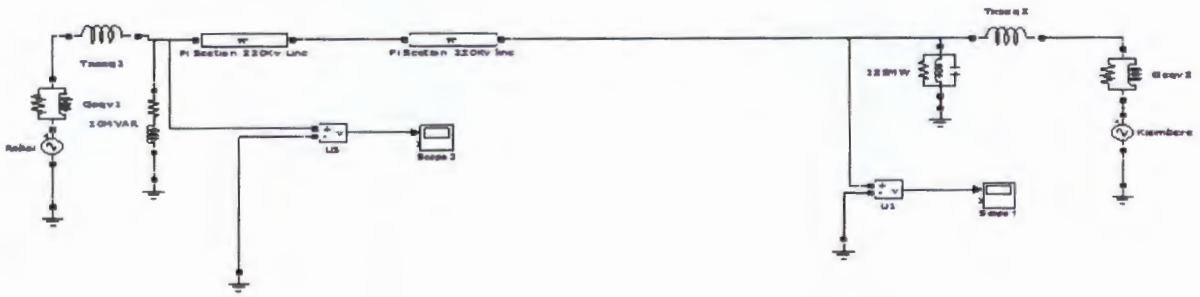

Figure 4.11 Model of the line with load and without CCS

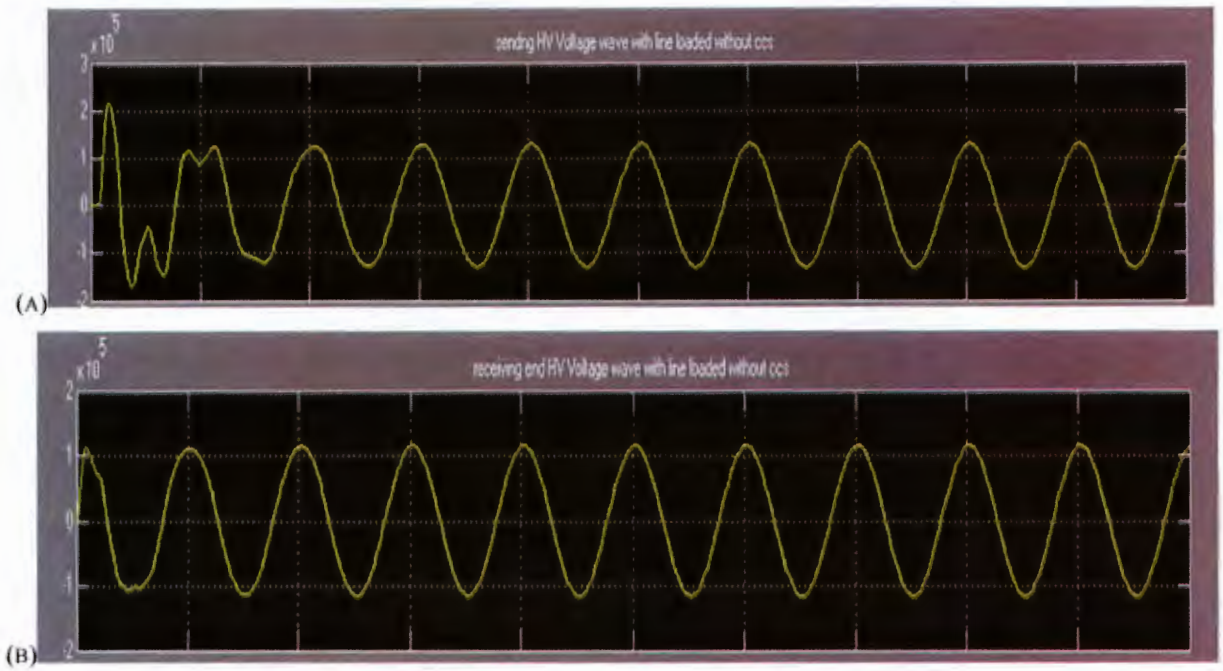

Figure 4.12 Sending and receiving voltage waveforms for line with load and without CCS

4.6 MODELS WITH CCS AND FSC FOR UNLOADED AND LOADED CONDITIONS

4.6.1 CCS AND FSC FOR UNLOADED LINE

Figure 4.13 shows the model with a CCS and FSC introduced midway the unloaded line length. The size of the CCS used in this case was derived from chapter 3. Different sizes of CCS may be considered, but for consistency the sizes derived for C_1 and C_2 were used. It was observed from the simulation results that the sending end voltage experiences some switching resonance that lasts for two cycles as seen in Figure 4.14. The HV voltages are 145.96kV and 129.64kV respectively. The over shoot was still experienced in one case.

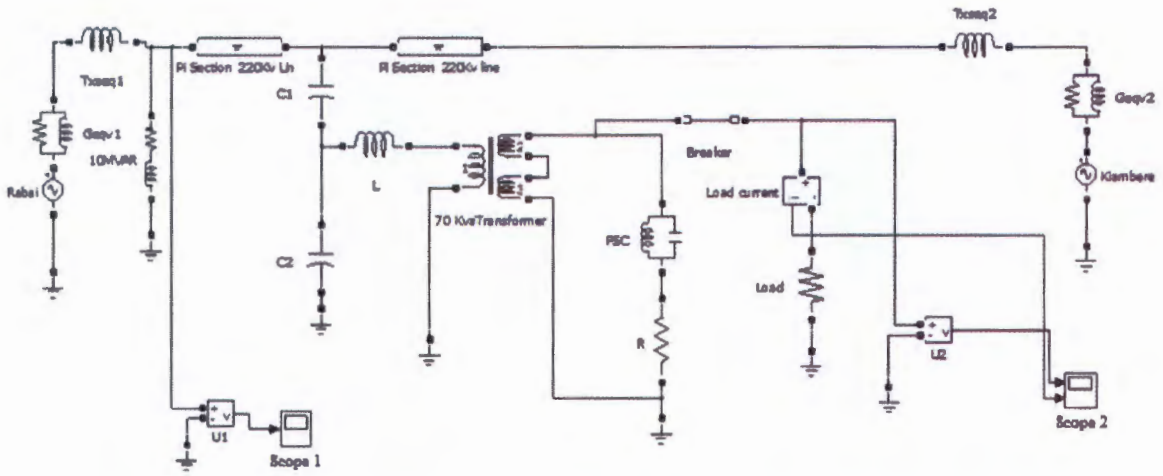

Figure 4.13 Models with CCS midway between the line and without Load

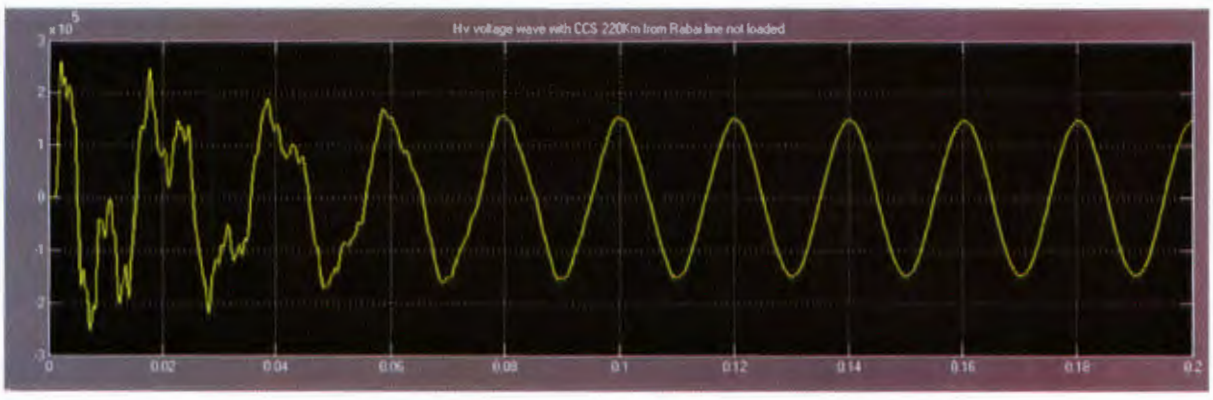

Figure 4.14 Simulation for HV voltage wave with CCS midway the unloaded line

4.6.2 MODEL WITH CCS WITH FSC MIDWAY A LOADED LINE

Figure 4.15 shows the model for a CCS with FSC for a loaded line of 125MW load and 10MVAr reactor. This scenario gives the probable practical situation of the transmission line under load conditions. In the figure the CCS is represented midway between the line.

It was observed from the simulation results that the receiving end voltage experiences Ferro-resonance lasting for a few cycles as shown in Figure 4.16. The HV steady state voltage was 147.75 kV, which presents an overshoot on the high voltage side.

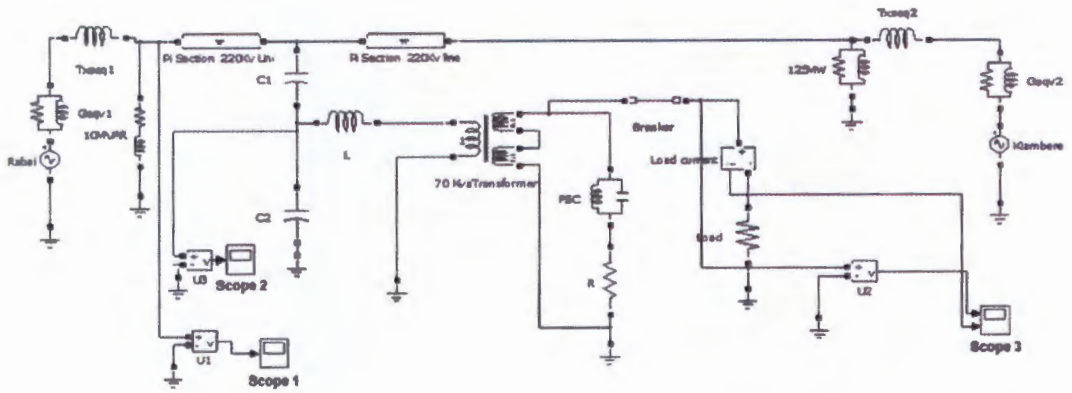

Figure 4.15 Models with CCS midway between the line and with load

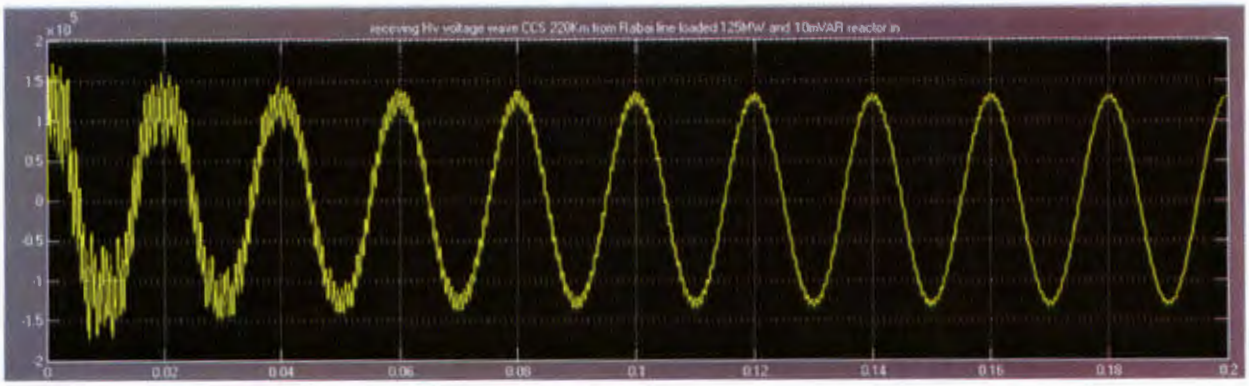

Figure 4.16 Receiving end voltage wave with CCS midway and line loaded

4.7 CCS WITH FSC AT DIFFERENT DISTANCES WITH LINE UNLOADED AND LOADED

Distances of the CCS from sources are altered by varying the length of the pi sections. Diagrams similar to those applied in section 4.6 are used for simulation. This is first done with the main line having no load and then with a loaded line of about 125MW (See Appendix A). The distances covered are spaced at 50km range. The assumption is that the lines are switched at different points on the wave. Different measurements are taken with regard to:

- Low side voltage (V_0) or load terminal voltage (V_L) and current
- Thévenin Voltage (V_{th}) at the point of capacitor divider or (V_D)
- High Voltage (V_{in}) or tap- off voltage (V_T).

The nature of distortion on high voltage and low voltage are also analyzed as shown in Tables C-1 to C-6 in appendix C.

4.7.1 CCS AT DIFFERENT DISTANCE WITH LINE UNLOADED

Tables C-1 to C-6 in appendix C, are the details of the measured parameters at different distances of the CCS.

Table C-1 show the transmission parameters at different distances with line not loaded. It was observed that in this scenario, the tap-off voltage or V_{in} overshoots to between 146.528 to about 148.920kV depending on the CCS distance from Rabai. It was observed that V_{in} reduces as the distance increases. On the other hand the low voltage or load terminal voltage decreased from about 250V to 217V as the distance from Rabai increases. The switching resonance for both high and low voltage varied between 3 and 5 cycles. This scenario requires compensation.

4.7.2 CCS AT DIFFERENT DISTANCES WITH LINE LOADED

Transmission line loaded at 125MW with CCS installed at distances of 50km. Simulations was repeated as in the unloaded case. Table C-2 shows the measured parameters of the transmission line under load. The table depicts similar results as those of the unloaded case with a slight decreased variation on the tap–off voltage or V_{in}.

4.8 EFFECT OF A REACTOR IN THE LINE

In this case we study the effect on the actual 10MVAr reactor (See appendix A) at Rabai on the voltage profile with the CCS installed. Voltages at source and receiving ends are recorded. Figure 4-17 shows the effect of the 125MW load with a 10MVAr reactor connected at one end of the line. It was noted that the high voltage is reduced to acceptable limits of ± 6%. Both the sending end and receiving end showed some switching resonance for a few cycles. The receiving end voltage (Figure 4-18b) shows a more intense resonance experience.

Table C-3 show the measured parameters with line loaded at 125MW and 10MVAr reactor at Rabai sub-station. It was observed that in this scenario, the tap-off voltage ranged between 128.595 to about 139.025kV. On the other hand the low voltage or terminal voltage ranged from about 227V to 221V as the distance from Rabai increased. The switching resonance for both high and low voltage varied between 3 and 5 cycles.

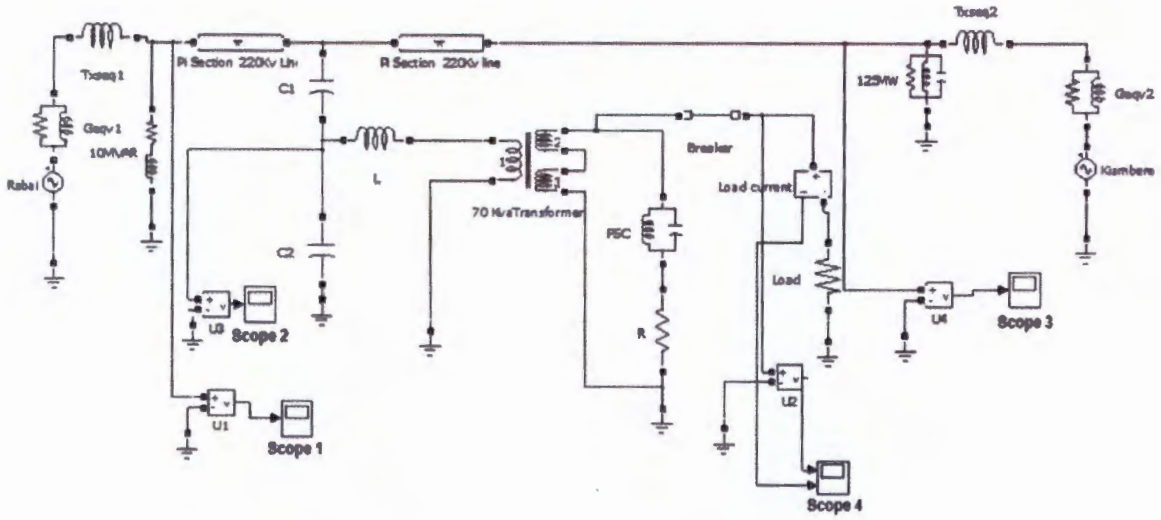

Figure 4.17 Model with CCS and 10 MVAR reactors at the receiving end

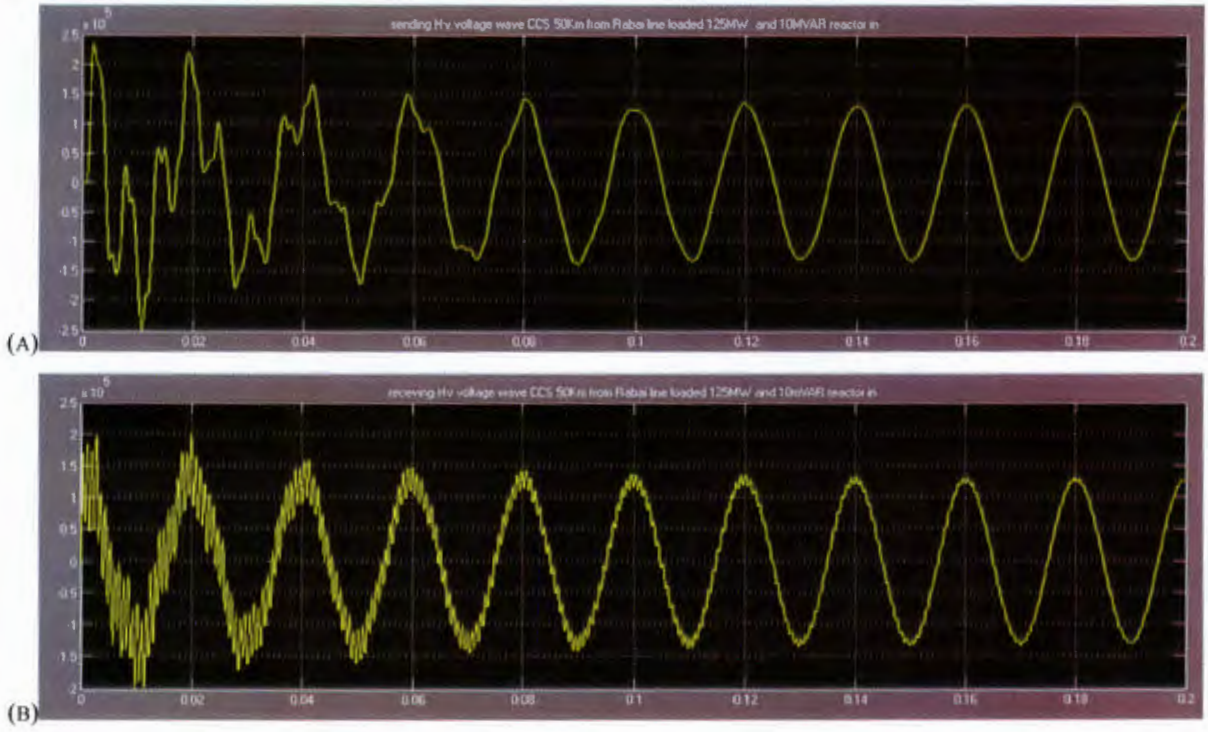

Figure 4.18 Effects of 125MW and 10MVAR reactor on the transmission line

4.8.1 TWO CCS WITHOUT REACTOR ON THE LINE

Two capacitor coupled substations were considered with the first substation being 50 km away from Rabai and the CCS being 50km apart from each other. Adjustment had to be done so that capacitor C_3 becomes 0.12 μF and C_4 was 0.4μF in order to obtain the correct output (see figure 4.19).

With the line fully loaded and the reactor switched off the steady state voltages obtained were as shown in Table C-4 in the appendix. Figure 4-20 (a-d) show the receiving and sending voltage waveforms simulation results. It was observed that the high voltage sending and receiving ranged between 129,342 to about 129,824kV and 147,625 and 151,383kV respectively. The low voltage ranged from about 241kV to 251kV (typical low voltage for domestic use in most SSA countries is 240V). The switching resonance for both high and low voltage was very minimal.

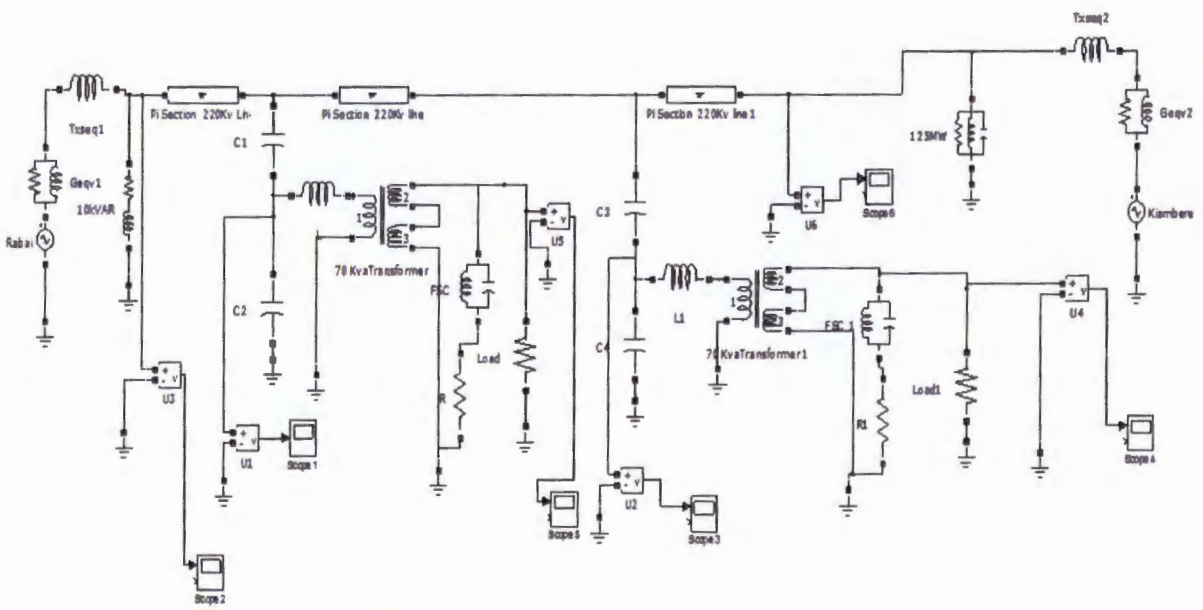

Figure 4.19 Model for two ccs connected on the transmission line

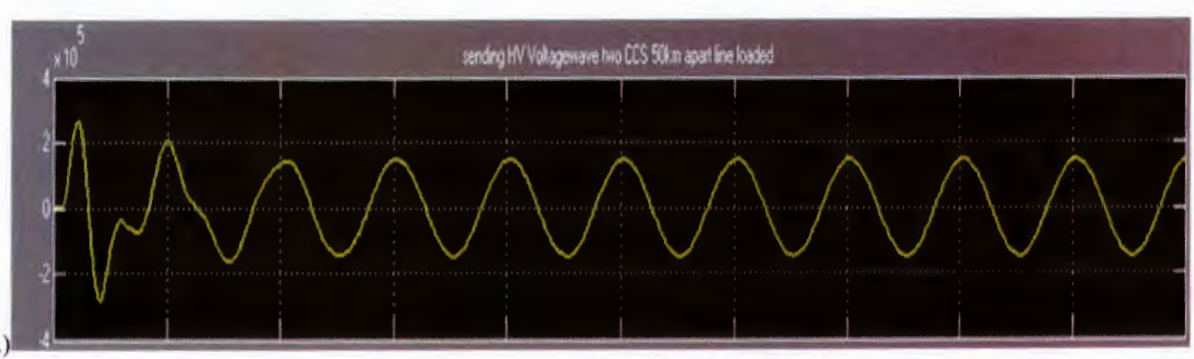

(A)

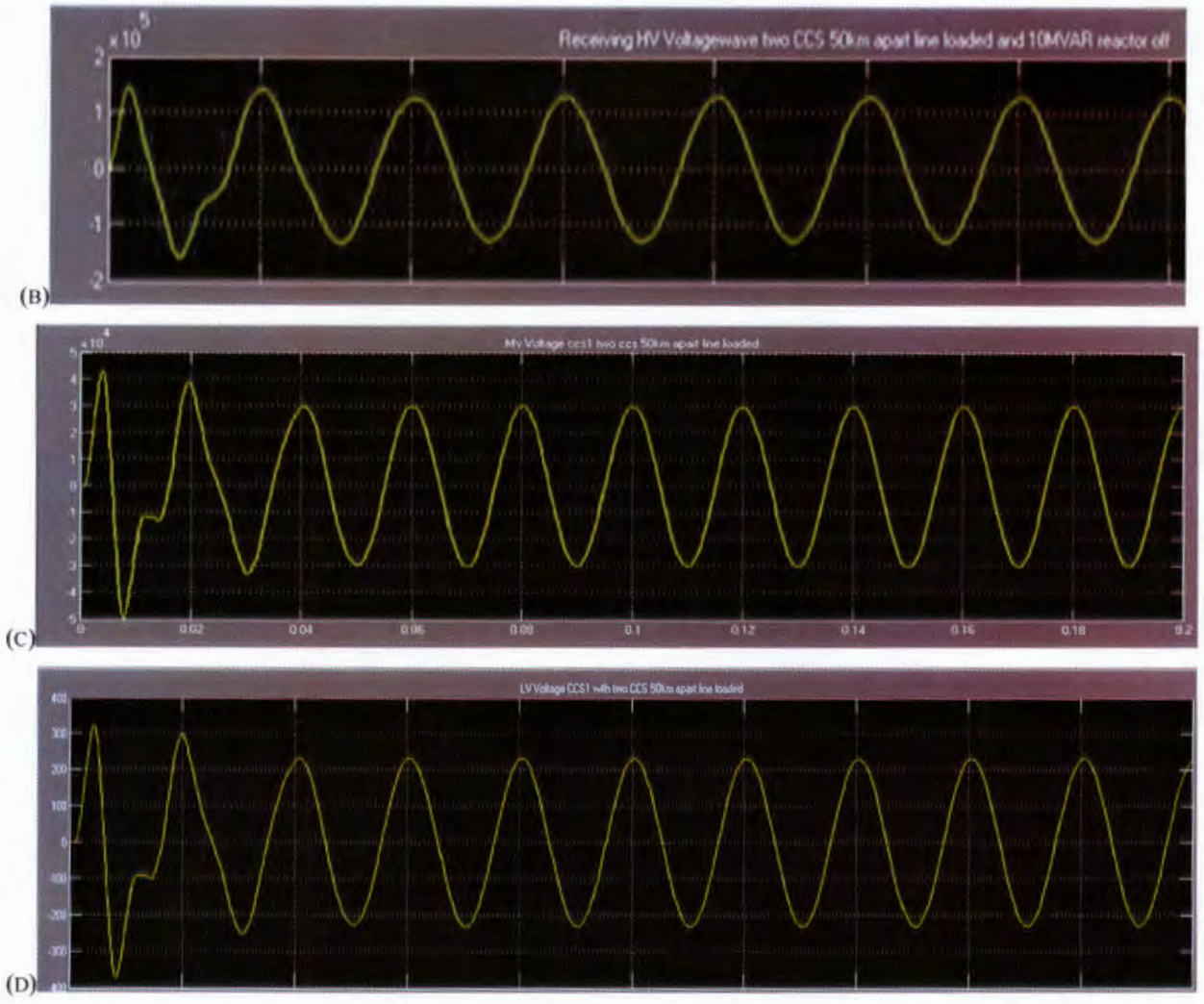

Figure 4.20 two ccs connected to loaded transmission line at different distances

4.8.1 TWO CCS WITH REACTOR ON THE LINE

This is a repeat of the previous case but with the reactor of 10MVAr added to the circuitry to reduce the over voltages at the sending and receiving ends. Table C5 in the appendix shows the measured parameters of the tests while Figure 4.21 shows the simulations.

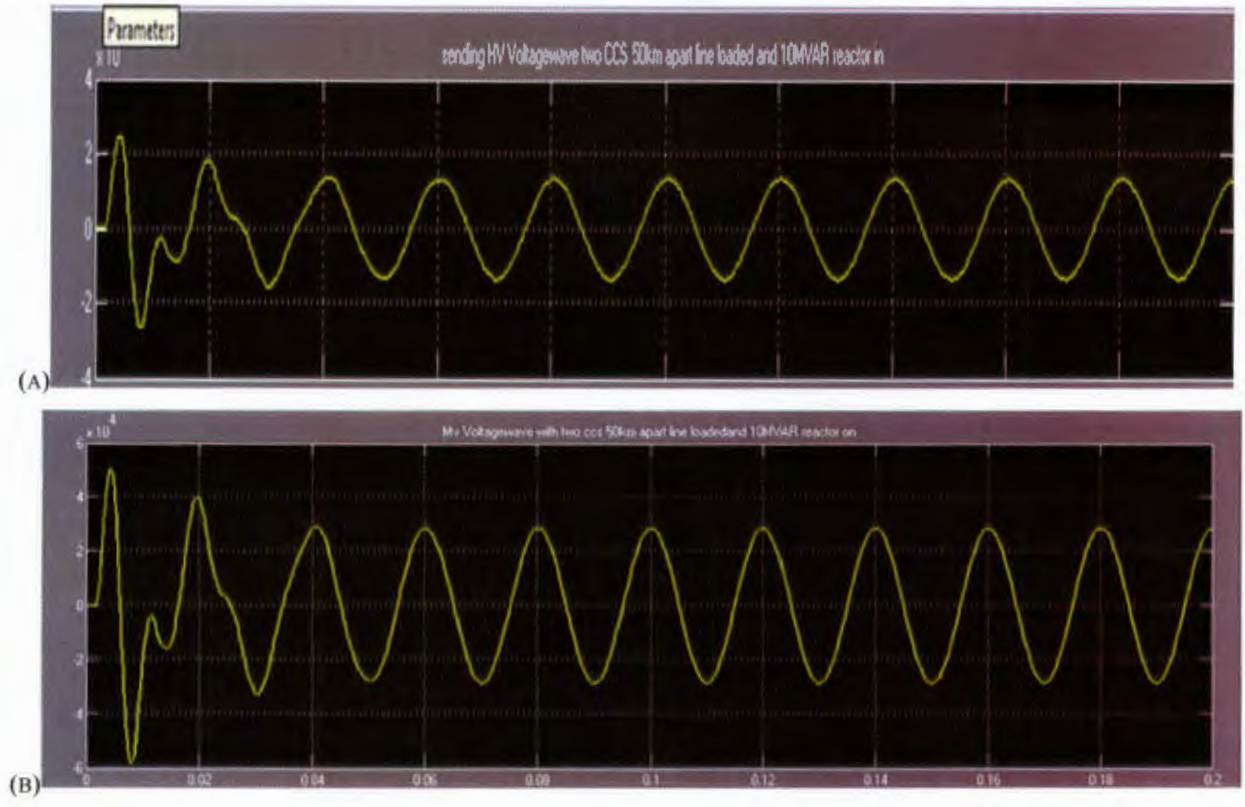

Figure 4.21 Voltage waveforms of two CCS with a 10MVAR connected at different distances

It was observed that with two CCS units connected in circuit and the 10MVAr reactor closed at Rabai. Both the low and high voltages ranged within ± 2.5% and 6% tolerance respectively. The switching resonance was also drastically reduced. This scenario showed a much improved performance than all the others.

4.9 THREE CCS WITH REACTOR ON AND OFF LINE

In this case three CCS were considered as shown in Figure 4.22 below, with the first sub-station being 50 km away from Rabai and the sub-stations being 50km apart from each other. No adjustment was required, so capacitor C_5 and C_6 were 0.12μF and 0.4μF same as C_3 and C_4. The transmission line was loaded at 125MW.

The low voltage was not loaded and the reactor switched on and then off. The steady state voltages obtained were as shown on table C-6. The simulation results for sending and receiving end high voltages are shown in Figure 4.23 (a) and (b) respectively. The results are similar to the two CCS scenarios when the reactor is in circuit. A slight increase in the receiving end high voltage was observed when the reactor is switched off.

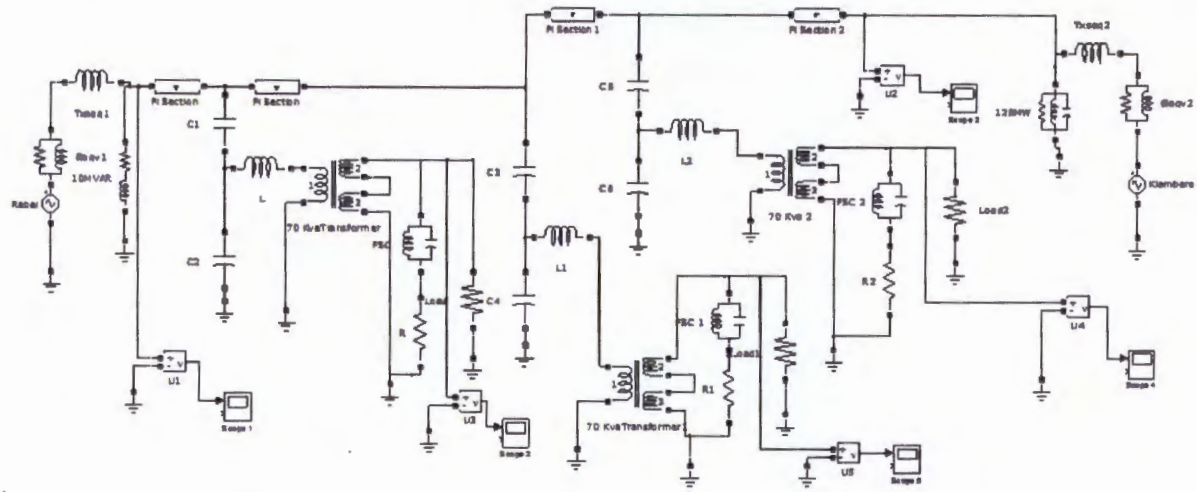

Figure 4.22 Models for three CCS at different distances

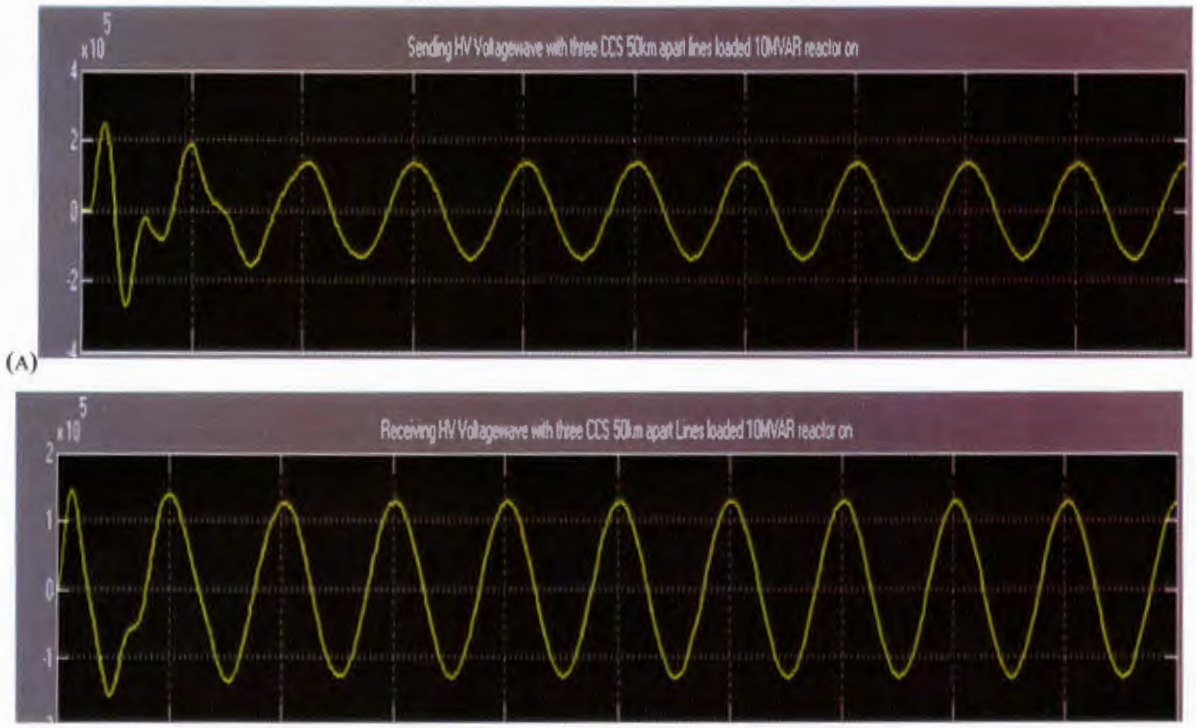

(A)

Figure 4.23 Simulation results for three CCS at different distances

4.10 CCS WITH FSC MODEL FOR TRANSIENT STABILITY CASE

In this section, a fault occurring on the MV side was considered by closing breaker 1 and opening it after 1-3 seconds. The objective was to observe the behavior of the voltage and current at the point of capacitor divider (VD).

Figure 4.24 shows the circuit diagram for transient stability simulations. While Figure 4-25 to 4-27 shows the MV and LV voltage with breaker closing at 1, 2, and 3 seconds respectively.

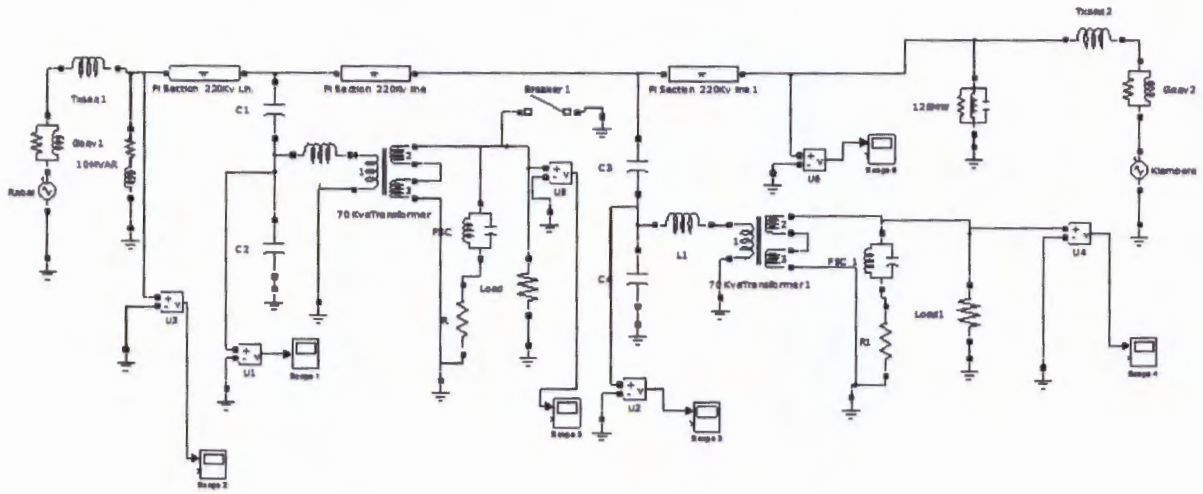

Figure 4.24 Models for transient stability simulation

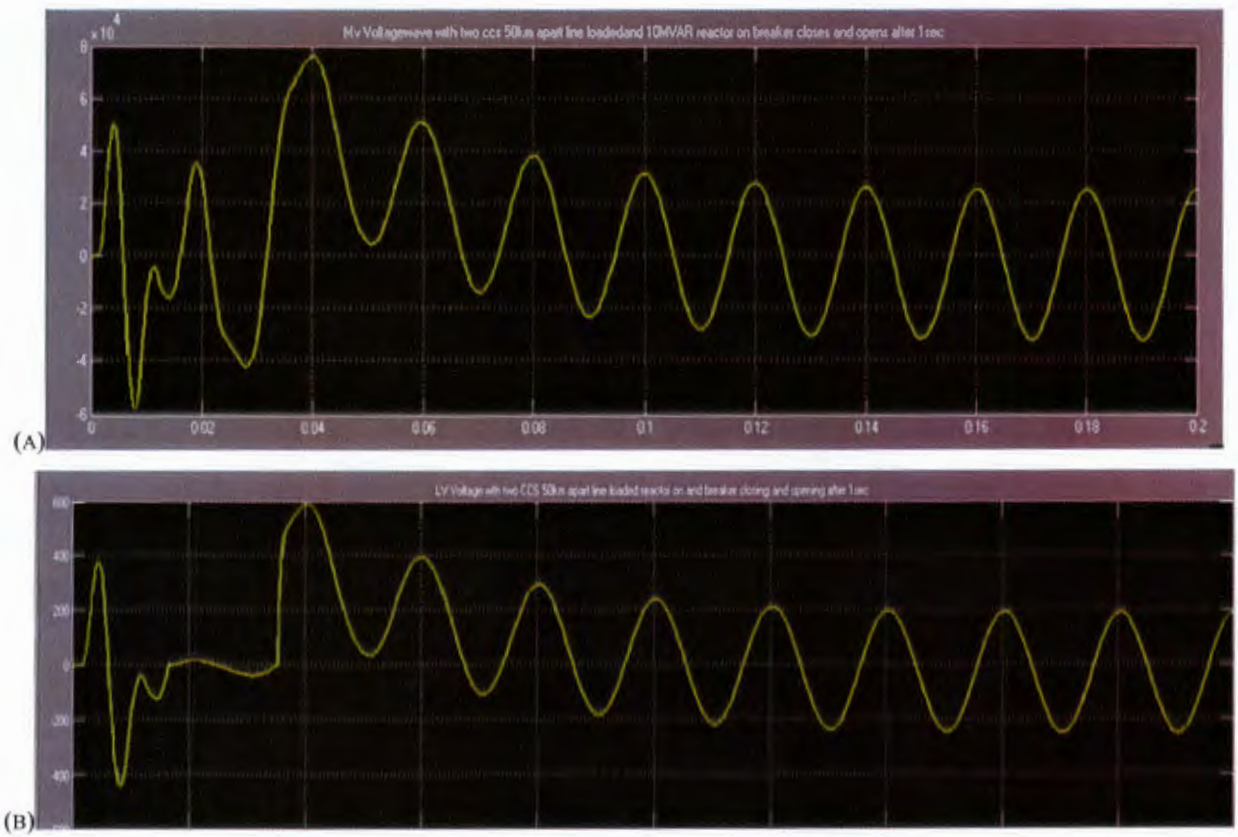

Figure 4.25 MV and LV voltage with breaker closing after 1 second

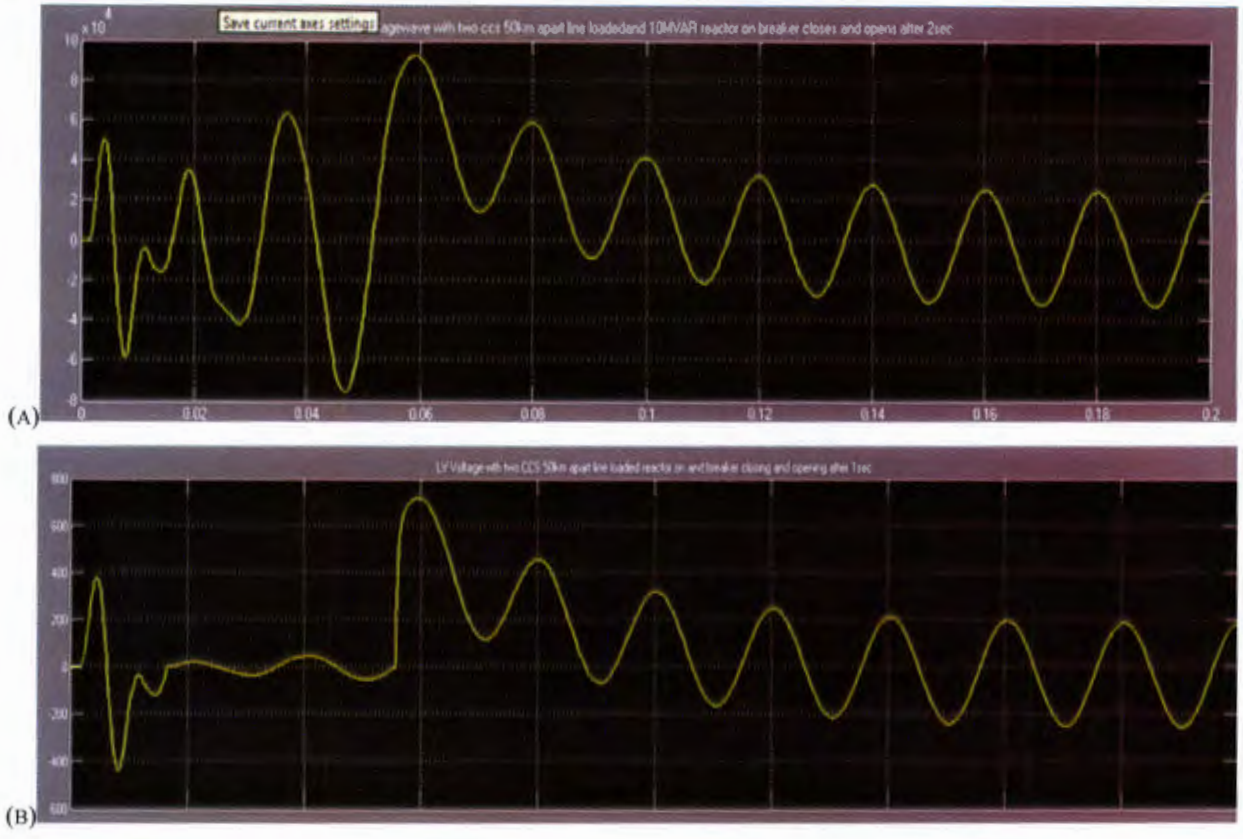

Figure 4.26 MV and LV voltage with breaker closing after 2 second

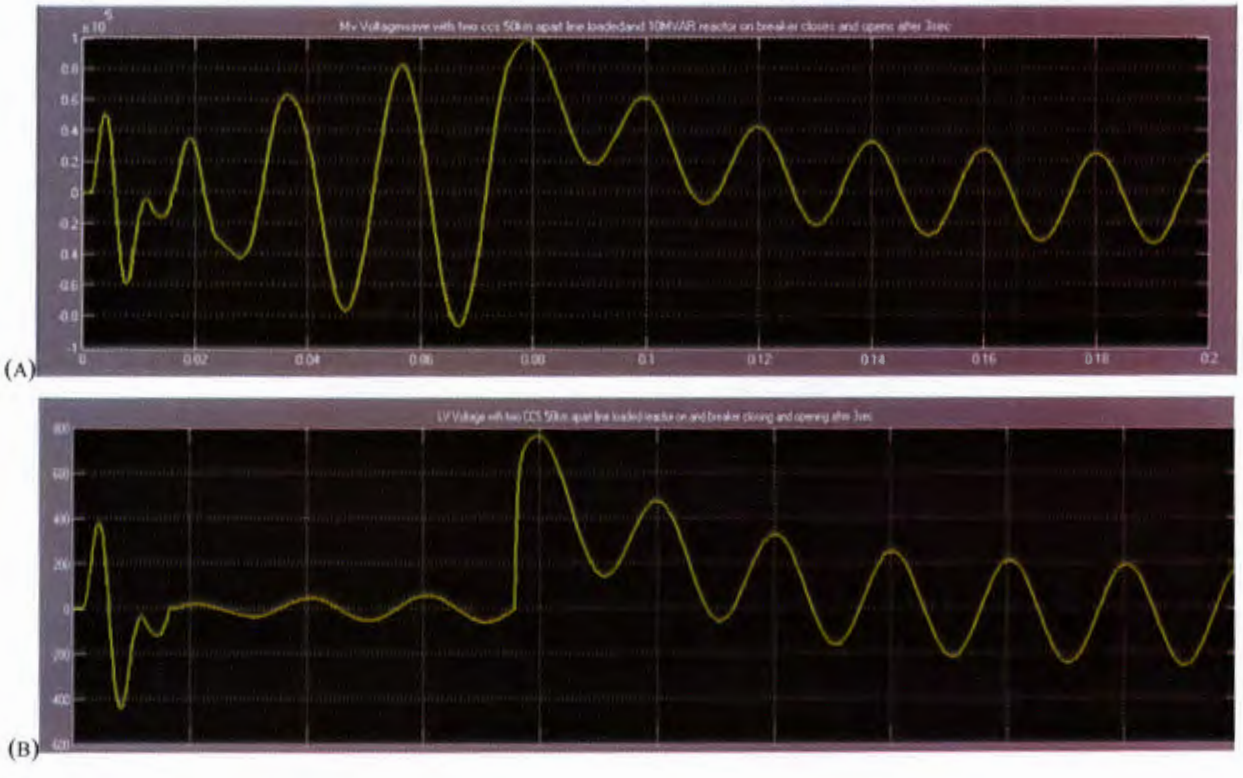

Figure 4.27 MV and LV voltage with breaker closing after 3 second

4.11 CCS LOADABILITY TEST

The loadability test was carried out to determine the optimum apparent power that can be supported before the voltage begins to collapse. The tests were carried out for six different demand levels. For each test, real power demand P_L was fixed and reactive power demand Q_L varied and operated at different load power factor between 0.2 lagging to unity. Simulation results were tabulated as shown in Table (E1-E6) in the appendix. The desired maximum voltage at the load terminal was ± 6% of 33kV (from 31.02 kV to 34.98 kV). The tests were done at variable power factor using series R-L load model. Simulations of the CCS system were carried out using the model circuit of Figure 4.28. Where;

Scope 1 U_1 - (kV) represents system tap-off voltage.

Scope 2 U_2 - (kV) represent capacitor banks voltage divider

Scope 3 U_3 (kV) - represent load terminal voltage

Scope 4 I_1 - (A) represent system current.

Scope 5 I_2 - (A) represent current flowing at the capacitor bank divider

Scope 6 I_3 - (A) represent load current

Q_L (MVA_R) - represent varied reactive power of the load

Figure 4.29; show the loadability test graph for the six different demand levels.

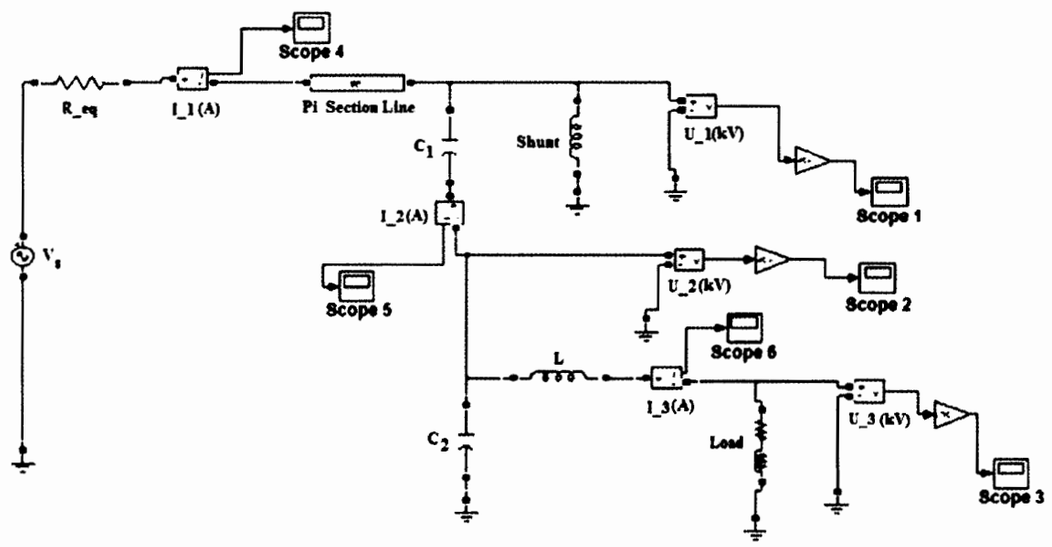

Figure 4.28 CCS loadability test model

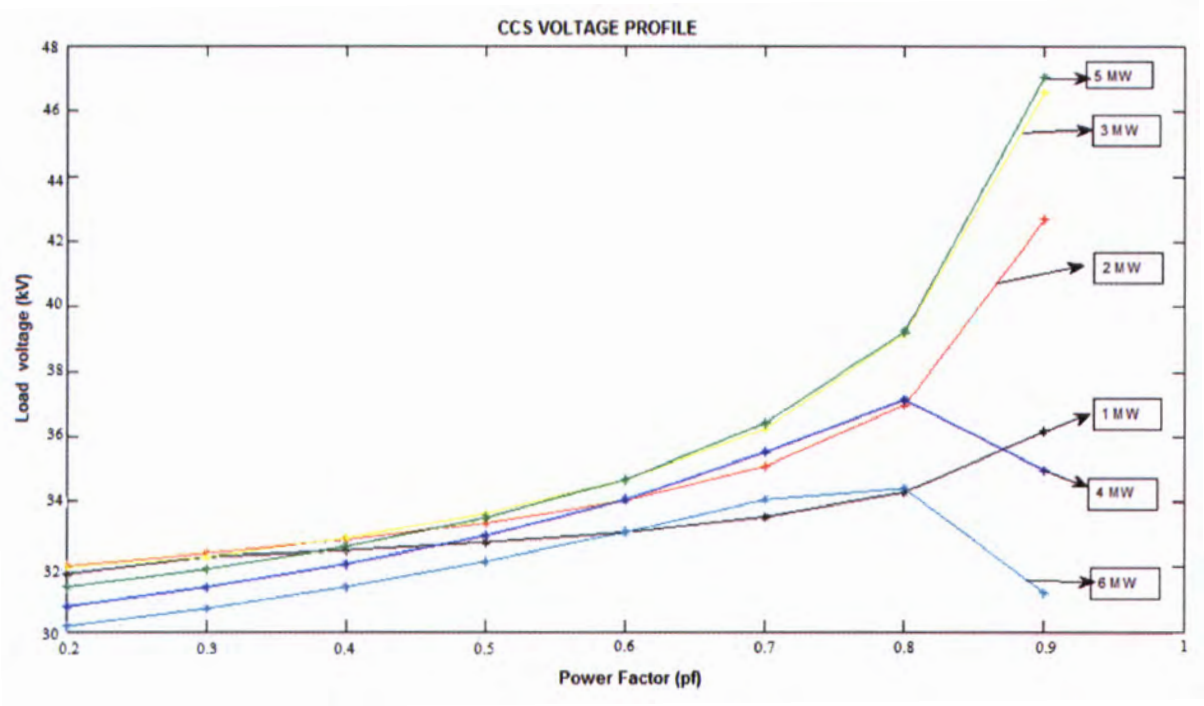

Figure 4.29 Voltage profile for loadability test

Simulation results clearly showed that CCS system can be operated within allowable voltage regulation if a load of 1MW at 0.5 to 0.8 power factor was connected at the load terminal. The load current at these power factors ranged between 35.28A to 21.05A. It is worth noting that the 6MW load gave a good voltage profile between 0.5 and 0.8 power factor, but the load currents were quite high i.e. between 215.56A and 125.94A (see appendix E1). For the other load demand scenarios, i.e. 2MW, 3MW, 4MW and 5MWthe system could operate between 0.2 and 0.6 power factor which would result to very high currents being drawn from the supply as shown in tables of appendix E2 to E5.

4.12 SHUNT COMPENSATION USING CCS

Compensation test was carried out using a similar diagram of Figure 4.28 shown above. The shunt reactor was modeled by varying values corresponding to the active and reactive power specified in the simulation design. The value of C_1 and C_2 were maintained as derived in chapter 3.

Additionally, in this scenario, it is worth noting that compensation meant with a loaded CCS and un-compensation without CCS. The simulation results showed that CCS model improved the line voltage profile as seen from the analysis given in Figure 4.30 below. Three load scenarios were simulated i.e. 40, 70 and 125MW.

These loadings were based on; when the transmission line is lightly, moderately and maximum loaded respectively. (Remember 125MW is the maximum loading of this line).

In all the three scenarios it was observed that the compensated system showed a higher voltage than the uncompensated. In this case, the line worked better at 40MW compensated load i.e. it operated within the ± 6 % of 127kV. The 70MW and 125MW load gave a lower voltage profile when compensated or uncompensated.

Therefore, CCS helps in mitigating line losses in a loaded line. Conversely, CCS model may be installed on a heavily loaded line to improve the line compensation. When the line is lightly loaded, CCS may increase the voltage profile.

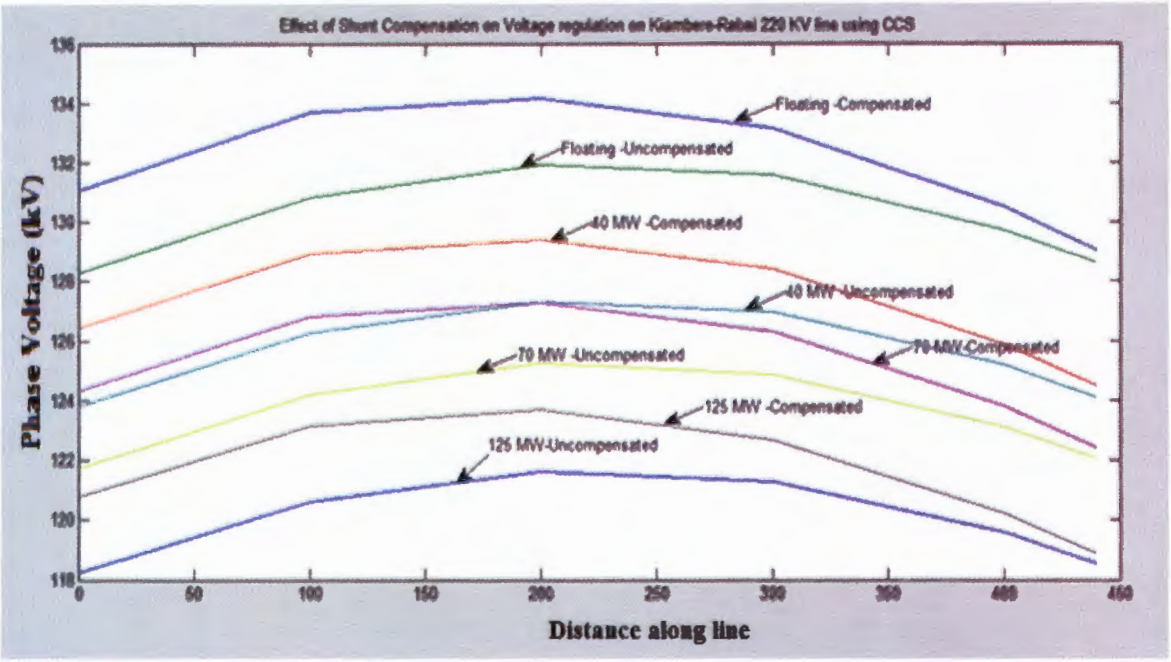

Figure 4.30 CCS voltage profile for compensated and uncompensated line

4.13 Analysis of Results

The steady state simulation results of CCS system showed that the tap-off voltage on the transmission line increased by 20.73% during light load period and 5.087% during heavy load periods with respect to the supply. In addition, there was a decrease of the terminal load voltage at light and heavy load of about 0.04% and 13.33% respectively.

4.11 CCS LOADABILITY TEST

The loadability test was carried out to determine the optimum apparent power that can be supported before the voltage begins to collapse. The tests were carried out for six different demand levels. For each test, real power demand P_L was fixed and reactive power demand Q_L varied and operated at different load power factor between 0.2 lagging to unity. Simulation results were tabulated as shown in Table (E1-E6) in the appendix. The desired maximum voltage at the load terminal was ± 6% of 33kV (from 31.02 kV to 34.98 kV). The tests were done at variable power factor using series R-L load model. Simulations of the CCS system were carried out using the model circuit of Figure 4.28. Where;

Scope 1 U_1 - (kV) represents system tap-off voltage.

Scope 2 U_2 - (kV) represent capacitor banks voltage divider

Scope 3 U_3 (kV) - represent load terminal voltage

Scope 4 I_1 - (A) represent system current.

Scope 5 I_2 - (A) represent current flowing at the capacitor bank divider

Scope 6 I_3 - (A) represent load current

Q_L (MVA_R) - represent varied reactive power of the load

Figure 4.29; show the loadability test graph for the six different demand levels.

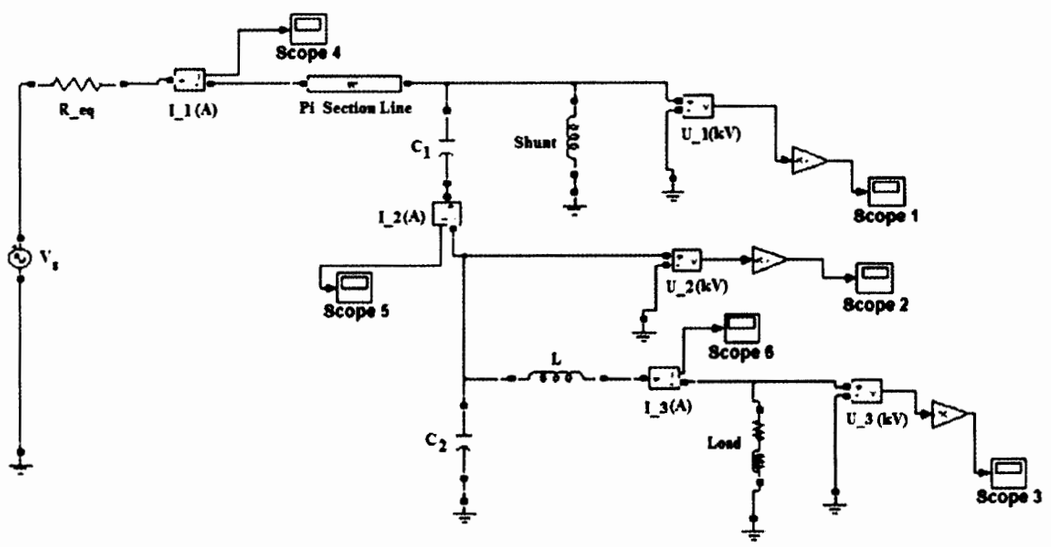

Figure 4.28 CCS loadability test model

The transient state simulation without the FSC circuit was carried out and different range of signals applied. During signals 1 to 4 the system was switched off and on, a spike current of about 8 to 10 time's normal system current was observed. Furthermore, a voltage overshot of about 1.3 to 1.5 time's normal tap-off voltage when the system was switched on or off was also noted. In addition, the effect of Ferro-resonance was experienced on the divider voltage, load current and load voltage waveform.

The loadability tests were also done at variable power factor using series R-L load model. Simulations of the CCS system were carried out in six different levels of demand (see appendix E1-E6). For each test real power demand (P_L) was fixed and reactive power demand (Q_L) varied to operate at different load power factor between 0.2 lagging to unity factor. The tests took into consideration the required load terminal voltage and the tap-off voltage constraints.

Simulation results showed that the designed CCS system can be operated within allowable voltage regulation if a load of up to 1MW at 0.5 to 0.8 power factor was connected. Shunt compensation results showed that, the CCS helps in mitigating line losses in a loaded line. Conversely, CCS model may be installed on a heavily loaded line to improve the line compensation. When the line is lightly loaded, CCS may increase the line voltage profile.

Various simulation studies were performed for different topologies of CCS design parameters. It was observed that penetration of a single CCS on the Rabai- Kiambere line caused increased Ferro-resonance resulting to the voltage waveform distortion towards the end of the transmission line. On switching, this distortion of impulses lasting about 3 to 6 cycles cumulatively may cause insulation failure of electrical equipment such as transformers connected to the line. In other words, Ferro-resonance problems persisted regardless of position of a single CCS along the line.

Subsequently, penetration of two CCS of similar values as that of the single CCS penetration provided much improved voltage profile characteristics for both transmission line and the load output voltage from the sub-stations. The switching resonance effect was limited to less than two cycles. However, with additional penetration of an extra CCS of similar value as the first two, a smaller input capacitor was required, that may put a ceiling on what is possible to manufacture. Meaning, this would introduce standardization problems.

Conversely, it was established that the CCS could be placed anywhere along the line. This meant that the maximum penetration point was not a function of the penetration level. Moreover, it was also proved through simulations at different distances on the line that penetration of the CCS per phase was dependent on the line parameters, the value of the CCS units installed and the loadability of the CCS. The requirement was to have the correct balance of all these parameters that could be accommodated without violating the maximum steady state voltage on the MV and HV side of the system.

It was further observed that fast operating switchgears (operating in less than 1sec) are required for isolating faults on the low voltage network. This is to ensure a reduced voltage rise on the voltage divider for the capacitors protection.

4.14 ONWARD

The most relevant aspects of the design, simulation and analysis of un-conventional CCS technologies have been presented in this chapter. Developing a rural supply distribution system from a CCS, based on its penetration level in a 220kV, 440km transmission line has been investigated. The CCS system was subjected to a series of repetitive simulations with regard to different distances, same loading conditions and different sizing of CCS units on the power network.

The loadability test and transient stability simulation were also carried out to establish the kind of protective scheme required. It was recognized that, there was a maximum number of CCS that could penetrate a particular line per phase based on the line parameter, the value of the CCS installed and the loading of the line.

The penetration level of the CCS was constrained by the allowable steady state voltage violation for a particular network. The transient state was tested to help in the design of the protective system. The next chapter presents a method of determining maximum allowable penetration level of CCS without steady state voltage violation derived from a modified distributed generation analogy. The method is based on the determination of voltage sensitivities from linearized power system model. This method is used to validate the repetitive power flow simulations results carried out in this chapter.

5 PENETRATION LEVEL OF CAPACITOR COUPLED SUB-STATIONS ON POWER NETWORKS

5.1 INTRODUCTION

The CCS system is always referred to as a capacitive transformer. However, there are major characteristic differences between CCS and distribution transformer. The CCS technology being proposed in this research project has great impact on the transmission and distribution network operation and structure when integrated into them; hence the knowledge of a quantifiable level of penetration of this URE technology in power networks is necessary. Penetration level of CCS on a power network has not been adequately researched as compared to penetration level of Distributed Generators (DG) in power networks.

Against this back drop, the feasible measure at present is to investigate on the maximum penetration level of CCS on an existing power network based on a modified DG analogy (as explained in section 5.2). The existing methods of calculating penetration level for DG mainly considers the capacity constraints from one or several aspects.

For example according to Chao Wang et al. [2007], the computation of maximum penetration level is analysed considering tap hunting constraints. The approach to calculate the maximum penetration without violating steady state voltage limits is also presented by Morren et al. [2008] and Ayres et al. [2010]. These approaches with some modification are considered in this chapter. The exact penetration limits depend critically on the steady state voltage quality, stability, and capacity constraints.

5.2 ANALOGY BETWEEN DG AND CCS

Distributed Generation (DG) units are mostly connected at the distribution level; this means that they are connected to the load bus. Load characteristics have a strong influence on the dynamic performance and stability of the system. The load model takes into account the effect of low voltage level tap changers in the equivalent high voltage level behavior [Kundur 1996]. When the penetration of DG is high, the generated power of DG units not only alters the power flow in the distribution system, but in the transmission system as well [Thong et al. 20004].

The penetration level can be calculated as function of the total DG power generation P_G over the total load demand P_L as shown in equation (5.1) below;

$$\text{Penetration level } (\%) = \frac{\sum P_{DG}}{\sum P_L} \times 100 \quad (5.1)$$

The connection of DG to the grid transmission line may influence the stability of the power system i.e. angle, frequency and voltage stability. On the other hand DG units have not been designed to support system stability during power system failure [Jenkins et al.2000].

DGs are usually made of small synchronous or induction generators with simple exciter and governor control schemes as compared to large central power generators. Induction generators are not able to control the reactive power at all.

Traditionally, power normally flow from the transmission network to distribution network. Therefore, the vice versa flow of reactive power from a distribution network to the transmission network affects the penetration level of the DG on the distribution and transmission network. To mitigate the effect of the DG penetration level on the transmission network, the system may be terminated on a slack bus. This is analogues to a CCS system when connected to a transmission line. Moreover; even the DG units connected via electronic power converters do not have large capabilities to control active and reactive power [Thong et al. 20004]. Furthermore; the system inertia of DG units is normally low.

Equally, the CCS is also usually connected to the load bus. Based on the assumption that the total CCS load is constant, this results to the system acting as a shunt capacitor. Therefore, the system responds to reactive power production depending on the transmission line loading. Similarly, since this operation is passive its analogues to a DG with low inertia.

Subsequently, it is justified to analyze the equivalence of the DG analogy for the CCS system using a slack bus treatment in load flow solutions as explained in section 5.3. The network under investigation can be represented using a modified DG analogy as shown in Figure 5.1. The network shows two active bus systems with a slack bus (bus 3) incorporated. The equivalent circuit diagram of the modification including the short-circuit impedance Z_{sc}.is shown in Figure 5.2.

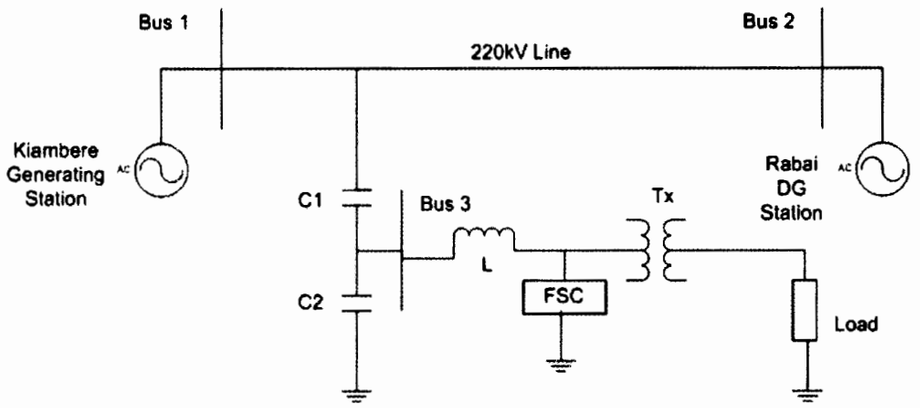

Figure 5.1 CCS modified version of the power network system

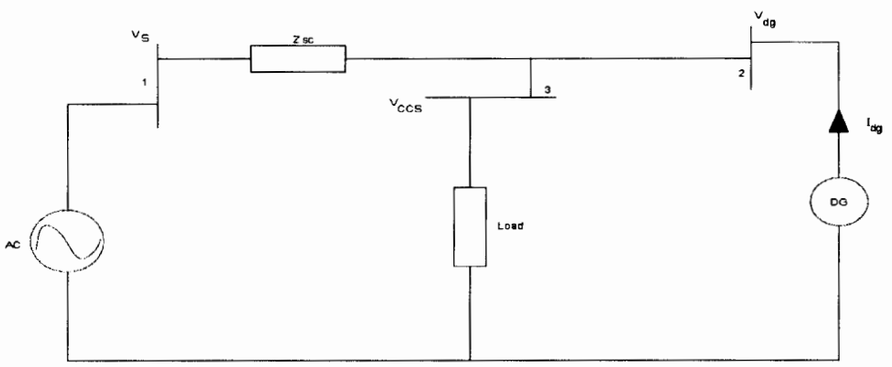

Figure 5.2 CCS equivalent circuit of the modification

5.3 SLACK BUS TREATMENT IN LOAD FLOW SOLUTIONS

The concept of slack bus as it is well known, is a mathematical necessity but has no physical relationship to any generator bus. Exception arises when a small system is linked to a much bigger system via a single tie line (single bus). In this case, one can represent the large system with an equivalent generator, which can hold the voltage constant and generate as much power as needed that is the slack bus characteristics. Similarly, in a distribution network fed by a CCS, the transmission network occasionally acts as a slack bus with respect to the distribution network.

The slack bus allows the solution of non-linear equations to be feasible. Since the power losses in the network are not known in advance, its role is to pick up the "slack" and balance the active and reactive power in the system.

This usually does not represent a problem in a well deterministic load flow problem [Dimitrovski and Tomsovic 2004]. However, in the case with uncertainty nodal powers, the slack bus also must absorb all the resulting uncertainties from the solution. As a result it has the widest nodal power possibility (probability) distribution in the system. This will frequently result in operating point well beyond its generating margins. Two of the most common ways of satisfying constraint imposed on a slack bus is explained below.

5.3.1 SLACK BUS – PV BUS CONVERSION

This method is analogous to that of PV bus to PQ bus conversion for PV buses with reactive power limits. During the course of solution of a load flow, a PV bus's produced reactive power extends beyond its limits, it is fixed at the violated limit and its voltage magnitude is relaxed. Thus, the PV bus has been converted into a PQ bus, with specified active and reactive power.

Later, during the solution, if the bus voltage shows tendency to return and the reactive power again falls within the limits, the bus will be converted back from PQ to PV [Dimitrovski and Tomsovic 2004].

Following the same approach as in PV bus to PQ bus conversion above; if the slack bus real power generation extends beyond predefined limits, it is fixed at the violated limit. Some other PV bus's active power generation then must be relaxed in order to be able to solve the load flow problem. The PV bus to choose seem to be a matter of preference, but it is logical to pick the one that has the highest margin from the current production to either its lowest or upper limit, depending on which limit was violated at the slack bus.

With the choice of a PV bus to relax, it is now possible to redefine the load flow problem by swapping only the equation for the real power at the chosen PV bus with the slack bus real power, without changing the unknown state variables.

In other words, the slack bus becomes PVθ bus and the PV bus becomes just V bus. We still have a system of n equations with n unknowns, only the known and the unknown variables have changed and the Jacobian loses symmetry. In this case, the system of equations will have the following form [Dimitrovski and Tomsovic 2004, Ayres et al. 2010]:

$$\begin{bmatrix} \Delta P_{Slack} \\ \Delta P_{PV-1} \\ \Delta P_{PQ} \\ \Delta Q_{PQ} \end{bmatrix} = \begin{bmatrix} \frac{\partial P_{Slack}}{\partial \theta^T_{PV+PQ}} & \frac{\partial P_{Slack}}{\partial V^T_{PQ}} \\ \frac{\partial P_{PV-1}}{\partial \theta^T_{PV+PQ}} & \frac{\partial P_{PV-1}}{\partial V^T_{PQ}} \\ \frac{\partial P_{PQ}}{\partial \theta^T_{PV+PQ}} & \frac{\partial P_{PQ}}{\partial V^T_{PQ}} \\ \frac{\partial Q_{PQ}}{\partial \theta^T_{PV}} & \frac{\partial Q_{PQ}}{\partial V^T_{PQ}} \end{bmatrix} \begin{bmatrix} \Delta \theta_{PV+PQ} \\ \Delta V_{PQ} \end{bmatrix} \quad (5.2)$$

Where;

PV is the set of all PV buses,

PV-1 is the set of all PV buses without the one with relaxed real power,

PQ is the set of all PQ buses,

$PV+PQ$ is the set of all PV and PQ buses,

P, Q are the real and reactive nodal power vector functions,

V, Q are the vectors of unknown state variables (voltage magnitude and angles), and

$\partial/\partial(.)^T$ Denotes Jacobian of the corresponding vector function.

The problem formulation as in equation 5.2 keeps the reference angle at the slack bus (usually 0^0). Another approach will be to relax the voltage angle of the slack bus and declare the voltage angle of the PV bus with relaxed real power as the reference (i.e. known). This will result to a complete slack to PV bus and PV to slack bus conversion. In this case the system of equations has the usual symmetry, with the slack bus completely swapped.

In the second, approach the original slack will change its voltage angle from the initial value during the course of solution. However, since angles are relative to each other, we can force it back to the initial value if desired, by subtracting that difference from each voltage angle obtained from the solution. In this way, we will obtain exactly the same solution as with the previous formulation.

Regardless of the treatment of the reference angle, the new slack bus takes over the balancing of power and, initially its production will be either decreased or increased, depending on the limit violation of at the previous slack bus.

During the course of solution, the production of the new slack bus will change and it is possible one of its limits gets violated also. In this case the procedure is repeated with some other PV bus capable of taking over the slack. If there is no such bus available, that is., all PV buses are on their limits, the problem is infeasible.

Evolving from the foregoing analysis, the succeeding section presents a method of determining maximum allowable penetration level of CCS without steady state voltage violation based on the determination of voltage sensitivities from linearized power system model.

5.4 VOLTAGE SENSITIVITIES DETERMINATION

The main factor that may limit the penetration level of CCS in a typical transmission system is the steady state voltage change. The maximum amount of reactive power supplied by CCS into the power network without causing voltage violation can be determined by using repetitive power flow studies as illustrated in Chapter 4.

In this research project the proposed method for estimating maximum allowable power injection into the network is based on voltage sensitivities related to active and reactive power injections [Ayres et al. 2010, Morren et al. 2008].

The network under investigation is represented using a modified DG analogy as shown in Figure 5.1. The network shows two active bus systems incorporating a slack bus. The equivalent circuit diagram of the modification including the short-circuit impedance Z_{sc}.is shown in Figure 5.2

The sensitivities are obtained from the load Jacobian matrix, which can be determined from the linearized power system model for a given base case (V^0, θ^0) as,

$$\begin{bmatrix}\Delta P \\ \Delta Q\end{bmatrix} = \begin{bmatrix}J_{P\theta} J_{PV} \\ J_{Q\theta} J_{QV}\end{bmatrix} \begin{bmatrix}\Delta\theta \\ \Delta V\end{bmatrix} \tag{5.3}$$

Where, Δ denotes small variations in the variables. The elements of Jacobian matrix (J) represent the sensitivity among the power variations (ΔP, ΔQ) and voltage variation (ΔV, Δθ) on the line.

In this research project Jacobian matrix (J) will be represented by;

$$J = \begin{bmatrix}J_{P\theta} J_{PV} \\ J_{Q\theta} J_{QV}\end{bmatrix} \tag{5.4}$$

5.4.1 V-P SENSITIVITY

Supposing that $\Delta Q = 0$ and $J_{Q\theta}^{-1}$ is non-singular, equation 5.2 can be rewritten as

$$\Delta P = (J_{PV} - J_{P\theta} J_{Q\theta}^{-1} J_{QV}) \Delta V = J_{RPV} \Delta V \tag{5.5}$$

And

$$\Delta V = J_{RPV}^{-1} \Delta P \tag{5.6}$$

Where J_{RPV} is a reduced Jacobian matrix, which gives the voltage magnitude variations due to active power injection variations. The inverse of $J_{Q\theta}$ matrix is feasible only if all buses are modeled as PQ buses, guaranteeing that $J_{Q\theta}$ is a square matrix. This situation only occurs in distribution systems, where the slack bus is the only bus that keeps a varying voltage magnitude [Jenkins et al. 2000, Morren et al. 2008].

This is analogous to the CCS system where $V_{th} = V_0$ (See Figure 3.4) and should be maintained at a varying value. In addition, DG plants are usually modeled as PQ buses since they do contribute to the voltage control of the system [Jenkins et al. 2000].

Similarly, when the CCS is modeled as Q instead of X_c, it can also contribute to voltage control. In our case, matrix J_{PV} can be used directly in order to indicate which buses of the system will be more or less affected by the installation of a CCS unit. However, matrix J_{PV} by itself does not give sufficient information about the sensitivities because the other matrices $J_{P\theta}$, $J_{Q\theta}$ and J_{QV} are neglected.

On the other hand matrix J_{RPV} is obtained without any approximation with respect to the characteristics of the system, since the relationship among variables V, θ P and Q are preserved.

Equation 5.5 can be used to estimate the impact of multiple CCS system by representing (ΔP) as a diagonal matrix, with one entry of active power component injection for each CCS unit.

In this case each column of ΔV will represent the impact of one CCS on the system voltage profile. The disadvantage of equation 5.5, however, is that only unity power factor CCS system can be considered, but in this research project a power factor of 0.2 to unity is considered. This draw back can be solved by using the V-Q sensitivity as explained in the next section.

5.4.2 V-Q SENSITIVITY

Analogous to V-P sensitivities, V-Q sensitivities can be determined by assuming ΔP = 0 in equation 5.2, resulting in

$$\Delta Q = (J_{QV} - J_{Q\theta} J_{P\theta}^{-1} J_{PV})\Delta V = J_{RQV}\Delta V \qquad (5.7)$$

And

$$\Delta V = J_{RQV}^{-1}\Delta Q \qquad (5.8)$$

Where J_{RQV} is a reduced Jacobian matrix, which states the voltage magnitude variations with relation to the reactive power variations.

Equation 5.7 allows the estimation of the impact of CCS systems with different power factor on the system voltage profile. Again ΔQ can be organized as a diagonal matrix, whose elements would represent the absorption or the injection of reactive power of each individual CCS unit.

5.4.3 APPLICATION OF V-P AND V-Q SENSITIVITIES SIMULTANEOUSLY.

The information obtained from these two sensitivities matrices (J_{RPV} and J_{RQV}) permits the estimation of voltage variations due to the installation of one or a group of CCS units with any desired power factor.

By considering P_{CCS} as a diagonal matrix whose elements represent the active power injection of each CCS unit and Q_{CCS} as a diagonal matrix whose elements represents reactive power injection/absorption into the network, the voltage profile due to these additional CCS units can be estimated respectively, as

$$\Delta V_{(P_{CCS})} = J_{RPV}^{-1} P_{CCS} \text{ and } \Delta V_{(QCCS)} = J_{RQV}^{-1} Q_{CCS} \quad \textbf{(5.8)}$$

Where $\Delta V_{(P_{CCS})}$ and $\Delta V_{(QCCS)}$ are, respective matrices that reflect the voltage profile deviation due to new active and reactive power injections of the CCS units assuming their installation at any distance on the network with respect to the base case. If just one CCS unit is considered, matrices ΔV will provide just a non-null column for each CCS, which should be summed in order to build up the new system voltage profile.

Therefore, the estimated voltage profile after installation of one or a group of CCS units can be analytically expressed by;

$$V = V^0 + \Delta V_{(Pccs)} + \Delta V_{(Q_{CCS})} \quad \textbf{(5.9)}$$

Where, V^0 is the voltage profile for base case. The reactive power impact on the voltage profile can be negative or positive depending on the CCS power factor. The capacitive power factor leads to a voltage rise and inductive power factor to a voltage drop.

Equation 5.9 allows one to estimate the voltage profile when the CCS at every possible distance of the power network, with any lead or lag power factor and any specified voltage level. The simultaneous usage of V-P and V-Q sensitivities to determine the voltage profile variation due to the installation of CCS units can be done through validation studies for different scenarios. These sensitivities can also be used for estimating the maximum allowable power injection of a CCS unit.

5.5 VALIDATION STUDIES FOR DIFFERENT SCENARIOS

In order to verify the accuracy of the proposed method, its results are compared with the results provided with the repetitive power flow solution shown in Chapter 4 and appendix C, which are taken as reference values. The usage of repetitive power flow to determine the maximum allowable active power flow per bus is summarized below as follows:

Step 1: Define active power in kW (step); CCS factor (Cos (Ø)), and maximum power to be investigated (P_{limit});

Step 2: Run power flow for the base case;

Step 3: Do k = 0 and $P_{CCS}^{max} = 0$;(Where k = is the CCS Bus).

Step 4: Do k =k+1 (index for bus under investigation: see fig 3.9);

Step 5: k >n (Where n is the number of buses);

Yes - finish process, No – go back to step 6

Step6: Do $P_{CCS}(k) = P_{CCS}(k) + step$ (increase the active power of generator k)

$Q_{CCS}(k) = P_{CCS}(k) \times \tan(a\cos(\cos(\phi))$ (vary reactive power of generator k):

Step 7: Run Power flow;

Step 8: Any nodal voltage > 1.05 or $P_{CCS}(k) > P_{Limit.}$

Yes – Do $P_{CCS}^{max}(k) = P_{CCS}(k) - step$, and return to step 4;

No – Go to step 6.

It is important to note that the usage of power flow studies to determine the maximum allowable steady state voltage violation limit is tied up to the reactive and active power flow in the line and is dependent on the position of the CCS and the line power capacity.as presented in section 3.4.2.

5.5.1 VALIDATION OF REPETITIVE POWER FLOW RESULTS BASED ON V-P AND V-Q SENSITIVITIES

Before installing a CCS unit, the distribution operator typically assess the worst operating scenarios, which are normally related to the maximum and minimum network demand, in order to ensure that the network voltage will not be adversely affected due to the presence of the CCS [Masters 2002, Baran and Wu 1989].

Figure 5.3 [KPLC 2007a], shows a single line diagram of a 34 bus Kenyan power system which can be analogized to an IEEE 30 to 34 bus shown in Figure 5.4. The Kenyan bus system numeration was modified to facilitate the graphical visualization of the maximum allowable active power injection per bus.

The line from bus 8 to 28 in Figure 5.4 was analogized to the 440 km, 220kV Kiambere - Rabai transmission line in Figure 5.3. The Olkaria II bus in Figure 5.3 was analogized to bus 22.

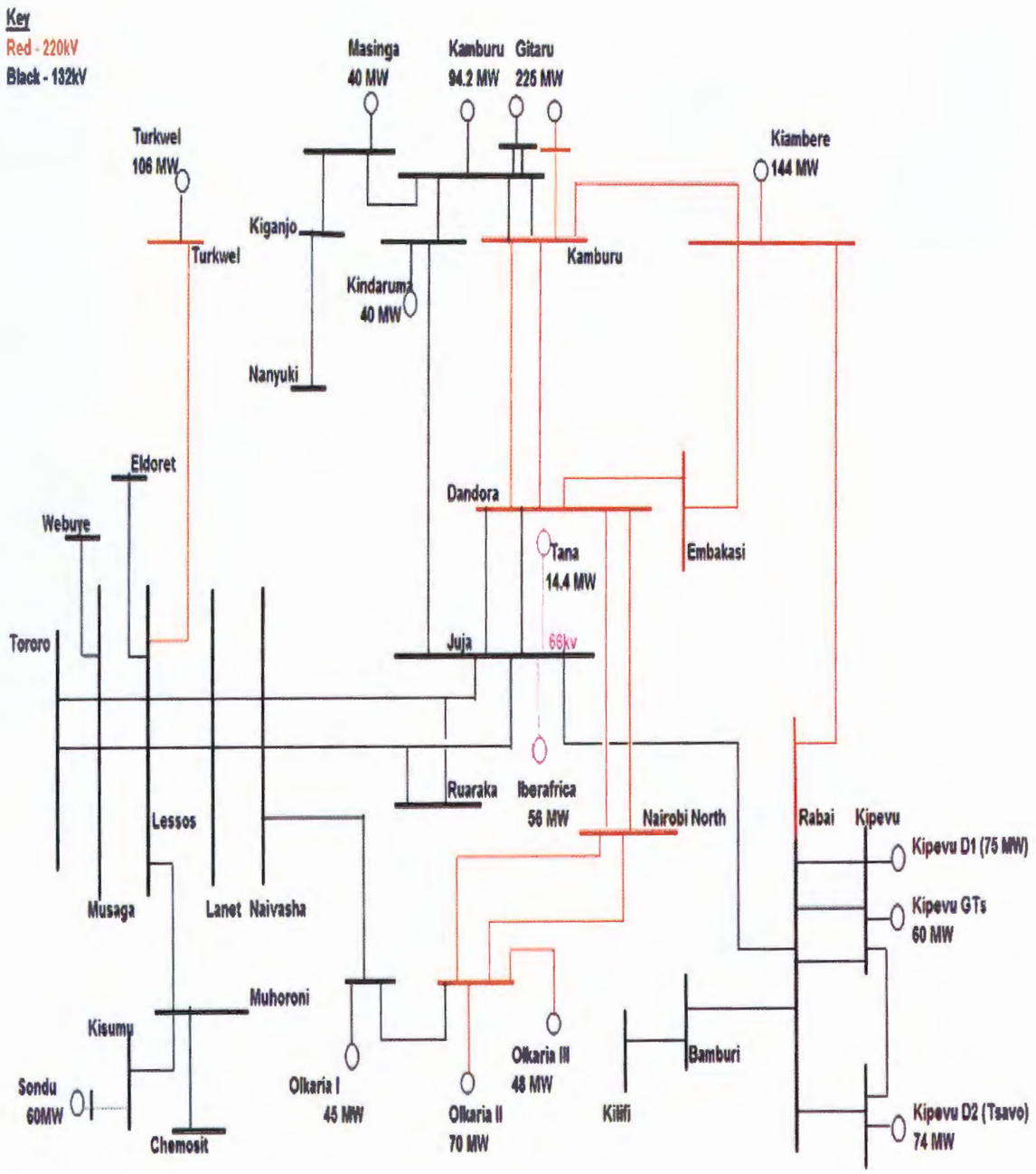

Figure 5.3 Single line diagram of Kenya transmission network

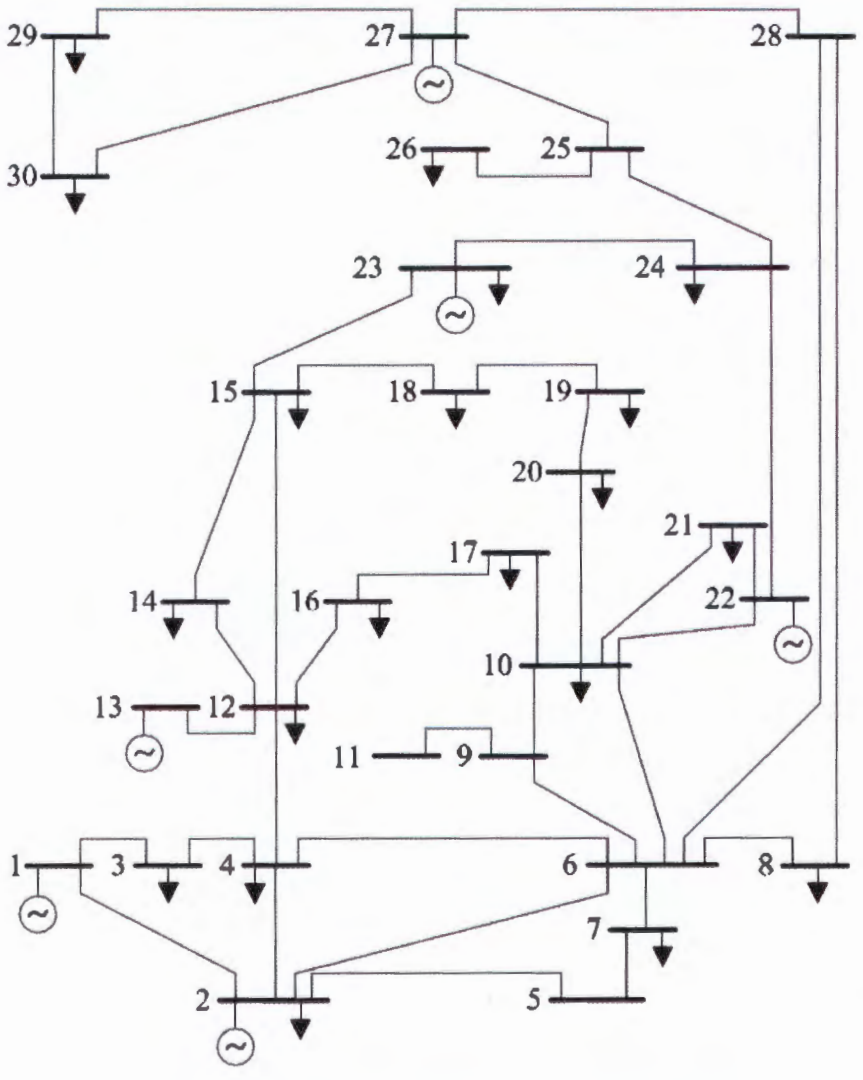

Figure 5.4 Single line diagram of the IEEE 30-bus test System

5.6 MAXIMUM PENETRATION LEVEL WITHOUT VIOLATING VOLTAGE LIMIT

As explained earlier, connecting CCS units to a transmission power network will result to a change in the voltage profile. With the increase of CCS, it may be difficult to keep the voltage on the load side feeders within the allowable range in all situations. This will limit the amount of CCS that can be connected in a network [Ayres et al. 2010, Jinfu et al. 2006].

The main goal of this research project is to determine the maximum (with respect to the voltage change they cause) allowable penetration level of CCS units in a power network without violating the steady state voltage limit of the system.

This section investigates how many CCS units can be allowed to penetrate the network when the voltage change caused by the CCS units is to stay below a certain limit.

The CCS in this case is assumed to produce as much reactive power as possible to limit the voltage increase they cause. The maximum allowable penetration will be determined when the CCS units use maximum possible reactive power to compensate the voltage change they cause [Morren et al. 2008].

The violation of the voltage limit is most likely to occur in high generation situations. In that case the CCS operates at or close to its nominal power and reactive power capability is limited. Similarly, the first way to increase the maximum penetration level of CCS is to use the CCS units to absorb reactive power from the grid.

In this way the CCS unit can compensate (a part of) the voltage change it causes. The maximum compensation that can be achieved is limited by the maximum current of the CCS. However the maximum amount of reactive power that can be consumed is given by;

$$Q_{CCS.max} = \sqrt{(V_{CCS} I_{CCS.max})^2 - P_{CCS}^2} \quad \textbf{(5.10)}$$

With Maximal CCS current defined as:

$$I_{CCS.max} = \frac{S_{dg} + S_S}{V_{CCS}} \quad \textbf{(5.11)}$$

Where; S_{dg} is the apparent power from the DG

S_s is the power absorbed by the CCS

And V_{CCS} is the CCS voltage.

The active power that is supplied to the grid will result in an increase in Vccs due to the voltage drop across the impedance. Since, P_{CCS} is independent of V_{CCS}, this results in a decrease of the active current ($P_{CCS} = V_{CCS} I_{CCS} \cos\phi$) and thus an increase of the reactive power margin. In this way the CCS unit can undo part of the voltage increase caused by its active power. First, only the margin obtained in this way will be used and the maximum penetration level determined. The voltage change caused by the CCS units' active and reactive power can be calculated from;

$$V_{CCS} = V_S + Z_{SC}\frac{S_{dg}}{V_{dg}} \quad (5.12)$$

The maximum number of installed CCS unit power ($P_{CCS.max}$) for a particular limit can be calculated by solving equation (5.10) to (5.12) iteratively.

5.7 VALIDATION TEST USING VOLTAGE SENSITIVITIES ANALYSIS.

The usage of V-P and V-Q sensitivities to determine the impact of an additional CCS on the system voltage profile by using equation 5.9 is described in this section. In the following studies three 100kVA, CCSs were added to the test system on buses 8, 22 and 28. The CCS at bus 8 operated at 0.95 inductive power factor, the CCS at bus 28 at unity power factor and the CCS at bus 22 at 0.95 capacitive power factor.

Figure 5.5 presents the voltage profile for the base case and the estimated voltage profile with the installation of one, two and three CCS, respectively, by using equation 5.9. The first CCS installed at bus 28 causes significant voltage rise even when operating at unity power factor. The buses on the main feeder are the most impacted, whereas the remaining buses suffer smaller voltage rise.

The second CCS installed at bus 8, has little impact on the system voltage profile. Due to the fact that it operates at an inductive power factor mode, hence, assist in balancing the reactive power of the line. The installation of a third CCS leads to voltage violations at the vicinity of bus 28, due to the combined effect of the two CCS. The CCS, installed at bus 22, drastically affects the whole voltage profile, since it injects simultaneous active and reactive power into the system. The combined impact of three CCS leads to severe voltage violation. This mainly takes place at the end of the main feeders (16-28).

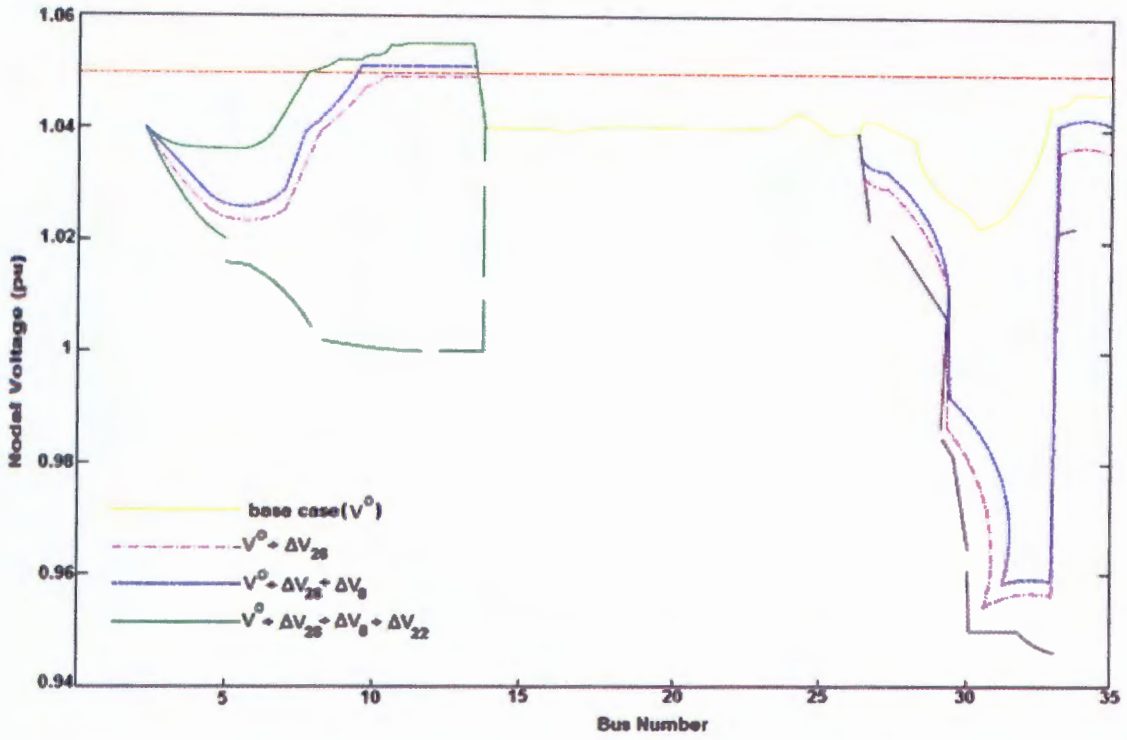

Figure 5.5 Voltage profiles with CCS units at buses 8, 22, and 28.

To justify why linearized equation 5.9 can be used, one CCS unit is considered to have been installed in bus 28 of the test network. Figure 5.6 illustrate the voltage behavior of bus 28.when the active power injection of the CCS is incremented by 1kW – steps until the superior voltage limit is reached. For each step a load flow is solved and then the graphic is plotted in Matlab software environment.

The analysis considers three different power factor operation (pf = 0.9 inductive, pf = 1.0 and pf = 0.9 capacitive) and the maximum demand scenario. The linear behavior of the nodal voltage can be observed. Indeed, the slopes of these lines are approximately equal to the sensitivity coefficients of J_{PQ} which are also shown in Figure 5.6.

These results explain why the maximum capacity of CCS can be estimated by using voltage sensitivity analysis which are linearized equations. The behavior of CCS systems within narrow voltage variation is close to linear. Figure 5.6 reveals that, as expected, the capacitive operating mode presents a higher sensitivity coefficient than that of the other operating modes. Therefore, the amount of power injected for this operating mode is the lowest for the three analyzed cases.

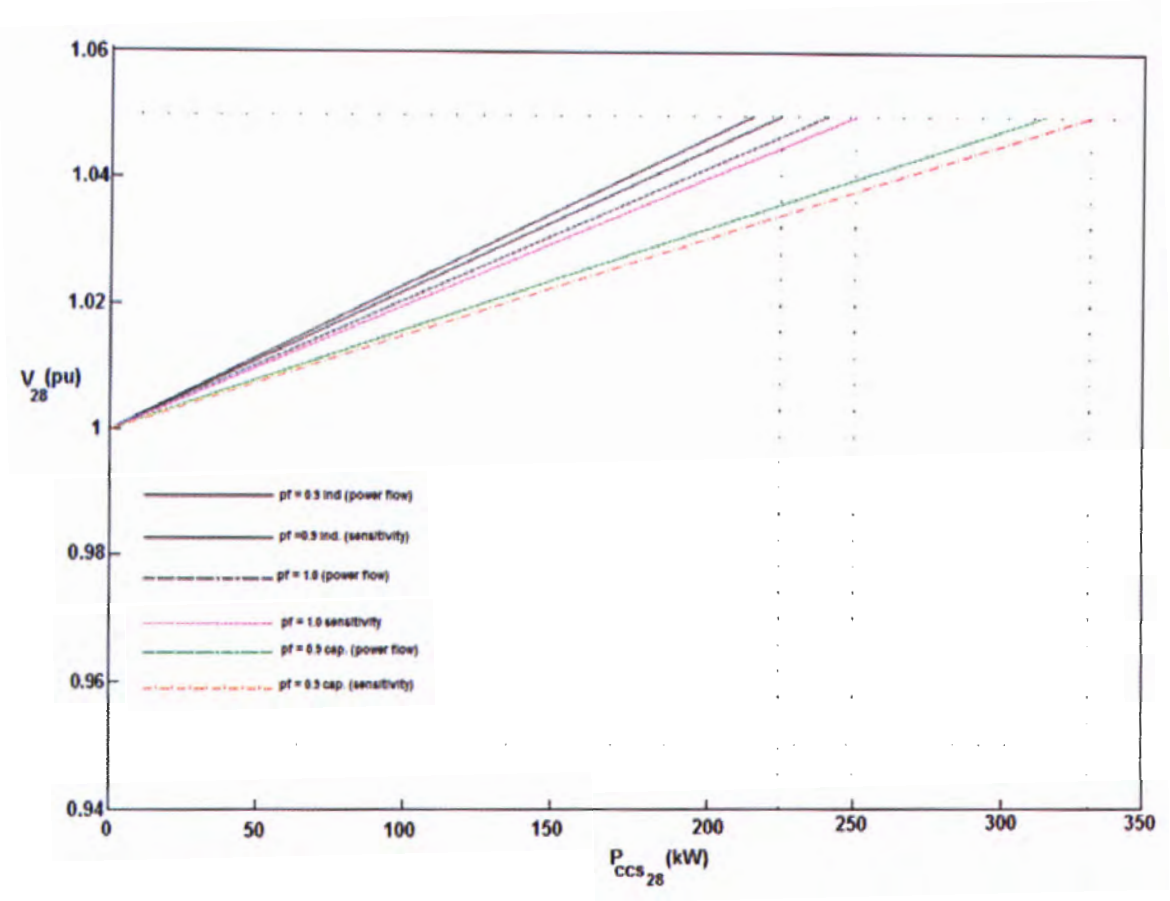

Figure 5.6 Maximum Allowable Power Of Bus 28.

In order to further validate the estimation of the system voltage profile with the addition of another CCS by using equation 5.9. A CCS unit of 100kW was installed at bus 11. The maximum demand scenario was considered and two different value of power factor were analyzed. The base case voltage profile (without any CCS unit) and the new voltage profile after the addition of the CCS are illustrated in Figure 5.7.

This reveals that the results provided by the voltage sensitivity based methodology are very close to those obtained by use of successive load flow solutions. The capacitive operating mode case presents the largest voltage variation. Consequently, the major error is related to this case.

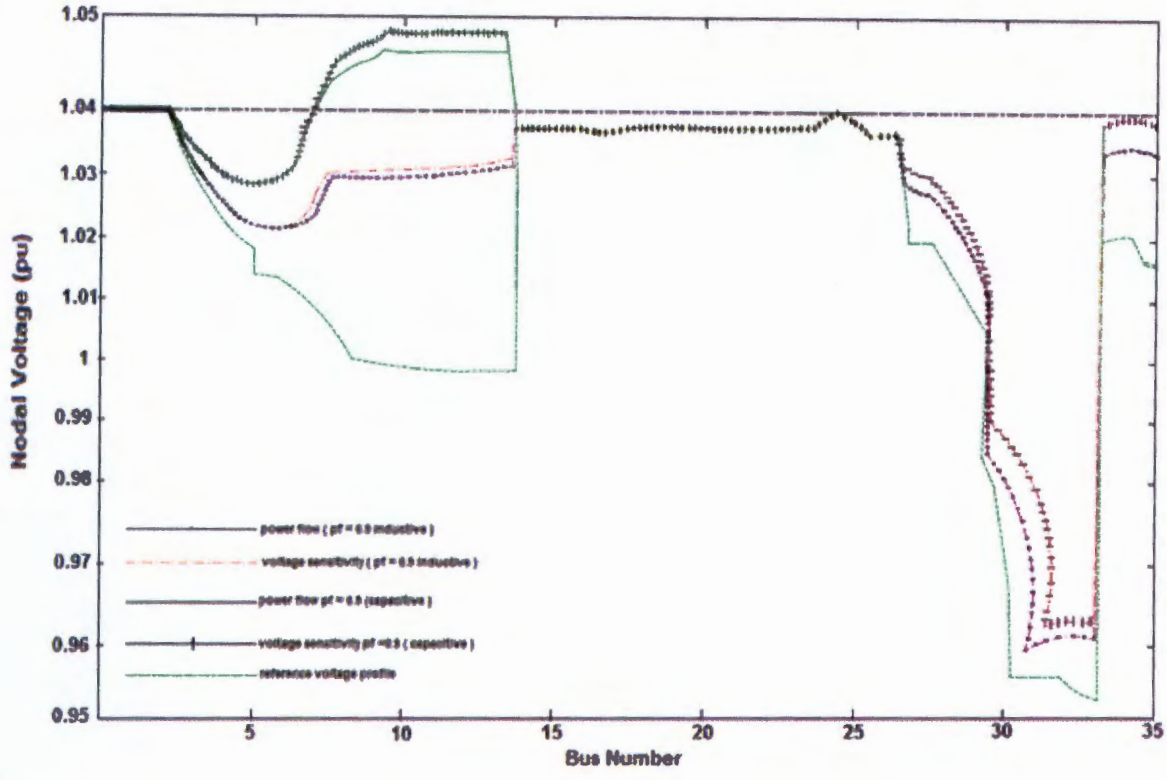

Figure 5.7 Voltage profile for different power factors for ccs unit

Figure 5.8 presents the evolution of the error between the estimated and compared voltage magnitude of bus 11 as a function of the active power injected by the CCS. Although, the error increases when the power is incremented, the maximum error is within an acceptable range for a linear method (lower than 0.2%).

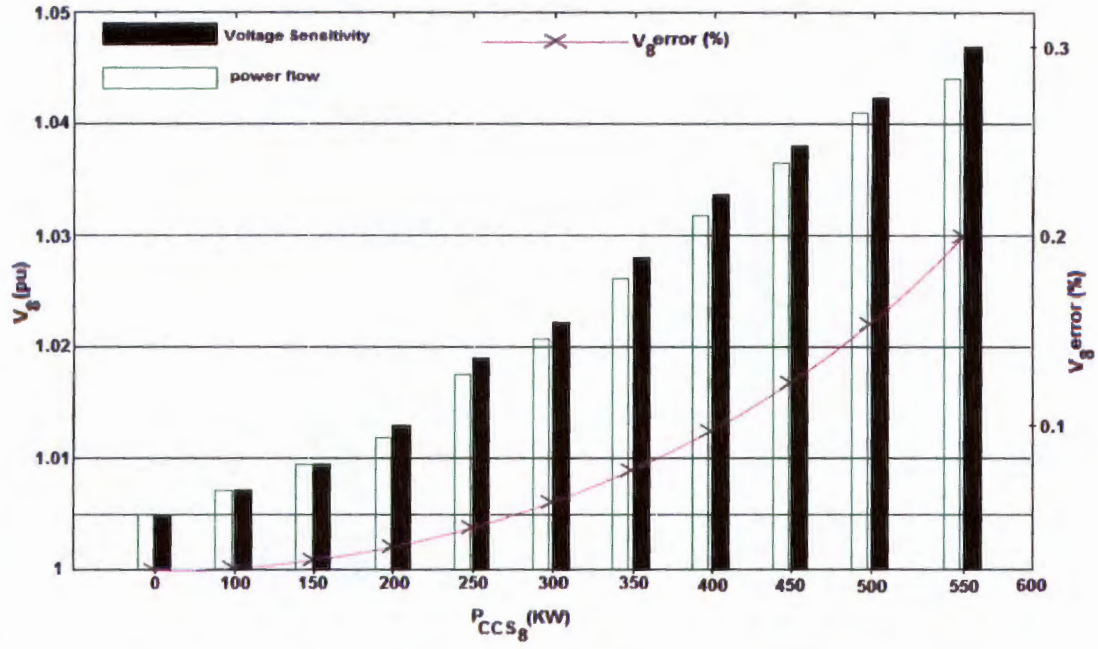

Figure 5.8 Assessment of voltage sensitivity

5.8 ONWARD

In this chapter, an analytical methodology based on voltage sensitivity was used to directly estimate the maximum allowable power that a CCS can inject into the system without causing steady state voltage violations and assuming no substantial changes in system structure. The results obtained by the proposed method were compared with those provided by repetitive power flow solutions in chapter 4. The accuracy of the proposed method was shown to be adequate. It is important to emphasize that, although the proposed method had presented good performance, this is an approximated approach due to linearization of the system model.

Further, it is important to call to attention that other technical aspects have to be analyzed when determining the maximum allowable CCS units in the system such as protection system and active power loses which cannot be addressed by the proposed method. Thus this method should be used only during preliminary investigation stages. The next chapter presents a case study of Auxiliary Service Voltage Transformers (ASVTs) in power networks.

6 AUXILIARY SERVICE VOLTAGE TRANSFORMERS ON POWER NETWORKS: (CASE STUDY)

6.1 INTRODUCTION

Auxiliary Service Voltage Transformers (ASVTs) are a relatively inexpensive way of supplying power to communities living in close proximity to high voltage power lines. ASVT sub-stations based on Instrument Voltage Transformer concept have been built and used successfully in Mexico, South America, with power rating ranging from 50kVA to 1MVA as described earlier in chapter 2 and 3.

An ASVT acts as an inductive feeder, when integrated into a power transmission line and may cause a significant change on long transmission line voltage profile depending on the penetration level of the ASVT units. Transmission lines utilize reactive power to support their magnetic fields. The magnetic field strength is dependent on the magnitude of the current flow in the line and line natural inductive reactance (X_L). It follows, then that the amount of MVAr used by a transmission line is a function of current flow and inductive reactance ($MVAr = I^2X_L$) [Miller 1982].

Therefore, in this chapter the 220kV, 440 km, (Kiambere – Rabai) line under study was integrated to ASVT units. First, the ASVT was designed using the reverse design approach developed in chapter three, then integrated to the transmission line. System energisations at no-load and on-load were carried out. Simulations were first done with the line not loaded followed by a loaded line and finally the line under short circuit conditions.

Voltage and power variable constraints were taken into considerations. The ASVT units were included at different distances. The line was cascaded with pi sections to increase the speed of convergence and reduce delays in the Sim Power software used.

6.2 ASVT DESIGN USING THE REVERSE DESIGN METHOD

In the reverse design approach the transformer is built up from the core outwards. The core cross-section dimensions (diameter for a circular core and side lengths for a rectangular core) are selected from cataloques of available materials. A core length is chosen. Lamination that are available can be specified in thickness. A core stacking factor can be estimated from the ratio of iron to total volume [Bell and Bodges 2007].

This type of design is suitable for ASVT models since they are meant for customized application [Karsai et al.1987, Dasguta 2002, Bell and Bodges 2007].

Figure 6.1 shows the proposed design procedures for the ASVT in form of a flow chart. The detailed design of the same along with a proto-type built and tested in the laboratory are presented in appendix F.

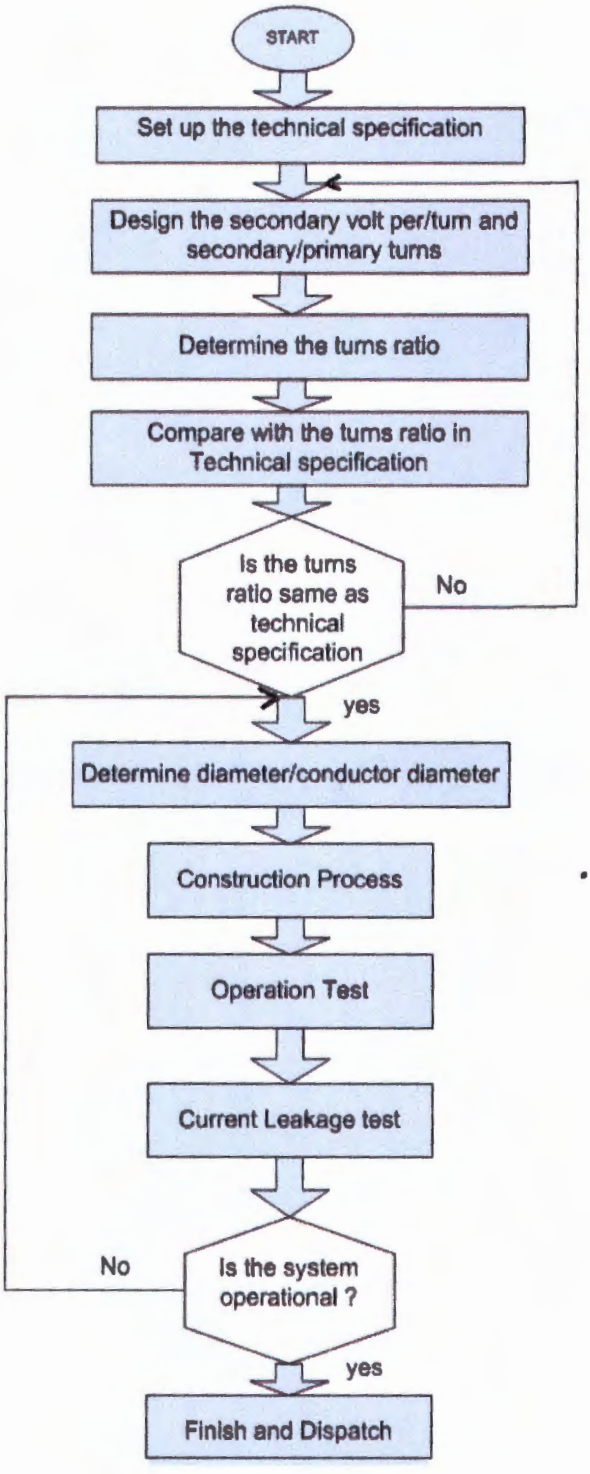

Figure 6.1 Flow chart for ASVT design

6.3 ASVT DESIGN FLOW CHART

The process was initialized by setting up the technical specifications, of the ASVT to be designed, using the power rating of the transformer as captured in the technical specification, secondary volt/ turn is determined. This secondary volt/turn is then used to determine the secondary turns. By use of the secondary/primary voltage ratio, the primary turns are determined. The primary and secondary turns are then used to determine the transformation ratio.

This calculated turns ratio is then compared with the turns ratio in the technical specifications, if not the processor transfers control to start off the process, if yes, the central processing unit proceeds to determine the core area then the core diameter, core stack, step width, number of coils per turn, weight of the core, conductor diameter and number of coils per turn. The prototype is then constructed and operational test and current leakage test administered. If the required parameters have not been achieved the process is repeated. If the system operates as expected, the process is finished and the system dispatched

6.4 SIMULATION SCENARIOS

To investigate both the transmission systems and the supply/load side maximum voltage violation limits under a varying ASVT penetration level. Several repetitive simulations scenarios are defined with respect to the distance of the ASVT unit relative to both ends of the line. The sending and receiving end voltage are measured and analyzed in each case. The simulation scenarios were classified as follows;

- Model for ASVT in the line at steady state with and without load
- Model for ASVT in the line at transient state with load
- Model for ASVT units(s) in the line without and with load, with reactor on/off circuit.
- Model for combined ASVT and CCS unit (s) in the line at different distances.

The ASVT unit(s) are also subjected to the same loading condition as the CCS indicated in section 4.3 of chapter 4. Loadability analysis was also carried out to show the variation of load voltage with load MVA

6.5 MODEL FOR ASVT IN THE LINE AT STEADY STATE CONDITION WITH LOAD

In this case, ASVT systems were connected at specific locations on a loaded transmission line and steady state measurements carried out for each simulation. The measurements carried out were with regard to tapped voltage (V_T) and load voltage (V_L). Figure 6.2 and Table 6.1 show the model used for Simulation of the system and the measured values respectively. Please note that the font of Figure 6.2 is somehow small and blurred due to the direct output from the simulation software used in this first scenario.

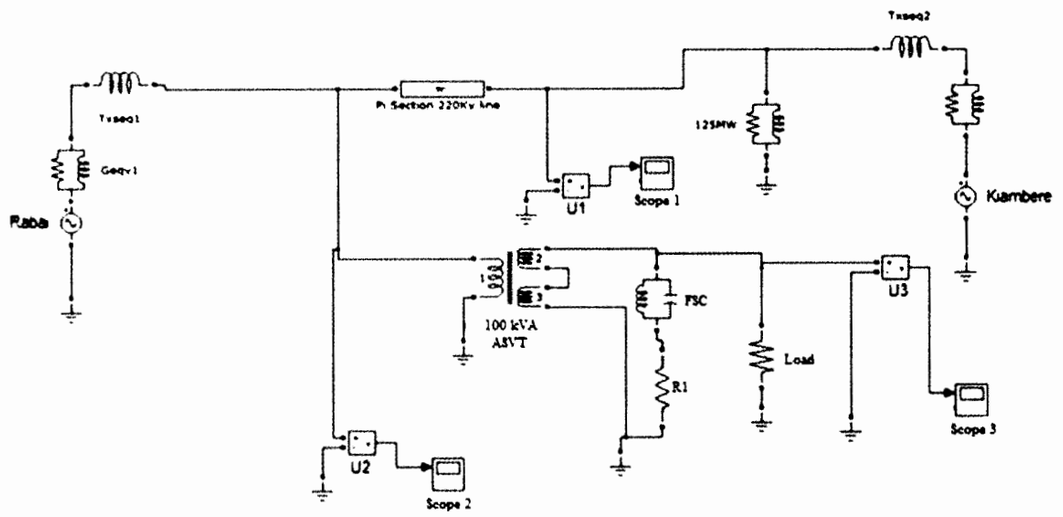

Figure 6.2 Model circuit with one ASVT (pi-section = 440km transmission line) line loaded

Table 6.1 Measurements for different penetration levels of ASVT at steady state

		LENGTH OF THE TRANSMISSION LINE IN KILOMETERS								
NO.OF ASVT	VOLTAGES	48.889	97.778	146.667	195.552	244.444	293.333	342.222	391.11	440
1	VT									154.61KV
	VL									0.266KV
2	VT				146.51KV					154.61KV
	VL				0.242KV					0.256KV
3	VT			143.00KV			151.67KV			154.6KV
	VL			0.248KV			0.263KV			0.268KV
4	VT		138.91KV		146.51KV		151.67KV			154.61KV
	VL		0.230KV		0.242KV		0.251KV			0.256KV
5	VT	133.64KV		139.4KV		143.56KV		146.09KV		146.93KV
	VL	0.221KV		0.230KV		0.237KV		0.242KV		0.243KV

VT-TAPPED VOLTAGE
VL-LOAD VOLTAGE

The objective of each measurement was to observe whether the allowable voltage limitation was being surpassed at different ASVT(s) penetration levels. Five configurations of the models were considered during simulation, ranging from a single ASVT penetration at the end terminal of the transmission line to five ASVT units penetrating the system. Different arrangements at specific distances on the transmission line were considered and measurements taken as shown in table 6.1.

The ASVT simulation results showed that the tap-off voltage *(V_T)* on the transmission line reduces as the number of ASVT penetration increased. The tap-off voltage drop for the five ASVT units connected on the transmission line did not conform to the allowable voltage drop of 6 % of the nominal voltage. (Please note that the nominal voltage is $220/\sqrt{3}=127$kV per phase).

Thus, voltage compensation technique was required for the five ASVT units penetration at steady state and with load. This meant that the system required some capacitive reactance injection to absorb the increased inductive reactance in the system. The magnitude of the load voltage (V_L) for four and five ASVT units' penetration was within the acceptable range of 2.5%, except for the first three ASVT penetrations, where the voltage appeared high. In summary it can be observed that penetration of five ASVT units gave an acceptable voltage profile on the load side. However, the tap-off side gave a slightly higher voltage profile.

6.5.1 MODEL FOR ASVT IN THE LINE AT STEADY STATE CONDITION WITHOUT LOAD

In this case, ASVT systems were connected at specific locations on unloaded transmission line as shown in Figure 6.3.

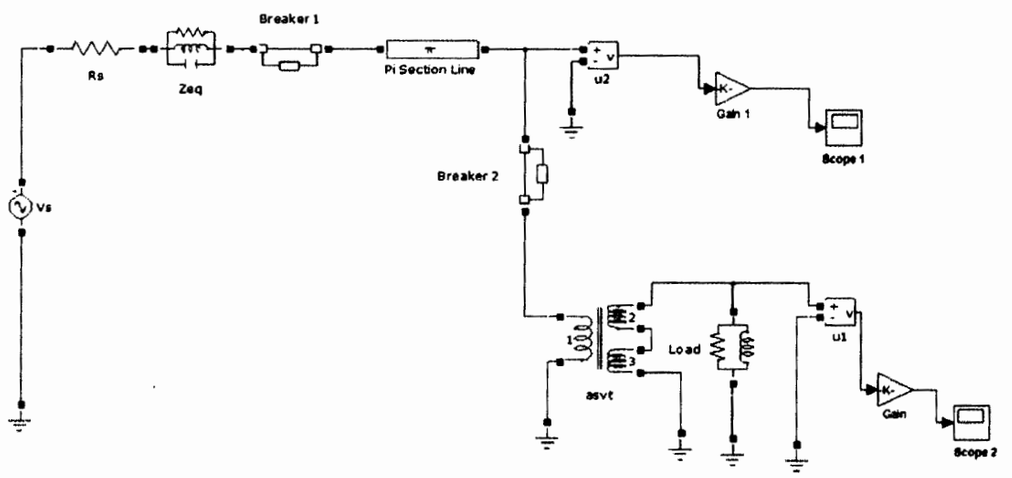

Figure 6.3 Model circuit with one ASVT without load

Steady state measurements were carried out for each simulation. Appendix G1 and G2 show the models used with two and three ASVT penetration respectively. The results showed that there was an overshoot in both the tapped voltage and the load voltage.

6.5.2 MODEL FOR ASVT IN THE LINE AT TRANSIENT STATE WITH LOAD

A number of disturbances were injected into the ASVT system and resulting transients observed. Figure 6.4 shows the layout of the ASVT including the positions of instruments for monitoring and injection of the disturbance. The observations were made at two points; tap-off point (V_T) and load terminal (V_L). The controlling signals (from the timer) are also shown in the layout. Simulation results are as shown in Figure 6.5 (a-c). The waveform measurements were displayed out as follows;

- Scope 1 measured the system current
- Scope 2 measured the tap off voltage (V_T)
- Scope 3 measured the load voltage (V_L)

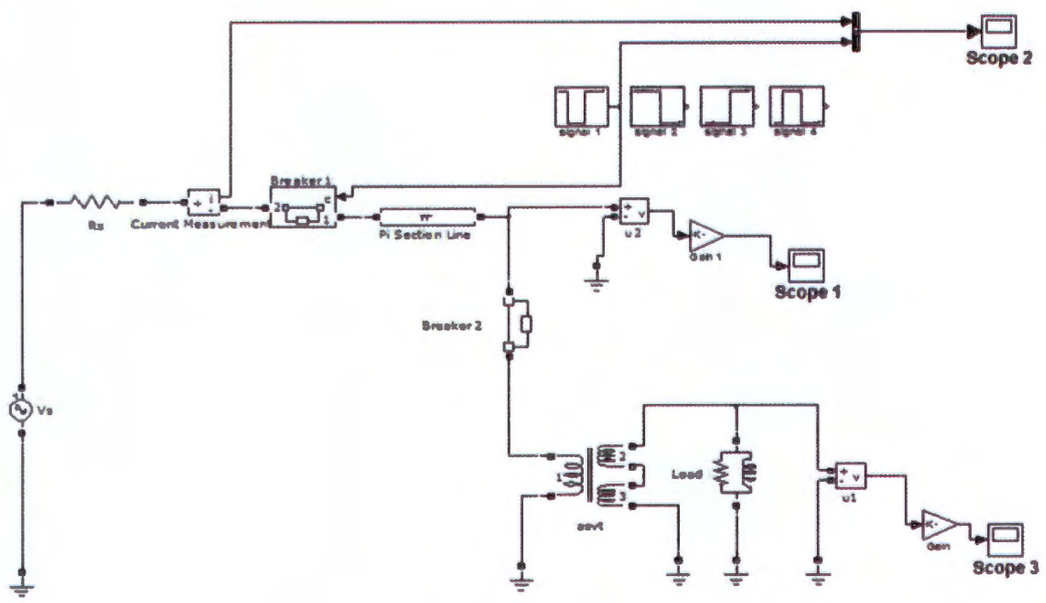

Figure 6.4 Model circuit with one asvt (pi-section =440km transmission line)

It is important to note that, all the graphs in this section are labeled as follows; Graph (a) waveforms represent graphs of current (A) against time in (seconds) and graphs (b), and (c) waveforms are graphs of per unit kilovolt (kV) against time (seconds).

The graphs in appendix H are also labeled in the same manner. Figure 6.4 illustrates a breaker 1 connected in series with the ASVT system on a 50Hz voltage source through a transmission line, the signal (1-4) in the model circuit simulates the switching in and out of the ASVT for a short duration. The switching time of the breaker block is controlled by Simulink signal which is defined by a logical signal (0 or 1) connected to the Simulink input.

Signal 1

The breaker device was initially closed, an opening order was given at t = 5 cycles and then closed again at t =15 cycles. Figure 6.5 illustrates that when the ASVT system was switched on, an inrush current of about 3 times normal system current and voltage overshot of about 1.3 times normal tap-off voltage was observed. When breaker was opened the voltage remained at a high level this could be attributed to the restricting voltage of the circuit breaker.

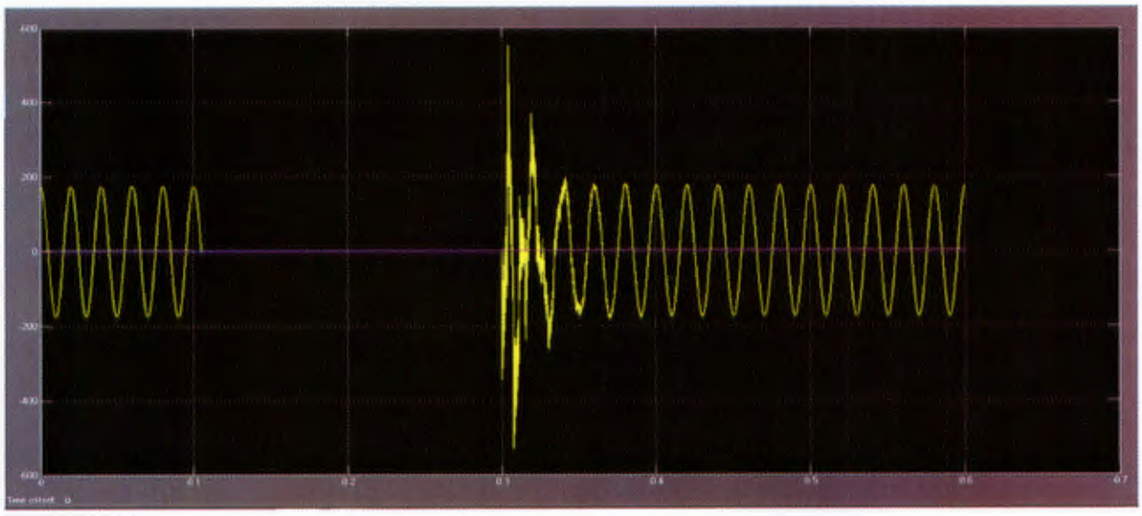

(C) SYSTEM CURRENT WAVEFORM.(SCOPE1)

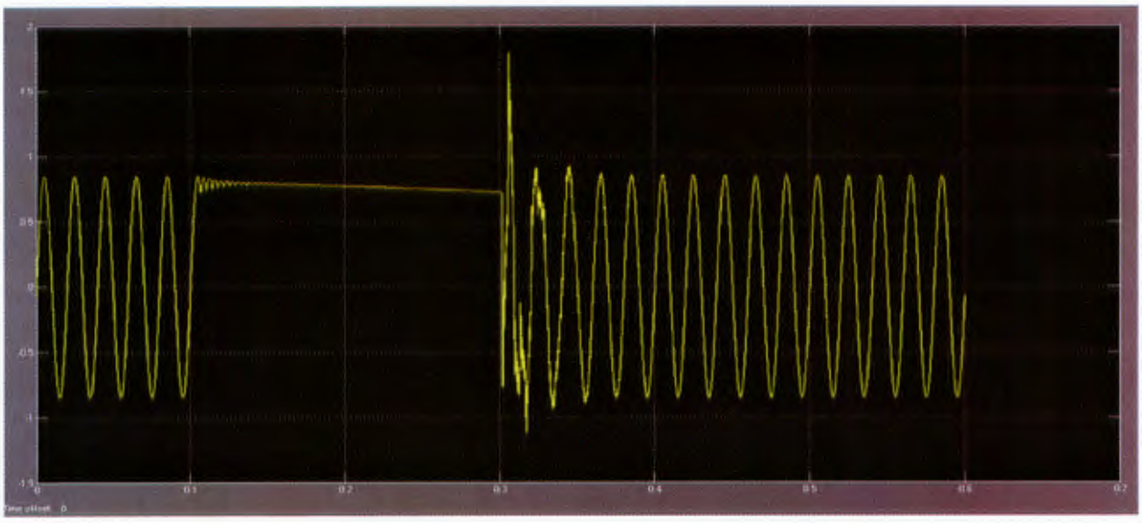

(D) TAP-OFF VOLTAGE WAVEFORM.(SCOPE 2)

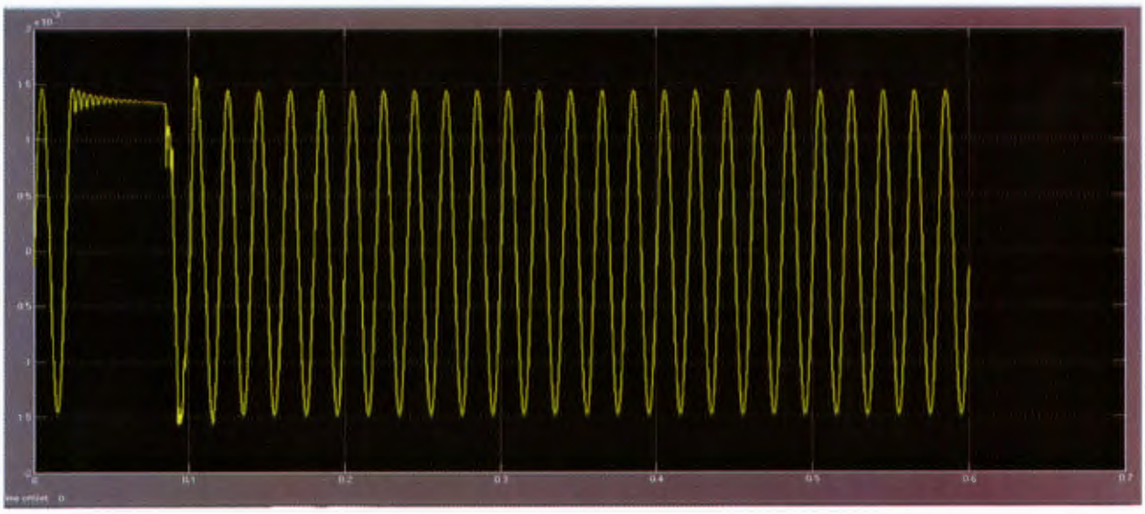

(E) LOAD VOLTAGE WAVEFORM.(SCOPE 3)

Figure 6.5Waveforms for signal 1 injection

Signal 2

In Figure 6.4 the breaker device was initially closed and an opening order was given at t =15 cycles. Here neither inrush current nor voltage overshot on the waveform was observed as shown in Figure 6.6 below.

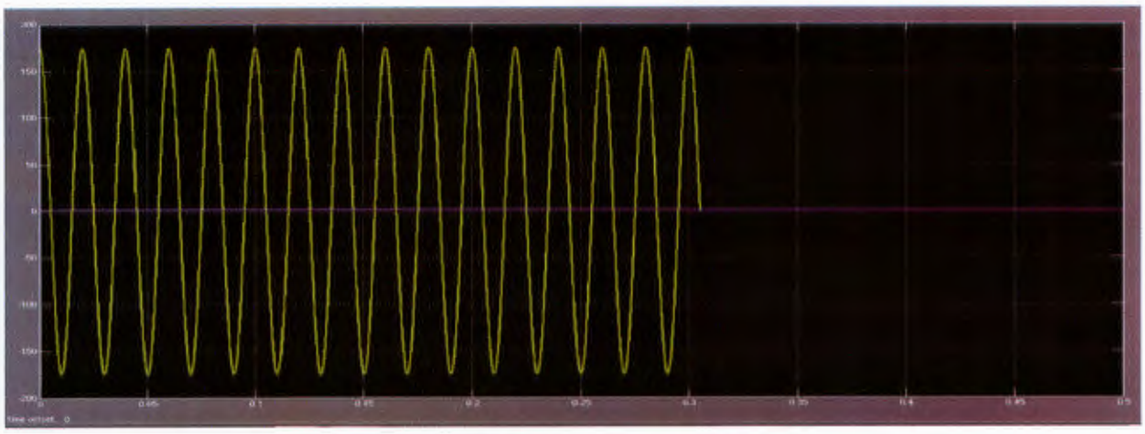

(A) SYSTEM CURRENT WAVEFORM.(SCOPE1)

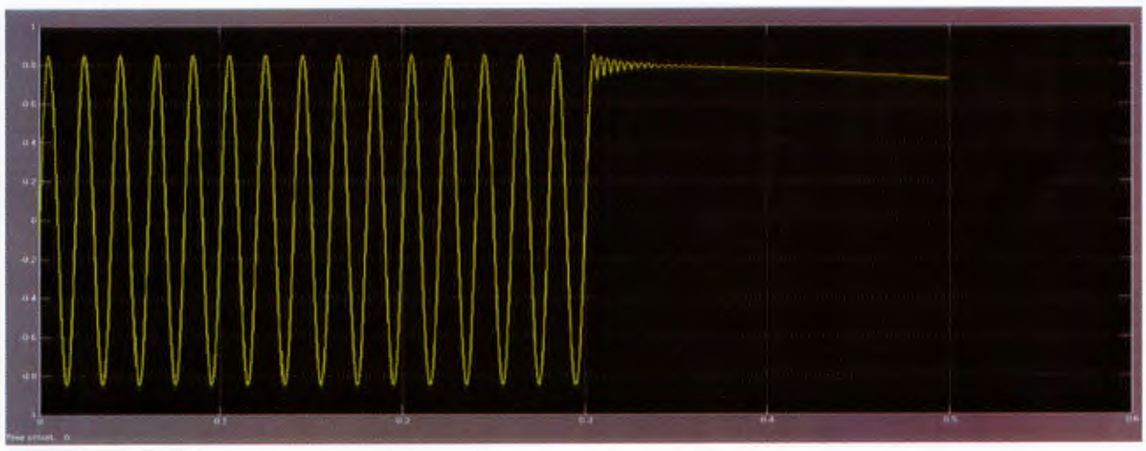

(F) TAP-OFF VOLTAGE WAVEFORM.(SCOPE 2)

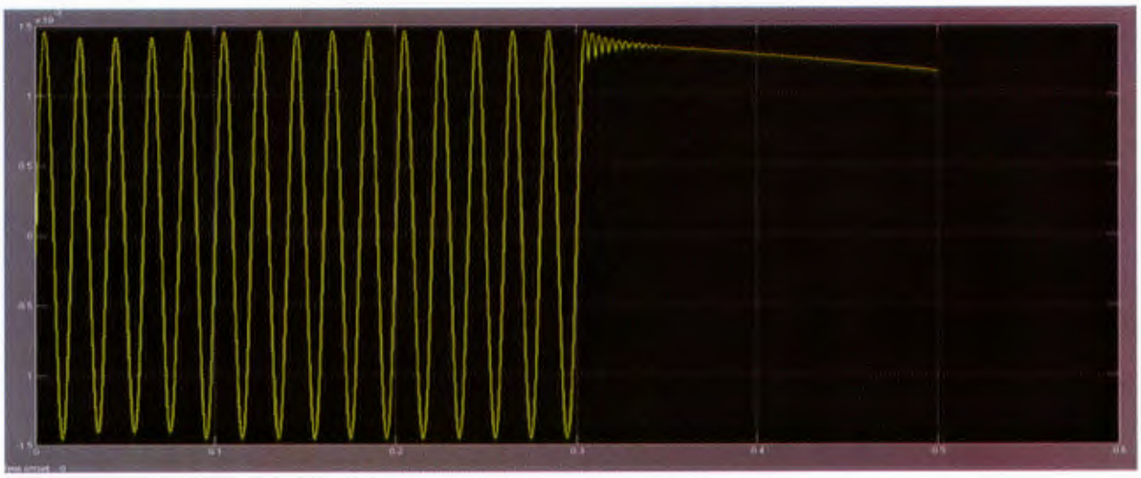

(C)LOAD VOLTAGE WAVEFORM.(SCOPE 3)

Figure 6.6 Waveforms for signal 2 injection

Signal 3

During simulation the breaker device was initially off and closing order was given at t =15cycle. Figure 6.7, shows an inrush current of about 1.2 time's normal system current. An overshot tap-off voltage of about 1.3 times the normal voltage and load voltage overshot of about 1.2 times the normal load voltage was observed.

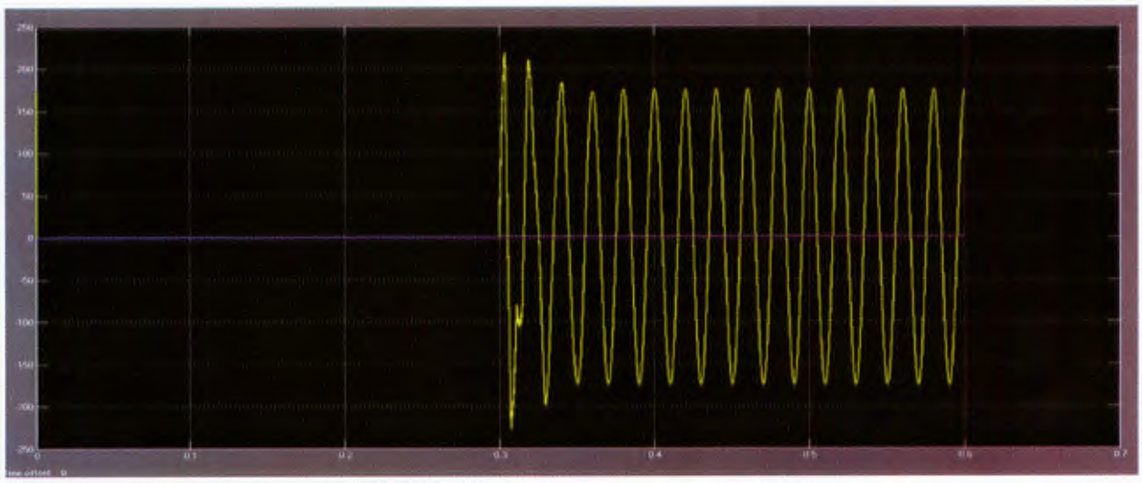

(A) SYSTEM CURRENT WAVEFORM.(SCOPE1)

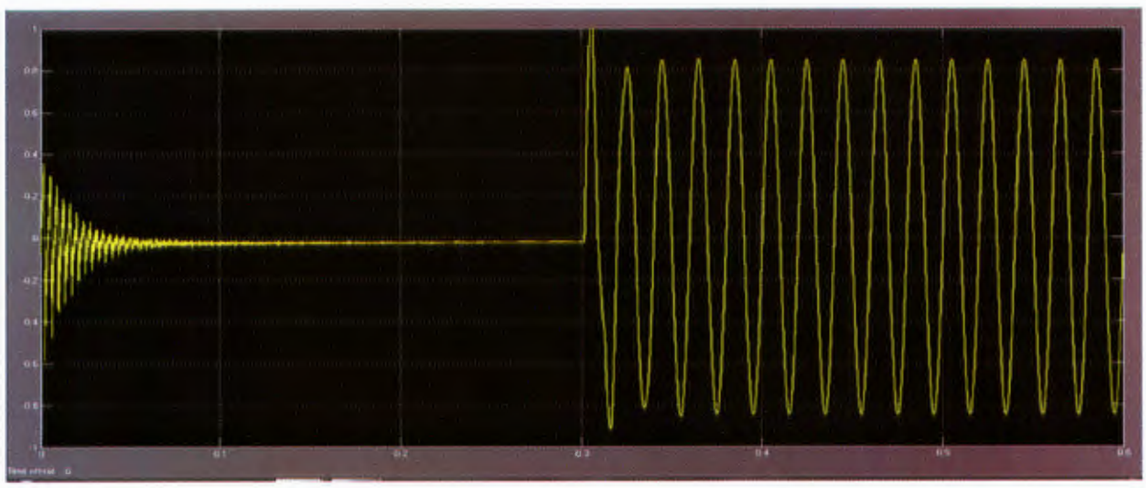

(B) TAP-OFF VOLTAGE WAVEFORM.(SCOPE 2)

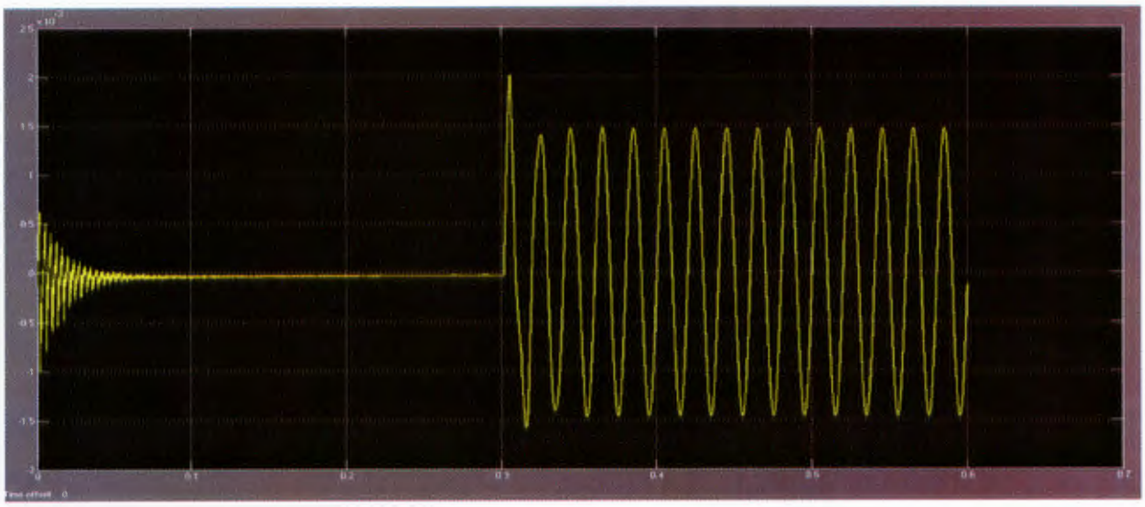

(C)LOAD VOLTAGE WAVEFORM.(SCOPE 3)

Figure 6.7 Waveforms for signal 3 injection

Signal 4

In this case the breaker device was initially off and a closing order was given at t = 5 cycles and then opened again at t = 15 cycles. An inrush current of about 1.2 times the normal system current was observed at t = 5 cycle, overshot of about 1.3 times normal tap-off voltage and 1.5 times normal load voltage are shown in Figure 6.8.

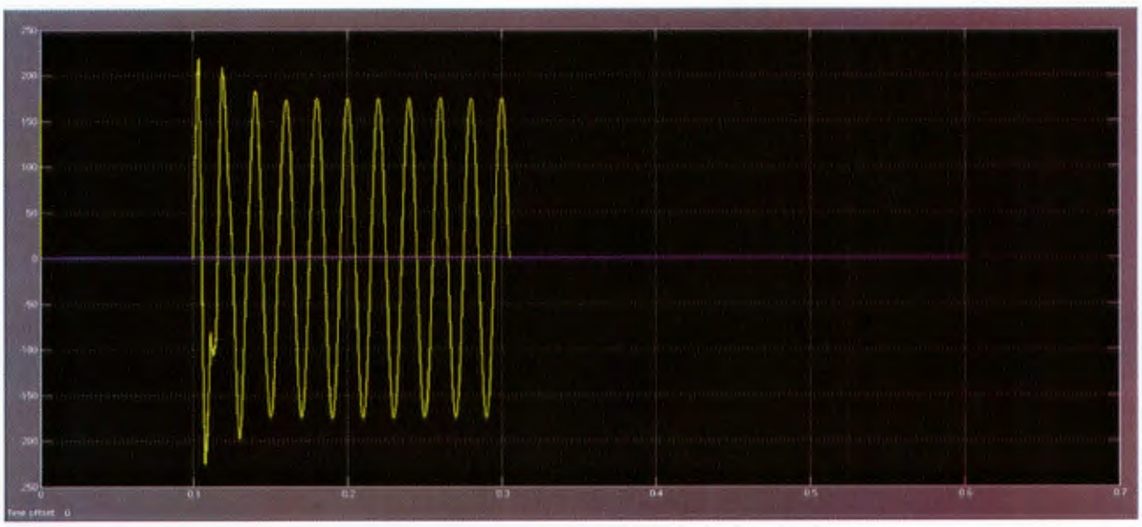

(A) SYSTEM CURRENT WAVEFORM.(SCOPE1)

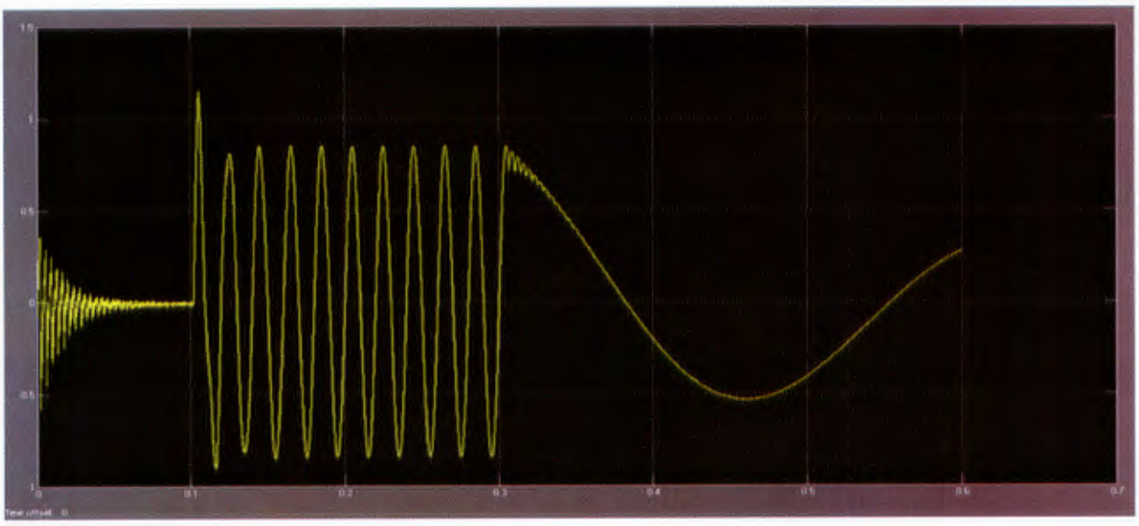

(B) TAP-OFF VOLTAGE WAVEFORM.(SCOPE 2)

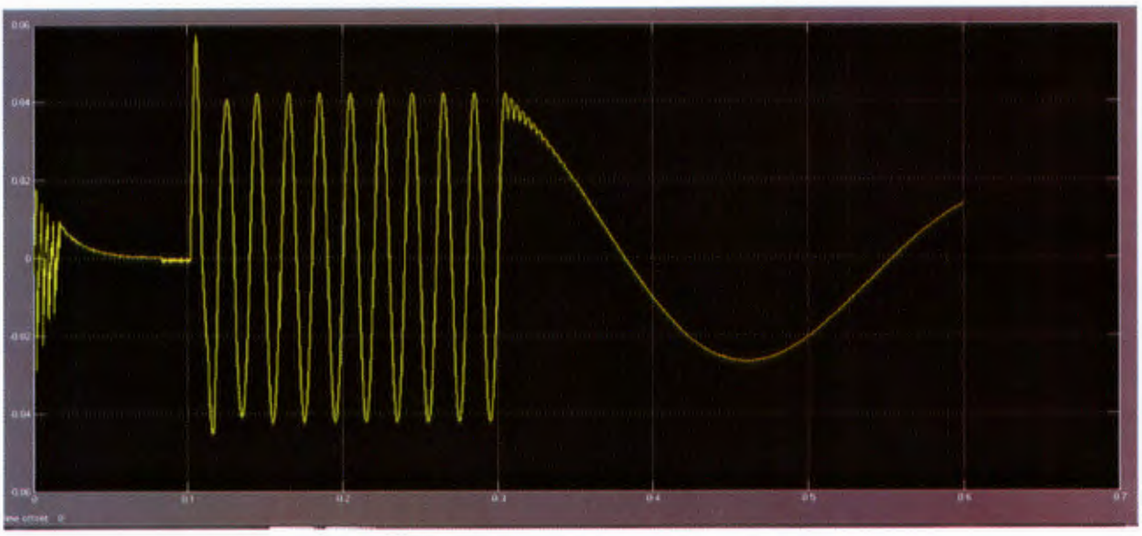

(C)LOAD VOLTAGE WAVEFORM.(SCOPE 3)

Figure 6.8 Waveforms for signal 4 injection

6.6 MODELS FOR ASVT IN THE LINE WITHOUT AND WITH LOAD AND REACTOR ON/OFF

In this case, we consider steady state behavior line voltage without the ASVT sub-station installed, then with the ASVT in circuit and finally with more than one ASVT units in circuit. The simulations were carried out with the line not loaded and later loaded with the reactor on/off at various instances. The models are shown in Figure 6.9 and 6.10 respectively. Figure 6.11(a)-(b) and Table G1 at the appendix shows simulated voltage waveforms for the sending and receiving end voltage and the analysis respectively.

It was seen that the receiving end load voltage (V_L) for the unloaded case ranged between 232V to 249V, while for the loaded was between 212V to 227V. Switching resonance was experienced for about two cycles as shown in Figure 6.11(a)-(b). The HV voltages were 145.926kV to 145.968kV respectively. Considering a per phase value of 127kV, there was an over shoot in both cases.

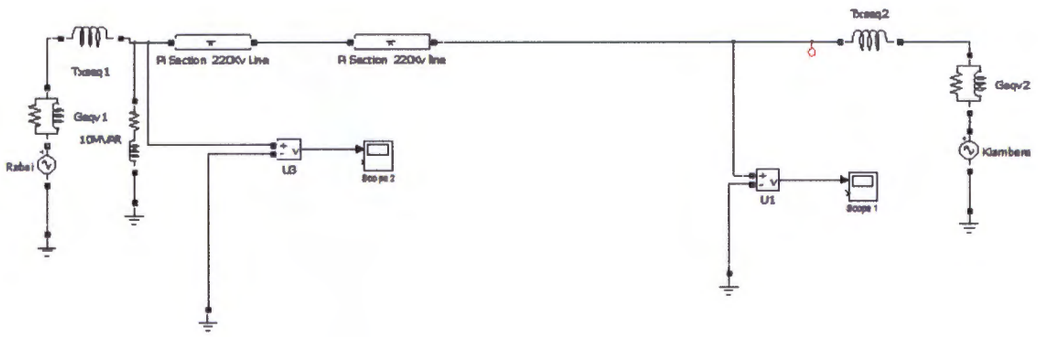

Figure 6.9 Model for the line without load and ASVT

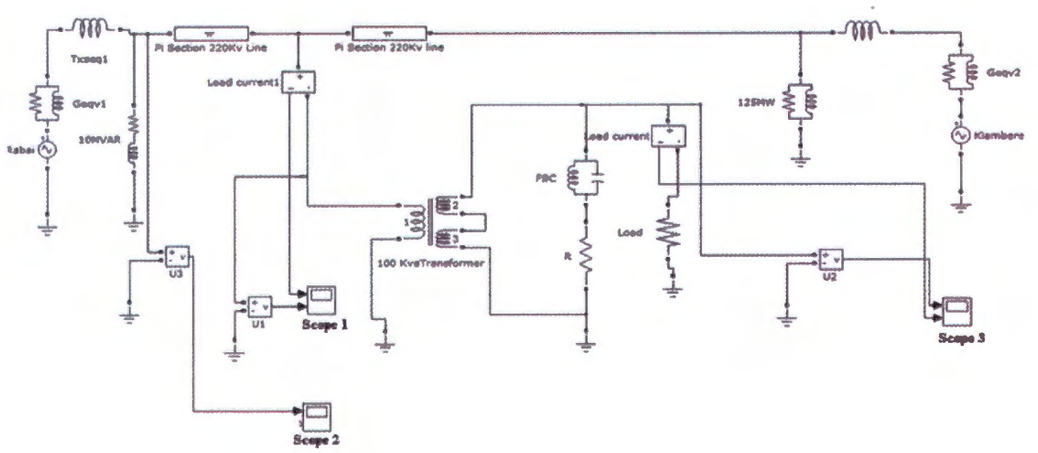

Figure 6.10 Model for the line with load and one ASVT

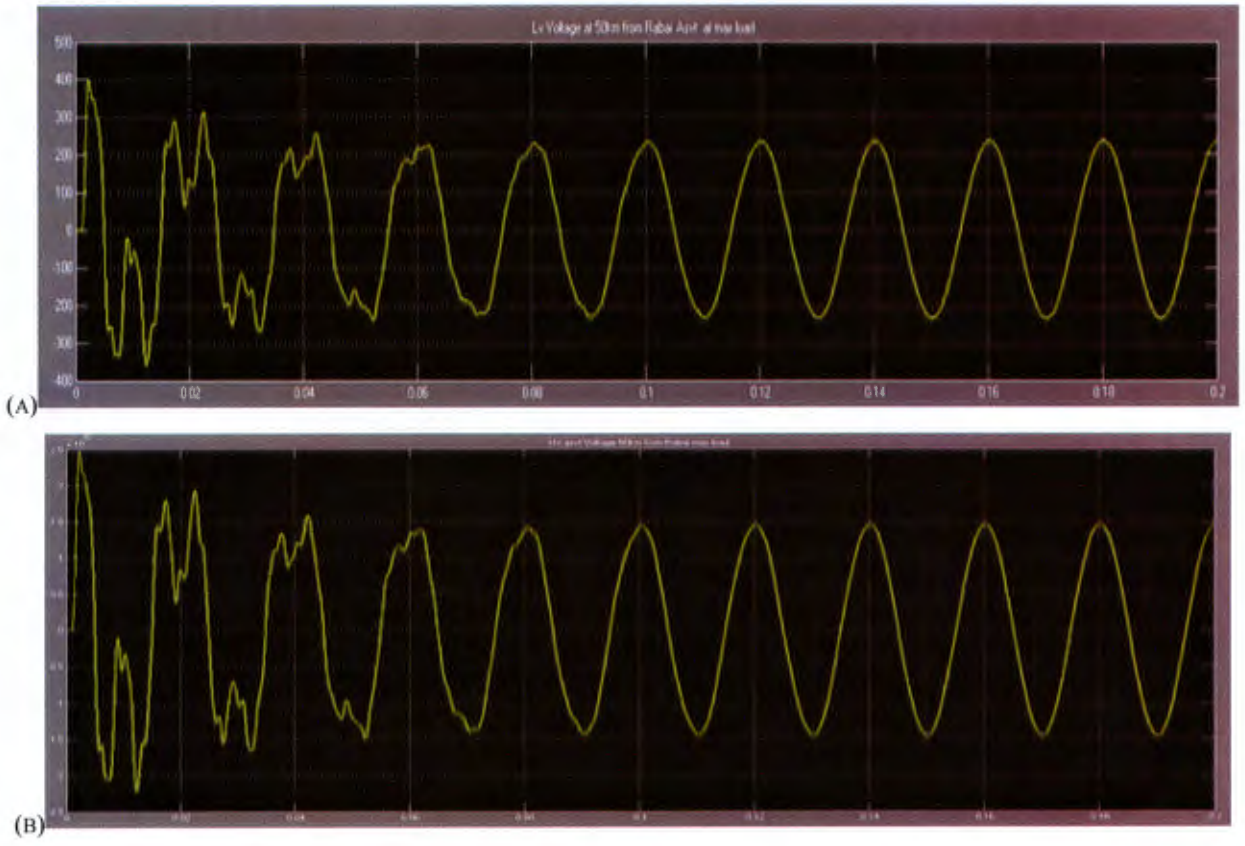

Figure 6.11 Receiving end LV and HV voltage

6.6.1 SIMULATION WITH TWO ASVT INSTALLED

Distances of the ASVTs from sources were altered by varying the length of the pi sections. This was done first with the main line having no load and then with a loaded line of about 125MW. Figure 6.12 shows the circuit used for simulation. The ASVT was tested for same loading conditions. The distance covered was spaced at 50km range. The assumption was that the lines were switched at different points on the wave. Different measurements were taken with regard to:

- Load terminal voltage (V_L) and current
- High Voltage (V_{in}) or Tap-off Voltage (V_T)

The nature of distortion on high voltage and low voltage was also analyzed. Table G3 at the appendix shows details of the measured parameters. It was observed that in this scenario, the high voltage overshot from 148.2kV to about 148.9kV depending on the ASVT distance from Rabai substation. Conversely, the low voltage decreased from 250V to about 217V as the distance from Rabai sub-station increased. Figure 6.13 shows the simulated waveforms. The switching resonance for both high and low voltage varied between 1 and 2 cycles. It was evident that low voltages were experienced on the ASVT low voltage network when the HV line was highly loaded.

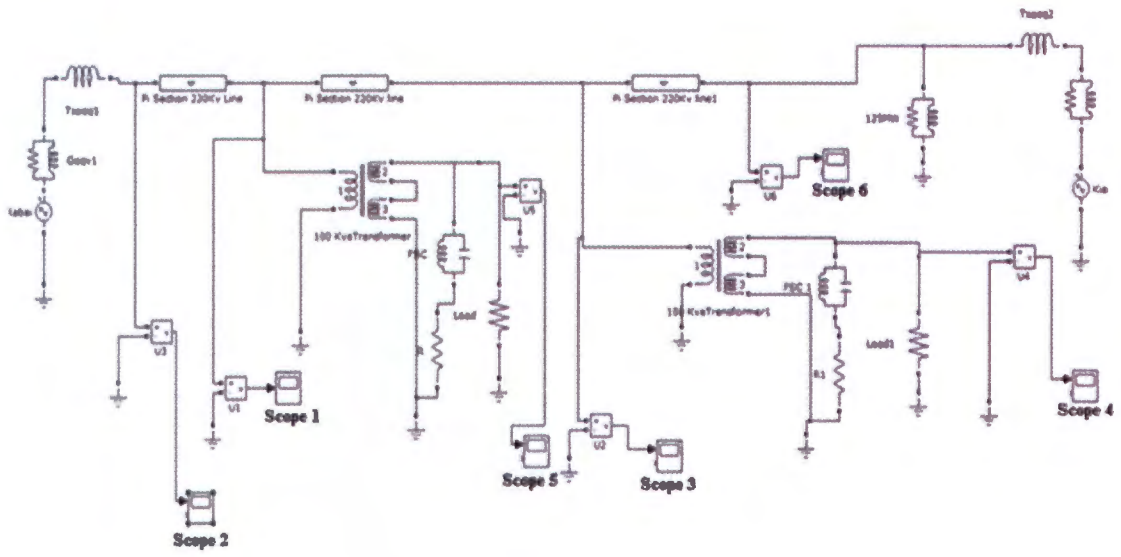

Figure 6.12 Model for the line with load and two ASVTs

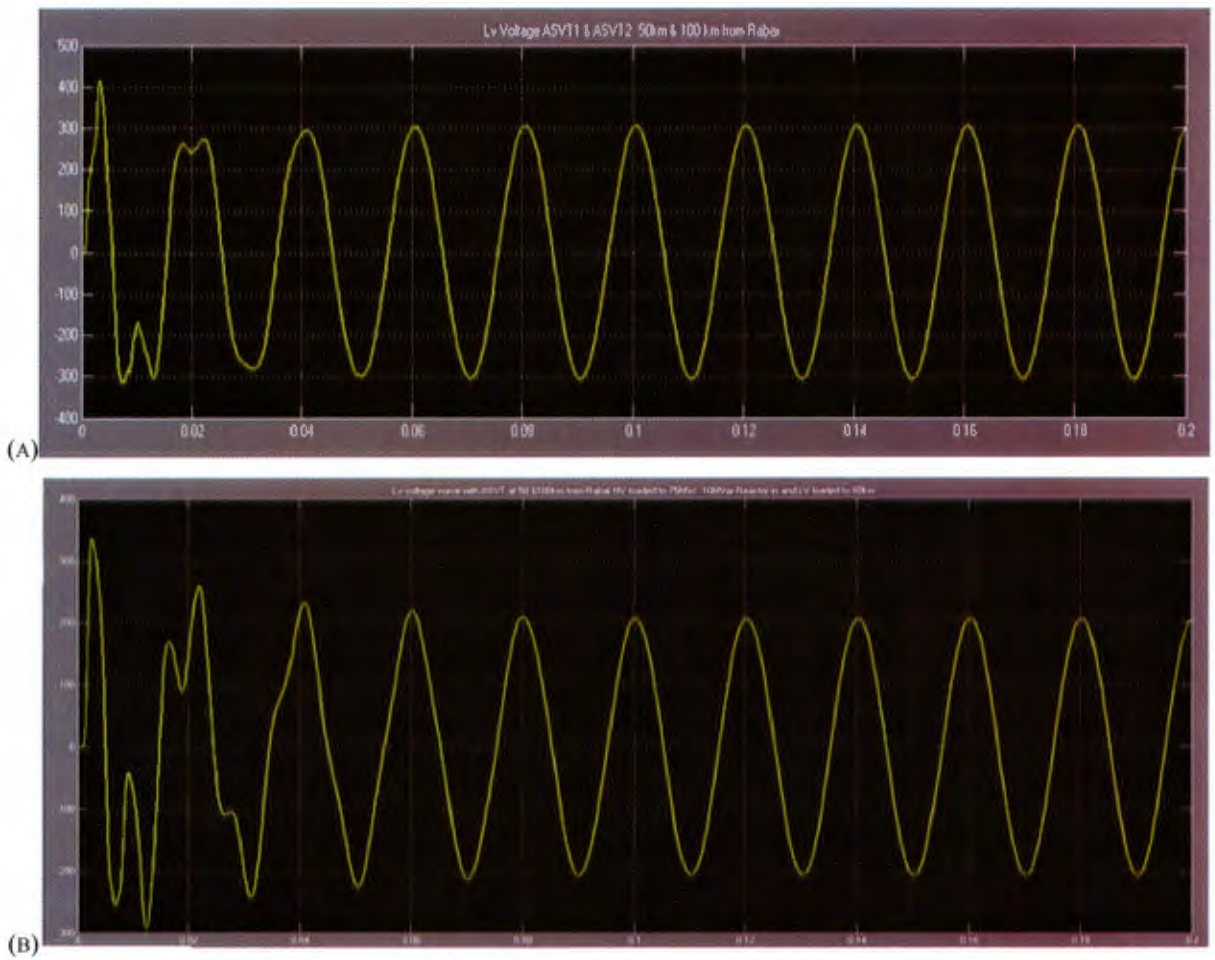

Figure 6.13 LV voltage at 50 and 100km from Rabai

6.6.2 SIMULATION WITH THREE ASVT INSTALLED

In this case we study the effect of three ASVTs installed on the line with a load of 125MW with a reactor of 10MVAr at Rabai substation. HV and LV voltages at distances of 50km apart successively from Rabai substation were recorded.

Figure 6.14 shows the system model. It was noted that the high and low voltage were below the acceptable limits of ± 6% at a loading of 125MW. However, after trying different loadings for the system, it was found out that at 75MW the voltages were within the acceptable limit of ± 6% of the nominal value. Both voltages showed some switching-resonance distortions as shown in Figure 6.15(a) and (b).

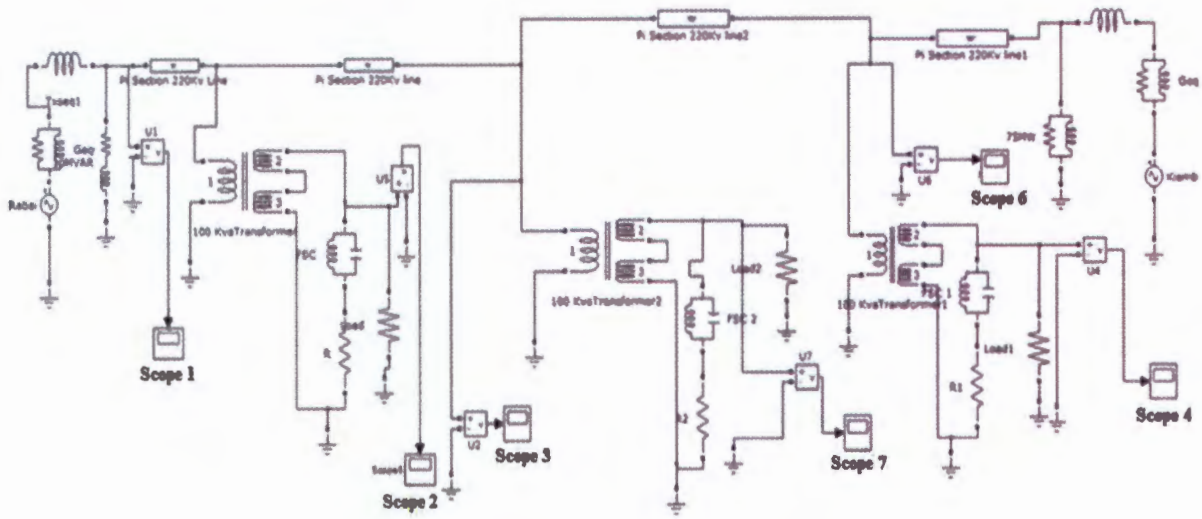

Figure 6.14 model for the line with load and three asvts

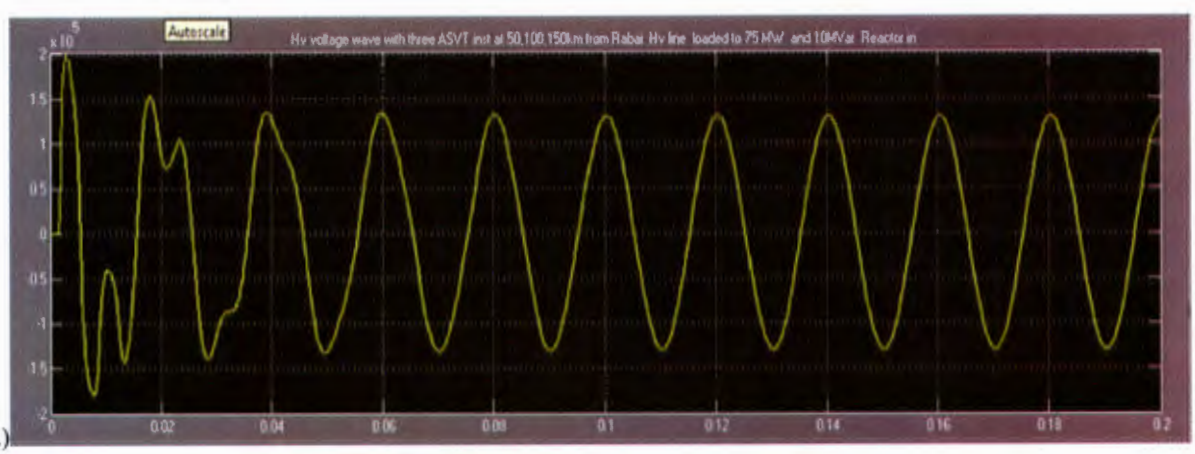

(A)

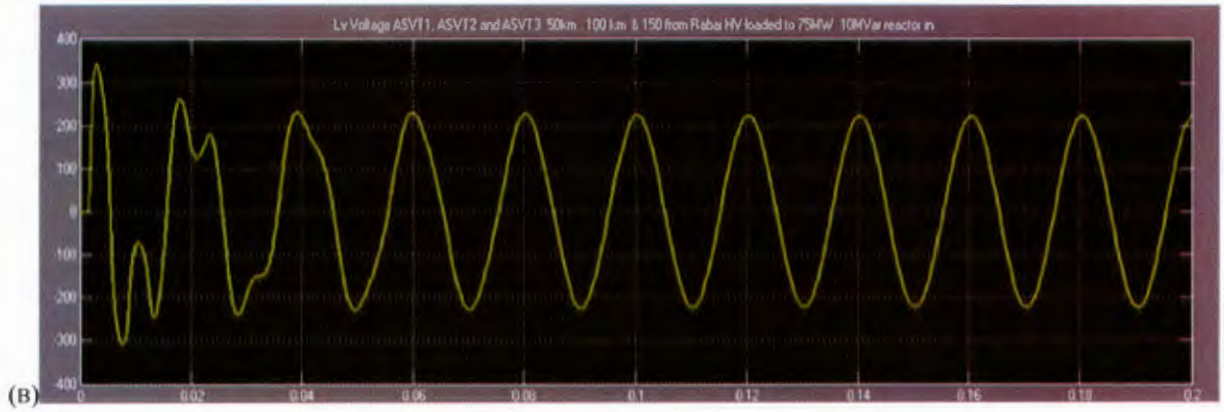

Figure 6.15 Model for the line without load and ccs

6.7 PENETRATION LEVEL OF COMBINED ASVT AND CCS UNIT(S) AT DIFFERENT DISTANCES

In this case, combinations of ASVT and CCS systems were connected at specific locations on the transmission line and steady state measurements carried out for each simulation. The measurements carried out were with regard to tapped voltage (V_T), divider voltage (V_D) and load voltage (V_L). Figure 6.16 and Table 6.5 show the model used for Simulation of the ASVT/CCS system and measured results respectively.

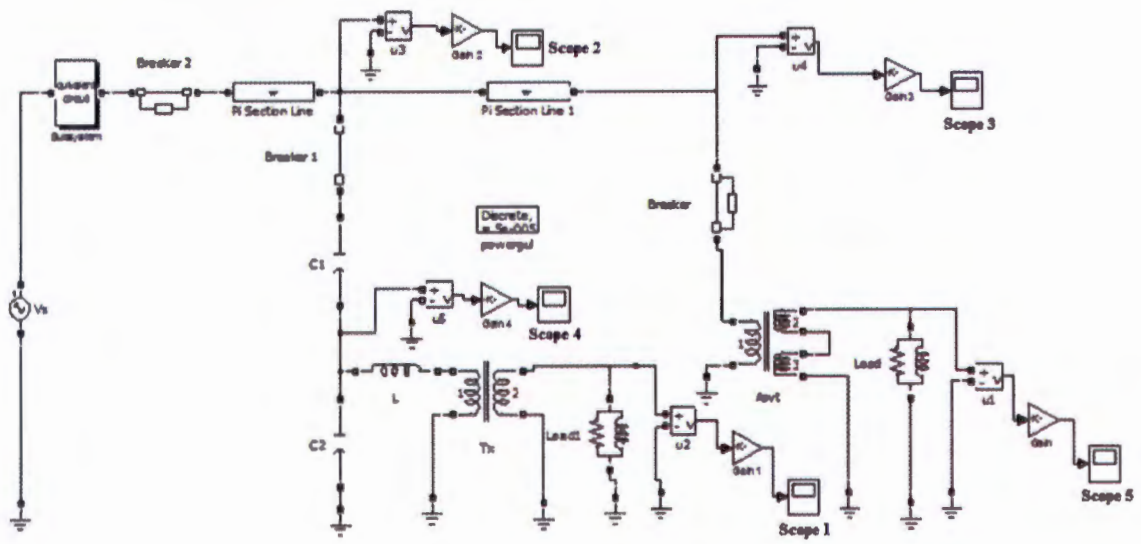

Figure 6.16 Model for combination of asvt and ccs

Table 6.2 Measurements for different penetration levels of ASVT/CCS at steady state

		LENGTH OF THE TRANSMISSION LINE IN KILOMETERS							
No. of CCS/ASVT	**VOLTAGE**	**48.89**	**97.78**	**146.67**	**195.55**	**244.44**	**293.33**	**342.22**	**440**
ONE/ONE	**V_T (kV)**				146.56				154.65
	V_D (kV)				36.64				N/A
	V_L (kV)				0.228				0.256
TWO/ONE	**V_T (kV)**			146.06			151.93		154.62
	V_D (kV)			36.52			N/A		38.66
	V_L (kV)			0.223			0.251		0.241
TWO/TWO	**V_T (kV)**		138.95		146.56		151.76		154.69
	V_D (kV)		34.13		N/A		37.94		N/A
	V_L (kV)		0.216		0.242		0.236		0.241
THREE/TWO	**V_T (kV)**	133.66		139.44		143.62		146.14	146.14
	V_D (kV)	33.42		N/A		35.91		N/A	36.54
	V_L (kV)	0.208		0.231		0.224		0.242	0.229

Four configurations of the models were considered during simulation, ranging from a single CCS/ASVT to three/two CCS and ASVT respectively as shown in table 6.5. Different arrangements at specific distances on the transmission line were considered and measurements taken.

The simulation results showed that the tap-off voltage *(V_T)* on the transmission line reduces slightly as the number of CCS/ASVT penetration increased. The magnitude of the load voltage (V_L) was within the acceptable range of 2.5% with the two/two CCS to ASVT penetration. Except for the 97.78km distance, where the voltage appeared low at 0.216kV. The rest of the distances showed acceptable voltages. The divider voltage *(V_D)* for the CCS portion appeared unacceptable except for the three/two scenario at 48.89km distance. In summary it can be observed that penetration of two/two and two/three CCS to ASVT units gave a reasonable acceptable voltage profile especially the load voltage (V_L) for the steady state scenario. The tap-off voltages (VT) for these two scenarios were a bit high. With some compensation these two scenarios may be made acceptable.

6.8 TRANSIENT CONDITIONS FOR ASVT/CCS AT DIFFERENT SWITCHING

Figure 6.17 illustrates combination model circuit for ASVT and CCS systems on a transmission line. The breaker devices are connected in series to the combination on 50Hz voltage source. The load conditions of the line are modeled in the pi section block.

The switching time of the breaker block are controlled by Simulink signal that is signal (1-4) as shown on the model layout below. Several simulations were carried out in this case study using different signal injections shown on the layout and resulting simulation for signal 1 injection are as shown in Figure 6.18. The waveform measurements for each signal injection were displayed out as follows;

Scope 1 measured the CCS system current

Scope 2 measured the ASVT system current

Scope 3 measured the ASVT tap off voltage (V_T)

Scope 4 measured the CCS tap off voltage (V_T)

Scope 5 measured the ASVT load current

Scope 6 measured the CCS load current

Scope 7 measured the ASVT load voltage (V_L)

Scope 8 measured the CCS load voltage (V_L)

Note that signals 2-4 injections are displayed in appendix G.

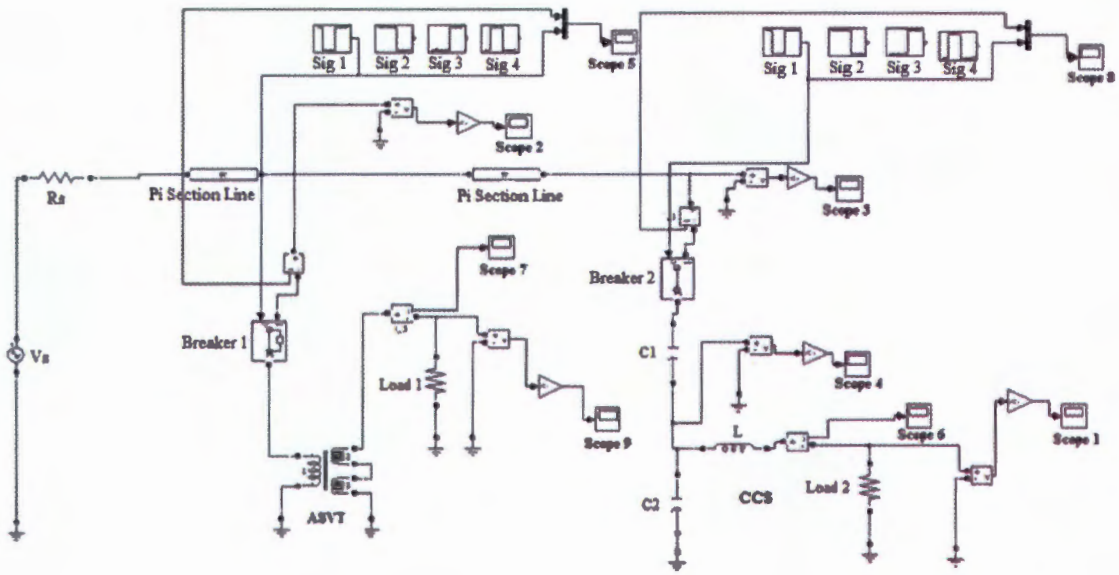

Figure 6.17 model for transient signal of ASVT/CCS combination

Signal 1

The breaker devices were initially closed, an opening order was given at t = 5 cycles and then closed again at t = 15 cycles. Here the ASVT system current waveform experienced a DC offset and small voltage rise on tap-off voltage, load current and load voltage during the switching on was experienced as shown on the waveforms.

Similarly, CCS system current experienced small spike current when the system was switched on with a small overshot experienced at the tap-off voltage, divider voltage and load current. No Ferro-resonance effects were exhibited.

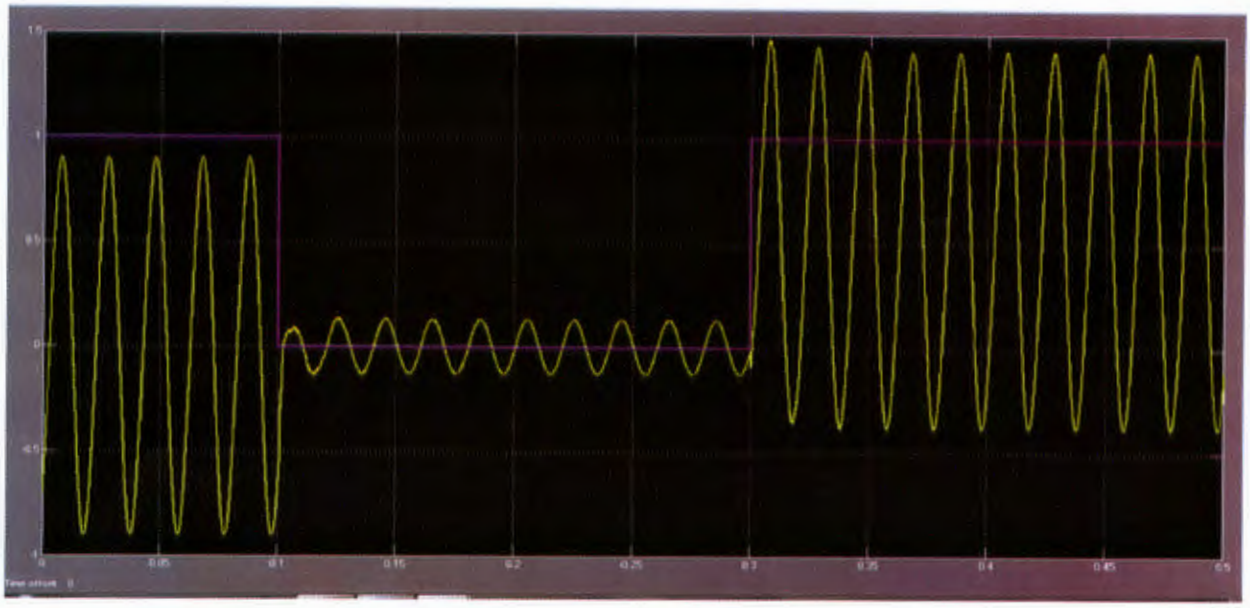

CCS SYSTEM CURRENT WAVEFORM (SCOPE1)

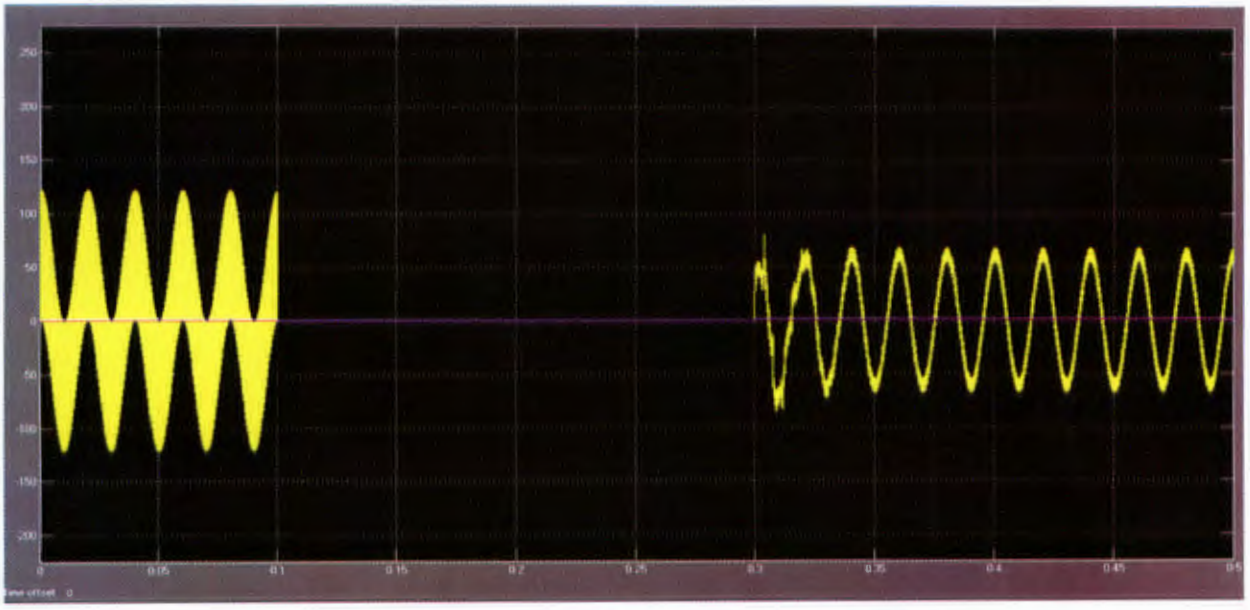

(C) CCS SYSTEM CURRENT WAVEFORM (SCOPE 2)

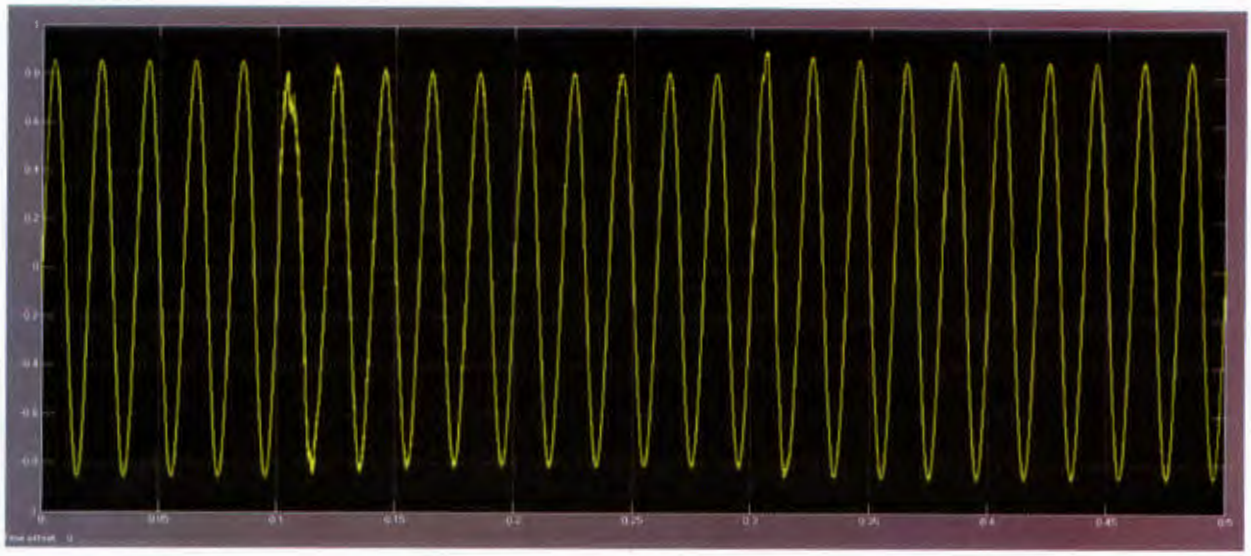

ASVT TAP-OFF VOLTAGE WAVEFORM (SCOPE 3)

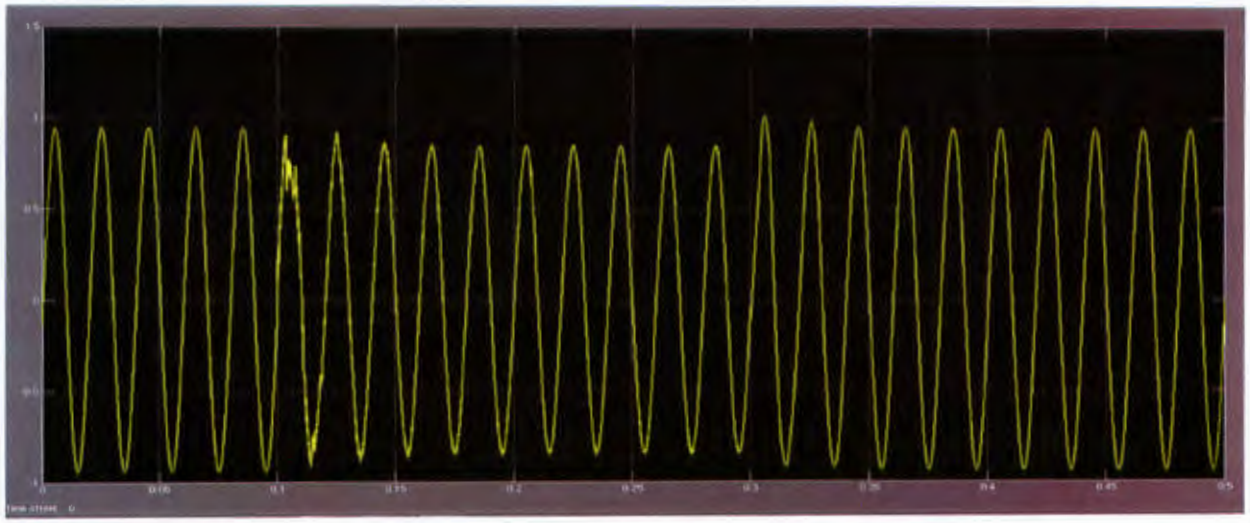

(D) CCS TAP-OFF VOLTAGE WAVEFORM (SCOPE 4)

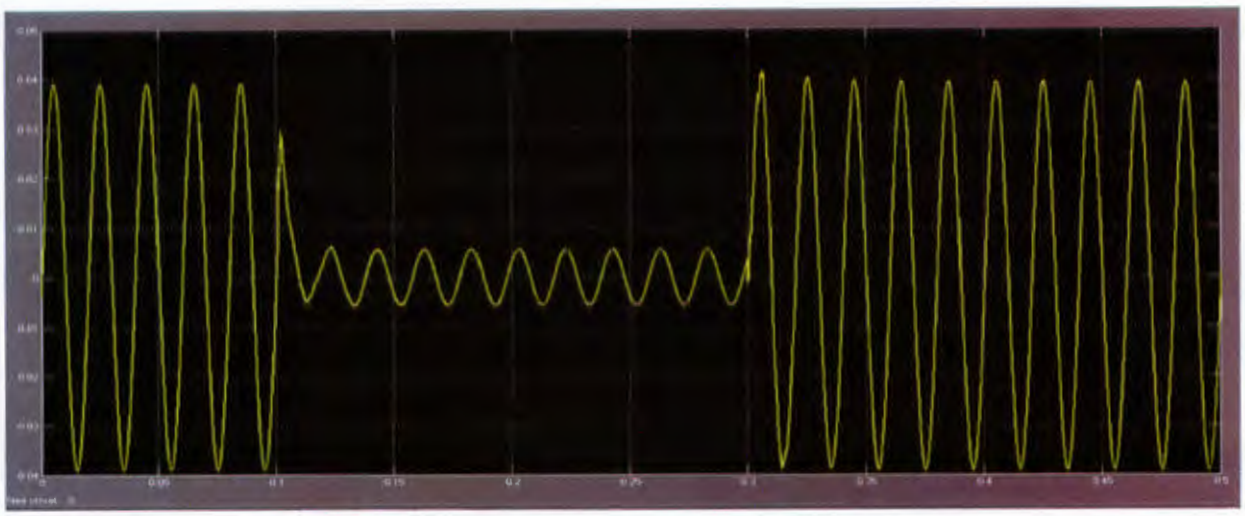

(E)ASVT LOAD CURRENT WAVEFORM (SCOPE 5)

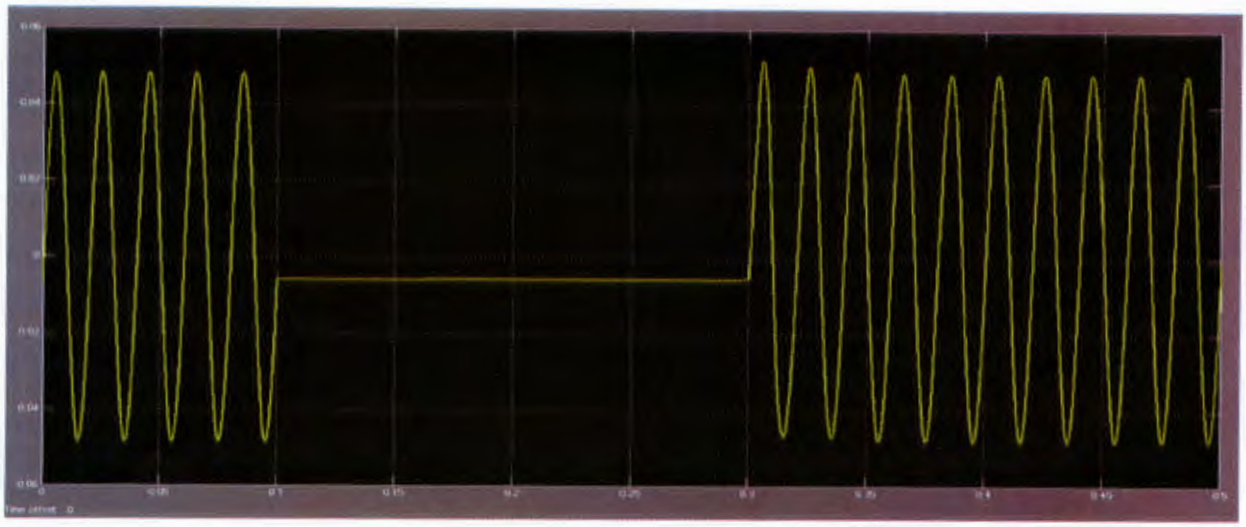

(E) CCS LOAD CURRENT WAVEFORM (SCOPE 6)

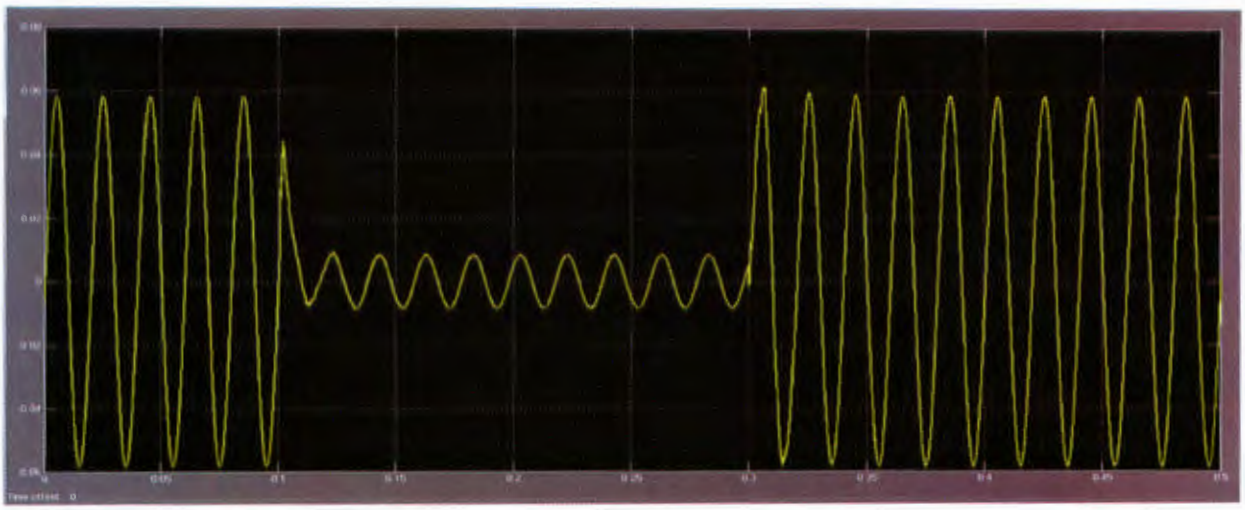

(G)ASVT LOAD VOLTAGE WAVEFORM (SCOPE 7)

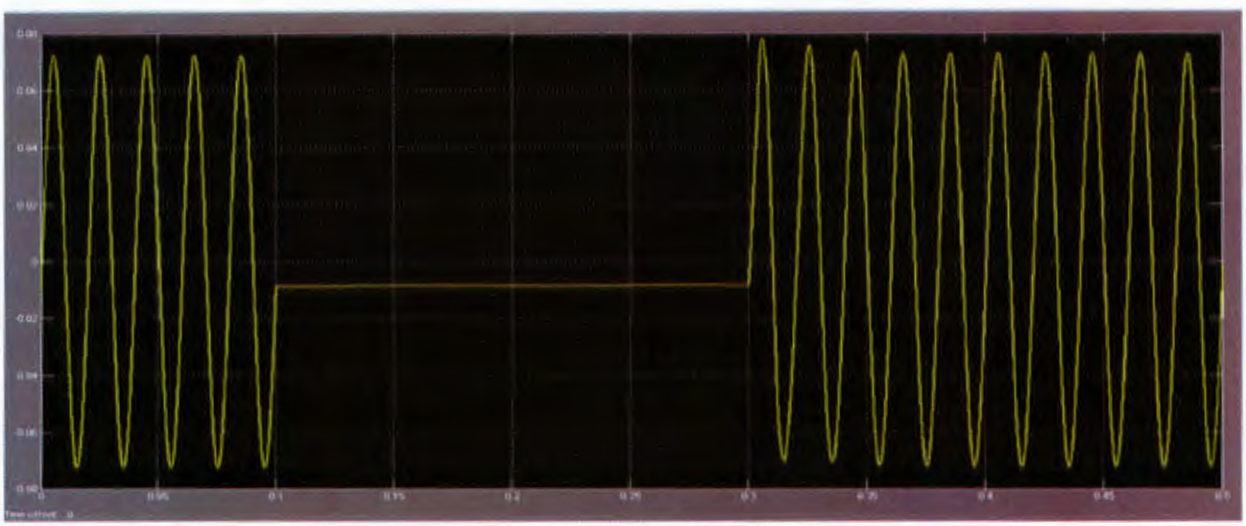

(H) CCS LOAD VOLTAGE WAVEFORM (SCOPE 8)

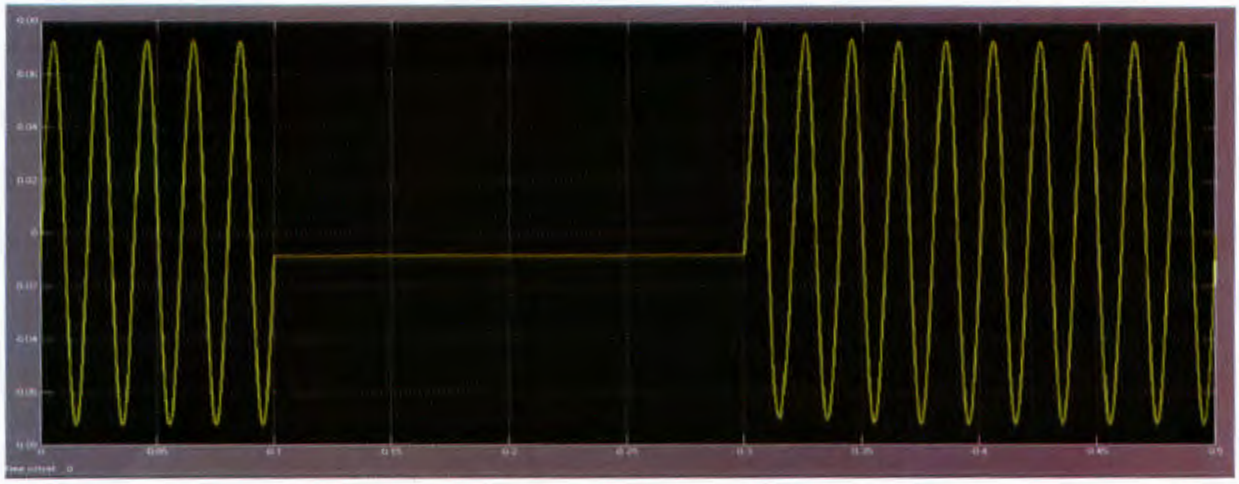

(I)ASVT LOAD VOLTAGE WAVEFORM (SCOPE 9)

Figure 6.18 waveforms for signal 1 injection

Signal 2

The breaker devices were initially closed and an opening order was given at t =15 cycles. The ASVT system current waveform was normal that is no effect was experienced after the circuit breaker was switched off. There was a small decrease on tap-off voltages. No Ferro-resonance effect was experienced on the load current and load voltage. Similarly, in the CCS system no Ferro-resonance effect was exhibited on the system current waveform. There was a considerable decrease on the tap-off voltage. Neither voltage overshot nor Ferro-resonance effect was experienced on the CCS system load voltage, load current and divider voltage. The simulation results of signal 2 are as shown in appendix G1.

Signal 3

The breaker devices were initially off and closing order was given at t =5 cycles. The ASVT system current waveform experienced DC offset at t = 15 cycles. The tap-off voltage waveform experienced a small increase. No major effects were observed on the load voltage and current. The CCS system experienced a spike current when the system was switched on. Tap-off voltage increased slightly. Neither voltage overshot nor Ferro-resonance effect was observed as shown in appendix G2.

Signal 4

In this test the breaker devices were initially off and closing order was given at t = 5 cycles and then commanded to open at t = 15 cycles. The ASVT system current waveform experienced a DC offset. Tap-off voltage waveform experienced a slight voltage increase while no effect was observed on the system load voltage and current waveforms.

For the CCS system, a spike current of about 1.2 time's normal system current was observed when switched on. No Ferro-resonance effect was observed on the load current, load voltage and the divider voltage as shown in appendix G3.

6.9 ASVT LOADABILITY TEST

Loadability tests were carried out to show the variation of load voltage with load MVA. The main issue of the loadability test was to find the optimum operating load MVA that can be supported before the voltage begins to collapse. The tests were done at variable power factor. Simulation results were tabulated as shown in Table (J1-J6) in the appendix. The desired maximum voltage at the load terminal was ± 6% of 33kV (Ranging from 31.02 kV to 34.98 kV).

Figure 6.19 below shows the model of the ASVT loadability test system used while Figure 6.20 is the loadability test graph. The load model used was that of series R-L. The system was tested in six different levels of demand. For each test, real power (P_L) was fixed and reactive power (Q_L) varied to operate at different load power factor between 0.2 lagging to unity. Simulations of the ASVT system were carried out using the model circuit of Figure 6.19.

Where;

Scope 1	.U_1 (KV) represents the system voltage
Scope 2	U_2 (KV) represents tap-off voltage
Scope 3	U_3 (KV) is the load voltage
Scope 4	I_1 (A) represents the system current
Scope 5	I_2 (A) represents load current
Q_L(MVAR)	represent the varied reactive power of the load

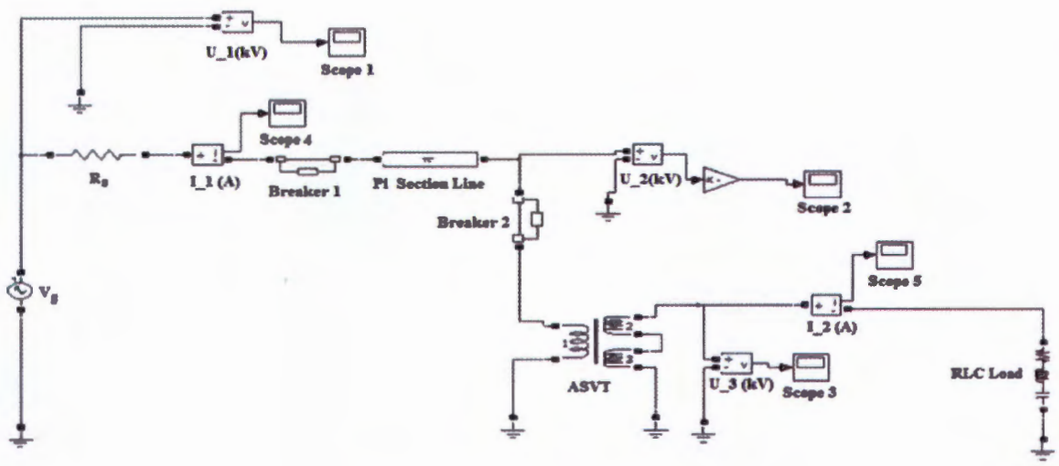

Figure 6.19 ASVT loadability model

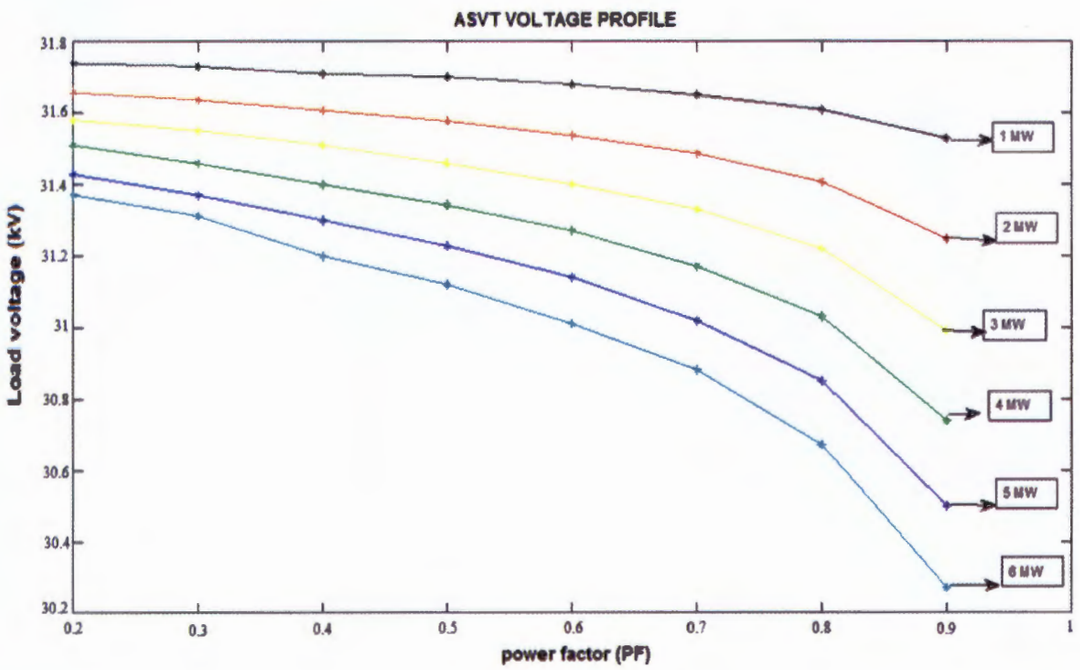

Figure 6.20 Loadability test of ASVT

Simulation results clearly showed that ASVT system can be operated within allowable voltage regulation if a load of 1MW at 0.3 to unity power factor was connected at the load terminal. The current at these power factors ranges between 61.35.07A to 19.37A (see appendix J1).

It is worth noting that the other loads i.e. 2MW, 3MW, 4MW, 5MW and 6MW have acceptable voltage profile between 0.2 and 0.6 power factors, although the load currents are quite high. It is only at 2MW load that the system can operate effectively at unity power factor (see appendix J2 to J6). The loadability tests for the ASVT showed that the system could operate almost at all power factors at 1MW loading. On the other hand, the CCS could operate from 0.5 up to a maximum of 0.9 power factor for similar loading conditions. Apparently, this indicated that the ASVT system was more flexible than the CCS and could be used for a wider variation of power factors or loading

Consequently, merging the two loadability graphs for CCS and ASVT in Figure 4.29 and 6.20 would produce an optimum power factor or operating range that these two systems could operate within when integrated together in power transmission lines. It is envisage that the two systems may present a more stable system when integrated together in the same power transmission line.

6.10 COMPARATIVE ANALYSIS OF ASVT WITH CCS

Figure 6.21, show a comparison of ASVT with CCS systems. This was done with respect to system current, tap-off voltage and load voltage at transient state.

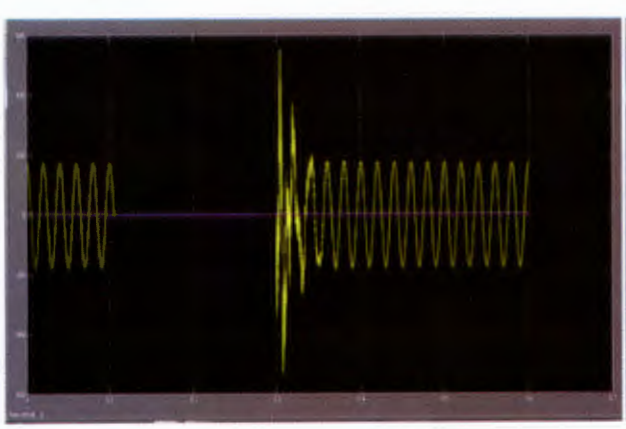

ASVT SYSTEM CURRENT

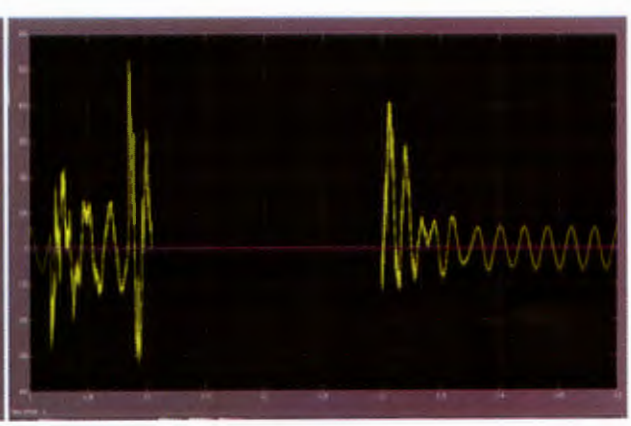

CCS SYSTEM CURRENT

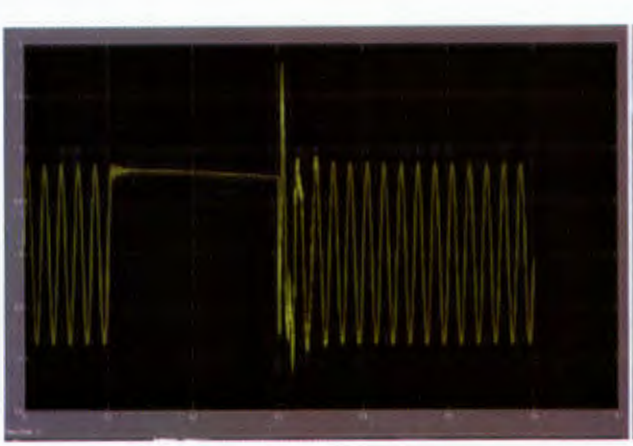

ASVT TAP-OFF VOLTAGE

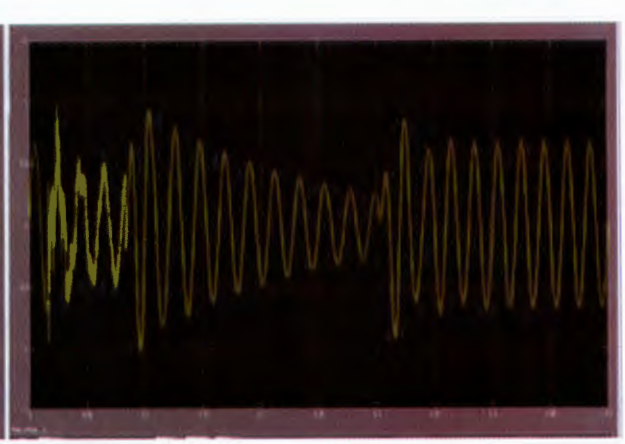

CCS TAP-OFF VOLTAGE

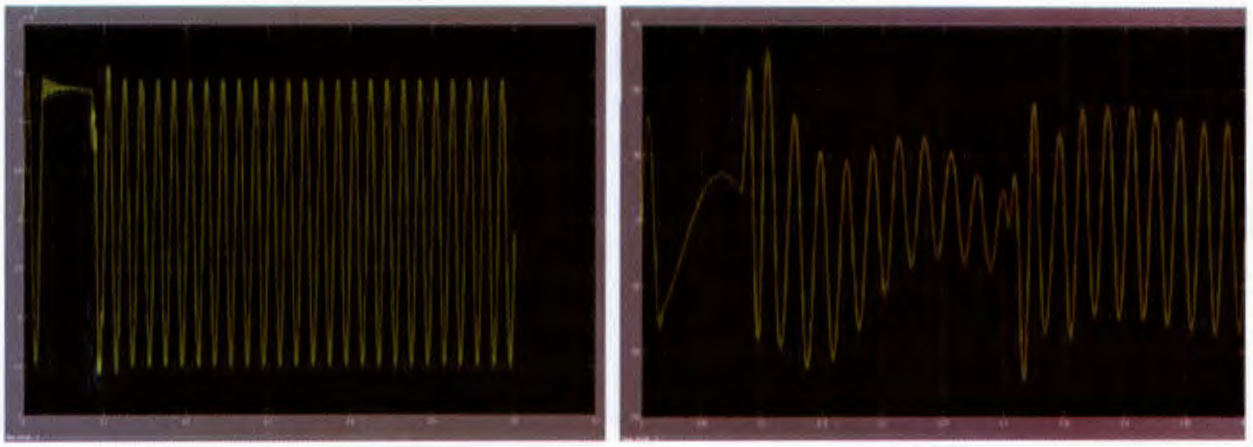

ASVT LOAD VOLTAGE CCS LOAD VOLTAGE

Figure 6.21 ASVT/CCS comparison.

Table 6.3 is a comparative analysis of the ASVT and CCS systems with regard to their operation principles at steady and transient states.

Table 6.3 Comparative analyses of ASVT and CCS

ASVT SYSTEM	**CCS SYSTEM**
Inductive system	Capacitive system
Uses the principle of instrument transformers	Uses the principle of capacitive voltage transformer
Joules effect loss due to the windings (in-rush current problem)	Has inherent poor voltage regulation due to high capacitive impedance introduced by capacitance equivalent of C_1 and C_2
Relatively higher tap-off voltage on the transmission line	Relative lower tap-off voltage on the transmission line.
Has very high thermal rating compared to conventional instrument transformer	Ferro-resonance effect due to the effect of capacitance and saturation of inductive elements in the system
Spike current of about 3 times normal current, voltage overshoot of about 1.3 times normal tap-off voltage.	Spike current of about 8 times normal current, voltage overshoot of about 1.8 times normal tap-off voltage
ASVT off, no spike was observed.	CCS off, spike current of about 10 time's normal current observed.
System can be operated within allowable voltage regulation if a load of 1MW at 0.3 to unity power factor was connected	System can be operated within allowable voltage regulation if 1MW at 0.5 to 0.9 power factor lagging load was connected

6.11 ANALYSIS OF RESULTS

The steady state simulation results of ASVT system showed that the tap-off voltage on the transmission line was high by 21.74% during light load period and 15.69% during heavy load periods with respect to the supply. Additionally, there was an increase of the load voltage at light and heavy load of about 10.8% and 1.25% respectively.

Transient condition tests were carried out by injecting several signals into the breaker. Signal 1 clearly illustrates that when ASVT system was switched on, an in-rush current of about 3 times normal system current and voltage overshot of about 1.3 times normal tap-off voltage was observed. When the breaker was opened the load voltage remained high momentarily, this could be attributed to the re-striking voltage of the circuit breaker. Signal 2 showed neither an in-rush current nor voltage overshot on the waveform. While signal 3 showed an in-rush current of about 1.2 times' normal system current, overshot tap-off voltage of about 1.3 times the normal tap-off voltage and load voltage overshot of about 1.2 times the normal load voltage was observed.
Signal 4 experienced an in-rush current of about 1.2 times the normal system current. It was observed that at t = 5 cycle, overshoot of about 1.3 times normal tap-off voltage and 1.5 times normal load voltage were experienced.

Loadability capacity of the system was tested and the resulting simulation showed that ASVT systems could be operated within allowable voltage regulation, if 1MW at 0.3 to 0.5 power factor lagging load was connected while CCS operated at 1MW at 0.5 to 0.8 power factor lagging. It was envisaged that the combination of both systems would give an optimum operating point since they were operating in a vice-versa mode.

A combination of ASVT and CCS units was also analyzed. Two configurations were investigated, that is with the ASVT positioned first as seen from the voltage source and secondly with the CCS in a similar position. The results showed that with the ASVT positioned first in the middle of transmission line, there was an increase of about 15.38% and a decrease of 1.25% for tap-off voltage and terminal voltage respectively. Whereas the CCS system at the end of the transmission line showed an increase of about 21.77% and 6.66% on the tap-off voltage and terminal voltage respectively during the light loads. This configuration also illustrated that the ASVT system at the middle of the transmission line experienced an increase of about 5.23% and a decrease of about 7.9% for tap-off voltage and terminal voltage respectively. The CCS system showed an increase of about 15% and decrease of about16.67% of tap-off voltage and terminal voltage respectively for heavy loads.

On the other hand, a CCS/ASVT configuration; showed that the CCS system experienced an increase of about 15.39% tap-off voltage and a decrease of 5% terminal load voltage, whereas the ASVT at the transmission line end showed an increase of about 21.77% tap-off voltage and 6.3% terminal load voltage at light load. During the heavy load period the CCS system as seen from the source side showed an increase of about 5.2% tap-off voltage and a decrease of 13.33% of terminal load voltage, the ASVT at the transmission line end showed an increase of about 15% and 6.66% of tap-off voltage and terminal load voltage respectively.

Transient conditions simulation of the combined ASVT/CCS system on the line was also carried out. Signal 1 injection showed that the system current waveform experienced a DC offset and a small voltage rise on tap-off voltage, load current and load voltage during the switching on. Similarly, CCS system current experienced some small spike current when the system was switched on and with small overshoot experienced on the tap-off voltage, divider voltage and load current.
No Ferro-resonance effects were exhibited. Signal 2 showed a normal ASVT system current waveform that is no overshooting effects were experienced after the circuit breaker was switched off. There was a small decrease on tap-off voltages. No effect was experienced on the load current and load voltage. Similarly, the CCS system experienced no effect on the system current waveform. Even though, there was a considerable decrease on the tap-off voltage. Neither voltage overshot nor Ferro-resonance effect was experienced on the CCS system load voltage, load current and divider voltage. With the application of signal 3, the ASVT system current waveform experienced a DC offset at t = 15 cycles. The tap-off voltage waveform experienced a small increase. Normal effect on the load voltage and current was observed. The CCS system in this case, developed a spike current on the system current waveform when the system was switched on. Tap-off voltage increased slightly. Neither voltage overshot nor Ferro-resonance effect was observed with the application of this signal.

Finally, signal 4 was applied and the ASVT system current waveform experienced a DC offset. Tap-off voltage waveform experienced a slight voltage increase while no effect was observed on the system load voltage and current waveforms. On the CCS system, a spike current of about 1.2 time's normal system current was observed when switched on. No Ferro-resonance effect was observed on the load current, load voltage and the divider voltage.

It may be concluded based on simulation results that in order to establish a voltage control mechanism at the tap-off point of the CCS and ASVT system, shunt inductances are required. In this research project the designed load capacity of both URE systems was about 100kVA. Therefore, reactance of 10MVAR and 5MVAR were required for the CCS and ASVT respectively.

Note that this particular line had a load capacity of 210MVA as indicated in appendix A. This was done to enable them operate without violating the voltage rise limitation base case of 127kV and 240V per phase for V_T and V_L respectively. Established on this finding, each transmission line may require a different size of reactance depending on the line parameters system and line loadings conditions.

Secondly, It was also observed that the waveform of the in-rush current of the ASVT when switched on was far from sinusoidal, it contained a lot of high frequency components; such harmonics stimulate resonances in the system causing significant magnification of voltage or current at various locations in the system. This may result to damage on the insulation, interference with sensitive electronic equipment's in the system, surge suppressor overheating, or capacitor fuse blowing.

Finally, When the two systems were connected on the same transmission line model the Ferro-resonance effects on the CCS was negligible, whereas ASVT system developed problem of DC offset on the system current during switching on.

Transient in-rush have a high DC-component and being rich in 1st and 2nd harmonics they affect the power quality and can trip sensitive protective relays. Therefore, these in-rush currents may be eliminated through;

- Controlled switching taking into account the residual flux.(using power electronic devices)
- Series resistance insertion
- Ground resistor insertion and
- Soft starting in case of motor loads

6.12 ONWARD

Several model configuration and circuits for ASVT systems on a transmission line were simulated, steady and transient state results were analyzed. Loadability tests were also carried out, results showed that that ASVT system could be operated within allowable voltage profile if 1MW at 0.3 to 0.5 power factor lagging load was connected, whereas CCS system could be operated within allowable voltage profile if 1MW at 0.5 to 0.8 power factor lagging load was connected.

The steady state simulation results for both ASVT and CCS system generally showed that the tap-off voltage on the transmission line is high during light load period and low during heavy load period. Further, the results showed that tap-off voltage in the transmission line where ASVT systems are connected have relatively higher voltage rise than that of the CCS systems when connected in transmission line of the same length and line parameters.

These two un-conventional systems have proved that they can be used individually or collectively when integrated to a transmission line. These two systems can be used to supply power to the rural community living in close proximity to the HV lines cheaply and reliably. This can be done as long as the voltage rise control mechanism and a reliable protection system are put in place. The next chapter analyses the penetration level of ASVT in a power network based on the surge impedance loading (SIL) of the line.

7 PENETRATION LEVEL OF AUXILIARY SERVICE VOLTAGE TRANSFORMERS

7.1 INTRODUCTION

The knowledge of penetration level of ASVTs in a power transmission network is necessary, since the integration of the system into the transmission network contributes to voltage stability limitations mostly in long lines. Normally, a line operated at Surge Impedance Loading (SIL) has a flat voltage profile. This means that the voltage magnitude is the same everywhere along the line. It is disadvantageous to allow the voltage to vary widely along the line. If it is too high, corona will appear on the conductors producing; radio interference, audible noise, and power loss especially in bad weather [Kimbark 1983, Glover and Sarma 2002].

When the voltage is too low, the current is increased for a given transmitted power, thereby increasing the I^2R loss. Therefore, there is an empirical assumption that voltages at both ends of a line are controlled to remain near to the rated value, but elsewhere especially at the mid-point of the line the voltage varies as a function of the transmitted power. This voltage is usually high at light load and low at heavy load. Only at natural load (or SIL) will the voltage have the same magnitude everywhere along the line [Glover and Sarma 2002, Nayak et al. 2006].

Consequently, it was acceptable to evaluate the penetration level of ASVT on a transmission line based on the Surge Impedance Loading (SIL) level of a particular line.

This was done by first building a model in SIMULINK with known elements and values. The results from the simulations were compared to the case study results of chapter six, that originated from the field data. The reason for this was to see how well this method would perform on real system. Accuracy was determined by what the utility accepts as the correct values of the actual transmission line under study.

The next step was to construct the surge impedance loading (SIL) curve from measured data. This curve was used to determine the loadability limit of the transmission line as well as to visually show the penetration level of ASVT in the transmission line. The curve was also useful as it provided insight into additional reactive power needed for a certain amount of active power transfer. The concept of drawing a SIL curve from actual measurements was first tested by means of simulation. The drawing of the proposed curve was also tested on actual measurements from the transmission line.

7.2 DETERMINATION OF TRANSMISSION LINE PARAMETERS

MATLAB Simulink environment was used to test the two-port ABCD parameters that were defined by [Wilson et al. 1999]. The ABCD parameters give the relationship between the voltages and currents at two points. For a transmission line this means that the ABCD parameters represent the influence that the capacitance, inductance and resistance of the line have on the voltage and current.

These relationships are developed in section 3.6.2 of chapter three. It is important to note that the point at which the ASVT is connected in the line become the receiving end point with respect to the sending end.

Figure 7.1 shows the Simulink model used. The length of the transmission line (T1) was varied to simulate different position of the ASVT load on the network. The transmission line model made use of distributed line parameters for the resistance, inductance and the capacitance resulting from appendix A This more closely mimics a real transmission line.

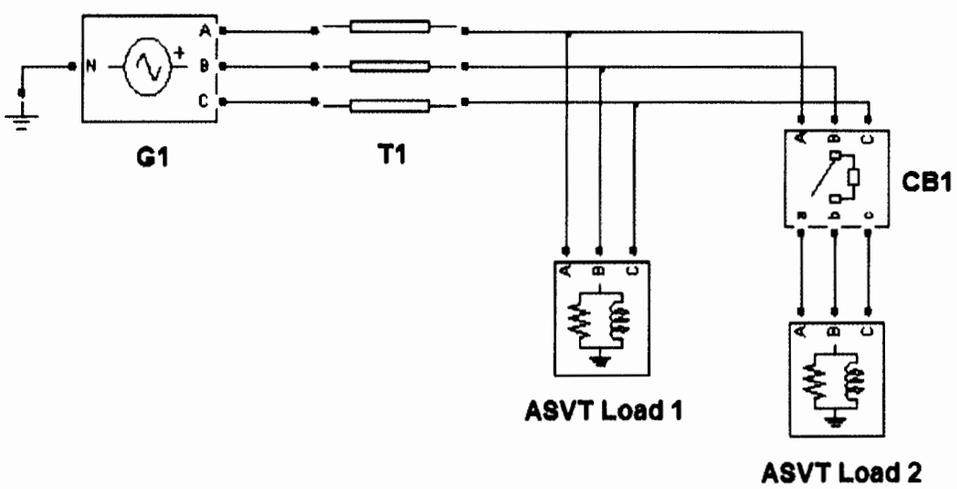

Figure 7.1 Simulation circuit used for line parameter determination

The three phase generator (G1) shown in Figure 7.1 was quantified as having a terminal voltage of 220kV with a system frequency of 50Hz. The parameters as well as line lenghts used for the simulation are given in table 7.1. In order for a sizeable current to flow in the lines, the loads were connected to the line of Figure 7.1. Only load 1 is connected during light loading conditions . During heavy conditions load 2 was swiched in with circuit breaker (CB1) which was also used for transient measurements.

Table 7.1 Load sizes

	Short line	Medium line	Long line
Light loading (VA)	44.77 + j 4.366	44.77 + j 4.366	44.77 + j 4.366
Heavy loading (VA)	89.54 + j8.732	89.54 + j8.732	89.54 + j8.732

This method relies in a change of load to determine the parameters. For this reason two loads were placed on the transmmission line. For the first second of the simulation a light load was placed on the transmission line. Thereafter, a circuit breaker switched in the second load. Under heavy loading the circuit was simulated for another second. This method used both sets of loading results to calculate the parameters for one second. Table 7.1 quantifies the two loads used in simulations. It is important to note that simulations were carried out for the three classifications of transmission lines for comparison purposes i.e. short, medium and long lines for comparison purpose. However, this reseach project was focused on long lines. The results for resistance (Figure 7.2 a), inductance (Figure7.2 b) and capacitance (Figure 7.2 c) for short line are presentsd below.

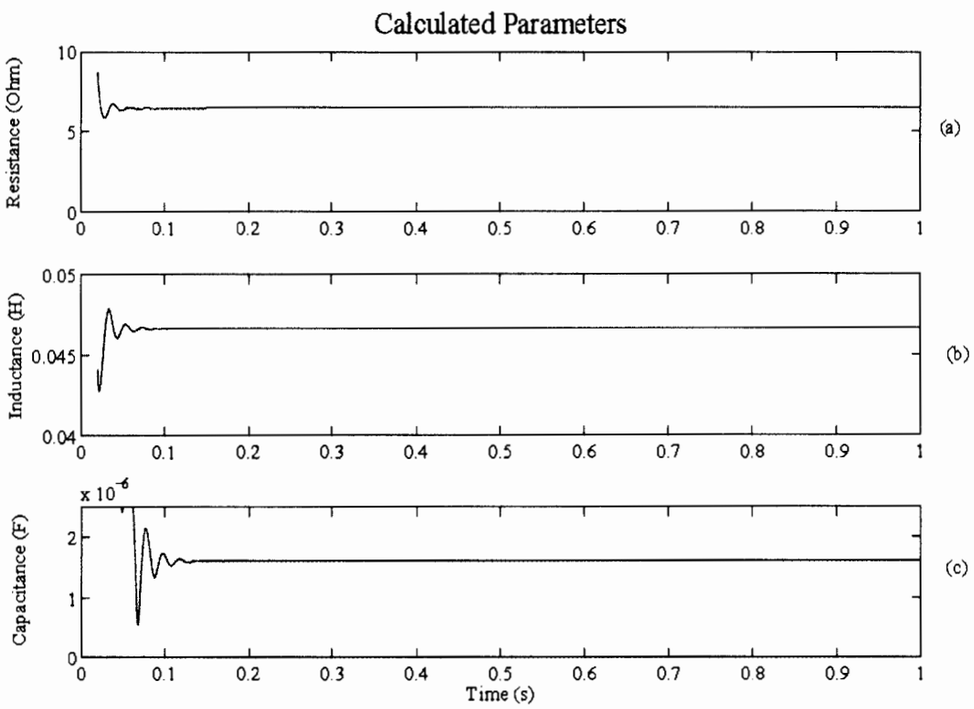

Figure 7.2Simulation results parameters for a 50km short line

The values measured in the simulation of this method are free from external influences like errors in measuring equipment, noise in the system and errors introduced by the method. This means that this results are stable even when the loading changes. Therefore, only one result is given in Table 7.2 for each of the line parameters.

Table 7.2 Errors introduced in the calculated parameters (short line)

	R	L	C
Measured values	4.96Ω	0.203mH	0.0089μF
Actual values	4.97Ω	0.204mH	0.00934μF
% errors	0.15%	0.02%	1.83%

The results for the medium and long lines are given in the same manner as the short line. First, the graph with the results are given, followed by a Table that summaries the results.

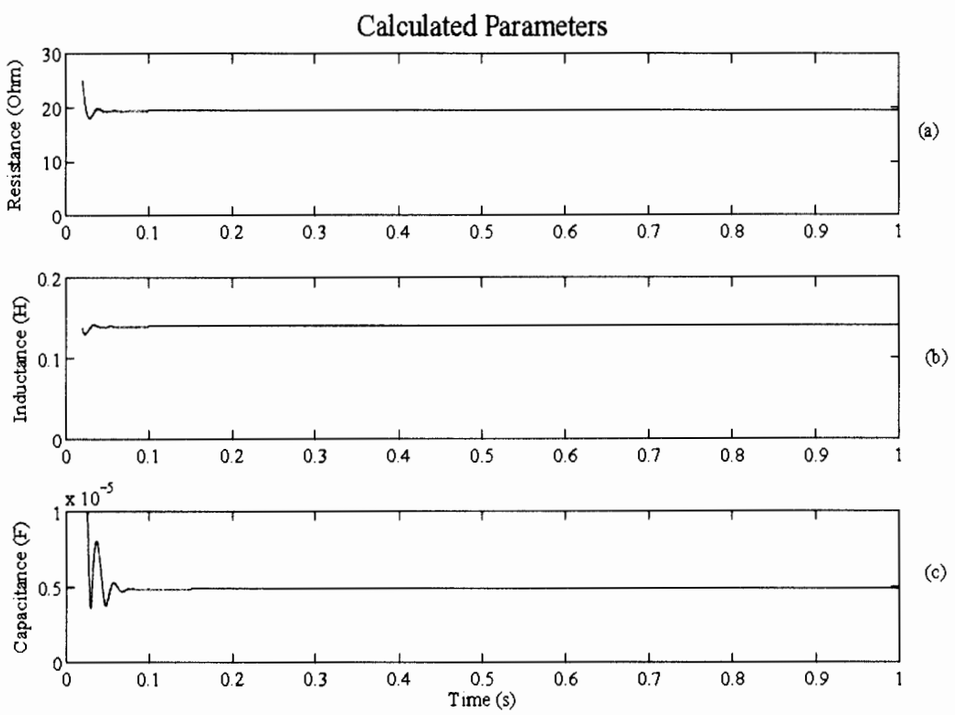

Figure 7.3 Simulation results parameters for a 150km medium line

Table 7.3 shows the errors introduced in the calculated parameters of a medium line transmission line.

Table 7.3 Errors introduced in the calculated parameters (medium line)

	R	L	C
Measured values	14.85Ω	0.617mH	0.027μF
Actual values	14.92Ω	0.613mH	0.028μF
% errors	0.36%	0.03%	0.20%

Figure 7.4 shows the results for a long line. This was the results that this research project was focused on, since the line under study is a 440 km long line.

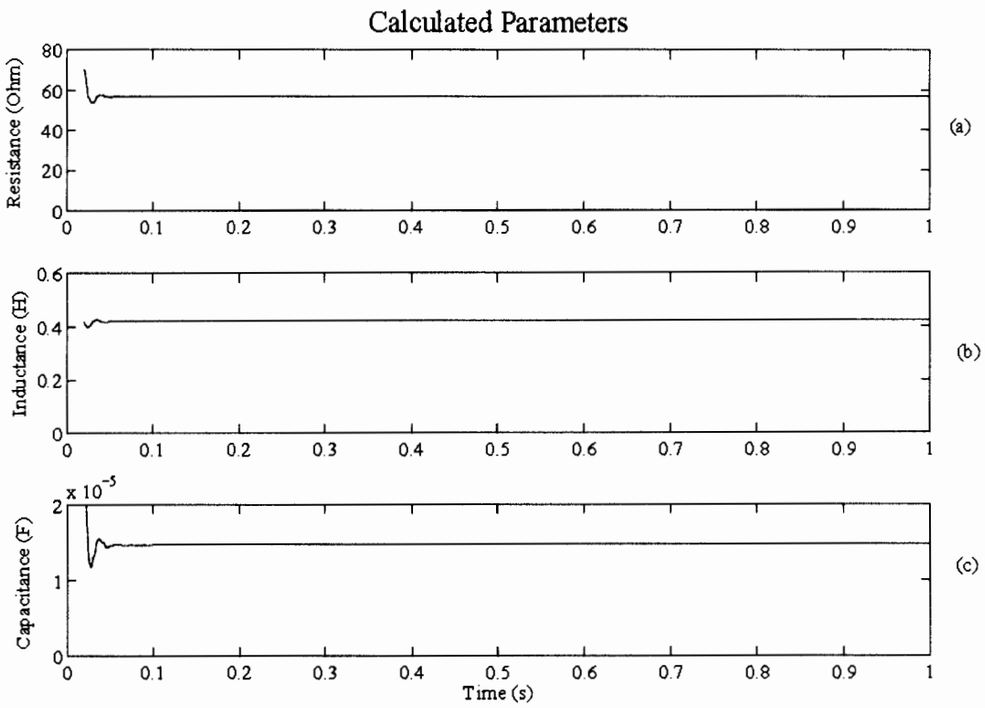

Figure 7.4 Simulation results parameters for a 440km long line

Table 7.3 shows the errors introduced in the calculated parameters of a medium line transmission line.

Table 7.4 Errors introduced in the calculated parameters (long line)

	R	L	C
Measured values	43.21Ω	2.78mH	0.083μF
Actual values	44.77Ω	1.84mH	0.084μF
% errors	2.67%	0.22%	0.07%

The impedance values were calculated with measured currents and voltages. These were compared to the impedance values calculated from the parameters in Table 7.5. By doing this the accuracy and feasibility of the method can be determined.

Table 7.5 Parameter for transmission lines shown in figure 7.1

	Transmission - line		
Parameters	**Short line**	**Medium line**	**Long line**
R (Ω)	4.97	14.92	44.77
L (mH)	0.204	0.613	1.84
C (μF)	0.00934	0.028	0.084
Length (km)	50	150	440

In conclusion, we can say that for a short transmission line the capacitance was ignored since it was small. The capacitance was accurate to 1.83% although it was small in comparison to other parameters. The medium transmission line results for resistance, inductance and capacitance measured had an error of less than 1% (see table 7.3).

The long transmission line model measured a resistance with an error of 2.67% (table 7.4). Both the inductance and capacitance values had errors less than 1%.

From the simulation results it can be seen that this method is very accurate. The transmission lines that were simulated ranged from 50km to 440 km. Therefore, against this back drop it is credible to say that the method used suits application to a long transmission line.

7.3 DETERMINING THE SIL CURVE

The next test was to determine whether it would be possible to draw a SIL curve from the measured data across a transmission line. The model that was used to determine the feasibility of the SIL curve is shown in Figure 7.5. The Figure shows seven loads with six circuit breakers. The circuit breakers were used to switch the selected load across the power line.

The simulations were done over a total of 4.9 seconds. It has become possible and viable to determine the parameters of long line in real-time. This can be done using GPS time stamping techniques. The effect of time here is that network losses can be determined in real-time. Although, for this research project approximate values for time estimates combined with the field data collected are used. The power factor of the load had to be the same for all the seven loads. The reason for this was that the transmission line reacts differently to different amounts of reactive power transferred.

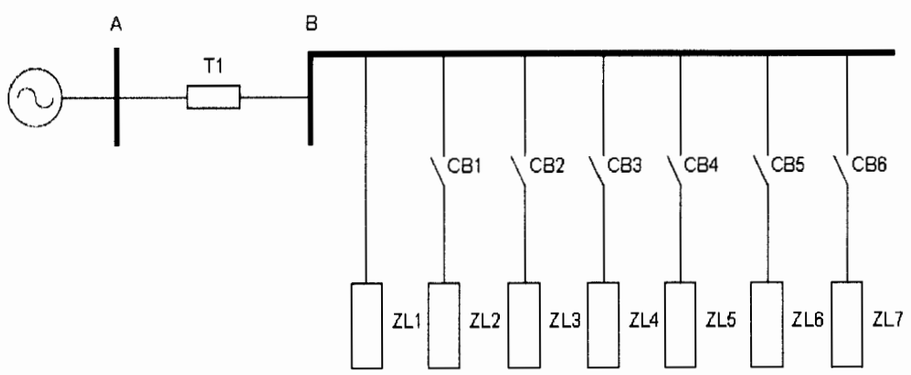

Figure 7.5 Simulation circuit used for drawing the SIL curve

For this part of the simulation three SIL curves were constructed under three distinct operating conditions for comparison purposes. For the first and second conditions the loads had a power factor of 0.5 and 0.9 respectively.

The last simulation was done for loads with varied power factors. Table 7.6 shows the loads that were used. This power factors were chosen based on the results obtained in chapter six. This was done in order to make the evaluation of loadability and penetration level of ASVTs rational.

Table 7.6 Size of impedance load in conjuction with time

	Load (MVA)		
Time (s)	**PF = 0.5**	**PF = 0.9**	**Mixed PF**
0 – 0.7	2	1.11	1.11
0.7 – 1.4	3	1.66	2.11
1.4 – 2.1	5	2.77	4.11
2.1 – 2.8	6	3.33	4.66
2.8 - 3.5	8	4.44	6.66
3.5 – 4.2	9	4.99	7.66
4.2 – 4.9	11	6.11	8.77

Figure 7.6 to 7.8 shows practical SIL curves drawn from measured data. The SIL curves were drawn for different power factors starting from a power factor of 0.5.In most cases a power factor of 0.5 is uneconomical. The typical values for power factors across a transmission line are in the range of 0.8 to 0.95. The reason for using a power factor of 0.5 was first to compare the results to the one presented in chapter six. Secondly, to see the difference in the SIL curves between power factors of 0.9 and 0.5. Both power factors are used in Figure 7.8. Figure 7.7 shows the SIL curve constructed for a power factor of 0.9. An individual SIL curve does not have to be drawn for every possible power factor. Rather, a SIL curve must be constructed for power factors within an operating step. It was decided to use a step size of 0.1.

In this case there were two SIL curves for the transmission line: one when the power factor ranges between 0.8 and 0.89 and another for the power factor equal to and larger than 0.9. The decision for the step change was based on the curve of Figure 7.8. For this SIL curve, the power factors of the loads were switched in varied between 0.5 and 0.9.

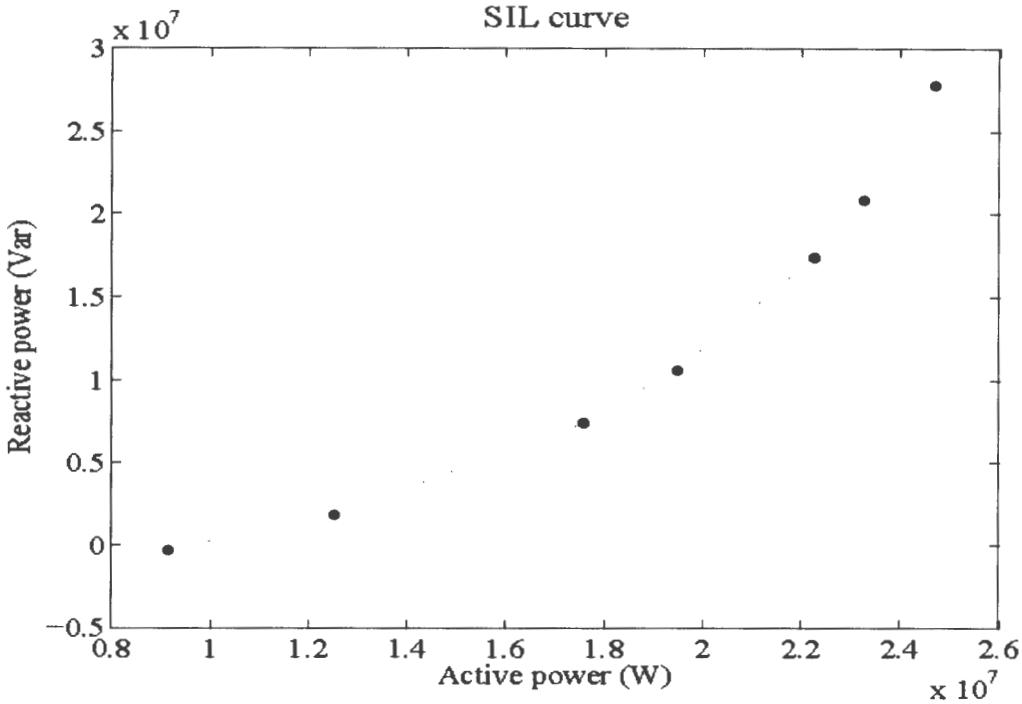

Figure 7.6 SIL curve with power factor of 0.5

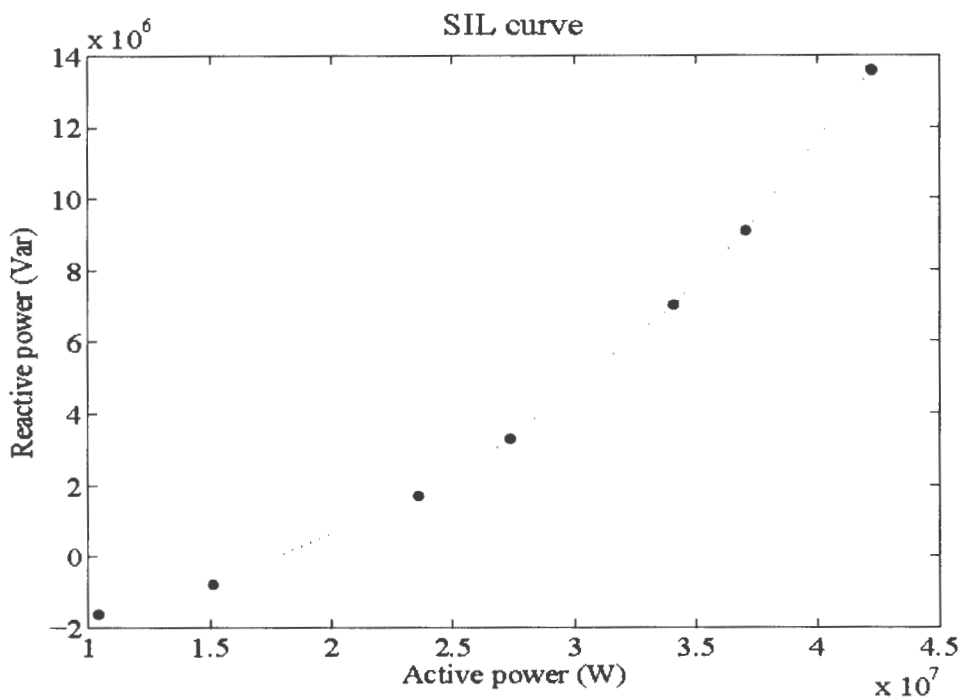

Figure 7.7 SIL curve with power factor of 0.9

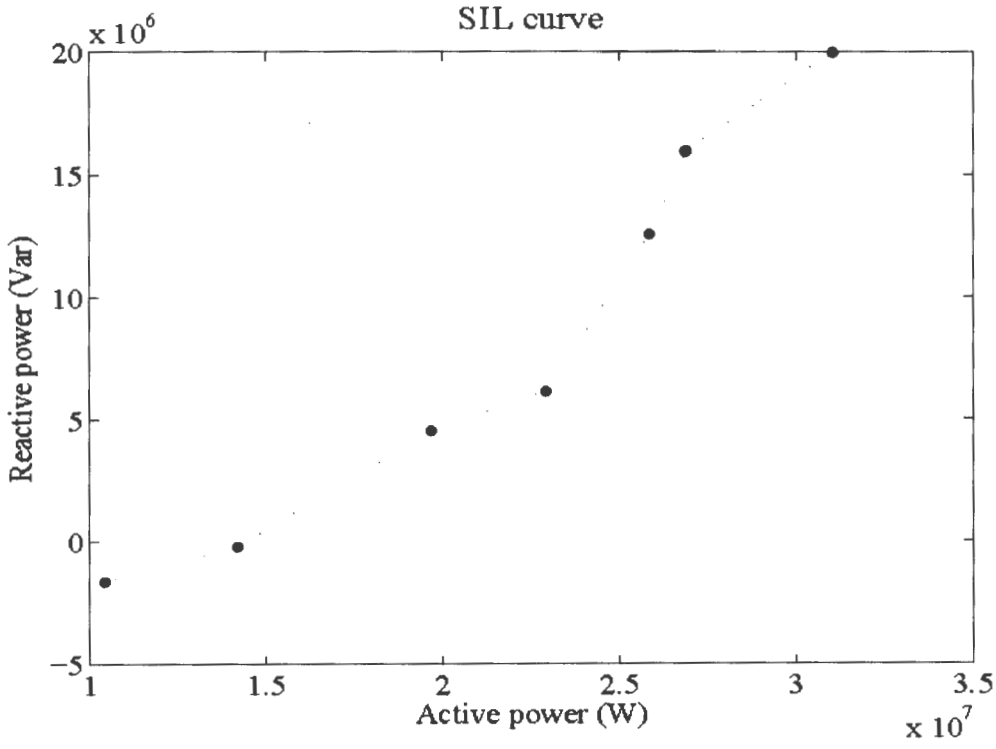

Figure 7.8 SIL curve with mixed power factors

Simulation results for the SIL curve proved that it is possible to construct the curve from measured data. It is important to note that a different SIL curve had to be drawn for a range of power factors. From Figure 7.8 it is evident that a mixed power factor will not result in a smooth SIL curve. Even though with the high difference in power factors, the SIL curve still retained its general shape.

Thus, we can deduce that a SIL curve will be smooth for a range of power factors. In addition, to the active and reactive power measurements needed for the construction of the SIL curve, the load side power factor has to be determined as well. This power factors were then used to determine the SIL curve to which the measured data can be added.

7.4 LINE LOADABILITY CURVES

The transmission network under investigation is a 220kV, 210MVA, 440km line (see appendix A). Therefore, considering an ASVT model rated at 127kV/240V, 100kVA with provision for load tap-changer. Line loadability curves in Figure 6.20 of chapter six were used for comparison with the results obtained in the forgoing section. Estimates of the power transfer capability value at 50Hz for other different voltages can also be determined. For example based on the line parameters determined and the load curve constructed for the 220kV line.

The loadability curve at a power factor of 0.5 showed that the reactive power was at 1.732MVA$_r$ with a load current and voltage of 60.34A and 11.5kV respectively. Conversely, the results of the 0.5 power factor SIL curve showed that for the same amount of reactive power, an active power of 2.2MW, with a load current of 11.56A may be connected to the system. Considering, the 0.9 power factor loadability curve. It showed that for a reactive power of 0.484MVA$_r$, the active power was approximately 1.70 MW. The load current and voltage were 80.02A and 11.6kV respectively.

The SIL curve at 0.9 power factor showed that for the same amount of reactive power, an active power of 1.75MW may be connected in the system. The mixed power factor (Figure 7.8) validates the results. It showed that for the two power factor that is 0.5 and 0.9, an active power of about1.70MW required almost a similar amount of reactive power of about 1.732MVA$_r$ This showed that it was uneconomical to operate the ASVT at low power factor (pf = 0.5). At this power factor it was proved that the loadability of the ASVT was quite low. In order to improve the loadabilty and stability of the system, the line had to be compensated as illustrated in the example shown in section 7.5 below.

7.5 COMPARISON OF STABILITY LIMITS.

The practical stability limits of power systems are the load angle 44^0 for the angular stability limit and the margin of 6% of the voltage stability limit [Dunlop et al. 1979, Hao and Xu 2008,]. Figure 7.9 and 7.10 show the power transfer capability curves with these realistic constraints. Figure 7.9 shows the limits when the line charging is included while Figure 7.10 shows the results when the charging is compensated to zero. [Kimbark 1983, Hao and Xu 2008].

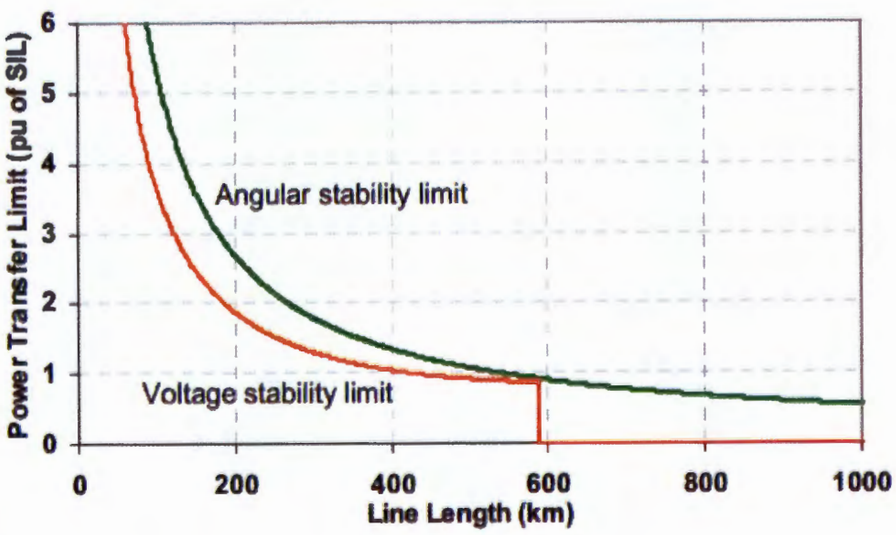

Figure 7.9 Comparison of realistic stability limits (uncompensated)

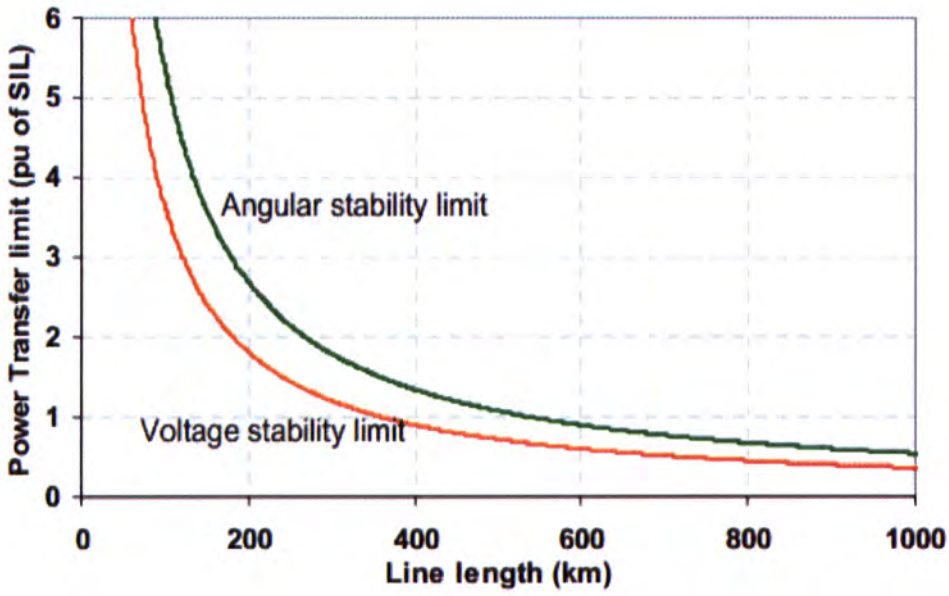

Figure 7.10 Comparison of realistic stability limits (compensated)

It can be observed from the Figure 7-9 and 7.10 that the angular stability limit is less restrictive than the voltage stability limit under the above mentioned assumptions. It is important to note that each transmission line has its own parameters hence different stability limits.

7.6 PENETRATION LEVEL OF ASVT

Based on appendix B parameters the 220kV line is estimated to have an X value of 0.3752pu at a SIL of 124MW. Consequently, considering the simulation results, when the transmission line designed with this SIL value was terminated to a single ASVT. The Penetration results exhibited increased distortion towards the sending end of the line. These distortions of impulses which last between 2 to 3 cycles on switching accumulatively could cause insulation failure on the ASVT and its associated gears connected to the line.

However, penetration of two similar ASVTs provided much improved characteristics for both transmission line and output of the sub-station while distortion effect was limited to less than two cycles. This may be attributed to the fact that with higher shunt compensation, it becomes possible to transfer power over long distance without violating the voltage stability or voltage quality limits. With addition of an extra ASVT, no significant change was observed. It would be right to deduce that the designed SIL did not accurately correlated to the line characteristics, but as the numbers of ASVT units were increased the line voltage profile improved as observed from the simulation results.

This indicates that when a line is terminated at its SIL the complex power gain (actually loss) is purely real. The implication of this is that the line (when terminated at SIL), only affects the real power (decreases it) but does not affect the reactive power at all. Whatever reactive power flows out of the line (and into the load) also flows into the line.

Therefore, a line terminated at SIL has a very special characteristic with respect to reactive power. The amount of reactive power consumed by an ASVT is exactly compensated by the reactive power supplied by the line for every length of the line. Consequently, the maximum penetration level of ASVT units in a power transmission network is governed by their surge impedance loading (SIL).

7.7 ONWARD

This chapter has presented penetration level of ASVT on a power transmission line. It first started by determination of line parameters. This led to constructing the SIL curve for the line under investigation. The analysis was based on the loadability curve developed in chapter six and St Clair curve. St Clair curve are generally accepted in the industry as a convenient reference for estimating the maximum loading limits of transmission lines as already mentioned in the foregoing chapter.

Therefore, integration of ASVTs on a transmission line was analyzed from a comparative evaluation of the constructed SIL curve and the simulation results presented in the case study of chapter six. The reactive power compensation perspective was also considered in the analysis, since the ASVT systems itself acts as a shunt compensator. It was observed that the voltage stability limit was the main constraints for long lines.

Both analytical and simulation results showed that for the uncompensated long line, it was not possible to transfer power without causing voltage stability problems. Though at some length of the line both voltage stability and voltage quality affects the penetration level of the URE systems. It is worth noting again that both the ASVT and CCS systems can be used individually or collectively when integrated into a power transmission line for the purpose of supplying power to the rural community living in close proximity to the HV lines cheaply and reliably. The next chapter concludes the finding of this research project.

8 CONCLUSION

This thesis develops:

- A method of determining maximum allowable penetration level of CCS without steady state voltage violation derived from a modified distributed generation analogy. The method was based on the determination of voltage sensitivities from linearized power system model. Consequently, this method was used to validate the repetitive power flow simulations carried out in the case studies of chapter 4.

- A method of establishing ASVT penetration level with regard to voltage quality and stability on a power network was developed. This was analyzed by comparing simulation results of ASVT(s) loadability curve, resulting from actual power flow measurements simulated by the SimPower software in chapter 6 with the constructed Surge Impedance Loading (SIL) curves of chapter 7. The later curves were derived from the ABCD parameters of the transmission line under investigation derived in chapter 3. Thus, tangible similarities were proven between constructed Surge Impedance Loading (SIL) curves and the ASVT(s) loadability curve.

- An integrated approach to steady and transient state simulation for both ASVT and CCS system. The results showed that the tap-off voltage on the transmission line is high during light load period and low during heavy load period for a CCS and vice versa for an ASVT. Further, the results showed that tap-off voltage in the transmission line where ASVT systems are connected have relatively higher voltage rise than that of the CCS systems when connected in transmission line of the same length and line parameters. This revelation helps in the design of the protection system.

Comprehensive simulation analyses have been presented in both case studies of chapter 4 and 6. While the developed penetration level approaches of both sub-stations based URE technologies have been presented in chapter 5 and 7. The thesis answered questions related to penetration level of URE technologies on power networks. The findings and implications drawn from the case studies and analyses are summarized below;

1) **Was there a consistent method of determining the percentage penetration level of URE technologies with regard to steady state voltage quality, stability, and capacity constraints**

The URE technologies have been tried successfully in some parts of the world. However, the literature review showed that no work had so far been done on penetration level of these technologies on power networks, especially the CCS and ASVT which both have ability to tap power from high voltage transmission lines.

A method of determining maximum allowable penetration level of CCS without steady state voltage violation derived from a modified distribution generation analogy was developed. The method was based on the determination of voltage sensitivities from linearized power system model. Apparently, this method was used to validate the repetitive power flow simulations carried out in the case study of chapter 4.

The amount of reactive power consumed by an ASVT is exactly compensated by the reactive power supplied by the line for every length of the line. Consequently, the percentage penetration level of ASVT units in a power transmission network is governed by their surge impedance loading (SIL). Therefore, it was reasonable to evaluate the maximum penetration level of ASVT on a transmission line based on its Surge Impedance Loading (SIL) level. It is worth noting that the voltage quality limit has dominating influence on the loadability of short lines while the voltage stability limit was the main constraints for long lines.

2) What was the scope of URE technologies to be considered?

The scope of this research was based on two options of URE sub-station technologies. The two URE technologies considered were the CCS and ASVT technologies. These two URE technologies offered a good opportunity to carry out some fundamental research in these areas. Analyses were required on these technologies with regard to steady state voltage quality, stability, and capacity constraint.

Consequently, system study applying extensive modeling, simulation and analysis were necessary for better understanding of the URE technologies and their adoptability in different situations and scenarios. This was done in order to maximize the predicted benefit of these technologies to the rural consumers and overall power system reliability.

3) What factors restrict each of the URE technologies highlighted?

The limitation of CCS and ASVT systems is that they are only applicable where HV power lines traverse rural areas and are in close proximity to rural communities. On the other hand, they are designed for rural electrification where most loads are single phase.

Due to this backdrop, single phase sub-station may introduce voltage imbalance on the entire system causing dangerous un- proportional currents to flow. This could be mitigated by installing CCS or ASVTs alternately on each phase on the transmission lines.

Conversely, voltage stability becomes a concern when dealing with long lines, while voltage quality is more problematic in short and medium lines. It is also important to note that too much compensation will cause excessive voltage during periods of light load and may affect the generator stability. Ferro-resonance ceased to be a problem after the application of the proposed FSC circuit. Lastly, the URE technologies for the electrification of rural and slum areas are not yet mature but still evolving. Hence, this may introduce standardization problems when implemented especially in the SSA regions.

4) **What criteria were used to compare the two URE sub-station technologies?**

The penetration level of CCS and ASVT technologies were analogized from different but relevant perspectives, with common constraints imposed on them. This kind of treatment required same capacity of the systems, use of same line parameters and subjection to similar analytical protocols. At some point both systems were analyzed on the same power line. It was established based on simulation results that in order to generate a voltage control mechanism at the tap-off point of the CCS and ASVT systems, shunt inductances were required. In this research project the designed load capacity of both systems was about 100kVA, while the line under study had a 210 MVA load capacity. Therefore, reactance of 10MVAR and 5MVAR were required in the transmission line for the CCS and ASVT respectively to enable them operate without violating the voltage rise limitation.

5) **What methods should be used to explore the implication and adaptability of implementing various URE technologies in SSA?**

Geographic Information Systems (GIS), a powerful tool for analyzing of information on where and how people live, can be used to improve people's access to services and markets. In this research project several model configurations and circuits for CCS and ASVT systems on a transmission line were simulated. Steady state and transient results were analyzed. The loadability tests for the ASVT showed that the system could operate almost at all power factors at 1MW loading. On the other hand, the CCS could operate from 0.5 up to a maximum of 0.9 power factor for similar loading conditions. Apparently, this indicated that the ASVT system was more flexible than the CCS and could be used for a wider variation of power factors or loading. Consequently, merging the two loadability graphs for CCS and ASVT produces an optimum power factor or operating range that these two systems could operate within when integrated in power transmission lines.

The steady state simulation results for both ASVT and CCS system generally showed that the tap-off voltage on the transmission line was high during light load period and low during heavy load period.
Further, the results showed that tap-off voltage in the transmission line where ASVT systems were connected had relatively higher voltage rise than that of the CCS systems when connected in transmission line of the same length and line parameters.

Two methods were used to explore the implication and adoptability of implementing these two technologies on power networks. First, was the use of voltage sensitivities analysis to determine the penetration level of CCS in a power network with regard to steady state voltage quality, stability, and capacity constraints without steady and transient state voltage violation.

Secondly, the application of surge impedance loading (SIL) of the line to analyze the penetration level of ASVT in power networks was used. This was analyzed by comparing simulation results of ASVT(s) loadability curve, resulting from actual power flow measurements simulated by the SimPower software in chapter 6 with the constructed Surge Impedance Loading (SIL) curves of chapter 7. The later curves were derived from the ABCD parameters of the transmission line under investigation derived in chapter 3.This were based on the voltage quality and stability constraints.

These two un-conventional systems have proved that they can be used individually or collectively when integrated to a power transmission line. Therefore, both systems are capable of supplying power to the rural community living in close proximity to the HV lines cheaply and reliably. This can be done as long as the voltage rise control mechanism and an ingenious protection system are put in place.

6) **Was there a consistent and reliable way to analyze the cost, reliability and performance implications of URE and conventional rural electrification technologies?**

The technology for the electrification of rural and slum areas are not yet mature but still evolving. It also comprises more than technology. Important observations from literature are that electrification of these areas needs a multi-disciplinary approach, and that decision makers need appropriate information, structures and tools as a basis for consistent and appropriate decision-making. The most suitable method of electricity provision (technology or institutional model) will usually depend on the combination of the geographic context, the consumer need, and the possibilities that are available and affordable to provide the energy requirements. Therefore, the most appropriate solutions in one place might be quite unsuitable in another.

7) What methods/tools/models would be appropriate for this research project?

It is evident that the two sub-station based URE technologies have their own modeling techniques using different tools. The normal approach to most distribution system designs is by:

- Mathematical modeling
- Iterative design methods
- Simulations.

There is no fixed methodology or set of tools for any given research activity. The choices of methodology or tools are determined by the depth of hypothesis and research questions one wishes to answer to validate it. However, it should be noted that the methodology choice made will most likely constrain the questions one can ask and conversely certain research questions can best be addressed using certain methodologies. In this research project all the three techniques were used at different aspects of the research work as described in section 3.7 of chapter three.

8) Do any environmental factors affect the choice of URE sub-station technologies?

In most SSA countries, where transmission systems are in place but a wide-spread distribution infrastructure is lacking, the URE technologies may be used as a compact sub-station to greatly reduce the electrification costs for small villages. The URE can either be used with its low voltage output to directly supply needed power for loads near the transmissions right of way, or simply step up the URE low voltage output through distribution transformers for a local distribution network or reticulation network.

Small sub-stations can be site specific to the load requirements without a large distribution network therefore becoming environmental friendly. Tapping from high voltage transmission line and connecting a CCS/ASVT with a small footprint sub-stations provides affordable, readily-available electricity to rural communities presently without power. In some cases the lightening protection might make the sub-station more expensive depending on the geographical topology of the region. In other cases the application for large loads might exceed the capacity of a CCS or ASVT (e.g. Meru CCS in South Africa).

8.1 IMPLICATION OF URE TECHNOLOGIES

The research hypothesis of this thesis was whether there is:

A maximum penetration level of sub-station based URE technologies on power networks with regard to steady state voltage quality, stability, and capacity constraints without steady and transient state voltage violation.

There was a need to re-evaluate rural electrification technologies especially the publicized cost reduction capability offered by sub-station based URE technologies. Maximum percentage penetration levels of two of these available technologies were analyzed.

The aim was to aid in improved policy making and sound transmission and distribution network planning. Results, analysis and performance of the URE systems have been presented and based on the findings; the hypothesis was validated. It was established from the analysis and simulations, that there was no apparent optimum point of penetration for CCS or ASVT on power networks. The sub-stations could be installed at any point along the transmission line.

However, it was recognized that there was a maximum number of CCS/ASVT units that could be installed in particular power networks. The maximum penetration level of CCS was dependent not only on the transmission line parameters, e.g. the size of the divider capacitors used, the length of the line and the real and reactive power of the load on the CCS, but also on the loadability of the entire transmission line.

The ASVT penetration level on a power network was based on the surge impedance loading at which the system was terminated. This was gauged using the voltage quality and stability of the line. Thus, the design aspect of the ASVT system with regard to the winding impedance level contributed highly to the maximum penetration level of the system.

Both innovative URE sub-station based technologies are applicable to any HV transmission line as long as the voltage level is maintained within the ± 6% tolerance when the load power factor is varied between 0.2 and unity power factor. These technologies may be applied in any transmission line in SSA, provided the line parameters are known, appropriate penetration level analysis may be performed with respect to voltage sensitivities for the CCS and Surge Impedance Loading (SIL) for the ASVT systems. The analysis should be based on the maximum penetration level of URE acceptable at steady and transient state without violating the allowable voltage limitation.

8.2 WAY FORWARD

The results obtained by the proposed voltage sensitivity method used for determining of penetration level of CCS technology were compared with those provided by repetitive power flow solution. The accuracy of the proposed method was shown to be adequate despite its simplicity. This is mainly for typical distribution and transmission system where the network is radial and the X/R relation is low. It is important to emphasize that, although the proposed method has presented good performance, this is an approximated approach due to the linearization of the system model. Consequently, it should be used as a first approximation and, then, the selected results should be confirmed and refined by using a complete power flow program.

In the case of ASVT, the line parameters were determined by using the voltage and current measurements from either side of the transmission line from a laboratory set up.

Though, an accurate reference signal is required to precisely compare the measured signal. The timing signal from GPS units should be used to reference the measurements. In a field implementation data transfer of the measured signal would be necessary which can be accomplished by GPRS modems. In other words, more investigations are still required to come up with accurate data to be used in the construction of the SIL curves. Since these curves are the one that determine the actual loadability of the transmission line as well as to visually show at what point the line is operating at any given time.

REFERENCES

ABB bulletin (2000): *Auxiliary power from high voltage transmission lines.* Type SSVT oil filled substation voltage transformer www.abb.ssvt.com [accessed 20 June2012]

ABB Kulman (2006): *High voltage instrument transformer'* www.abb.com/highvoltage [accessed 7 June 2012]

Anderson, G.O., Yanev, K., (2010): *Non-Conventional Sub-station and Distribution System for Rural Electrification.* 3rd IASTED Africa PES 2010, Gaborone, Botswana, September 2010.

Anil, R.C., Barnes, D.F., Agawam, S.G., (2005): *Productive uses of energy for rural development* Energy sector management assistance program (ESMAP) World Bank Washington DC.

ANSI C93-1990, for power-line Carrier Coupling Capacitor and Coupling Capacitor Voltage Transformers (CCVT) – Requirements, Section 5.1.10 Burdens.

Araujo, A.E.A., Marti J.R., Soudac, A.C., (1993): *Ferro resonance in power systems: Chaotic behaviour* IEEE Proceedings, vol 140, No 3, May 1993.

Arteche Instrument transformer manual (2010): ASVT – 245 and ASVT 145 Manuals and technical brochures.

Arthur, R.B., Vijay, V., (2000): *Power Systems Analysis.* 2nd edition, ISBN 0-13-691990-1, Prentice Hall Inc 2000.

Ashok, K., (2007): *Optimised model for community-based hybrid energy system* Renewable energy 32 (2007) pp1155-1164

Asensi, R., Cobos, J.A., Garcia, O., Prieto, R., Uceda, J., (1994): *A full procedure to model high frequency transformer windings.* IEEE Power Electronics Specialist Conference PESC 94 June 1994 vol 2 pp856-863.

Ayres, H.M., Freitas, W., De Almeida M. C., Da Silva, L.C.P., (2010): *Methods for determining the Maximum Allowable Penetration Level of Distributed Generation without steady-state voltage violation* IET Generation, Transmission and Distribution 2010 Vol 4, pp495-508.

Baran, M.E., Wu, F.F., (1989): *Optimal Capacitor Placement on radial distribution systems.* IEEE Transaction on power delivery, vol 4, No.1, pp725-734.

Barnes, D.F., (2005): *Transformative power: Meeting the challenge of rural electrification.* ESMAP, Knowledge exchange series No 2.

Barnes, D.F., (2007): *The challenge of Rural Electrification: Strategies for developing countries.* Vol 3 pp1-18 Washington DC.

Barnes, D.F., Foley, G., (2004): *Rural Electrification in the developing world: A Summary of successful programs.* Joint UNDP/World Bank Energy Sector Management Assistance Program (ESMAP) World Bank, Washington DC.

Bekker, B., Eberhard A., Gaunt C.T., Marquand, A., (2008): *South Africa rapid electrification programme: Policy, institutional, planning, financial and technical innovations.* Energy policy 36 (2008) Pg 3115-3127.

Bekker, B., Gaunt C.T., (2007): *Sustainable electrification projects through a multi-criteria informed logical frame work approach CIGRE* SC-C6 working group (Coll 2007) IWD, Topic 4

Bell, S.C., Bodgers P.S., (2007) *Power Transformer Design Using Magnetic Theory Finite Element Analysis-Comparison of Techniques* Proceeding of AUPEC 2007 Perth, Western Australia 9-12 December 2007.

Bergen, A.R., and Vittal V., (2000) *Power System analysis 2nd*, ed upper saddle river, New Jersey 07458, prentice hall, 2000 p85.

Bodgers, P.S., Liew, M.C. Johnson, P.T., (2000) *Comparison of Conventional and reverse transformer design* Proceeding of AUPEC 2000 Brisbane, Australia, September 2000, pp80-85.

Bolduc, L., Bouchard B., Beaulieu G., (1997): *Capacitor divider substation* IEEE Transaction power delivery, vol 12 No 3 pp1202-1209, July 1997.

Cecelski, E., (2002): *Enabling equitable access to rural electrification: Current thinking on energy, poverty and gender.* Energy News Vol 5 nr 3 (2002).

Celli, G., Ghiani E., Mocci S., Pilo F., (2005): *A multiobjective evolutionary algorithm for the sizing and siting of distributed generation.* IEEE Trans Power system, 2005. 20 (2) pp750-757.

Celli, G., Pilo F., Pisano, V., Cicoria, R., Iaria, A., (2004): *Meshed Vs radial mv distribution network in presence of large amount of DG.* Power system conference and exposition 2004 IEEE PES pp709-714 vol 2, 2004.

Chapman, N., (2001): *When One Wire is enough*, Advance Energy Transmission & Distribution World, April 2001.

Chakravarthy, S.K., Nayar, C.V., (1995): *Ferro resonance Oscillations in Capacitor Voltage Transformer* IEE Proceedings Circuits Devices System Vol 142, No1 February 1995.

Chao Wang, Hua Hu., Yang He.,(2007): *Maximum Penetration level computation of Distributed Generators in Distribution network by considering Tap hunting constraints* Automation of electric power system vol 19 pp36-41 2007

CSA., (1979): *Capacitor Voltage Transformers.* CAN 3-C13.1M79. March 1979.

Dagbjartsson, G., Gaunt C.T., Zomers A.N., (2007): *Rural electrification: a scoping report.* CIGRE SC-C13/WD5 working group (Coll 2007) "Rural Electrification".

Damstra, G. C., (1997): *Ferro-resonance in Gas-Insulated Substation Voltage Transformer*, Power Technology International, pp. 87-91, 1994.

Dasguta, I., (2002): *Design of transformers.* 2nd Edition, Tata McGraw- Hill education Publishers 2002.

Daqing, H., Roberts J., (2000): *Capacitive Voltage Transformers: Transient Overreach Concerns and Solutions for Distance Relaying.* Schweitzer Engineering Laboratories, Inc. Pullman, WA, USA.

Deokar, D.N., Lingayat N.S., Khaparde S.A., Sukhatme S.P., (1988): *Modelling power plant at saphale,* IEEE Region 10 International conference on global connectivity in energy, TENCON 98, Vol 2, 17-19 December 1998, pp544-547.

DFID, (2007): *Energy planning in sub-Saharan Africa –facing the challenges of equitable access, secure supply and climate change* the environmental change institute Oxford, Ref: P01304.

Dimitrovski, A., Tomsovic, M., (2004) *Slack Bus Treatment in Load Flow Solutions with Uncertain Nodal Powers*, Proceeding of the 8th International Conference on Probalistic Methods Applied to Power Systems, Iowa State University, Ames, Iowa September 2004.

Dunlop, R.D., Gutman, R., Marchenko, P.P., (1979): *Analytical Development of loadability Characteristics for EHV and UHV Transmission lines.* IEEE Transactions on Power Apparatus and Systems, vol 1 PAS – 98, No 2 March/April 1979.

Donnelly, M.K., Dagle, J.E., Trudnowski, G.J., Rogers J., (1996): *Impacts of the distributed utility on transmission system stability*, IEEE Transaction on Power Systems, 11 (2) 1996 pp741-746.

Eberhard, A.A., (1986): "*Energy consumptions patterns in underdeveloped areas in South Africa*" Energy Research Institute, University of Cape Town.

Elgerd, O., (1982): *Electric Energy Systems Theory: An Introduction*, 2nd edition, McGraw-Hill, 1982.

EPRI TR, (1993): *Voltage Stability/Security Assessment and on line control,* EPRI-TR-101931, April 1993.

Enslin, J.H.R., (2004): *Interconnection of distributed power to the distribution network,* IEEE Young Researchers Symposium: Intelligent Energy Conventions, Delft, March 2004

Eskom, (1988): *Workshop on developing areas.* Collection of minutes and papers delivered at the workshop held on 5th February 1988 Eskom, Sandton

Fernandez Jr, D., Neves, W.L.A., Vasconcelos, J.C.A., (2003): *A Coupling Capacitor Voltage Transformer Representation for Electromagnetic Transient Studies.* International Conference on Power Systems Transients, IPST 98, 2003 New Orleans.

Ferracci, P., (1998): *"Ferro resonance"* Groupe Schneider: Cahier technique no190: www.scneiderelectric.com/en/pdf//ect190pdf,pp1-28 March 1998.

Gaunt, C.T., (2003): *Electrification Technology and Processes to meet Economic and Social Objectives in Southern Africa.* PhD Thesis: University of Cape Town.

Gaunt, C.T., (2005a): *The outlook for Dispersed Generation in South Africa CIGRE* SC-C6 working group (Coll 2005) ...IWD Topic D4. Cape Town

Gaunt, C.T., (2005b): *HV SWER and Single phase systems CIGRE* SC-C6 working group (Coll 2005) IWD Topic E2. Cape Town

Gaunt, C.T., (2007): *Economics, Social and environmental dimension of access to electricity. CIGRE* SC-C6 working group (Coll 2007) "Rural Electrification" Topic A.

Glover, J.D., Sarma, M. S., (2002): *Power System Analysis and Design*,(3rd ed) Brooks/Cole, CA: 2002.

Gish, W.B., Feero, W.E., Greuel, S., (1987): *Ferro resonance and loading relationship for DSG installations* IEEE Trans on power delivery, Vol PWRD - 2, pp953-959, 1987.

Gomez, R.G., Solano, A.S., Acosta, E.A., (2010): *Rural Electrification Project Development, Using Auxilliary Transformers. Location of Tubares, Chihuahua, Mexico. CIGRE* C6-305- 2010 working group (Coll 2010) "Rural Electrification" Calgary.

Gonen, T., (2008): *Electric Power Distribution System Engineering* CRC Press 2008, 2nd Edition.

Gozel, T., Hocaoglu, M.H., (2009): *An analytical method for the sizing and siting of distributed generators in radial systems.* Electrical Power System, Res, 2009. 79 pp912-918.

Haanyika, C.M., (2008): *Rural electrification in Zambia: A Policy and institutional analysis.* Energy policy 36 (2008), pp 1044-1058.

Hao, J., Xu W., (2008): *Extended Transmission Line Loadability Curve by including Voltage Stability Constraints.* IEEE Electrical Power and Energy Conference, Alberta, 2008.

IEG C57.13- 1993, 'IEEE Standard requirement for Instrument transformer'

Iliceto, F., Gatta, P., Debebe, M., (2005): *Rural electrification in Ethiopia with the simplified wire scheme*, Proceeding of the 18th International Conference on Electricity Distribution, Turin June 6-9 2005.

Iliceto, F., Gatta, P., Masato, H. Sysoulah, P., (2004): *Rural electrification in developing countries with the shield wire scheme application in Laos*, CIGRE paper C6-301, 2004 Session, Paris.

Ilskog, E., (2008): *Indicators for assessment of rural electrification –An approach for the comparison of apples* and *pears* Energy policy 36 (2008) pp2665-2673.

Instrument Transformer Manual by ABB (2004): Technical information and application Guide by ABB inc (www.abb.com/medium voltage) accessed 8th November 2012.

Invernizzi, A.G., Dagbjartsson A., Zomers A.N., (2007): SC C6 General Report *Electrification and Dispersed Generation: a debate between local and international professionals* Electra Nr 235. Cigre, Paris

Invernizzi, A.G., Gaunt C.T., (2006): SC C6 General Report *Electrification and Dispersed Generation: a debate between local and international professionals* Electra Nr 226. Cigre, Paris

Iravani, M.R, Wang X., Polishscuk, I., Ribeiro, J., Sarshar, A., (1998): *Digital time-domain investigation of Transformer transient Behaviour of Capacitor Coupling Voltage Transformer* IEEE Trans on Power Delivery, vol 13, No 2 pp 622-629.

Jacobson, D.A.N., (2000): *Example of Ferro-resonance in high voltage power system.* Proceedings of the 2000 Intl conference on power system transients- (IPST), June 2000.

Jacobson, D.A.N., Menzies, R.W., (2001): *Investigation of station service transformer Ferro-resonance in Manitoba Hydro's 230kV Dorsey converter station.* Proceedings of the 2001 Intl conference on power system transients, June 2001.

Jacobson, D.A.N., Marti, L. Menzies R.W., (1999): *Modelling Ferro-resonance in a 230kV transformer terminated double circuit line.* Proceedings of the 1999 Intl conference on power system transients (IPST) pp 451-456, June.

Jenkins, N., Allan, R., Crossly, P., Kirschen, D., Strbac, G., (2000): *Embedded Generation*, no 31in Power Energy series, London IEE 2000.

Jinfu, C., Rongqi, F., Xianzhaong, D, Jingliana, C., (2006): *Penetration level optimization for DG considering reliable action of relay protection device constraints.* IEEE Transaction on Power Systems vol 17, No3 2006.

Juhari, A.B., Kamaruzzan, S., Yusoff, A., (2007): "*Optimisation of renewable energy hybrid system by minimizing excess capacity*" International Journal of Energy Vol 1 issue 3 (2007) pp77-81.

Kaijuka, E., (2007): *GIS and rural electricity planning in Uganda.* Journal of Cleaner Production 15, 203-217.

Karsai, K., Kerenyi D., Kiss L., (1987): *Large Power Transformers* Elsevier Journal, New York, USA 1987.

Kenya Electricity Generation Company (KenGen), 2008. http://www.kengen.co.ke/map.aspxS (accessed August 2011).

Kenya Power and Lighting Co. Ltd., and Ministry of Energy, (2007a) Update of Kenya's Least Cost Power Development Plan 2008-2028.

Kenya Power and Lighting Co. Ltd., and Ministry of Energy, (2007b). Kenya Power and Lighting Company 2006/2007 *Annual Report.* Available at: http://www.kplc.co.ke/display.

Kersting W.H., (2001): *Distribution System Modelling and Analysis*, ISBN 0-8493-0812-7, CRC Press Boca Raton, Florida 33431.

Khatib, H., (1996): *Financial and Economic Evaluation of Projects with Special Reference to Electrical Power Industry* Power Engineering Journal February 1996, Vol 10, issue 1 pp 42-54.

Kirchesch, P., (2002): *Non-Conventional instrument transformers in high voltage substations* Electrotechnik and information e&i Journal, Vol 119, issue 1 2002, pp10-14

Kirubi, C. (2006): *How important is mordern Energy for micro-enterprises? Evidence from rural Kenya.* Jomo Kenyatta University of Agriculture and Technology, Masters thesis.

Kimbark, E.W., (1983): *A new look at shunt compensation.* IEEE Transaction on Power Apparatus and Systems vol, PAS-102, No1 January 1983.

Kooijman-van Dijk, A.L., (2008): *The power to produce: the role of energy in poverty reduction through small scale enterprises in the Indian Himalayas.* University of Twenty, Enschede, PhD thesis.

Kooijman-van Dijk, A.L., Clancy J., (2009): *Impact of electricity access to rural enterprises in Bolivia, Tanzania and Vietman.* Energy for sustainable development 14(2010) 14-21

Kothari, D.P., Nagrath, I.J., (2006): *Modern Power System Analysis* Mc Graw Hill, 2006.

Kundur, P., Paserba J., (2004): *"Definition and Classification of Power System Stability"*, IEEE Trans. on Power Systems. Vol. 19, No. 2, 2004.

LaMeres, B.J., Nehrir, M.H., Garez, A., (1999): *Controlling the Average Residential Water heater Power Demand Using Fuzzy Logic:* Electrical Power System Research vol 52 (1999) pp267-271.

Loughton, M.A., (2002): *Fuel cells,* IEE Engineering Science and Education Journal, 11 2002 pp7-16

LCPDP Report., (2009): *"Update of the Least Cost Power Development Plan 2009-2029"*Kenya Power and Lighting and Ministry of Energy Nairobi.

LCPDP Report, (2010): *"Update of the Least Cost Power Development Plan 2010-2030"*Kenya Power and Lighting and Ministry of Energy Nairobi.

Ledwich, G., Martino P., Calderon F., Gaunt C.T., (2007): *International practices in Rural Electrification CIGRE* SC-C6 working group (Coll 2007) ...IWD Topic E.

Leuven, (1987): EMTP Center, ATP – *Alternative Transient Program* – Rule Book, Heverlee Belgium, July 1987

Lindbolm, A., Isberg, J., Bernhoff, H., (2004): *Calculating the coupling factor in a multilayer coaxial transformer with air core*, IEEE Transaction on magnetics, Nov 2004, Vol.40, issue 5, pp3244-3248.

Liu, E., Bebic J., (2008): *Distribution System Voltage Performance Analysis for High-Penetration Photovoltaics* National Renewable Energy Laboratory Report – NREL/SR-581-42298

Longland, T., Hunt, W., Brecknell, W.A., (1985): *Power capacitor handbook* Butterworth London.

Mainali, B., Silveira, S., (2010): *Financing rural electrification: Country case Nepal.* Energy (2010), doi:10.1016/j.energy.2010.07.004.

Mandano, L., (1947): Rural Power Supply Especially in Back Country Areas, Proceeding of the New Zealand Institute of Engineers, 1947, Volume 33.

Mangwengwende, S.E., (2002): *Tariff and subsidies in Zimbabwe's reforming electricity industry: steering a utility through turbulent times* Energy policy 30 947-958

Margueron, X., Keradec, J.P., (2007): *Design of equivalent circuit and characterization strategy of n-input coupled inductors.* IEEE Transactions on Industry Applications Jan- Feb 2007, vol 43, Issue 1, pp14-22

Masters, C.L., (2002): *Voltage Rise: The big issue when connecting embedded generation on a long 11kV overhead line*, Power Engineering Journal 2002, vol 6, No 1, pp 5-12.

Mayer, J., Hossein-Zadeh, N., Wolfs, P., (2005): *Investigation of voltage quality and distribution capacity issues on rural three phase distribution lines supplying SWER system* AUPEC 2005 proceedings, Vol 2,pp333-350,September 2005.

Mathworks.com.(2008):http://www.mathworks.com/help/physmod/sps/powersys/ug/building-and-simulating-a-simple-circuit.html (accessed November 2013).

McLyman, W.N., (2004): *Transformer Inductor and Design Handbook,* 3rd edition, 2004.

Dekker, New York, USA,

Miller, T.J.E., (1982): *Reactive Power Control in electric systems, John* Wiley & Sons, New York.

Mohamedi, S., Lefebvre, S., Ba, O.A., Houle, A., (2007): *Comparative Study of the Symmetric and Asymmetric Approaches to Increase Power Transfer Capacity of a Corridor*. irep Symposium for Bulk Power System Dynamics and Control – VII Revitalizing Operational Reliability, August 19-24, 2007, Charlestone, SC, USA.

Morren, J., De Haan., and Sjoerd, W.H., (2008): *Maximum Penetration level of distributed generation without violating voltage limits* .CIRED Seminar: Smart Grid for Distribution paper No 0074.

Mrimal, K.P., (1991): *Voltage stability Condition considering load characteristics* IEEE Power Engineering Society 1991

Munasighe, M., (1988): *The economics of Rural Electrification Projects* Energy Economics 10 (1), 3-17.

Mutale, J., Gaunt, C.T., Konjic T., (2007): *Electricity service requirements in rural areas for domestic consumption and for productive use and services.* CIGRE SC-C13 working group (Coll 2007) "Rural Electrification".

Nasser, H., Rattray, J., (2008): *Economics of Upgrading SWER Distribution systems* AUPEC 2008 Proceedings, September 2008.

Nasser, H., Wolfs, P., (2009): *Distribution of Electrical Power to Rural Areas – Australian Experience and Implantation Possibility in Developing Countries.* AUPEC 2009 Proceedings, 2009.

Nayak, R.N., Sehgal, Y.K.,Subir, S., (2006): *EHV Transmission Line Capacity Enhancement Through Increase in Surge Impedance Loading Level* IEEE Transaction power delivery, vol 12 No 3 pp1202-1209, July 2006.

Neimane, V., (2001): *On Development Planning of Electricity Distribution Networks* Doctoral Dissertation, Royal Institute of Technology Stockholm.

Paatero, J.V., Lund P. D., (2006): *A Model of generating electricity house profile* International Journal of Energy Research Vol.30, issue 5, pp 273-290.

Pasand, M.S., Aghazadeh, R., (2003).*Capacitive Voltage Substations Ferro resonance Prevention using power electronics devices International* conference on power system transients- IPST 2003 in New Orleans.

Paul, C.R., Nasar, S. A., Unnewehr, L.E., (1986): *Introduction to Electrical Engineering* McGraw-Hill, Singapore, 1986.

Raphalalani, T.V., Ijumba N.M., Jimoh, A.A., (2000): *Capacitive Divider System for feeding a distribution network from an EHV line.* Powercon 2000 Lusaka.

Reeves K, Gaunt C.T., Braae M., (2011): *Modeling and dynamic systems analysis of instability in a capacitor-coupled substation supplying an induction motor.* Electric Power Systems Research, 81, Issue 4, April 2011, pp 888-893

REA, (2007): *Rural Electrification Authority Strategic Plan.* Nairobi: Government Printers

Sarmiento, H.G., De la Rosa F., Carrillo, V., and Villar J., (1990): *Solving Electric Energy Supply to Rural areas: The Capacitor Voltage Divider.* IEEE Transaction on power delivery, Vol 5, No 1, January 1990.

Saulo, M.J., Gaunt, C.T.,and Oliver,D.,. (2010) *Comparative Assessment of Short term Electricity Distribution System Planning with Long term Vision Oriented Planning* Proceeding of the 3rd IASTED African conference power and energy systems (Africa PES 2010) Sept 2010 Gaborone Botswana.

Saulo, M.J and Gaunt, C.T., (2010) *Implication of National Policy on Electricity Distribution System Planning in Kenya*, Proceeding of the 19th South African Universities Power Engineering Conference, SAUPEC 2010pp132-137.

Saulo, M.J., Gaunt, C.T., and Mbogho, M.S., (2011) *Implication of Non-Conventional Rural Electrification Technologies on Electricity Distribution System Planning in Kenya: A Review*, Proceeding of the 46th International Universities Power Engineering Conference, UPEC 2011 Soest Germany

Saulo, M.J., and Mbogho,M.S., (2011): *Implication of Capacitor Coupling Substation on Rural Electrification Planning in Kenya*, Proceeding of the 3rd International Kenya Society of Electrical and Electronics Engineers Conference, KSEEE 2011.

Saulo, M.J., and Mbogho, M.S., (2012): *Electricity Distribution System Planning in Kenya Based Multiple Criteria Decision Making,* Proceeding of the 9th International Conference on Power Systems Operation and Planning, ICPSOP 2011 Nairobi, pp 66-71

Saulo, M.J., Gaunt C.T., and Mbogho, M.S., (2012a): *Comparative Assessment of Capacitor Coupling Sub-station and Auxiliary Service Voltage Transformer for Rural Electrification* 2nd annual Kabarak international conference at Kabarak University 16th -18th October 2012 Nakuru, Kenya.

Saulo, M.J., Gaunt C.T., and Mbogho, M.S., (2012b): *Optimum Penetration level of un-conventional sub-station on a power transmission network.* Proceedings of the 1st Applied Research Conference in Africa. 29th – 31st August 2012 Elmina, Ghana.

Schilder, M., Britten A.C., Mathebula M.E., Singh A., (2005): *Eskom Experience with On-Site Field Tests of Capacitive Coupled Substation.* IEEE PES 2005 Conference and Exposition in Africa Durban, July 2005

SEM500 (Unitrode Seminar Manual)., (1987): *How to design a transformer with Fractional turns.* Unitrode Seminar Manual 1987.

SEM600 (Unitrode Seminar Manual)., (1988): *Eddy Current Losses in Transformer winding and Circuit Wiring* Unitrode Seminar Manual 1988.

Shukla, M., Sekar A., (2003): *Study of the effect of X/R Ratio of lines on Voltage Stability.* IEEE Transaction on power delivery, vol 2, No.3, pp83-97.

Sim Power System and PSS/E 25, On line documentation, Schenectady, US: Power Technologies Inc., December 1997.

Susa, Dejan., (2005): *Dynamic Thermal Modeling of Power Transformers*, PhD. thesis, Helsinki University of Technology.

Theirry Van Custem, T., (1988): *Voltage Stability of Electric Power systems,* Kluwer Academic Publishers, 1988.

Thong, V.V., Vanden, E., Soens J., Dommelan, D.V., (2004): *Influence of Large Penetration of Distributed Generation on N-1 Safety Operation.* IEEE Transaction on power delivery, vol 2, No.4, pp43-47.

Tobich, G.R., (1989): *The electrification of under developed areas: A case study in Ciskei.* MSc Thesis: University of Cape Town.

Transmission Line Reference Book (1987): *345 kV and Above,* Electric Power Research Institute, 2nd Edition, 1987.

Wadhwa, C.L., (2010): *Electrical Power Systems,* 6th Edition New Age International Publishers ISBN 8122424686, 2010

Wamukonya, J., Davis, M., (2001): *Social- economic impacts of rural electrification in Namibia: Comparisons between grid, solar and un-electrified households* Energy for sustainable development Vol No 3 (2001).

WEO (2011): World Energy Outlook, SBN: 978-92-6412413-4 International press

Wilson, R. E., Zevenbergen G. A., Mah, D.L., Murphy, A. J., (1999): *Calculation of transmission line parameters from synchronised measurements* Taylor and Francis, Vol 27, pp1269-1278, 1999.

Wolfs, P., Senini S., Seyoun, D., Loveday, A., (2004): *A proposal to investigate the problems of three – phase distribution feeders supplying power to SWER systems* AUPEC 2004 Proceedings, September 2004.

World Bank, (2000): *Energy Sector Reform and Power Development Project*, Kenya Report No. 16001-KE, Washington DC: World Bank.

Zomers, A.N., (2001): *Rural electrification*, PhD. thesis, University of Twente.

Zomers, A.N., (2003): *The Challenges of rural electrification* Energy for sustainable development Vol VII No 1 (2003).

APPENDICES

APPENDIX A: Line Parameter

TABLE A

KIAMBERE - RABAI LINE PARAMETERS [SOURCE: KPLC 2007A, KPLC 2007B, REA 2007, LCPDP 2010]

Code word	Nominal Area (mm^2)	Eqv. Area HDCC (mm^2)	Stranding And Wire Dia. (mm)		Overall Dia.(mm)	Areas (mm^2)			Weight (Kg/km)			Nominal Breaking Load		Max.D.C Resistance Ω/Km.20°C)	Rating (amps)	
Goat	300	194	Al	St		Al	St	Total	Al	St	Total	N	Kgf		Temperate	Tropical
			30/3.71	7/3.71	25.97	324.3	75.67	400.0	896	593	1.489	135.700	13.838	0.08910	542	200

A1. Towers:

The line has 940 towers with the first tower at Kiambere and the last tower at Rabai substation.

Tower of interest is no. 381 at Kasala Village. The village is located immediately after Tsavo East National Park.

A2. Line distance

The line is 440 km from the Kiambere Hydro-Generation station to Rabai station

A3. Line Loading

The 220kV line carries a maximum of 210 MVA. This can flows in either direction. During dry seasons, when hydrogenation is low, the flow is towards Kiambere and whereas during wet seasons the flow is towards Rabai

Line reactance X_L= 0.375200p.u Line Capacitive reactance Charging (B) 1/Xc =0.57600 p.u line rating =210 MVA

Line resistance= 0.0925 pu Z= Mva base at Rabai = 100MVA Base at hydros =100MVA

Stability limitation for the line is 125MVA/125 at unity p.f (because of length of line the line is mostly loaded at 70% of this limit), angle 44^0

A4.Transformer and Loading

Rabai Transformer 2x90MVA 22,000 GRY/138600 GRY, positive sequence impedance

(HV-LV 9.97Ω, HV TV 32.57) vector GYy0d1

Generation Transformer 2x75MVA 11/138kV SC impedance 18.32% vector group YNd11

Two reactors (inductors for compensation) 2x10MVAr

At Kiambere 1x87.5 MVA and 1x100MVA Transformers YN0d1 impedance at nominal tap 14.5%

Kiambere generators 2x 84.7MVA

APPENDIX B: Line Calculations

B1. 220kV Line Calculations

Base MVA = 100MVA, Line Capacity =210MW, Prevailing transfer Capacity =125MVA

Base voltage = 220KV

(i) Line inductance

At rated power:

$$\text{Base current} = \frac{BasePower}{\sqrt{3} \times BaseVoltage} = \frac{100 \times 10^3}{\sqrt{3} \times 220} = 262.43A$$

Given that the line reactance is 0.3752p.u

The line inductance is therefore $= \frac{220^2 \times 0.3752}{100 \times 2\pi \times 50} = 0.578\Omega$

Inductance per km $= \frac{0.578}{440} = 0.001314\Omega$

(ii) Line capacitance

Given susceptance =0.576p.u

So capacitive reactance $\frac{1}{B} = \frac{1}{0.576} = 1.736 p.u$

Therefore total capacitance = $\frac{100}{220^2 \times 1.736 \times 2\pi 50} = 3.7884\Omega$

Capacitance per Km = $\frac{3.7884 \times 10^{-6}}{440} = 8.61 \times 10^{-9} \mu F$

(iii) Resistance

Given the resistance of the line = 0.0925p.u

Total resistance of the line $= \frac{0.0925 \times kV^2}{100} = \frac{0.0925 \times 220^2}{100} = 44.77\Omega$

Resistance per km = $\frac{44.77}{440} = 0.102\Omega$

DC Resistance is 0.089Ω

B2. Transformer Calculations

Rabai Transformers

2x90MVA Auto-Transformers

Impedance at nominal tap given as 9.72% transformers are 90MVA so using 100MVA base:

$Z_{PU} = j0.0972 \times \frac{100}{90} = j0.108$

Since the two transformers are identical and working in parallel;

$Z_{eq} = j0.054$

For the use of Sim Power Systems software we need to convert these SI units:

Base impedance $= \frac{(BaseVoltage)^2}{BasePower(VA)} = \frac{127.07^2 \times 10^6}{\frac{180}{3} \times 10^6} = 268.8\Omega$

Base inductance $= \frac{268.8}{2\pi 50} = 0.8559 pu$

So inductance of combined transformers= 0.855 x 0.054 = 0.046H

(ii) Generator Transformers

2X75MVA

Using the above procedure the combined inductance = 0.044 H

The two types of transformers (Auto and generator transformers) can be represented as a series equivalent of:

.044 = 0.09H

(iii)Kiambere Transformers

For 1X87.5MVA transformer, the impedance at nominal tap = 14.8%

$$Z_{PU} = j0.148 \times \frac{100}{87.5} = j0.16914$$

For 1X100MVA Transformer, the impedance at nominal tap =14.48%

$$Z_{PU} = j0.1448 \times \frac{100}{100} = j0.1448$$

Since the transformers are working in parallel:

$$Z_{eq} = \frac{-(0.16914 \times 0.1448)}{j(0.16914 + 0.1444)} = j0.078$$

Base reactance for the 87.5MVA transformer $= \frac{127.017^2}{\frac{87.5}{3}} = 553.14\Omega$

Base inductance $= \frac{553.14}{2\pi 50} = 1.7607H$

Base reactance for the 100MVA transformer $= \frac{127.017^2}{\frac{100}{3}} = 483.99\Omega$

Base inductance $= \frac{483.99}{2\pi \times 50} = 1.541H$

Equivalent base inductance $= \frac{1.7607 \times 1.541}{1.541 + 1.7607} = 0.822H$

Total inductance for the two transformers in parallel

0.0657H $0.0779 \times 0.822 = 0.0657H$

APPENDIX C: Simulation Results and Tables for CCS

C1. Simulations showing voltage wave forms at the sending end with a single capacitor coupled sub-station at different distances from Rabai.

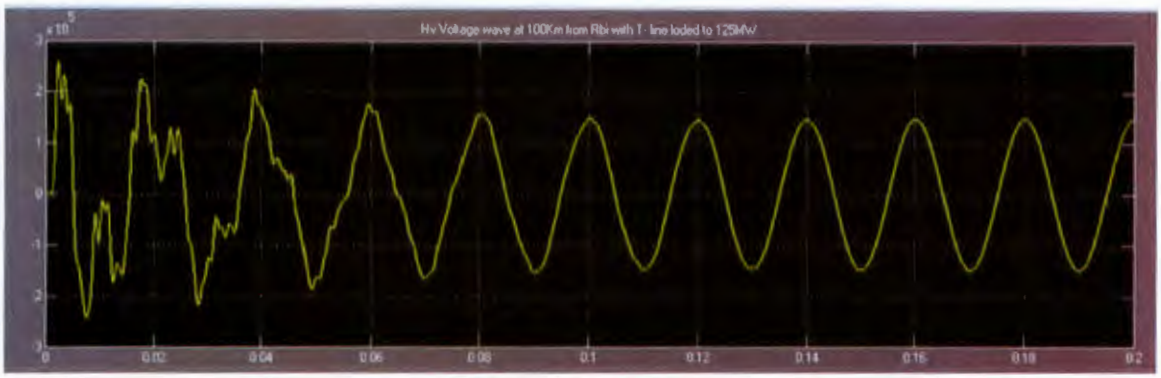

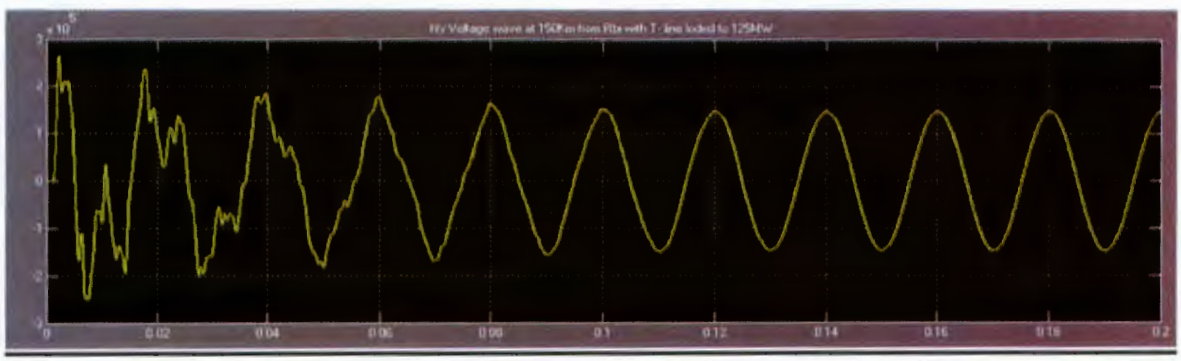

C2. Simulations showing voltage wave forms at the Sending and receiving end with a two capacitor coupled sub-station at different distances from Rabai

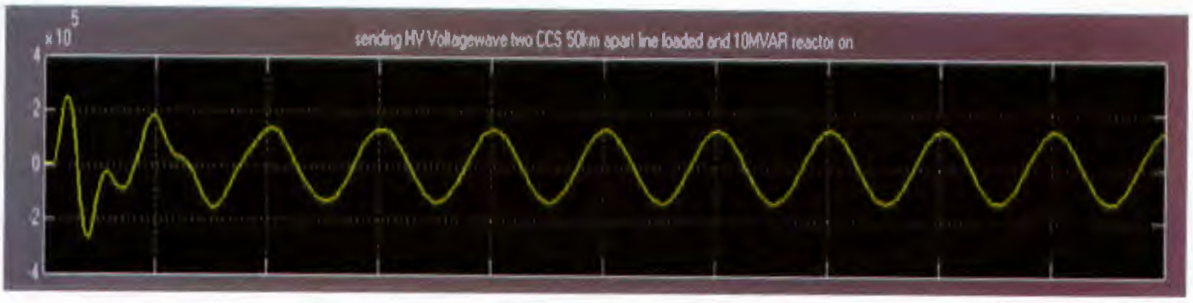

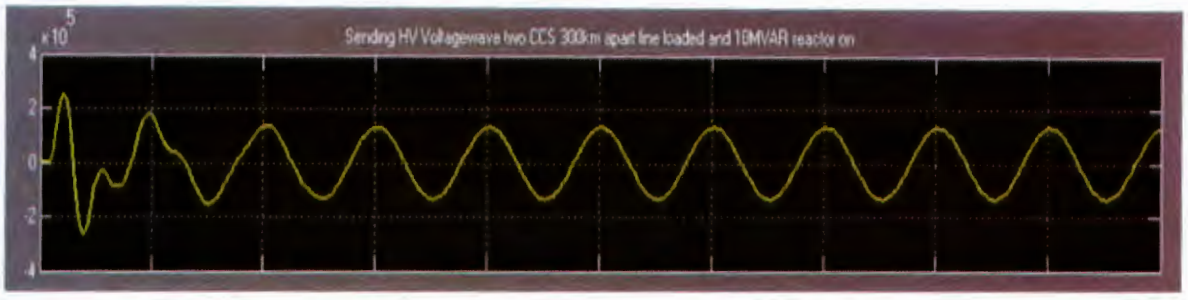

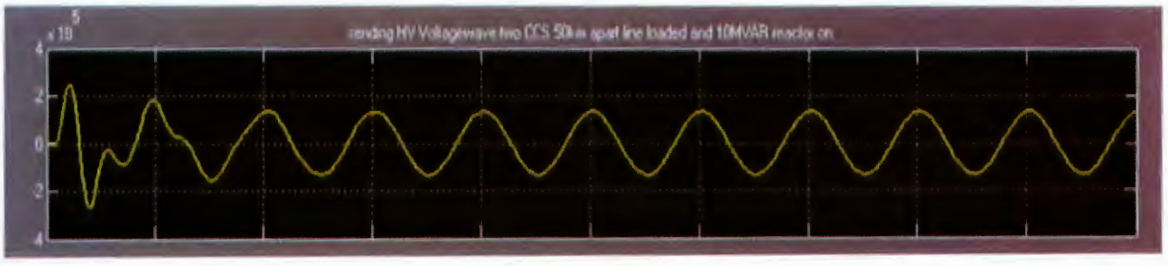

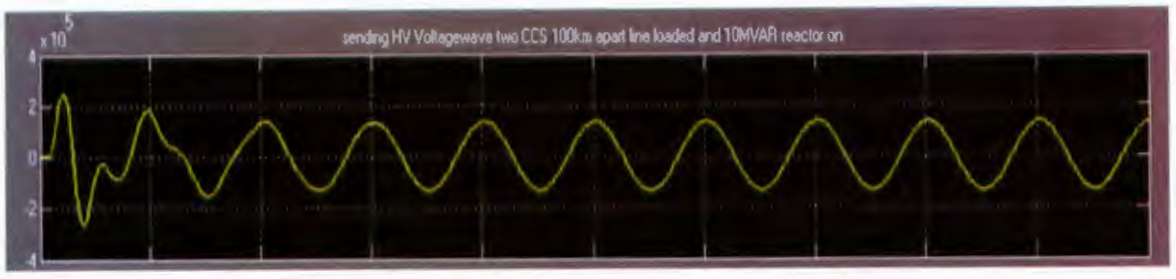

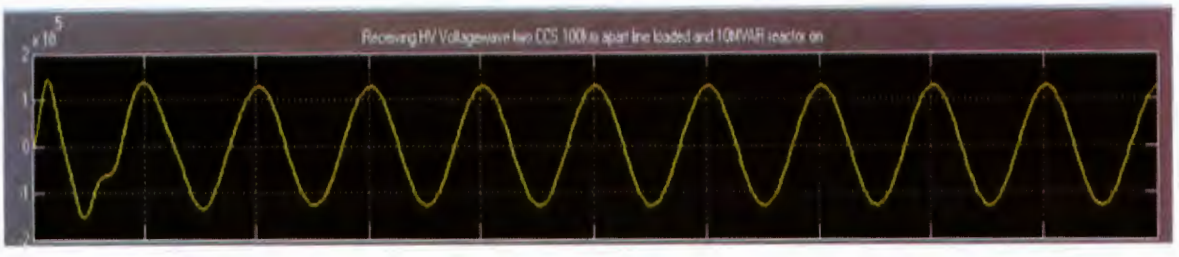

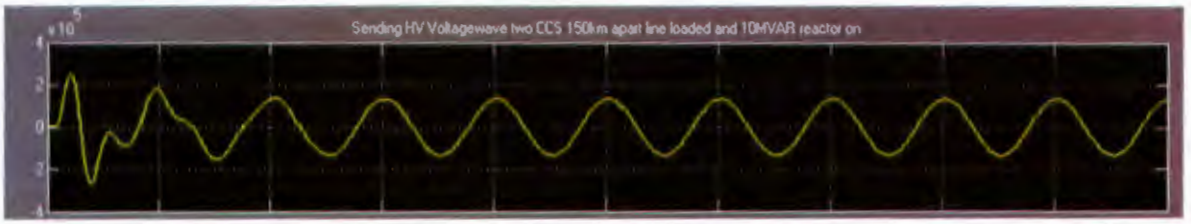

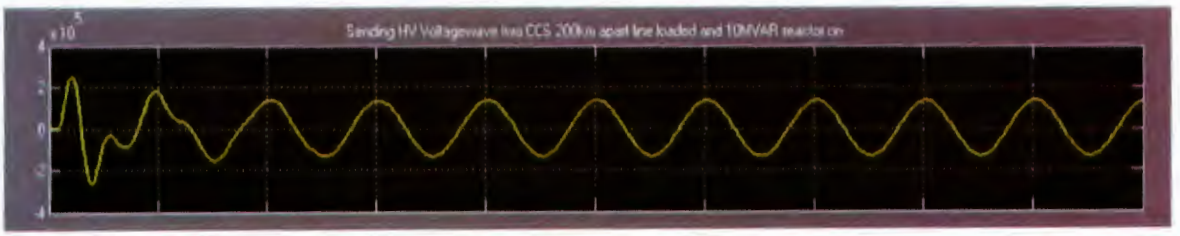

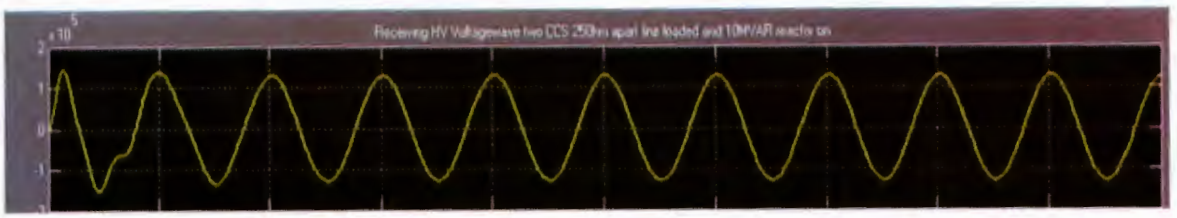

C3. Simulations showing voltage wave forms at the receiving end with three capacitor coupled sub-station at different distances from Rabai.

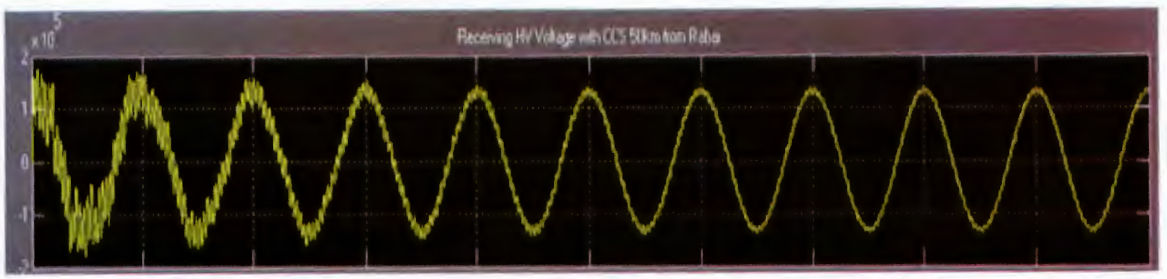

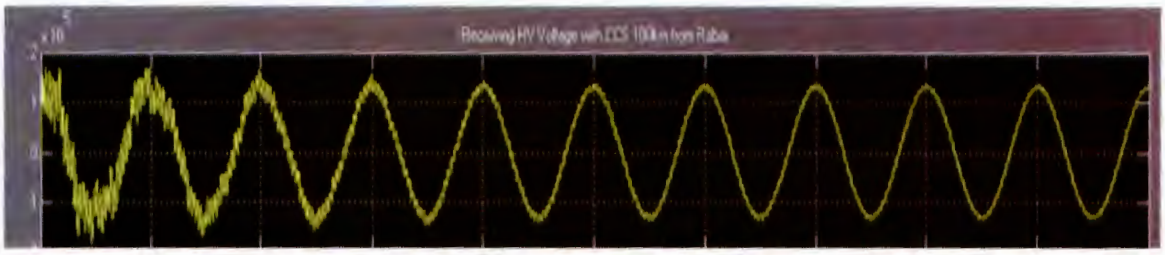
Receiving HV Voltage with CCS 100km from Rabai

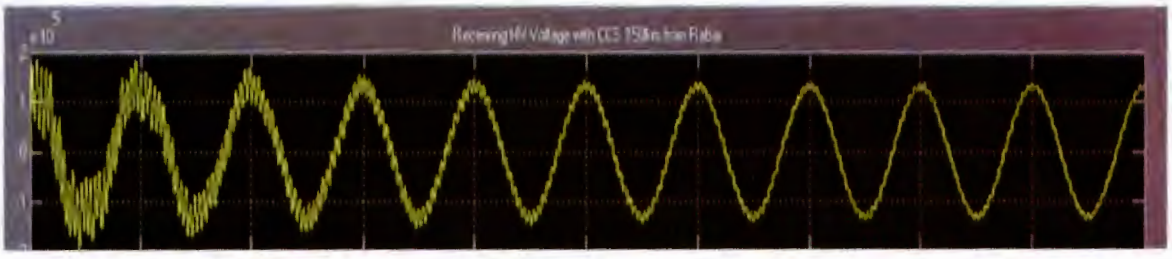
Receiving HV Voltage with CCS 150km from Rabai

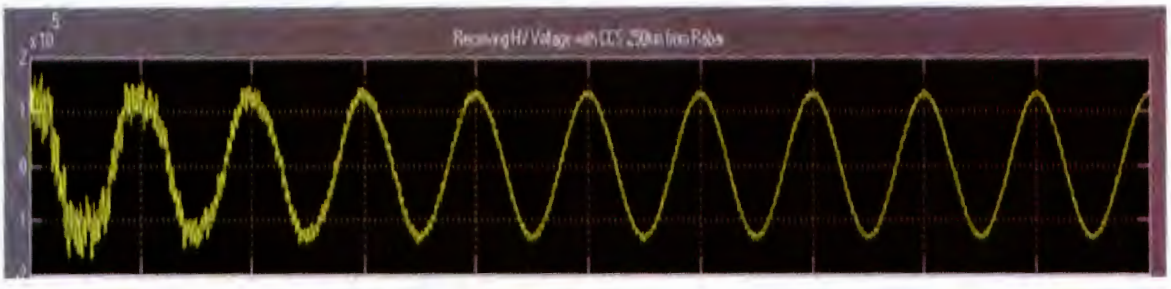
Receiving HV Voltage with CCS 200km from Rabai

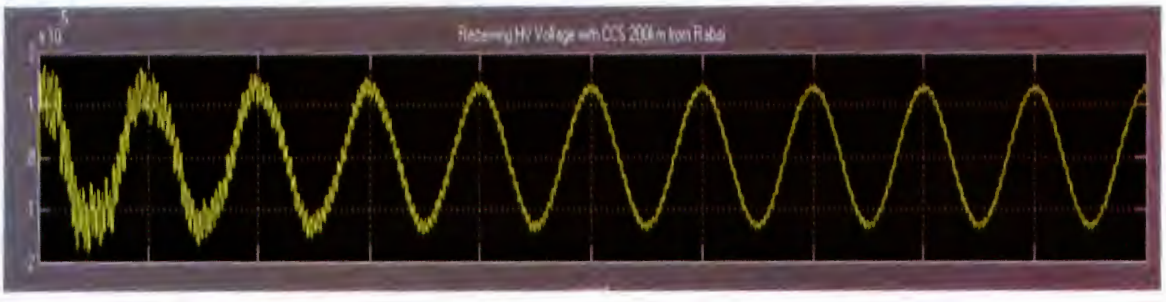
Receiving HV Voltage with CCS 250km from Rabai

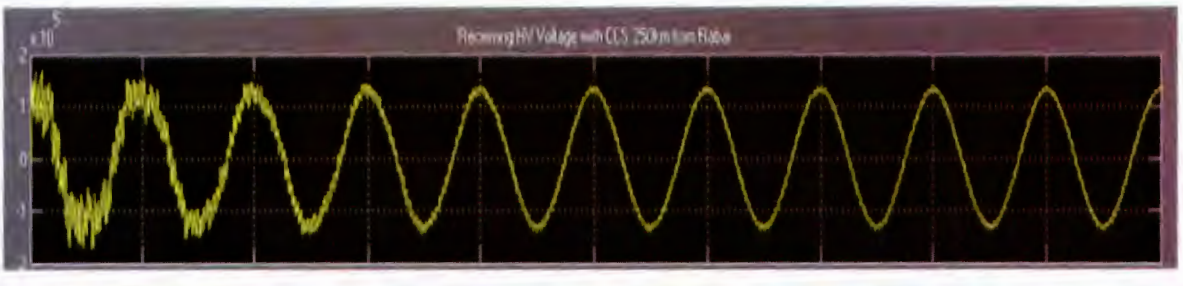
Receiving HV Voltage with CCS 300km from Rabai

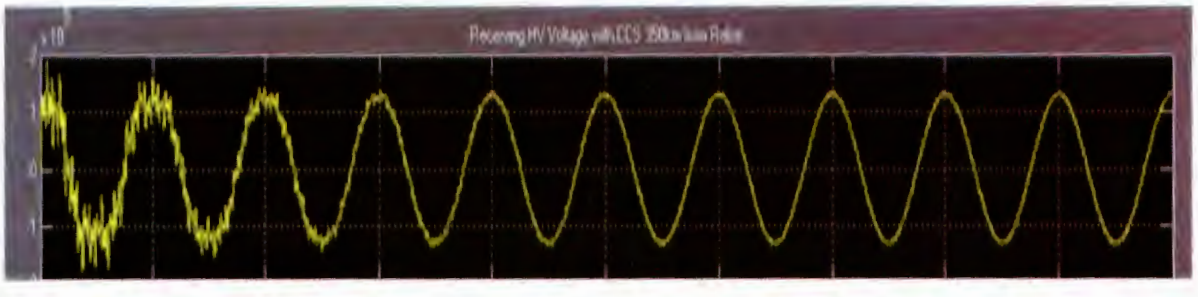
Receiving HV Voltage with CCS 350km from Rabai

TABLE C- 1TRANSMISSION PARAMETERS AT DIFFERENT DISTANCES WITH LINE NOT LOADED

with transmission line not loaded	CCS at 50km from Rabai		CCS at 100km from Rabai		CCS at 150km from Rabai		CCS at 200km from Rabai	
	Min Load 1kW	Max Load 100kW	Min Load 1kW	Max Load 100kW	Min Load 1kW	Max Load 100kW	Min Load 1kW	Max Load 100kW
Low Voltage	250V	241V	248V	239V	246V	237V	243V	234V
Current	4 A	51 A	4 A	49 A	4 A	47 A	4A	44A
Medium Voltage V_m	31,343V	31,531V	31,142V	31,330V	30,854V	31,040V	30,480V	30,664V
High Voltage V_{in} (Volts)	148,920	148,898	148,588	148,569	148,247	148,230	147,900	147,887
Value of capacitors in µF	C_1 0.4		0.4		0.4		0.4	
	C_2 1.5		1.5		1.5		1.5	
Value of inductor	2.5H		2.5H		2.5H		2.5H	
Voltage V_{th} at point of capacitor divider	Initial over shoots that that are about 50kV settles to32kV after 3cycles		Initial over shoots that that are about 50kV settles to32kV after 3cycles		Initial over shoots that that are about 50kV settles to32kV after 3cycles		Initial over shoots that that are about 50kV settles to32kV after 3cycles	
Nature of Distortion on High voltage	Serious Initial over shoots that are up to 250 kV settles to145kV after 5cycles		Serious Initial over shoots that that are up to 240kV settles to143kV after 3cycles		Serious Initial over shoots that are up to 280kV settles to142kV after 4cycles		Serious Initial over shoots that are up to 300 kV settles to142 kV after 4cycles	
Nature of Distortion on low voltage	Distorted waveform with harmonics of about 350 V which clears after 3 cycles		Distorted waveform with high harmonics of about 350V which clears after 4cycles		Distorted waveform with harmonics of about 350 V which clears after 3 cycles		Distorted waveform with high harmonics of about 350V which clears after 3cycles	

Continued..	CCS at 250km from Rabai		CCS at 300km from Rabai		CCS at 350km from Rabai		CCS at 400km from Rabai	
	Min Load 1kW	Max Load 100kW	Min Load 1kW	Max Load 100kW	Min Load 1kW	Max Load 100kW	Min Load 1kW	Max Load 100kW
Low Voltage	239V	231V	235V	227V	230V	222V	224V	217V
Current	4A	40A	4A	36A	4A	31A	4A	26A
Medium Voltage V_m	30,022	30,204	29,483	29,662	28,865	29,042	28,173	28,345

(V)								
High Voltage V_{in} (Volts)	147,551	147,541	147,205	147,197	146,865	146,858	146,531	146,528
Value of capacitors (μF)	C_1	0.4	0.4		0.4		0.4	
	C_2	1.5	1.5		1.5		1.5	
Value of inductor (H)	2.5		2.5		2.5		2.5	
Voltage V_{th} at point of capacitor divider	Initial over shoots that t are about 42kV settles to32kV after 3cycles		Initial over shoots that are about 40kV settles to32kV after 4cycles		Initial over shoots that are about 35kV settles to32kV after 4cycles		Initial over shoots that are about 35kV settles to32kV after 5cycles	
Nature of Distortion on High voltage	Initial over shoots that are up to 200 kV settles to145kV after 5 cycles		Initial over shoots that that are up to 240kV settles to143kV after 3 cycles		Initial over shoots that are up to 280kV settles to142kV after 4 cycles		Initial over shoots that are up to 300kV settles to142kV after 4 cycles	
Nature of Distortion on low voltage	Distorted waveform with high harmonics of about 320V which clears after 3cycles		Distorted waveform with high harmonics of about 300V which clears after 4cycles		Distorted waveform with high harmonics of about 300V which clears after 4cycles		Distorted waveform with high harmonics of about 250V which clears after 4cycles	

TABLE C- 2

TRANSMISSION PARAMETERS OF THE LINE UNDER A 125MVA LOAD

Case 3b Transmission line loaded at 125 MVA	CCS at 50km from Rabai		CCS at 100km from Rabai		CCS at 150km from Rabai		CCS at 200km from Rabai	
	Min Load 1kW	Max Load 100kW	Min Load 1kW	Max Load 100kW	Min Load 1kW	Max Load 100kW	Min Load 1kW	Max Load 100kW
Low Voltage	250.29V	241.39V	248.69V	239.85V	246.38V	237.63V	243.39V	234.75V
Current	4.35A	51.44A	4.32A	49.84A	4.28A	47.53A	4.23A	44.53A
Medium Voltage V_m	31,343V	31,531V	31,142V	31,330V	30,854V	31,040V	30,480V	30,664V
High Voltage V_{in}	148,920V	148,898	148,588V	148,569V	148,247	148,230	147,900V	147,887V
Value of capacitors in μF	C_1 0.4		0.4		0.4		0.4	
	C_2 1.5		1.5		1.5		1.5	
Value of inductor	2.5H		2.5H		2.5H		2.5H	
Voltage V_{th} at point	Initial over shoots that		Initial over shoots that that		Initial over shoots		Initial over shoots that t	

of capacitor divider	that are more than 42kV settles to32kV after 5cycles	are more than 42kV settles to32kV after 5cycles	that that are more than 42kV settles to 32kV after 5cycles	are more than 40KV settles after 4 cycles
Nature of Distortion on High voltage	Initial over shoots that that are up to 250 kV settles to145kV after 5cycles	Serious Initial over shoots that that are up to 240kV settles to143kV after 3 cycles	Serious Initial over shoots that that are up to 280kV settles to142kV after 4 cycles	Serious Initial over shoots that that are up to 300kV settles to142kV after 4cycles
Nature of Distortion on low voltage	Distorted waveform with high harmonics but wave not more than 400V	Distorted waveform with high harmonics but wave not more than 400V	Distorted waveform with high harmonics but wave not more than 400V	Distorted waveform with high harmonics but wave not more than 400V

Case 3b Continued..	CCS at 250km from Rabai		CCS at 300km from Rabai		CCS at 350km from Rabai		CCS at 400km from Rabai	
	Min Load 1kW	Max Load 100KW	Min Load 1kW	Max Load 100kW	Min Load 1kW	Max Load 100kW	Min Load 1kW	Max Load 100kW
Low Voltage	239.74V	231.23V	235.43V	227.08V	230.50V	222.33V	224.97V	217.00V
Current	4.16A	40.86A	4.09A	36.54A	4.00A	31.60A	3.91A	26.04A
Medium Voltage V_m	30,022V	30,204V	29,483V	29,662V	28,865V	29,042V	28,173V	28,345V
High Voltage V_{in} (Volts)	147,551	147,541	147,205	147,197	146,865	146,858	146,531	146,528
Value of capacitors in µF	C_1 0.4		0.4		0.4		0.4	
	C_2 1.5		1.5		1.5		1.5	
Value of inductor	2.5H		2.5H		2.5H		2.5H	
Voltage V_{th} at point of capacitor divider	Initial over shoots that that are more than 42kV settles to32kV after 5cycles		Initial over shoots that that are more than 42kV settles to32kV after 5cycles		Initial over shoots that that are more than 42kV settles to 32kV after 5cycles		Initial over shoots that t are more than 40kV settles after 4 cycles	
Nature of Distortion on High voltage	Initial over shoots that that are up to 200 kV settles to145kV after 5cycles		Serious Initial over shoots that that are up to 240kV settles to143kV after 3cycles		Serious Initial over shoots that that are up to 280kV settles to 142kV after 4cycles		Serious Initial over shoots that that are up to 300kV settles to142kV after 4cycles	
Nature of	Distorted waveform with high harmonics but		Distorted waveform with high harmonics but wave		Distorted waveform with high harmonics		Distorted waveform with high harmonics but wave	

Distortion on low voltage	wave not more than 400V	not more than 400V	but wave not more than 400V	not more than 400V

TABLE C- 3TRANSMISSION PARAMETERS WITH LINE LOADED AT 125MVA AND 10MVAR REACTOR

Case3c with trans- line loaded 125 MVA and 10MVAR in	CCS at 50km from Rabai		CCS at 100km from Rabai		CCS at 150km from Rabai		CCS at 200km from Rabai	
	Min Load 1kW	Max Load 100kW	Min Load 1kW	Max Load 100kW	Min Load 1kW	Max Load 100kW	Min Load 1kW	Max Load 100kW
Low Voltage	221V	221V	221V	221V	230V	221V	227V	221V
Current	4A	29A	4A	28A	4A	29A	4A	29A
Medium Voltage V_m	27,691V	28,883V	27,776V	28,974V	28,806V	28,980V	28,851V	28,904V
High Voltage V_{in} (Volts)	130,393 128,595	135,171 129,395	130,140 128,597	134,919 129,395	134,663 129,399	134,650 129,398	134,900 129,396	134,372 129,397
Value of capacitors in μF	C_1 0.4		0.4		0.4		0.4	
	C_2 1.5		1.5		1.5		1.5	
Value of inductor	2.5H		2.5H		2.5H		2.5H	
Voltage V_{th} at point of capacitor divider	Initial over shoots that that are more than 42kV settles to32kV after 5cycles		Initial over shoots that that are more than 42kV settles to32kV after 5cycles		Initial over shoots that that are more than 42kV settles to32kVafter5cycles		Initial over shoots that t are more than 40kV settles after 4 cycles	
Nature of Distortion on High voltage	Initial over shoots that that are up to 250 kV settles to145kV after 5cycles		Serious Initial over shoots that that are up to 240kV settles to143kV after 3cycles		Serious Initial over shoots that that are up to 280kV settles to142kV after 4cycles		Serious Initial over shoots that that are up to 300kV settles to142kV after 4cycles	
Nature of Distortion on low voltage	Distorted waveform with high harmonics but wave not more than 400V		Distorted waveform with high harmonics but wave not more than 400V		Distorted waveform with high harmonics but wave not more than 400V		Distorted waveform with high harmonics but wave not more than 400V	

TABLE C- 4TRANSMISSION PARAMETERS OF TWO CCS CONNECTED AT DIFFERENT DISTANCES

Case 4a Transmission line loaded 125 MVA	CCS1 ,CCS2 at 50km,100km from Rabai respectively		CCS1, CCS2 50km,150km from Rabai respectively		CCS1, CCS2 50km,200km from Rabai respectively		CCS1, CCS2 250km,252km from Rabai respectively	
	CCS1	CCS2	CCS1	CCS2	CCS1	CCS2	CCS1	CCS2
Low Voltage	242V	254V	241V	251V	241V	248V	239V	252V
Medium Voltage V_m	31,308V	32,853 V	31,287	32,534V	31,265V	32,125V	30,994V	32,706V
High Voltage $V_{S,\&}V_R$	147,828V 129,842V		147,727V 129,344V		147,625V 129,342V		151,383V 129,807V	
Value of capacitors in μF	C_1 0.4	0.12	0.4	0.12	0.4	0.12	0.4	0.12
	C_2 1.5	0.4	1.5	0.4	1.5	0.4	1.5	0.
Value of inductor	2.5 H		2.5 H		2.5 H		2.5 H	
Voltage V_{th} at point of capacitor divider	Initial over shoots that are more than 42kV settles to 32kV after 1cycles		Initial over shoots that are more than 42kV settles to32kV after 1cycles		Initial over shoots that are more than 42kVsettles to32kV after 1cycles		Initial over shoots that are more than 42kVsettles to32kV after 1cycles	
Nature of Distortion on High voltage	Initial over shoots that are up to 250 kV settles to146KV after 2cycles		Initial over shoots that are up to 240kV settles to145KV after 2cycles		Initial over shoots that are up to 230kV settles to145kV after 2cycles		Initial over shoots that are up to 230kV settles to146kV after 2 cycles	
Nature of Distortion on low voltage	Initial overshoot to 300V but settles to set voltage after 2 cycles Almost no distortion on waveform		Initial overshoot to 300V but settles to set voltage after 2 cycles Almost no distortion on waveform		Initial overshoot to 300V but settles to set voltage after 2 cycles Almost no distortion on waveform		Initial overshoot to 300V but settles to set voltage after 2 cycles Almost no distortion on waveform	

Case 4a transmission line loaded 125 MVA	CCS1 ,CCS2 at 50km,250km from Rabai respectively		CCS1, CCS2 50km,300km from Rabai respectively		CCS1, CCS2 50km,350km from Rabai respectively		CCS1, CCS2 50km,400km from Rabai respectively	
	CCS1	CCS2	CCS1	CCS2	CCS1	CCS2	CCS1	CCS2
Low Voltage	241V	244V	241V	240V	249V	243V	241V	229V
Medium Voltage V_m	31,243V	31,627 V	31,221V	31,042V	32,317V	31,459V	31,179V	31,580V
High Voltage	147,522V		147,420V		152,592V		147,221V	

$V_{S,}$ & V_R	129,339V			129,336V		129,826V		129,329V	
Value of capacitors in μF	C_1	0.4	0.12	0.4	0.12	0.4	0.12	0.4	0.12
	C_2	1.5	0.4	1.5	0.4	1.5	0.4	1.5	0.4
Value of inductor	2.5 H			2.5 H		2.5 H		2.5 H	
Voltage V_{th} at point of capacitor divider	Initial over shoots that that are more than 42kV settles to32kV after 1cycles			Initial over shoots that that are more than 42kV settles to32kV after 1cycles		Initial over shoots that that are more than 42kV settles to32kV after 1cycles		Initial over shoots that that are more than 42kV settles to32kV after 1cycles	
Nature of Distortion on High voltage	Initial over shoots that that are up to 250 kV settles to146kV after 2cycles			Initial over shoots that are up to 240kV settles to145kV after 2cycles		Initial over shoots that are up to 230kV settles to145kV after 2cycles		Initial over shoots that are up to 230kV settles to146kV after 2cycles	
Nature of Distortion on low voltage	Initial overshoot to 300V but settles to set voltage after 2 cycles Almost no distortion on waveform			Initial overshoot to 300V but settles to set voltage after 2 cycles Almost no distortion on waveform		Initial overshoot to 300V but settles to set voltage after 2 cycles Almost no distortion on waveform		Initial overshoot to 300V but settles to set voltage after 2 cycles Almost no distortion on waveform	

TABLE C- 5 TRANSMISSION PARAMETERS OF TWO CCS WITH A 10MVAR CONNECTED AT DIFFERENT DISTANCES

Case 4b transmission line loaded 125 MVA & 10MVAR Reactor	CCS1 ,CCS2 at 50km,100km from Rabai respectively		CCS1, CCS2 50km,150km from Rabai respectively		CCS1, CCS2 50km,200km from Rabai respectively		CCS1, CCS2 250km,252km from Rabai respectively	
	CCS1	CCS2	CCS1	CCS2	CCS1	CCS2	CCS1	CCS2
Low Voltage	221V	234V	221V	234V	221V	234V	225V	238V
Medium Voltage V_m	28,683V	30,378 V	28,666V	30,366V	28,648V	30,269V	29,168V	30,790V
HighVoltage $V_{S,}$ & V_R	134,188V 127,912V		134,108V 127,912V		134,025V 127,911V		136,006V 128,321V	
Value of capacitors in μF	C_1 0.4	0.12	0.4	0.12	0.4	0.12	0.4	0.12
	C_2 1.5	0.4	1.5	0.4	1.5	0.4	1.5	0.4
Value of inductor	2.5 H		2.5 H		2.5 H		2.5 H	
Voltage V_{th} at point	Initial over shoots that that are more than 42kV settles		Initial over shoots that that are more than		Initial over shoots that that are more		Initial over shoots that that are more	

of capacitor divider	to32kV after 1cycles	42kV settles to 32kV after 1cycles	than 42kV settles to32kV after 1cycles	than 42kV settles to32kV after 1cycles
Nature of Distortion on High voltage	Initial over shoots that that are up to 250 kV settles to146kV after 2cycles	Initial over shoots that are up to 240kV settles to145kV after 2cycles	Initial over shoots that are up to 230kV settles to145kV after 2cycles	Initial over shoots that are up to 230kV settles to146kV after 2cycles
Nature of Distortion on low voltage	Initial overshoot to 300V but settles to set voltage after 2 cycles Almost no distortion on waveform	Initial overshoot to 300V but settles to set voltage after 2 cycles Almost no distortion on waveform	Initial overshoot to 300V but settles to set voltage after 2 cycles Almost no distortion on waveform	Initial overshoot to 300V but settles to set voltage after 2 cycles Almost no distortion on waveform

Case 4b with trans-line loaded 125 MVA & 10MVAr Reactor	CCS1 ,CCS2 at 50km,250km from Rabai respectively		CCS1, CCS2 50km,300km from Rabai respectively		CCS1, CCS2 50km,350km from Rabai respectively		CCS1, CCS2 50km,400km from Rabai respectively	
	CCS1	CCS2	CCS1	CCS2	CCS1	CCS2	CCS1	CCS2
Low Voltage	221V	232V	221V	230V	221V	227V	220V	224V
Medium Voltage V_m	28,630V	30,087 V	28,612V	29821V	28,593V	29473V	28,575V	29,043V
High Voltage V_S &V_R	133,940V 127,910V		133,854V 127,909V		133,768V 127,907V		133,683V 127,905V	
Value of capacitors in μF	C_1 0.4	0.12	0.4	0.12	0.4	0.12	0.4	0.12
	C_2 1.5	0.4	1.5	0.4	1.5	0.4	1.5	0.4
Value of inductor	2.5 H		2.5 H		2.5 H		2.5 H	
Voltage V_{th} at point of capacitor divider	Initial over shoots that are more than 42kV settles to 32kV after 1cycles		Initial over shoots that are more than 42kV settles to32kV after 1cycles		Initial over shoots that are more than 42kV settles to32kV after 1cycles		Initial over shoots that are more than 42kV settles to32kV after 1cycles	
Nature of Distortion on High voltage	Initial over shoots that are up to 250 kV settles to146kV after 2cycles		Initial over shoots that are up to 240kV settles to145kV after 2cycles		Initial over shoots that are up to 230kV settles to145kV after 2cycles		Initial over shoots that are up to 230kV settles to146kV after 2cycles	
Nature of Distortion on low voltage	Initial overshoot to 300V but settles to set voltage after 2 cycles Almost no distortion on waveform		Initial overshoot to 300V but settles to set voltage after 2 cycles Almost no distortion on waveform		Initial overshoot to 300V but settles to set voltage after 2 cycles Almost no distortion on wave		Initial overshoot to 300V but settles to set voltage after 2 cycles Almost no distortion on wave	

TABLE C- 6 TRANSMISSION PARAMETERS FOR THREE CCS AT DIFFERENT DISTANCES

Case 4c transmission line loaded 125 MVA & 10MVAR Reactor off	CCS1 ,CCS2, CCS3 at 50,100and 150 Km from Rabai respectively			CCS1, CCS2,CCS3 50,150, 250km from Rabai respectively			CCS1, CCS2 CCS3 at 50,200 350 km from Rabai respectively		
	CCS1	CCS2	CCS3	CCS1	CCS2	CCS3	CCS1	CCS2	CCS3
Low Voltage	272V	270V	259V	269V	262V	259V	266V	257V	258V
Medium Voltage V_m (Volts)	32,51	34,180	33,847	32,442	33,799	32,852	32374	33,322	31,499
High Voltage $V_{S,}$ & V_R	148,660V 129,462V			148,349V 129,454V			148041V 129,445V		
Value of capacitors in μF	C_1	0.42	0.12	0.12	0.42	0.12	0.12	0.42	0.12	0.12
	C_2	1.5	1.5	0.4	1.5	0.4	0.4	1.5	0.4	0.4
Value of inductor	2.5 H			2.5 H			2.5 H		
Voltage V_{th} at point of capacitor divider	Initial over shoots that that are more than 42kV settles to 32kV after 1cycles			Initial over shoots that that are more than 42kV settles to 32kV after 1cycles			Initial over shoots that that are more than 42kV settles to 32kV after 1cycles		
Nature of Distortion on High voltage	Initial over shoots that that are up to 250 kV settles to146kV after 2cycles			Initial over shoots that are up to 240kV settles to 145kV after 2cycles			Initial over shoots that are up to 230kV settles to145kV after 2cycles		
Nature of Distortion on low voltage	Initial overshoot to 300V but settles to set voltage after 2 cycles Almost no distortion on waveform			Initial overshoot to 300V but settles to set voltage after 2 cycles Almost no distortion on waveform			Initial overshoot to 300V but settles to set voltage after 2 cycles Almost no distortion on waveform		

APPENDIX D: Circuits for Different Scenarios of CCS.

D1. MODEL CIRCUIT WITH TWO CCS EACH PI SECTION REPRESENTING 220KM

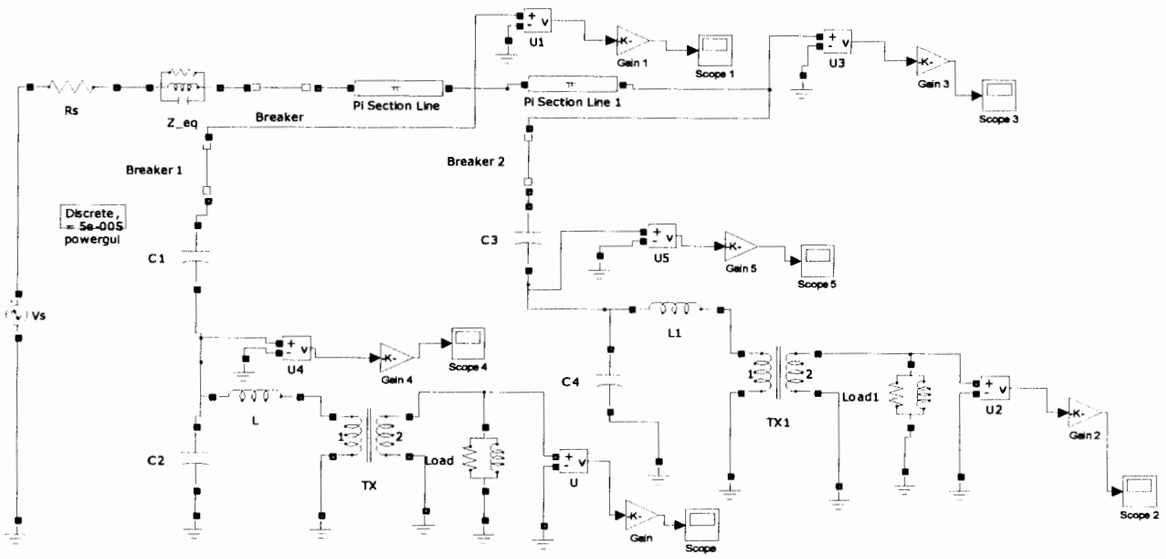

D2. MODEL CIRCUIT WITH THREE CCS EACH PI SECTION REPRESENTING 147KM

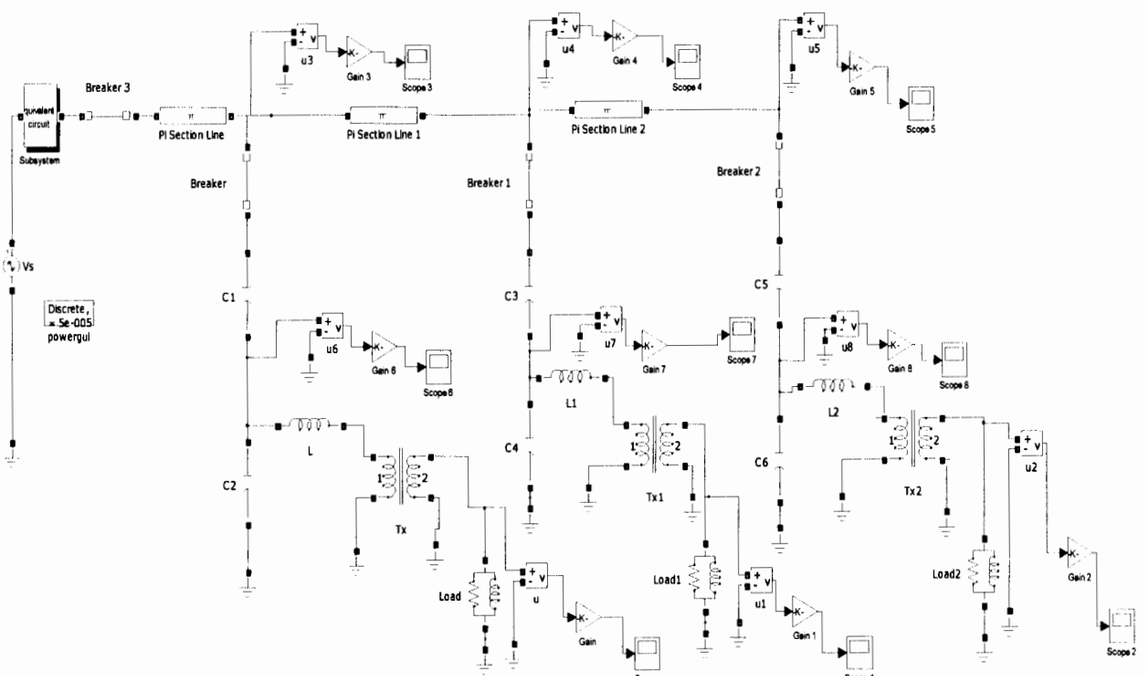

APPENDIX E: CCS Loadability Test Results

Tables E1 to E6 are the CCS loadability test results derived from the simulation of the model in Figure 4.28.

Where;

Scope 1 U_1 - (kV) represents system tap-off voltage.

Scope 2 U_2 - (kV) represent capacitor banks voltage divider

Scope 3 U_3 (kV) - represent load terminal voltage

Scope 4 I_1 - (A) represent system current.

Scope 5 I_2 - (A) represent current flowing at the capacitor bank divider

Scope 6 I_3 - (A) represent load current

QL (MVAR) - represent varied reactive power of the load

The calculations for currents were done using $P = \sqrt{3} V_L I_L \cos\phi$.

Where; P is the load power, V_L is the line voltage, I_L is the line current and $\cos\phi$ is the power factor. Assuming a star connected load $I_{ph} = {}^{I_L}/_{\sqrt{3}}$ where; I_{ph} is the phase current.

Note that the values given in table E1 to E6 for the capacitor divider current and load current are line currents. While for the system current is given in phase value. The stability limitation of the line was 125MW (see appendix A). Therefore, assuming a 70% loading per phase, the system load was 29.17MW.

E1. SIMULATION RESULTS FOR 1MW LOAD AT VARIED POWER FACTOR

U_1(KV)	U_2(KV)	U_3(KV)	1_I(A)	I_2(A)	I_3(A)	Q_L(MVAR)	PF
130.55	31.76	31.76	645.01	90.89	90.89	4.898	0.2
130.38	33.09	32.27	430.56	58.16	59.64	3.179	0.3
130.32	33.57	32.48	323.07	42.99	44.44	2.291	0.4
130.24	34.14	32.73	258.62	33.82	35.28	1.732	0.5
130.14	34.88	33.05	215.68	27.59	29.11	1.333	0.6
129.99	35.92	33.51	185.08	22.96	24.61	1.02	0.7
129.75	37.67	34.27	162.25	19.16	21.05	0.75	0.8
129.15	41.99	36.15	144.89	15.28	17.74	0.484	0.9
130.55	31.92	31.81	129.00	18.09	18.73	0	1.0

E2. SIMULATION RESULTS FOR 2MW LOAD AT VARIED POWER FACTOR

U_1(KV)	U_2(KV)	U_3(KV)	1_I(A)	I_2(A)	I_3(A)	Q_L(MVAR)	PF
130.42	34.34	31.99	645.65	168.13	180.48	14.693	0.2
130.26	35.57	32.27	430.96	108.21	119.27	9.538	0.3
130.08	37.06	32.88	323.67	103.86	87.79	6.873	0.4
130.63	38.94	33.63	257.85	59.31	68.67	5.196	0.5
129.56	41.58	34.65	216.65	46.28	55.54	3.999	0.6
129.14	45.70	36.22	186.30	36.09	45.54	3.06	0.7
128.46	53.60	39.17	163.87	26.92	36.85	2.25	0.8
128.46	56.99	46.15	145.67	22.51	27.80	1.453	0.9
130.67	32.32	30.97	128.88	35.73	37.28	0	1.0

E3. SIMULATION RESULTS FOR 3MW LOAD AT VARIED POWER FACTOR

U_1(KV)	U_2(KV)	U_3(KV)	1_I(A)	I_2(A)	I_3(A)	Q_L(MVAR)	PF
130.42	34.34	31.99	645.65	252.19	270.72	14.693	0.2
130.26	35.57	32.27	430.96	162.31	178.91	9.538	0.3
130.08	37.06	32.88	323.67	116.84	131.69	6.873	0.4
130.63	38.94	33.63	257.85	88.96	103.00	5.196	0.5
129.56	41.58	34.65	216.65	69.43	83.31	3.999	0.6
129.14	45.70	36.22	186.30	54.14	68.31	3.06	0.7
128.46	53.60	39.17	163.87	40.39	55.27	2.25	0.8
128.46	56.99	46.15	145.67	33.77	41.70	1.453	0.9
130.67	32.32	30.97	128.88	53.59	55.92	0	1.0

E4. SIMULATION RESULTS FOR 4MW LOAD AT VARIED POWER FACTOR

U_1(KV)	U_2(KV)	U_3(KV)	1_I(A)	I_2(A)	I_3(A)	Q_L(MVAR)	PF
130.60	35.05	31.35	644.77	329.44	368.32	19.591	0.2
130.44	36.58	31.92	430.37	210.44	241.16	12.717	0.3
130.27	38.47	32.61	323.20	150.07	177.05	9.164	0.4
130.06	40.88	33.48	258.97	112.98	137.95	6.928	0.5
129.81	44.26	34.65	216.23	86.96	111.08	5.333	0.6
129.55	49.50	36.39	185.71	66.65	90.66	4.08	0.7
128.59	58.60	39.22	163.71	49.26	84.12	3.00	0.8
133.04	59.98	41.07	140.65	42.78	62.48	1.938	0.9
130.87	32.58	30.40	128.68	70.88	75.96	0	1.0

E5. SIMULATION RESULTS FOR 5MW LOAD AT VARIED POWER FACTOR

U_1(KV)	U_2(KV)	U_3(KV)	1_I(A)	I_2(A)	I_3(A)	Q_L(MVAR)	PF
130.86	35.62	30.78	643.49	405.21	468.93	24.488	0.2
130.73	37.35	31.37	429.41	257.63	306.74	15.897	0.3
130.60	39.47	32.07	322.38	182.84	225.04	11.455	0.4
130.47	42.19	32.94	258.16	136.84	175.27	8.66	0.5
130.38	45.92	34.05	215.28	104.77	141.30	6.667	0.6
130.49	51.36	35.53	184.37	80.29	116.07	5.1	0.7
131.44	59.31	37.12	160.16	60.84	97.21	3.75	0.8
134.79	63.19	34.97	138.83	50.76	91.72	2.421	0.9
131.12	32.87	29.80	128.44	87.82	96.87	0	1.0

E6. SIMULATION RESULTS FOR 6MW LOAD AT VARIED POWER FACTOR

U_1(KV)	U_2(KV)	U_3(KV)	1_I(A)	I_2(A)	I_3(A)	Q_L(MVAR)	PF
131.17	36.03	30.14	641.30	480.72	574.67	29.386	0.2
131.08	37.87	30.71	428.27	304.91	376.00	19.076	0.3
131.01	40.09	31.36	321.37	216.02	276.16	13.747	0.4
130.99	42.90	32.14	257.14	161.49	215.56	10.392	0.5
131.09	46.59	33.05	214.12	123.92	174.69	7.999	0.6
131.53	51.47	34.02	182.92	96.15	145.46	6.121	0.7
132.86	56.96	34.38	158.45	86.88	125.94	4.50	0.8
135.16	56.49	31.17	138.44	68.14	123.48	2.906	0.9
131.36	33.1O	29.18	128.21	104.65	118.71	0	1.0

APPENDIX F: ASVT DESIGN

ASVT parameters of a 100kVA rating alongside a prototype of 100VA rating are presented in this appendix. Basic concept of selection of number of turns for the transformer based on the equation F1 is presented

$$E_t = k\sqrt{Q} \qquad \text{(F1)}$$

From the number of turns and the approximate flux- density (assumed) the gross core area can be calculated. Once the core area is known, the core diameter can easily be found using the formula

$$A_g = K_1 \pi d^2 \qquad \text{(F2)}$$

Where d is the core diameter and k is a factor to be selected from the number of core steps.

Selection of the approximate area of winding wires and strip are done on the basis of the rated current and available current density, which is generally restricted to 1.5A/sqmm for aluminum and 3.0A/sq/mm for copper material.

The diameter of round conductor for high voltage winding can be calculated from the equation

$$Area = \frac{\pi d^2}{4} \qquad \text{(F3)}$$

The size of the strip and their disposition is very important to minimize the skin effect. However, while selecting the strip, the limitation of size as the ratio of width and depth must remain 2 and 4.

F1 DESIGN SPECIFICATION

TABLE – F1 DESIGN SPECIFICATIONS FOR THE PROTO-TYPE

	TRANSFORMER DESIGN	**PROTO TYPE DESIGN**
Power rating	100KVA	100VA
No load voltage ratio	220,000 /220 Volts	240/24 volts
No of phase / frequency	3 phase/ 50Hz	1 phase/ 50Hz
Connection	delta / star	neutral grounded
Winding material	copper	copper
Tapping on HV	At + 2.5% to 5% for HV variation	At + 2.5% to 5% for HV variation
No – load and load loss (max)	520/3520 (max)	
Impedance	4.5%	4.5%
Maximum flux density	1.6 tesla s	1.6 tesla s
Maximum current density	3.0A / sq.mm	3.0A / sq.mm
All other specifications are as per ISO- 2026, ISO – 1180 and REC – 2/71		

TABLE – F2 PRIMARY COIL CONNECTED IN DELTA

TRANSFORMER DESIGN	**PROTO TYPE DESIGN**
Voltage per phase $V_{ph} = 220{,}000/\sqrt{3}$ V	240V
The current per phase $I_{ph} = \frac{power\ rating}{3x phase\ voltage} = \frac{100{,}000}{3x127{,}000} = 0.2624A$	$\frac{100}{\sqrt{2}x240} = 0.2946A$
Current density (cd) assumed = 3.0 A/sq mm (max)	3.0 A/sq mm (max)

$conductor\ area = \frac{current\ per\ phase}{current\ density}$ $= \frac{0.2624}{3.0} = 0.0874$	$\frac{0.2946}{3.0} = 0.0982$
Equivalent conductor $Area = \frac{\pi d^2}{4} = 0.0505$	$Area = \frac{\pi d^2}{4} = 0.1473$
$d^2 = \frac{0.0505x4}{\pi}$	$= \frac{0.14731x4}{\pi} = 0.1250$
Conductor diameter d= 0.0643mm	d = 0.3257mm
The designer proposed to use the next round figure	
d = 0.3 mm	d = 0.35mm
Area of the proposed conductor $= \frac{\pi d^2}{4} = \frac{0.3^2\pi}{4} = 0.0707 sq.mm$	$\frac{0.35^2\pi}{4} = 0.096 sq.mm$
$working\ current\ density = \frac{current\ per\ phase}{area\ of\ proposed\ conductor}$	
$= \frac{0.2624}{0.0707} = 3.711 A/sq.mm$	$\frac{0.2946}{0.0982} = 3A\ per\ sq.mm$

From equation (1), the value of 'k' for copper wound transformer ranges from 0.40 to 0.50

The commonly used value for k (assumed) = 0.45

TABLE – F3 NUMBER OF TURNS

TRANSFORMER DESIGN	PROTO TYPE DESIGN
$E_t = 0.45\sqrt{100} = 4.5V\ per\ turn$	$0.45\sqrt{250} = 1.13\ V\ per\ turn$
Number of secondary turns = secondary phase voltage /E	
$= \frac{127\sqrt{2}}{4.5} = 89.8T$ rounded off to 90T	$\frac{0.24\sqrt{2}}{1.13} = 3T$
$No.of\ primary\ turns = \frac{primary\ phase\ voltage \times secondary\ turns}{secondary\ phase\ voltage} = 38647T$	
$= \frac{127000 \times 90}{127\sqrt{2}} = 63{,}639.6T$	$\frac{240 \times 3}{24} = 30T$

Additional turns 5% tapping voltage = 63,639.6 x 5% = 3,182	30x5% = 1.5T
Total primary turns =63,639.6 + 3,182= 66822T	30+1.5=31.5T
$no.\ of\ coils\ per\ phase\ (assumed) = 4Turns$	(Assumed)= 5 turns
Turns per coil = $\frac{66822}{4} = 16{,}706T$	$\frac{31.5}{5} = 6.3T$
The H.V winding design proceeds as follows	
TRANSFORMER DESIGN	**PROTO TYPE DESIGN**
$V_{ph} = 127000\ V$	= 240V
$I_{ph} = 0.2624\ A$	=0.2946A
Wire size =0.3 mm	0.35mm
Area =0.0707 sq mm	Area = 0.096sq.mm
Current density =3 A/sq mm	= 3A/sq.mm
Secondary turns = 90T	3T
Primary turns = 16706 T	or 31.5T

Description	**Length**	**Radial**	**Proto type**
Bare conductor	0.3 mm	0.3 mm	0.35mm
Covering thickness towards DPC	0.2 mm	0.2 mm	0.2mm
Covered conductor	0.5 mm	0.5mm	0.55mm
Gap between two consecutive conductor (assumed) insulated size of conductor with	0.05 +0.55mm	0.05+0.55mm mm for mil inter layer insulation	0.05mm +1.00mm
Working tolerance			
$\frac{16706+0.55}{100} \times 387$ Turns per layer			280/17 Turns per layer.
Axial length of H.V Coil	212.85mm		65mm
Rounded – off to	213mm		

TABLE – F4 ESTIMATED CORE WINDOW (SECONDARY COIL)

Transformer connected in star	**Prototype single phase neutral earthed**
Total axial length of four coils: 387x 4 = 1548mm Gap between yoke to top and bottom coil : 2x30 = 60mm Gap between two tap coils at the Centre : 1x 15mm = 15mm Gap between plain coils : 2x10 = 20mm Core window height 1643mm	Total axial length of four coils: 65x4 = 260mm Gap between yoke to top and bottom coil : 2x15 = 30mm Gap between two tap coils at the center 1x5 = 5mm Gap between plain coils : 2x5 = 10mm Core window height 305mm
Voltage per phase = $220/\sqrt{3} = 127\,\text{kV}$	$240/\sqrt{3} = 138.56V$
Current per phase = $\frac{63639.6 \times 0.2624}{90} = 185.54A$	$\frac{31.5X0.2946}{3} = 3.09A$
Current Density (Assumed) = 3.0 A/ sq mm (max)	Current Density (Assumed) = 3.0 A/ sq mm (max)
Conductor area = $\frac{185.54}{30} = 6.18 sqmm(mil)$	$\frac{2.946}{3} = 0.982 sq\ mm\ (mil)$
Number strips proposed to be used in parallel = 4	= 2
Approximate area of each strip = $\frac{6.18}{4} = 1.545 sqmm(mil)$	$\frac{0.982}{2} = 0.491\cdots sq\ mm\ (mil)$
Disposition of each strip = 1 width x 2 depth	Disposition of each strip = 1 width x 2 depth
No *of* turns per phase (as calculated earlier) = 90T	No *of* turns per phase (as calculated earlier) = 3T
Space required to accommodate 35T =90 +1 = 91T	Space required to accommodate35T= 3+1 = 4

NB: Since the strips are placed one above the other, we need to keep some space for transposition, which creates the need for space for one more additional turns,

as such space required to accommodate transposition	90 +1 = 91 T	31+1 =32T
Gap between LV coil to yoke at the top and bottom	15 mm	15mm
Window height of core (w/h) as calculated before	1643 mm	305mm
Axial length available to accommodate transposition	90T = 1643 - (4x15) =1583 mm	3T= 305-2x15 = 275mm
Approximate width of LV strip, including DPC covering and with Working tolerance = Axial length/space required.	$\frac{1583}{90} = 17.58mm$	$\frac{275}{32} = 8.594mm$
Air gap between two consecutive conductors (assumed)	0.1 mm	0.1mm
Therefore width of the above conductor taking into consideration the covering thickness- 0.2	17.58 mm – (0.2 + 0.1) =17.28 mm	8.594mm - (02+.1) =8.294mm
The design conceived a strip having bare width of	35mm (which is around figure)	0.35mm
Area of each strip (as calculated before) $= area\ of\ strip \times number\ of\ turns$	= 21.86x90=1858.1sq mm	0.0962sq mm
Therefore the approximate depth of the bare conductor	$\frac{1858.1}{35} = 53.09mm$	$\frac{0.0962}{0.35} = 0.275mm$

LV WINDING DESIGN

	TRANSFORMER DESIGN	**PROTO TYPE DESIGN**
Voltage per phase	127kV	138.56V
Current per phase	185.54A	2.946A
Strip size	35 x 54 x 2 numbers in parallel	0.35x0.275x1
Area of strip	21.867 sq mm	0.491 sq mm
Current density	3A/sq mm	3A/sq mm

Number of coils per phase	4	1
Turns per coil	90T	3T
No of layers	2	2
Turns per layer	43.5	14
Transposition	to be provided	to be provided

	Transformer		**Prototype**	
DESCRIPTION	**LENGTH**	**RADIAL**	**LENGTH**	**RADIAL**
Bare strip size	35 mm	54 mm	14mm	
Covering thickness towards DPC covered strip size	0.4 mm 35.4 mm	10.4 mm 58.4 mm	0.2	6.0mm 10.5mm
Gap between two consecutive strip (assumed)	0.1 mm	58.4 mm + 0.1 mm	0.1mm	10.1mm
Insulated size of strip with working tolerance	35.5 mm	58.5 mm		10.1
Placement of strip (1w x 2D)	1W	2D	1W	2D
Effective dimension of each turn	35.5 x 40mm	117 mm (builds for 1st layer) + 0.25 mm (10mil inner layer insulation + 10 mm (build for 2nd layer.	14 x17mm	20.2 +0.2+ 6mm
Length of LV coil	1420 mm +	127.25 mm +	240mm	59.25mm
Use end packing of 5mm or either side of the coil (i.e. 5 x 2) = 10 mm	10mm	255 (round off)	10mm	12.00
Length of LV coil with packing	1430 mm	255 (radial build of LV coil)	250mm	12.00

In conclusion the LV coil per phase having 90T with 35.5 T per layer. length of coil is 1430 mm , the radial build of the coil is 25.5mm and inter layer insulation is 10 mil		In conclusion the LV coil per phase having 3T with 14.0 T per layer length of coil is 240 mm the radial build of the coil is 12mm and inter layer insulation is 10 mil

TABLE – F5 CORE DIAMETER

	Transformer	Prototype
Voltage per turn	$E_t = 220/\sqrt{3}/90 = 1.411kV$	$E_t = 240/\sqrt{3}/32 = 4.33V$
Flux density (available from specification) (B_m)	1.6 Tesla	1.6 Tesla
Stacking factor (assumed)	0.97	0.97
Gross core area (to be calculated)	Ag in sq cm.	

$$E_t = 4.44 \times f \times B_m \times A_g \times 0.97 \times 10^{-4} = 4.44 \times 50 \times B_m \times A_g \times 0.97 \times 10^{-4}$$

A_g =	51.898 sq cm	13.322sq cm

The design considered a core stack of 9 steps having rounding off factor of 0.935 (assumed)

STEP WIDTH

Transformer	**Prototype**
The core limb has a diameter of 300mm and has 9 steps.	The core limb has a diameter of 100cm and has 2 steps.
The first and 9th steps may be taken as 300 mm and140mm respectively. The balance 7 steps may be chosen as 280mm , 260mm, 240mm,	The first and 2nd steps may be taken as 100mm and60mm respectively. The

220mm,200mm,180mm, and 160mm.	balance 1 step may be chosen as 80mm ,
While selecting the step width, we must bear in mind that there should be at least a difference of 20 mm between the consecutive steps and they should be in descending order.	

F 2 CORE STACK

Calculation of the core stack (K)

$K = \sqrt{d^2} - l^2$ Where, d is the core diameter and l is the step width.

TABLE – F6 CORE STACK

Step no.	**Transformer**	**Prototype**
1	$l_1 = 300mm \quad K_1 = \sqrt{310^2} - 300^2 = 78.1mm$	$l_1 = 100mm$ $K_1 = \sqrt{110^2} - 100^2 = 45.83mm$
2	$l_2 = 280mm\ K_2 = \sqrt{310^2} - 280^2 = 78.1mm$ (-) 78.1= 54.94mm	$l_2 = 80mm$ $K_2 = \sqrt{110^2} - 80^2 = 75.498mm$
3	$l_3 = 280mm\ K_3 = \sqrt{310^2} - 260^2(-)54.94 = 113.87mm$	
4	$l_4 = 240mm\ K_4 = \sqrt{310^2} - 240^2(-)113.87 =$ 82.34mm	
5	$l_5 = 220mm\ K_5 = \sqrt{310^2} - 220^2(-)82.34 = 136.06mm$	
6	$l_6 = 200mm\ K_6 = \sqrt{310^2} - 200^2(-)13606 = 100.79mm$	
7	$l_7 = 180mm\ K_7 = \sqrt{310^2} - 180^2 = (-)100.79 = 151.59mm$	
8	$l_8 = 160mm\ K_8 = \sqrt{310^2} - 160^2(-)151.59 = 113.92mm$	
9	$l_9 = 140mm\ K_9 = \sqrt{310^2} - 140^2(-)113.92 = 162.66mm$	
	$K = K_1 + K_2 + K_3 + K_4 + K_5 + K_6 + K_7 + K_8 + K_9$ =78.1+54.94+113.87+82.34+136.06+100.79+151.9+113.92+162.66 =994.58	$K = K_1 + K_2$ = 45.83 + 75.498= 121.328mm

F3 CORE AREA

Step no.	TRANSFORMER			PROTO-TYPE		
	Step width (mm)	Core stack (mm)	Gross core area (sq mm) (l x K)	Step width (mm)(l)	Core stack (mm)(k)	Gross core area (sq mm) (l x k)
1	300 l_1	78.1 (K_1)	23430 $l_1 + K_1$	100 (l_1)	45.83 (k_1)	4583
2	280 l_2	54.94 (K_2)	15383.2 $l_2 + K_2$	80 (l_2)	75.498 (k_2)	6039.84
3	260 l_3	113.87 (K_3)	29606.2 $l_3 + K_3$			
4	240 l_4	82.34 (K_4)	19761.16 $l_4 + K_4$			
5	220 l_5	136.06 (K_5)	29933.2 $l_5 + K_5$			
6	200 l_6	100.79 (K_6)	20158 $l_6 + K_6$			
7	180 l_7	151.59 (K_7)	27286.2 $l_7 + K_7$			
8	160 l_8	113.92 (K_8)	18227.2 $l_8 + K_8$			
9	140 l_9	162.66 (K_9)	22772.4 $l_9 + K_9$			
	Total gross core area $(mm)^2$		**206,557.76**			**10622.84**

The net core area can be calculated as:

Net core area = Gross core area × stacking factor

The stacking factor may be assumed as 0.97 for all practical purposes.

Therefore, the net core area =206557.76 × 0.97 = 200,361.03sq mm

And net core area =10622.84× 0.97 = 10304.1548 sq mm for the prototype

F4 COIL DIAMETER AND CORE LIMB CENTRE

	Transformer	Prototype
Core diameter (previously calculated)	310 mm	100mm
Radial build of LV coil (previously calculated)	25.5 mm	17mm
Radial build of HV coil (previously calculated)	31.5 mm	17mm
Radial clearance between core to LV coil (assumed)	3 mm	3mm
Radial clearance between LV and HV (assumed)	10 mm (For 132 KV Transformer)	5mm

NB: Based on the above parameters, the coil, diameter and limb center can be calculated as follows

	Transformer		prototype	
	Radial	**Diameter**	**Radial**	**Diameter**
Core diameter Rx2Radial gap between core to LV coil	155x2 (+) 3	310 mm +6mm = 316mm	50 mm x2 +3	100mm + 6 =106mm
LV coil inside diameter Radial build of LV coil	158x2 (+) 21	316 mm + 21 mm = 337mm	53x2 +17	106mm+17mm =123mm
LV coil outside diameter Radial gap between LV and HV Coils	179 x2 (+) 10	358mm + 21 mm = 379 mm	70x2 +5	140mm+17mm =157mm
HV coil inside diameter Radial build coil	189 x 2 (+) 28	378mm + 28mm = 406mm	78x2 (+) 17	156 +17 = 173mm
Core limb centre	217x2	443mm + 13mm = 456 mm	95x2	173+17mm= 190mm

F5 CORE DETAILS

CORE FRAME SIZE AND OTHER CORE DETAILS:

	Transformer	**Prototype**
Core diameter	310 mm	100mm
Window height (w/h)	1643 mm	305mm
Limb center (c/L)	220 mm	184mm
Grade of core	27 – M_4	kapton covered
No of core steps	9	2
Core step width	300/280 /260/ 240 / 220 / 200 / 180 / 160 / 140mm	100/80
Core stack	78.1/ 54.94 / 113.87 / 82.34 / 136.06 / 100.79 / 151.59 /113.92 /162.66 mm	45.83/ 75.498
Total core stack	994.27 mm	121.328mm

F6 APPROXIMATE WEIGHT OF CORE

The weight of core is calculated using the following formula:

Weight of the complete set of core in Kg

= [3x W/H + 4x(C/L) + (2 x Width of 1^{st} x 0.86) x gross core area x density of core material x 0.97 x 10^{-3}

Where W/H, C/L, and width of the *l* step are in cm, gross core area in sq cm and density material 7.65g/ cc

The approximate core weight of the complete set of core:

= [(3 x 91.9 + 4 x 22.0) + (2 x 11x0.86) 2065.57 x 7.65 x 0.97 x10^{-3}] = 290 Kg

= [(3 x 30.5 + 4 x 18.4) + (2 x 11x0.86) 1062.284x0.35 x 0.97 x10^{-3}] = 1.6823Kg for the prototype

CORE CHART SPECIFICATION

Material	CRGO, Grade	
Thickness	027 mm	0.35mm
Widow height	1643 mm	305
Limb centre	220 mm	84
Core stack	994.27 mm	121.328mm
Weight / set	290 K g	1.683kg

F7 WINDING DETAILS:

LOW VOLTAGE WINDING

DESCRIPTION	TRANSFORMER DESIGN PARAMETERS	PROTOTYPE DESIGN PARAMETERS
Conductor material	Copper	copper
Type of coil	Spiral	spiral
Connection	Star	Neutral earthed
Size of bare conductor	11x4.5mm (parallel)	1.024x4.5mm
Covering	DPC- 0.4 mm	DPC- 0.4 mm
Size of covered conductor	11x11.4x4.9mm	1.024x11.4x4.9mm
Conductor disposition	1width x 2depth = (1Wx2D)	1width x 2depth = (1Wx2D)
Turns per phase	90T	3T
No. of coils per phase	1	1
Turns per coil	90 T	3T
No. layers	2	2
Turns per layer	35.5 T	17 T
Inter- layer - Insulation	10 mil	5mil
Tapping details	Nil	Nil
Inside drum of coil	337mm	64mm
Outside drum coil	379mm	100mm
Winding length of coil	460mm	120mm
End packing details	5 mm on either side	5 mm on either side
Overall length of coil	470mm	135mm
Approximate bare weight of conductor per Transformer	27.1Kg	0.200kg
Approximate covered weight of Conductor per TX including leads	27.1 × 1.07 = 29.0 Kg	0.200x1.07= 0.214kg

HIGH VOLTAGE WINDING:

PARAMETERS DESCRPTION	**TRANSFORMER**	**PROTO-TYPE**
Conductor material	copper,	copper,
Type of coil	crossover or sectional	crossover or sectional
Connection	Delta	Delta
Size of bare conductor	0.3 mm diameter	0.812 mm diameter
Covering	DPC – 0.2 mm	DPC – 0.2 mm
Size of covered conductor	1.9 mm diameter	0.812 mm diameter
Conductor disposition	Nil	nil
Transposition (if provided)	Nil	nil
Turns per phase	147225+7362for tapping = 154587T	
No. of coils per phase	4	1
Turns per coil	147225 T	
No. of layers	100 layers	17
Turns per layer	387/100 T (averaged)	30/31T
Inter- layer insulation	4 mil (0.1mm)	2mil(0.05mm)
Tapings details	0- (700)-(794)-(878) (F)	
Inside diameter of coil	182mm	67mm
Outside diameter of coil	252mm	100mm
Winding length of coil	104 mm	35mm
End packing details	Nil	nil
Approximate bare weight of conductor per TX	45 kg	0.200kg
Approximate covered weight of conductor per TX,	45x1.14=51.5kg	0.300kg

LENGTH OF LV AND COPPER

PARTICULARS	LV COIL	HV COIL :
Inside diameter of coil (D1)	337mm	182mm
Outside of coil (D2)	162mm	252mm
Mean diameter of coil	$Dm = \frac{D_1 + D_2}{2} = 141mm$	217mm
Mean length of turns	$(l_t)(K_t)=\pi D_m$ = 443mm	682 mm
No of turns (T)	87T	8511+ 426= 8937T
Total length of conductor L=l_txT	394485mm	2395184mm

F8 PROTOTYPE TRANSFORMER TESTS

NO-LOAD TESTS

TEST	VALUE
No-load supply Voltage	235V
No-load output voltage-	23.5V
Primary winding resistance	2.7Ω
Secondary winding resistance	0.6Ω

TRANSFORMER UNDER PURELY CAPACITIVE LOAD TEST

V_s (volts)	C_l (μF) x10-1	V_o (volts)	I_o (Amps)
235	10	25.2	0.007
235	9	25.2	0.006
235	8	25.3	0.005
235	7	25.2	0.005
234	6	25.2	0.004
235	5	25.2	0.004
234	4	25.2	0.003

235	3	25.2	0.001
235	2	25.2	0.001
235	1	25.2	0.00
235	0	25.2	0.00

TRANSFORMER UNDER PURELY RESISTIVE LOAD TEST RESULTS

V_s (volts)	R_l (Ω)	V_o (volts)	I_o (Amps)	Z=Vo/Io (Ω)
229	50	25.0	0.42	59.5
229	100	25.1	0.24	104.5
230	200	25.1	0.12	209.29
230	300	25.1	0.082	306.10
231	400	25.0	0.06	416.7
231	500	25.0	0.048	520.83
231	600	25.1	0.040	627.50
231	700	25.1	0.034	738.25

TRANSFORMER PURELY INDUCTIVE LOAD TEST

V_s (volts)	L_l (H)x10-1	V_o (volts)	I_o (Amps)
238	10	25.5	0.009
239	9	25.5	0.011
238	8	25.5	0.012
238	7	25.4	0.013
239	6	25.5	0.016
239	5	25.5	0.021
239	4	25.5	∞

TRANSFORMER INDUCTIVE AND CAPACITIVE (SHUNT) LOADING

V_s (volts)	C_l (μF) x10-1	V_o (volts)	I_o (Amps)	L_l (H)x10-1
235	10	25.2	0.011	10
235	10	25.2	0.011	9
235	10	25.2	0.012	8
235	10	25.2	0.013	7
235	10	25.2	0.015	6
235	10	25.2	0.020	5

V_s (volts)	C_l (μF) x10-1	V_o (volts)	I_o (Amps)	L_l (H)x10-1
235	8	25.2	0.010	10
235	8	25.2	0.011	9
235	8	25.2	0.012	8
235	8	25.2	0.013	7
235	8	25.2	0.014	6
235	8	25.2	0.020	5

V_s (volts)	C_l (μF) x10-1	V_o (volts)	I_o (Amps)	L_l (H)x10-1
235	6	25.2	0.009	10
235	6	25.2	0.010	9
235	6	25.2	0.011	8
235	6	25.2	0.012	7
235	6	25.2	0.013	6
235	6	25.2	0.020	5

V_s (volts)	C_l (μF) x10-1	V_o (volts)	I_o (Amps)	L_l (H)x10-1
234	4	25.1	0.009	10
234	4	25.1	0.010	9
234	4	25.1	0.011	8
234	4	25.1	0.012	7
234	4	25.1	0.013	6
234	4	25.1	0.020	5

V_s (volts)	C_l (μF) x10-1	V_o (volts)	I_o (Amps)	L_l (H)x10-1
234	2	25.1	0.008	10
234	2	25.1	0.009	9
234	2	25.1	0.011	8
234	2	25.1	0.012	7
234	2	25.1	0.015	6
234	2	25.1	0.020	5

TRANSFORMER- PARALLEL CAPACITIVE-INDUCTIVE- RESISTIVE LOADING

V_s (volts)	C_l (μF) x10-1	V_o (volts)	R_l (Ω)	L_l (H)x10-1	I_o (Amps)
233	10	25.1	700	5	0.008
233	10	25.1	600	5	0.010
233	10	25.1	500	5	0.012
233	10	25.1	400	5	0.014
233	10	25.1	300	5	0.018
233	10	25.1	200	5	0.025
233	10	25.1	100	5	0.54
233	10	25.1	50	5	1.20

V_s (volts)	C_l (µF) x10-1	V_o (volts)	R_l (Ω)	L_l (H)x10-1	I_o (Amps)
234	5	25.1	700	5	0.008
234	5	25.1	600	5	0.009
234	5	25.1	500	5	0.012
234	5	25.1	400	5	0.014
234	5	25.1	300	5	0.018
234	5	25.1	200	5	0.025
234	5	25.1	100	5	0.54
234	5	25.1	50	5	1.20

V_s (volts)	C_l (µF) x10-1	V_o (volts)	R_l (Ω)	L_l (H)x10-1	I_o (Amps)
233	2	25.1	700	5	0.008
233	2	25.1	600	5	0.010
233	2	25.1	500	5	0.012
233	2	25.1	400	5	0.014
233	2	25.1	300	5	0.018
233	2	25.1	200	5	0.025
233	2	25.1	100	5	0.54
233	2	25.1	50	5	1.20

APPENDIX G: Simulation Results Tables for ASVTs

G1. Model circuit with two ASVTs each Pi section representing 220km

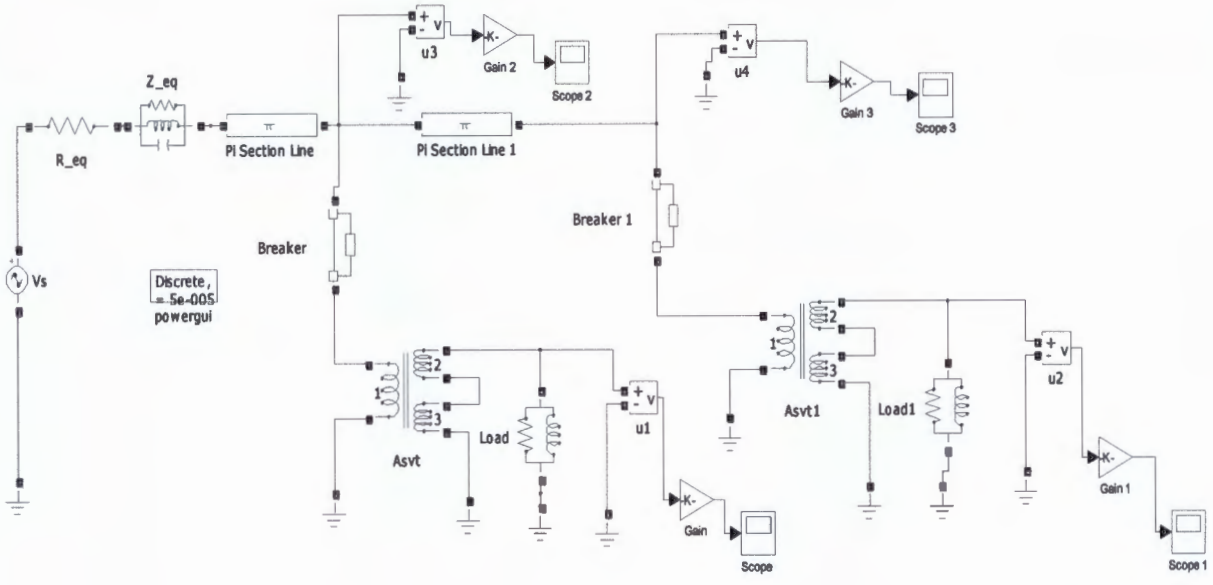

G2. Model circuit with two ASVTs each Pi section representing 147km

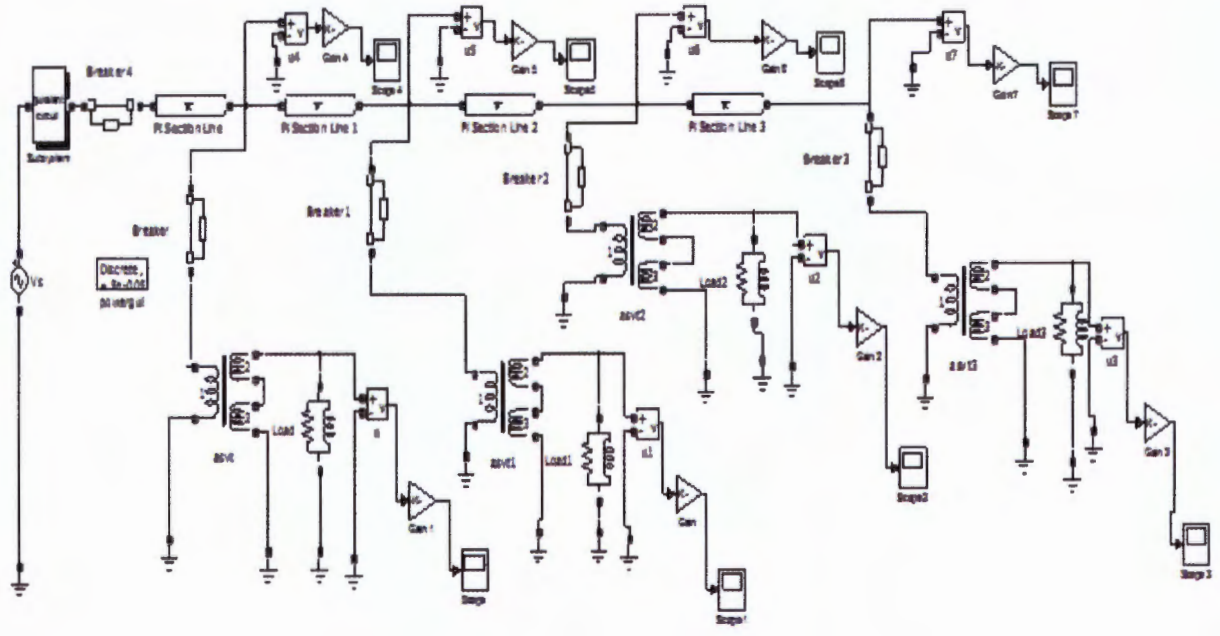

TABLE G-1: HV AND LV VOLTAGES WITH HV LINE NOT LOADED

HV line not loaded and no reactor,	ASVT 50km from Rabai		ASVT 100km from Rabai	ASVT 150km from Rabai	ASVT 200km from Rabai	ASVT 250km from Rabai	ASVT 300km from Rabai	ASVT 350km from Rabai
No load On LV (volts)	LV	249	248	246	244	240	237	232
	HV	145,954	145,957	145,960	145,963	145,967	145,971	145,974
Loaded LV (volts)	LV	227	226	224	222	219	216	212
	HV	145,926	145,932	145,938	145,945	145,952	145,960	145,968
Value of HV winding	R	300 Ω						
	L	1.8 H						
Value of LV winding	R	0.06Ω						
	L	2.2e-5						

TABLE G- 2: TWO ASVT INSTALLED WITH HV LINE NOT LOADED

Low Voltage line not Loaded	ASVT at 50 and 100km from Rabai		ASVT at 50 and 150km from Rabai		ASVT at 50 and 200km from Rabai		ASVT at 50 and 250km from Rabai		ASVT at 250 and 252km from Rabai		ASVT at 50 and 300km from Rabai	
	LV 50	249	50	249	50	249	50	249	250	242	LV 50	233
	HV 50 (kV)	145,70	50	145,732	50	145,734	50	145,737	250	141749	50	145,718
	LV100	248	150	246	200	243	250	240	252	242	300	237
	HV 100	145,72	150	144,113	200	142,692	250	145,732	252	141,75	300	138,682
Low Voltage line loaded to 100kW	LV 50	233	50	233	50	233	50	233	250	227	50	233
	HV 50	145,68	50	145,691	50	145,696	50	145,702	250	141,70	50	145,712
	LV100	232	150	230	200	228	250	225	252	226	300	222
	HV 100	145,08	150	144,082	200	142,672	250	140,871	252	141,647	300	138,678

TABLE G- 3 : TWO ASVT INSTALLED WITH HV LINE LOADED

Low Voltage line not Loaded	ASVT at 50 and 100km from Rabai		ASVT at 50 and 150km from Rabai		ASVT at 50 and 200km from Rabai		ASVT at 50 and 250km from Rabai		ASVT at 250 and 252km from Rabai		ASVT at 50 and 300km from Rabai	
	LV 50	220	50	220	50	220	50	220	250	224	50	220
	HV50	128864	50	128,865	50	128,867	50	128,870	250	131,477	50	128,872
	LV100	222	150	223	200	224	250	224	252	224	300	223
	HV 100	129959	150	130,695	200	131,066	250	131,071	252	131,463	300	130,711
Low Voltage line loaded to 100kW	LV 50	206	50	206	50	206	50	206	250	210	50	206
	HV 50	128834	50	128,838	50	128,841	50	128,846	250	131,461	50	128,850
	LV100	208	150	209	200	209	250	209	252	210	300	209
	HV 100	129932	150	130,671	200	131,045	250	131,054	252	131,457	300	130,698

TABLE G- 4: THREE ASVT INSTALLED WITH HV LINE LOADED

Low Voltage line not Loaded	ASVT at 50,100 150km from Rabai		ASVT at 50, 150 and 200km from Rabai		ASVT at 50 ,200 and250km from Rabai		ASVT at 250,252 and 254km from Rabai		ASVT at 50,250 and 300km from Rabai	
	LV 50	249	50	249	50	249	250	242	50	249
	HV 50	146	50	145,912	50	145,925	250	146,821	50	145,932
	LV 100	248	150	246	200	240	252	242	250	237
	HV100	147,1	150	144,09	200	142,683	252	141,652	250	140,881
	LV 150	246	200	243	250	243	254	242	300	240
	HV 150	144,1	200	142,681	250	140,872	254	141,575	300	138,682
Low Voltage line loaded to 100kW	LV 50	233	50	233	50	233	250	226	50	233
	HV 50	145,8	50	145,043	50	145,876	250	146,793	50	145,891
	LV 100	232	150	232	200	225	252	226	250	222
	HV100	145,1	150	145,044	200	142,641	252	141,623	250	140,853
	LV 150	230	200	230	250	228	254	226	300	225
	HV 150	144,2	200	144,047	250	140,845	254	141,541	300	138,650

TABLE G- 5: TWO ASVT AND ONE CCS INSTALLED WITH HV LINE NOT LOADED

Low Voltage line not Loaded	ASVT at 50,100 150km from Rabai		ASVT at 50, 150 and 200km from Rabai		ASVT at 50 ,200 and250km from Rabai		ASVT at 250,252 and 254km from Rabai		ASVT at 50,250 and 300km from Rabai	
	LV 50	219	50	219	50	219	250	223	50	223
	HV 50	126,912	50	126,703	50	126,908	250	127,317	50	129,041
	LV 100	221	150	222	200	223	252	223	250	226
	HV 100	129,443	150	130,172	200	130,541	252	130,942	250	132,742
	LV150	222	200	223	250	223	254	223	300	226
	HV 150	130,221	200	130,173	250	130,553	254	130,948	300	132,375
Low Voltage line loaded to 100kW	LV 50	205	50	205	50	205	250	209	50	208
	HV 50	126,824	50	126,865	50	126,871	250	127,282	50	129,007
	LV 100	207	150	208	200	209	252	209	250	212
	HV100	129,346	150	130,572	200	130,512	252	130,918	250	132,709
	LV 150	208	200	209	250	209	254	209	300	211
	HV 150	130,137	200	130,514	250	130,518	254	130,906	300	132,705

TABLE G- 6: TWO ASVTS ON A 125MW LOADED LINE INCORPORATING A BREAKER

Low Voltage line not Loaded	ASVT1 at 50km,CCS100km and ASVT2 at 150km from Rabai		ASVT1 at 50km,CCS150Km and ASVT2 at 200km from Rabai		ASVT1 at 50Km,CCS200 Km and ASVT2 at 250km from Rabai		ASVT1 at 250Km,CCS252Km and ASVT2 at 254km from Rabai		ASVT1 at 50Km,CCS250Km and ASVT2 at 300km from Rabai	
	LV 50	253	50	253	50	252	250	245	50	251
	HV 50	147,723	50	146,361	50	144,597	250	143,272	50	142,429
	LV 100	248	150	246	200	243	252	241	250	239
	HV 100	148,576	150	148,222	200	147,874	252	148,508	250	147,535
	LV 150	250	200	247	250	243	254	244	300	239
	HV 150	146,423	200	144,637	250	142,262	254	143,176	300	139,917
Low Voltage line loaded to 100kW	LV 50	237	50	236	50	236	250	229	50	235
	HV 50	147,612	50	146,323	50	144,557	250	143,234	50	142,391
	LV 100	242	150	239	200	237	252	234	250	233
	HV100	148,584	150	148,162	200	147,835	252	148,465	250	147,492
	LV 150	234	200	231	250	228	254	229	300	224
	HV 150	146,324	200	144,595	250	142,432	254	143,147	300	139,883

APPENDIX H: Transient conditions for ASVT and CCS combination

H1.Waveform for ASVT/CCS Under transient conditions (Signal 2)

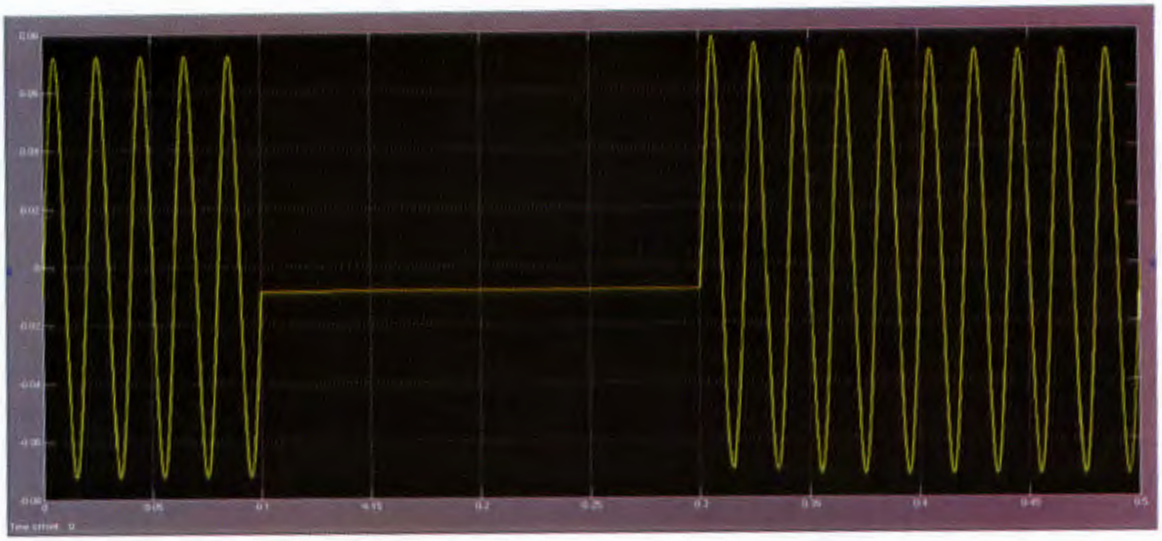

CCS DIVIDER POINT VOLTAGE WAVEFORM (SCOPE 1)

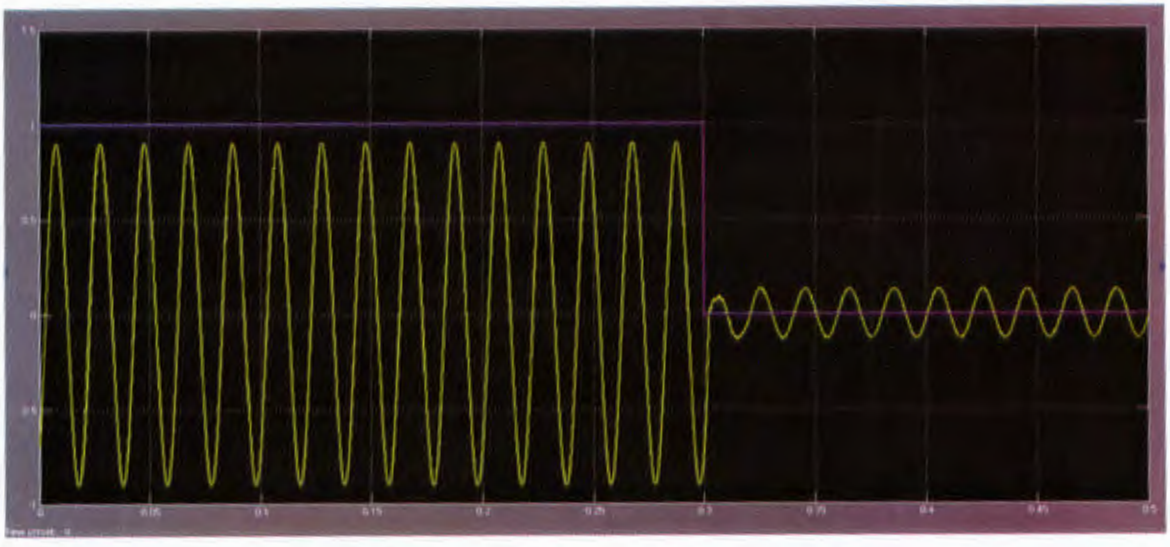

(B) ASVT SYSTEM CURRENT WAVEFORM (SCOPE 2)

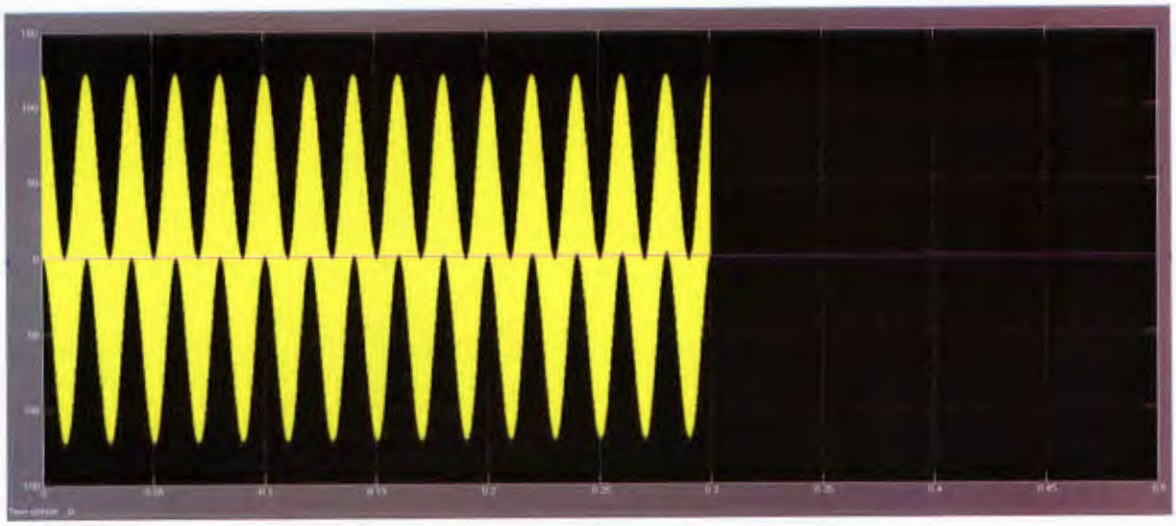

CCS SYSTEM CURRENT WAVEFORM (SCOPE 3)

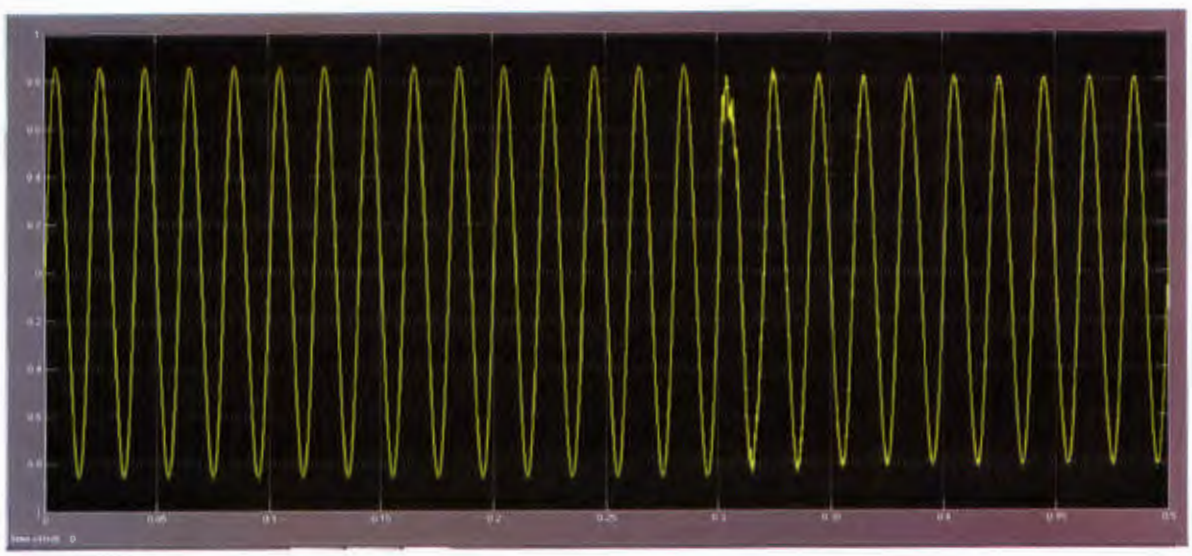

ASVT TAP-OFF VOLTAGE WAVEFORM(SCOPE 4)

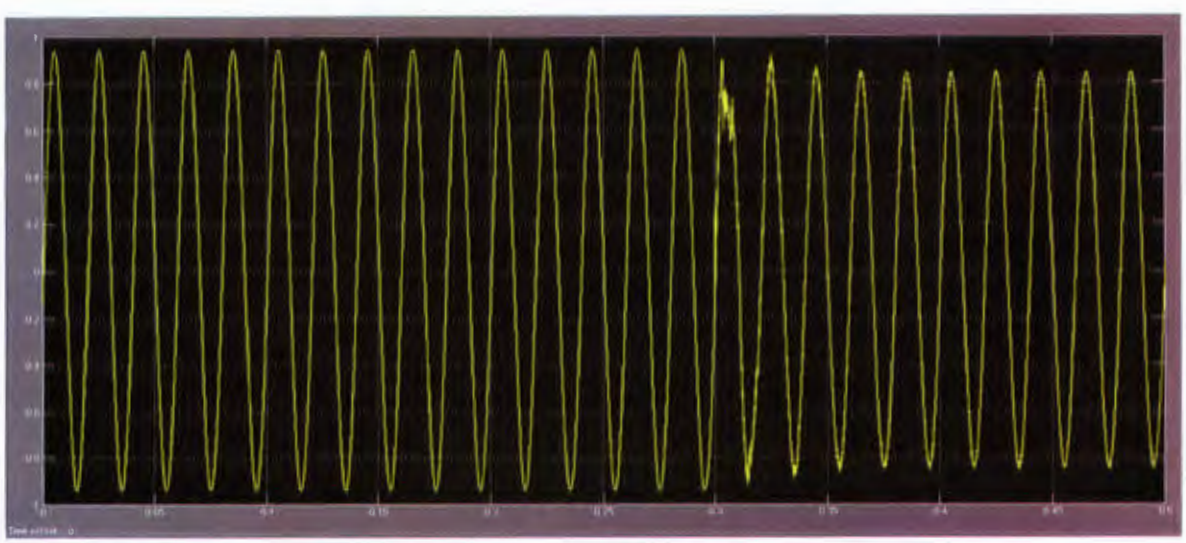

CCS TAP-OFF VOLTAGE WAVEFORM(SCOPE 5)

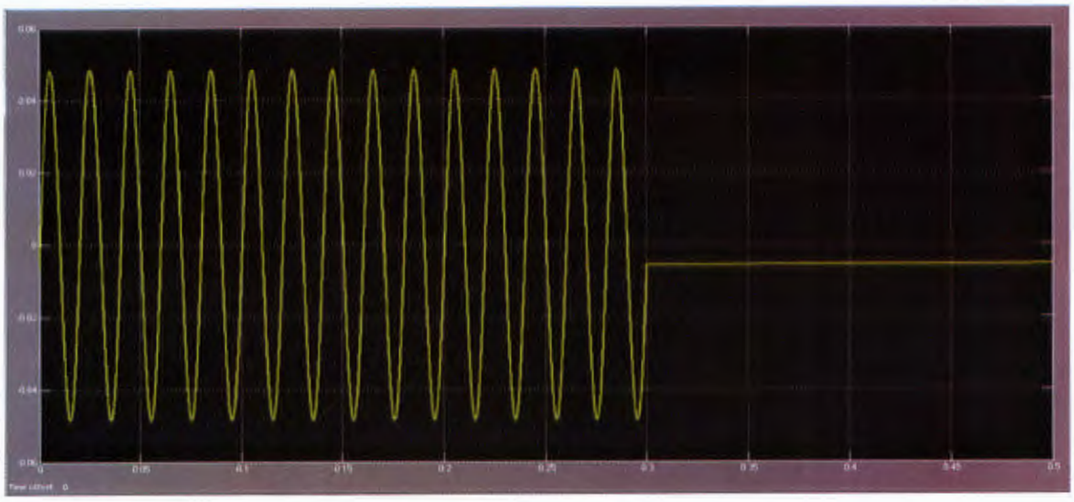

(F) CCS LOAD CURRENT WAVEFORM (SCOPE 6)

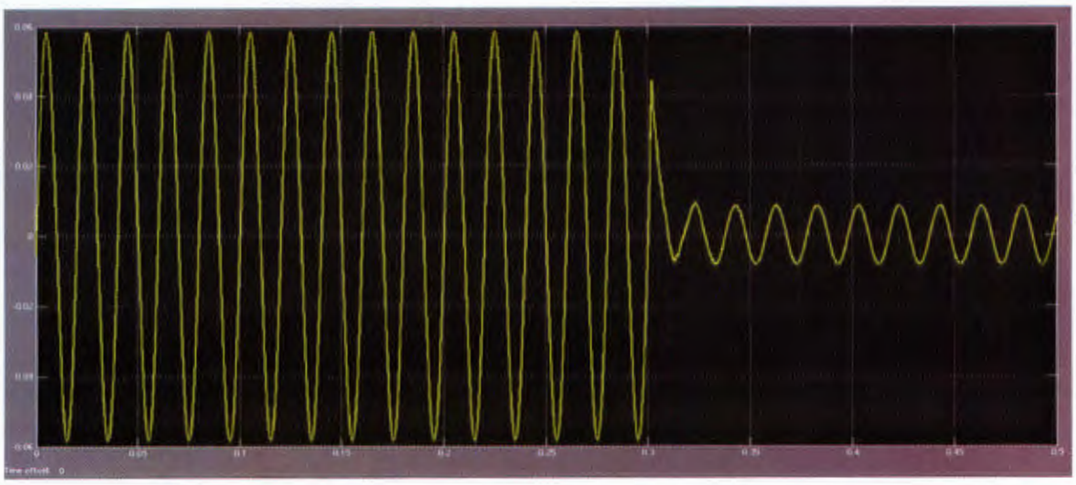

(G)ASVT LOAD VOLTAGE WAVEFORM (SCOPE 7)

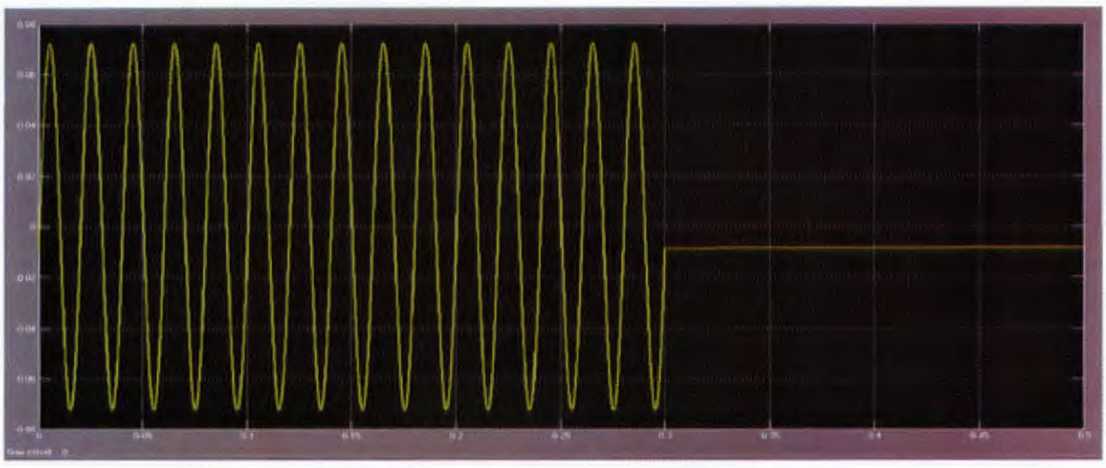

(H) CCS LOAD VOLTAGE WAVEFORM (SCOPE 8)

H2.Voltage waveform for ASVT/CCS under transient conditions (Signal 3)

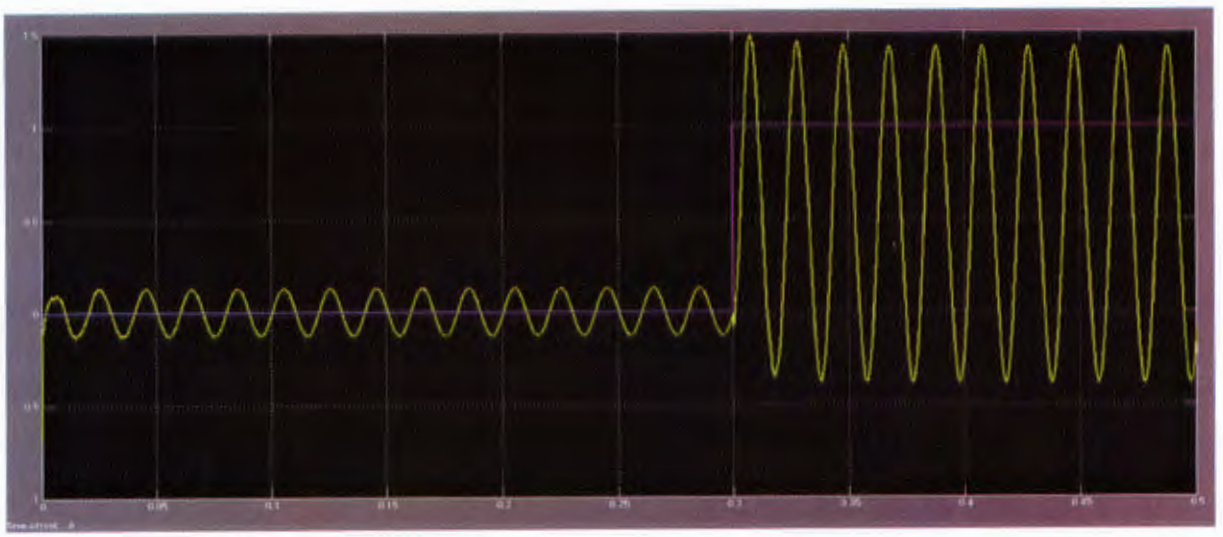

ASVT SYSTEM CURRENT WAVEFORM (SCOPE 1)

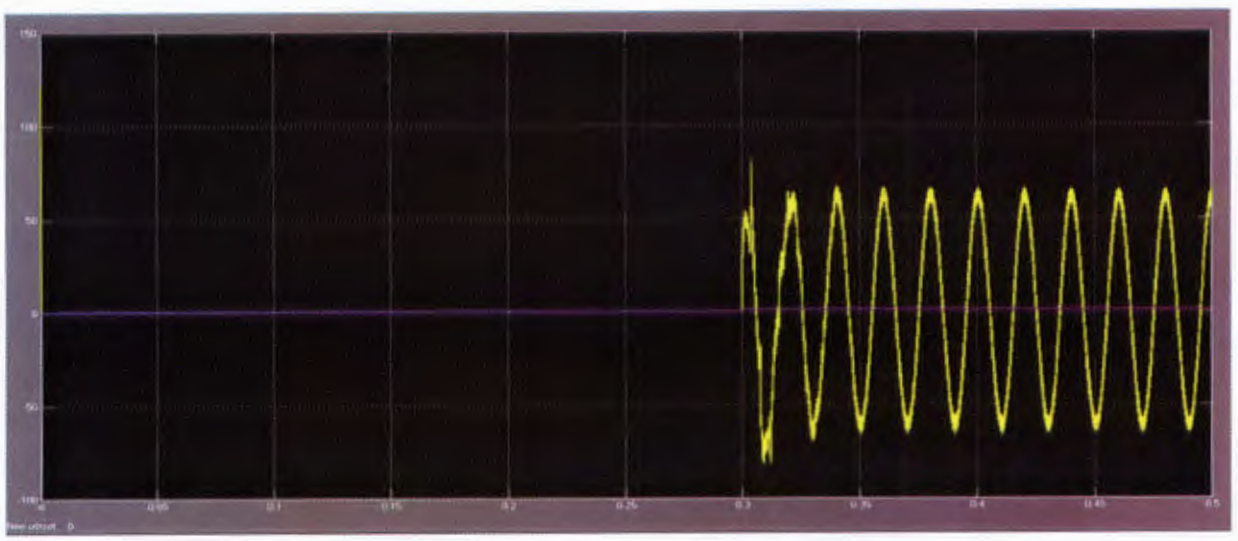

CCS SYSTEM CURRENT WAVEFORM(SCOPE 2)

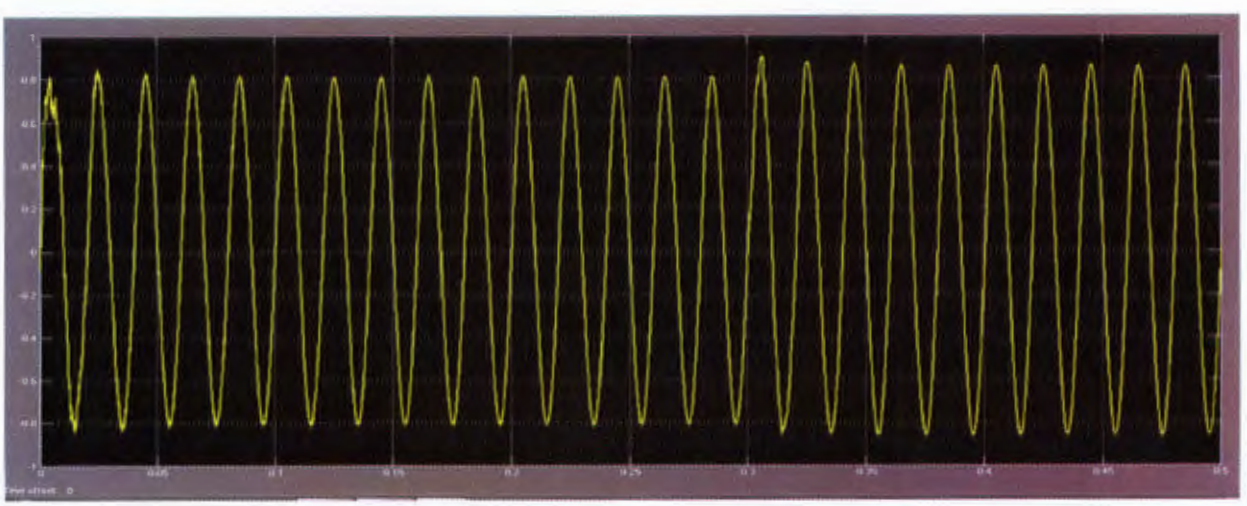

(C) ASVT TAP-OFF VOLTAGE WAVEFORM (SIGNAL 3)

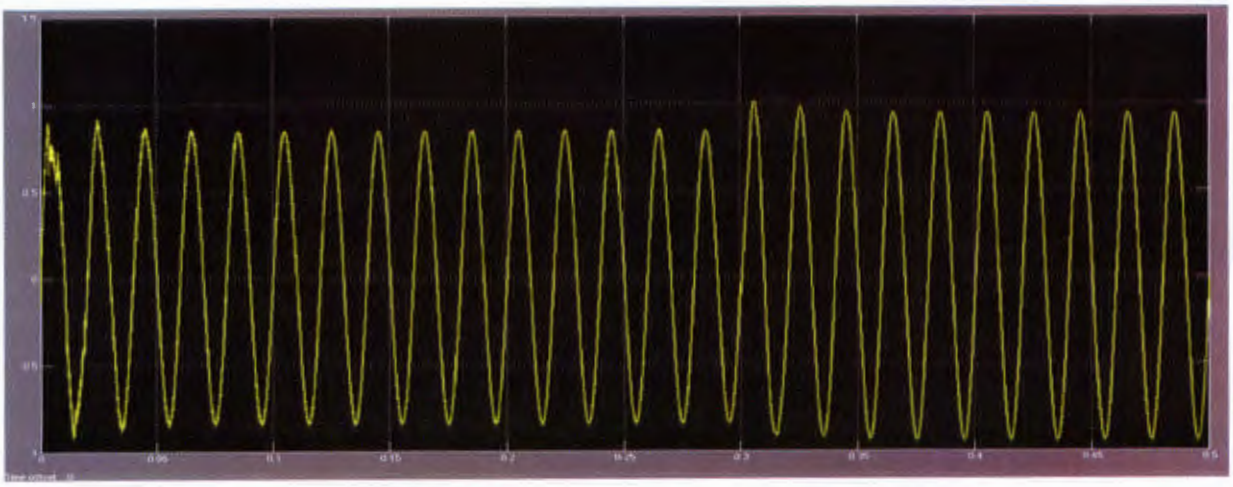

CCS TAP-OFF VOLTAGE WAVEFORM (SCOPE 4)

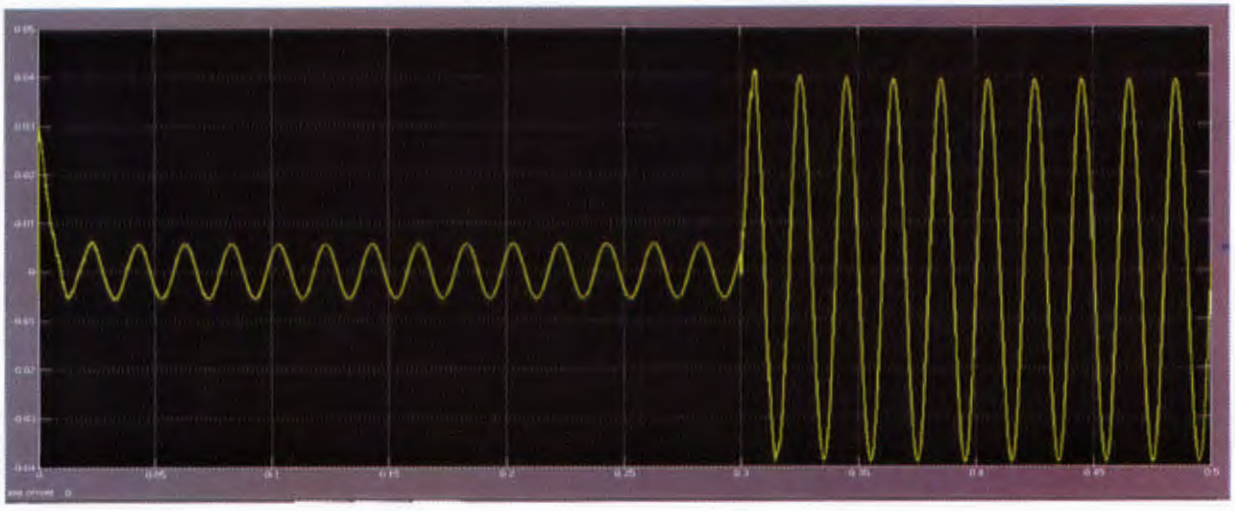

(E)ASVT LOAD CURRENT WAVEFORM (SCOPE 5)

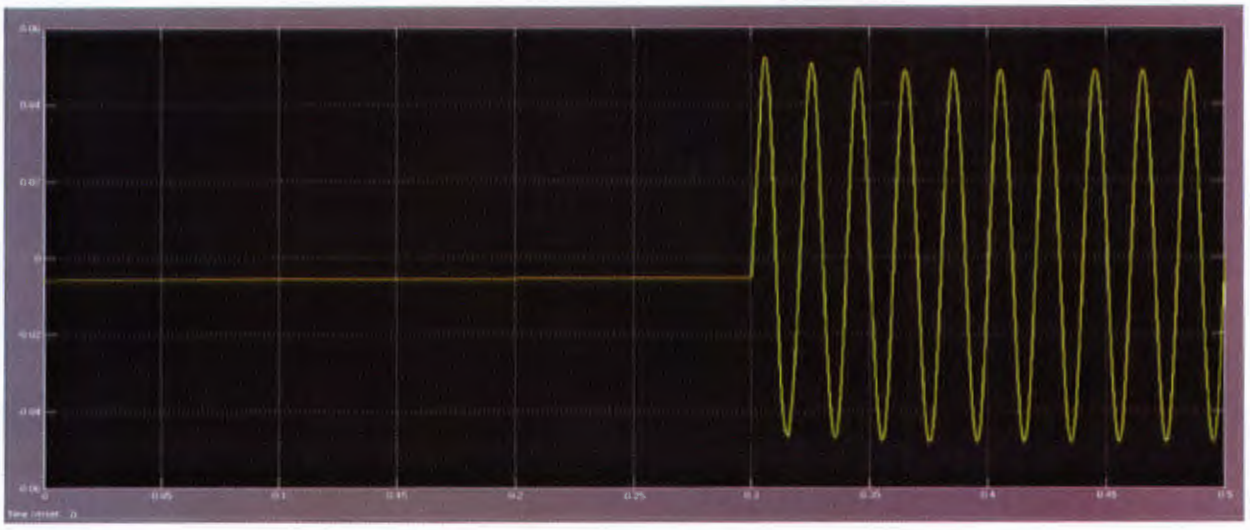

CCS LOAD CURRENT WAVEFORM (SCOPE 6)

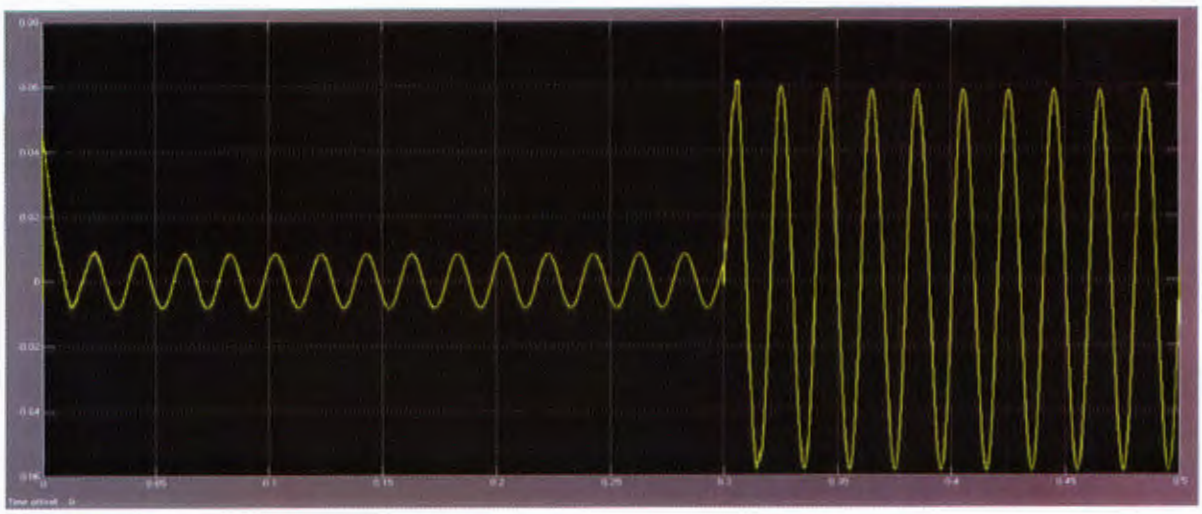

(G)ASVT LOAD VOLTAGE WAVEFORM (SCOPE 7)

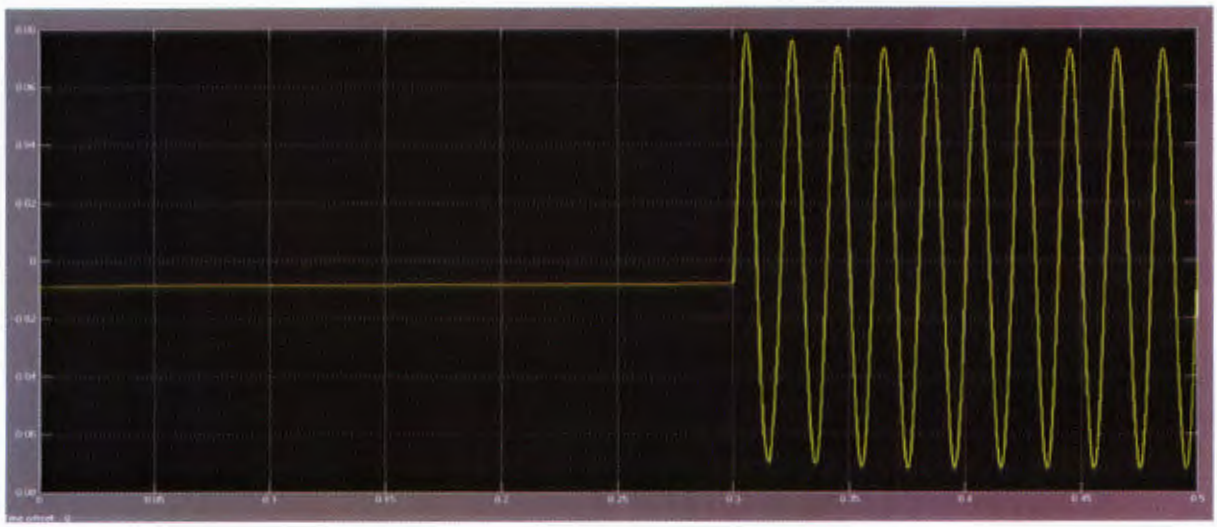

(H) CCS LOAD VOLTAGE WAVEFORM (SCOPE 8)

H3.Waveform for ASVT/CCS Under transient conditions (Signal 4)

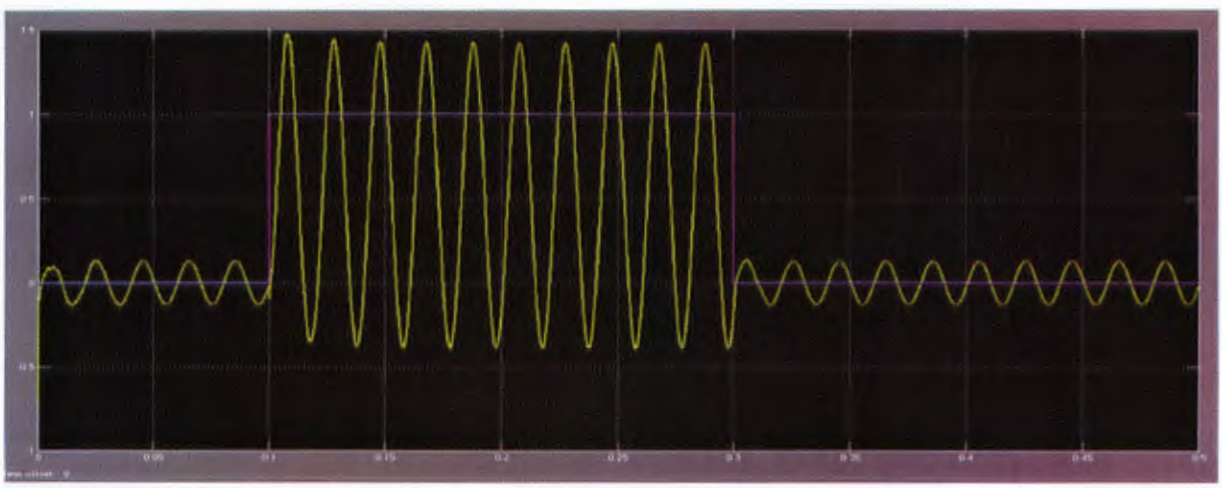

(A)ASVT SYSTEM CURRENT WAVEFORM (SCOPE 1)

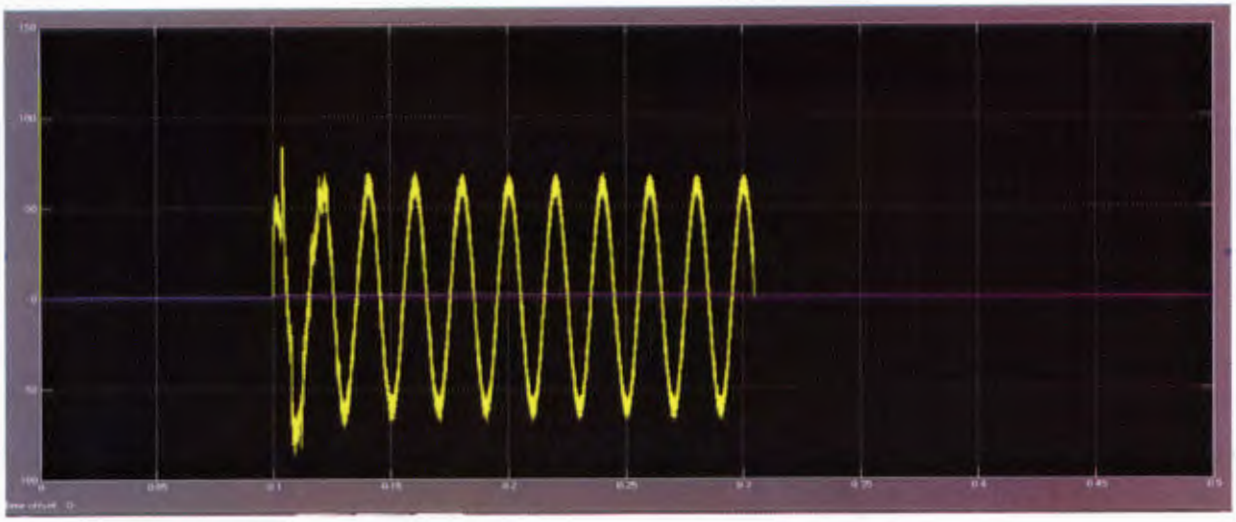

(B)CCS SYSTEM CURRENT WAVEFORM (SCOPE 2)

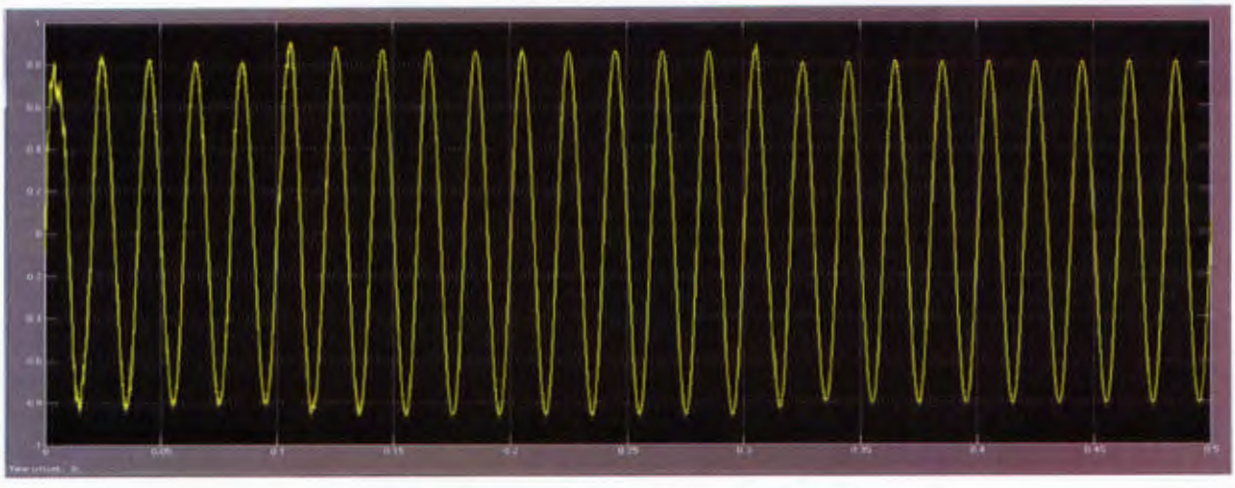

ASVT TAP-OFF VOLTAGE WAVEFORM(SCOPE 3)

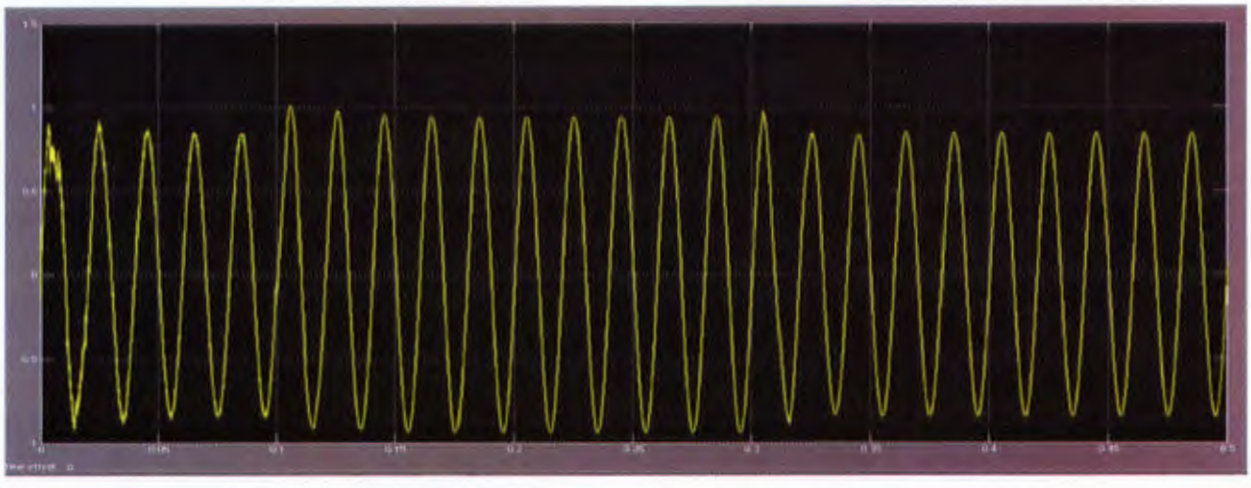

(D) CCS TAP-OFF VOLTAGE WAVEFORM (SCOPE 4)

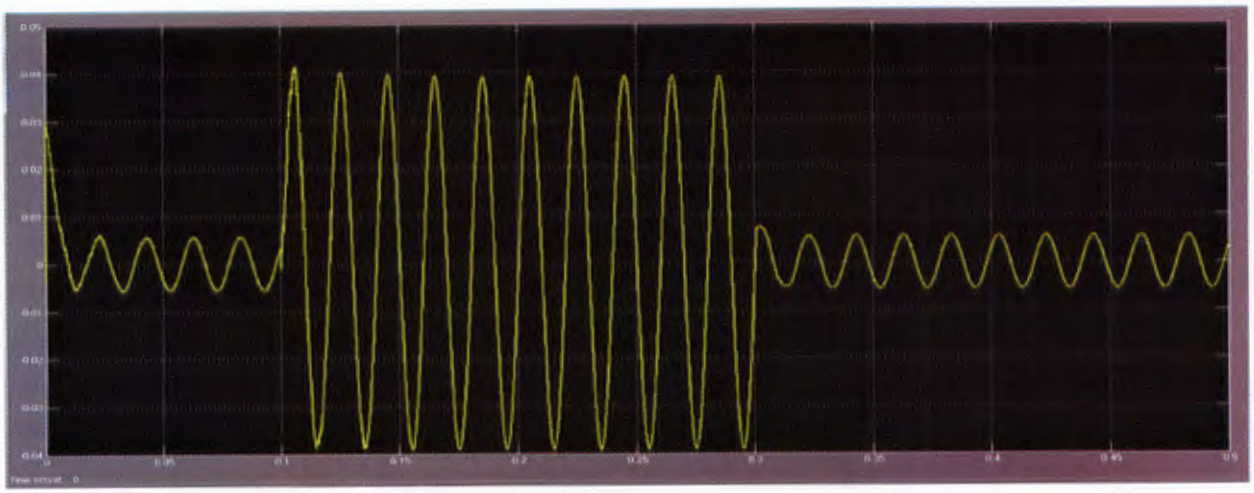

(E)ASVT LOAD CURRENT WAVEFORM (SCOPE 5)

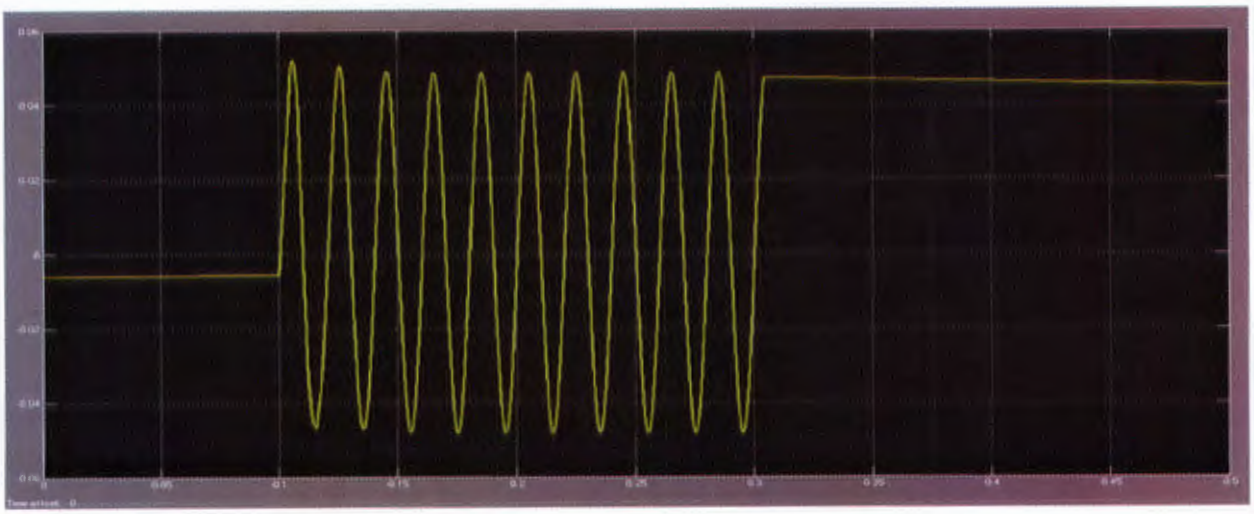

CCS LOAD CURRENT WAVEFORM (SCOPE 6)

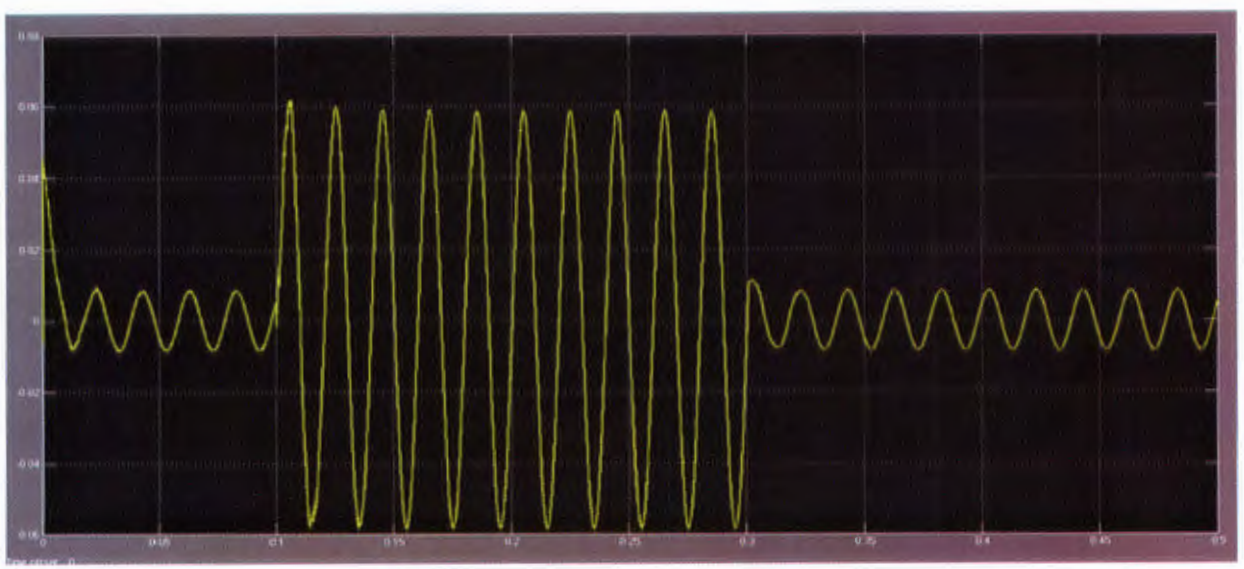

(G)ASVT LOAD VOLTAGE WAVEFORM (SCOPE 7)

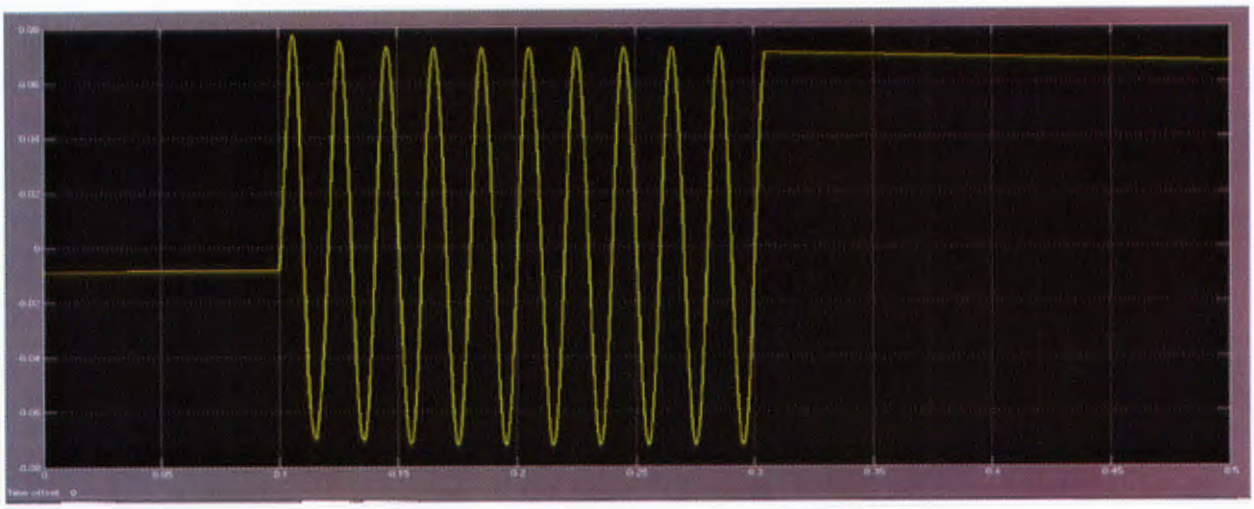

(H)CCS LOAD VOLTAGE WAVEFORM (SCOPE 8)

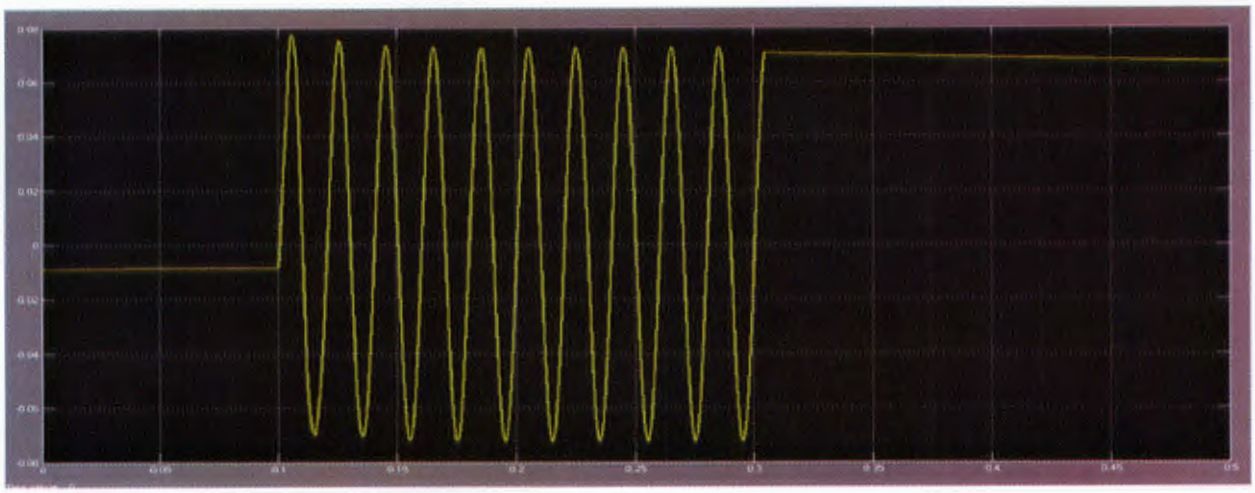

(I) CCS DIVIDER POINT VOLTAGE WAVEFORM (SCOPE 9)

APPENDIX J: ASVT LOADABILITY TEST RESULTS

Tables J1 to J6 are the ASVT loadability test results. .Simulations of the ASVT system were carried out using the model circuit of Figure 6.19.

Where;

Scope 1 .U_1 (KV) represents the system voltage

Scope 2 U_2 (KV) represents tap-off voltage

Scope 3 U_3 (KV) is the load voltage

Scope 4 I_1 (A) represents the system current

Scope 5 I_2 (A) represents load current

Q_L(MVAR) represent the varied reactive power of the load

Note that the values given in table J1 to J6 for the load current are line currents. While for the system current is given in phase value. The stability limitation of the line was 125MW. Therefore, assuming a 70% loading per phase, the system load was taken as 29.17MW (see appendix A). Calculations were carried out applying the same methodology used in appendix E.

J1. ASVT LOADABILITY FOR A CONSTANT REAL POWER OF 1MW AND VARYING Q_L

U_1(KV)	U_2(KV)	U_3(KV)	I_I(A)	I_2(A)	Q_L(MVAR)	PF
130.55	130.86	30.78	643.49	93.78	4.898	0.2
130.38	130.73	31.37	429.42	61.35	3.179	0.3
130.32	130.60	32.07	322.38	45.00	2.291	0.4
130.24	130.47	32.94	258.16	35.05	1.732	0.5
130.14	130.38	34.05	215.28	28.26	1.333	0.6
129.99	130.49	35.53	184.37	23.21	1.02	0.7
129.75	131.44	37.17	160.16	19.42	0.75	0.8
129.15	134.79	34.97	138.82	18.34	0.484	0.9
130.55	131.12	29.80	128.44	19.37	0	1.0

J2. ASVT LOADABILITY FOR A CONSTANT REAL POWER OF 2MW AND VARYING Q_L

U_1(KV)	U_2(KV)	U_3(KV)	1_I(A)	I_2(A)	Q_L(MVAR)	PF
130.42	129.98	31.66	647.84	182.36	9.795	0.2
130.26	129.88	31.63	432.23	121.69	6.359	0.3
130.08	129.77	31.61	324.44	91.32	4.582	0.4
130.63	129.65	31.58	259.80	73.13	3.464	0.5
129.56	129.49	31.54	216.76	61.02	2.667	0.6
129.14	129.29	31.49	186.09	52.38	2.04	0.7
128.46	128.97	31.41	163.23	45.95	1.50	0.8
128.46	128.34	31.25	145.80	41.06	0.969	0.9
130.67	130.17	31.71	129.38	36.41	0	1.0

J3. ASVT LOADABILITY FOR A CONSTANT REAL POWER OF 3MW AND VARYING Q_L

U_1(KV)	U_2(KV)	U_3(KV)	1_I(A)	I_2(A)	Q_L(MVAR)	PF
130.42	129.98	31.66	647.84	273.54	14.693	0.2
130.26	129.88	31.63	432.23	182.53	9.538	0.3
130.08	129.77	31.61	324.44	136.99	6.873	0.4
130.63	129.65	31.58	259.80	109.69	5.196	0.5
129.56	129.49	31.54	216.76	91.53	3.999	0.6
129.14	129.29	31.49	186.09	78.58	3.06	0.7
128.46	128.97	31.41	163.23	68.93	2.25	0.8
128.46	128.34	31.25	145.80	61.58	1.453	0.9
130.67	130.17	31.71	129.38	54.62	0	1.0

J4 ASVT LOADABILITY FOR A CONSTANT REAL POWER OF 4MW AND VARYING Q_L

U_1(KV)	U_2(KV)	U_3(KV)	1_I(A)	I_2(A)	Q_L(MVAR)	PF
130.60	129.10	31.43	652.26	367.39	19.591	0.2
130.44	128.87	31.37	435.61	245.39	12.717	0.3
130.27	128.61	31.30	327.37	184.46	9.164	0.4
130.06	128.31	31.23	262.51	147.90	6.928	0.5
129.81	127.96	31.14	219.36	123.60	5.333	0.6
129.55	127.49	31.02	188.71	106.36	4.08	0.7
128.59	126.79	30.85	166.03	93.57	3.00	0.8
133.04	125.39	30.50	149.23	84.13	1.938	0.9
130.87	129.54	31.54	130.00	73.22	0	1.0

J5 ASVT LOADABILITY FOR A CONSTANT REAL POWER OF 5MW AND VARYING Q_L

U_1(KV)	U_2(KV)	U_3(KV)	1_I(A)	I_2(A)	Q_L(MVAR)	PF
130.86	129.10	31.43	643.49	459.24	24.488	0.2
130.73	128.87	31.37	429.41	306.74	15.897	0.3
130.60	128.61	31.30	322.38	230.57	11.455	0.4
130.47	128.31	31.23	258.16	184.87	8.66	0.5
130.38	127.96	31.14	215.28	154.50	6.667	0.6
130.49	127.49	31.02	184.37	132.94	5.1	0.7
131.44	126.79	30.85	160.16	116.97	3.75	0.8
134.79	125.39	30.50	138.83	105.16	2.421	0.9
131.12	129.54	31.54	128.44	91.53	0	1.0

J6 ASVT LOADABILITY FOR A CONSTANT REAL POWER OF 6MW AND VARYING Q_L

U_1(KV)	U_2(KV)	U_3(KV)	1_I(A)	I_2(A)	Q_L(MVAR)	PF
131.17	128.89	31.37	641.96	552.14	29.386	0.2
131.08	128.66	31.31	428.27	368.80	19.076	0.3
131.01	128.23	31.20	321.37	277.57	13.747	0.4
130.99	127.88	31.12	257.14	222.63	10.392	0.5
131.09	127.46	31.01	214.12	186.18	7.999	0.6
131.53	126.92	30.86	182.92	160.36	6.121	0.7
132.86	124.10	30.67	158.45	141.18	4.50	0.8
135.16	124.49	30.27	138.44	127.15	2.906	0.9
131.36	129.32	31.48	128.21	110.04	0	1.0